HIGH-PRESSURE (HP), GRANULITE-FACIES THRUSTING IN A THICK-SKINNED THRUST SYSTEM IN THE EASTERN GRENVILLE PROVINCE, CENTRAL LABRADOR

JASON B. KRAUSS

National Library of Canada
Acquisitions and Bibliographic Services
395 Wellington Street
Ottawa ON K1A 0N4
Canada

Bibliothèque nationale du Canada
Acquisitions et services bibliographiques
395, rue Wellington
Ottawa ON K1A 0N4
Canada

Your file Votre référence

Our file Notre référence

0-612-73606-7

Canada

Memorial
University of Newfoundland

This is to authorize the Dean of Graduate Studies to deposit two copies of my thesis/report entitled

High-pressure (HP), granulite-facies thrusting in a thick-skinned thrust system in the eastern Grenville Province, central Labrador

in the University Library, on the following conditions. I understand that I may choose only ONE of the Options here listed, and may not afterwards apply for any additional restriction. I further understand that the University will not grant any restriction on the publication of thesis/report abstracts.

(After reading the explanatory notes at the foot of this form, delete TWO of (a), (b) and (c), whichever are inapplicable.)

The conditions of deposit are:

(a) that two copies are to be made available to users at the discretion of their custodians,

OR

(b) that access to, and quotation from, this thesis/report is to be granted only with my written permission for a period of one year from the date on which the thesis/report, after the approval of the award of a degree, is entrusted to the care of the University, namely, _____ 19 ____, after which time the two copies are to be made available to users at the discretion of their custodians,

OR

(c) that access to, and quotation from, this thesis/report is to be granted only with my written permission for a period of _____ years from the date on which the thesis/report, after approval for the award of a degree, is entrusted to the care of the University; namely, _____, 19 ____; after which time two copies are to be made available to users at the discretion of their custodians.

Date Dec 11/2001 Signed Jason Kamis

Dean of Graduate Studies Witnessed by Maureen Moore

NOTES

1. *Restriction (b) will be granted on application, without reason given.*

   However, applications for restriction (c) must be accompanied with a detailed explanation, indicating why the restriction is thought to be necessary, and justifying the length of time requested. Restrictions required on the grounds that the thesis is being prepared for publication, or that patents are awaited, will not be permitted to exceed three years.

   Restriction (c) can be permitted only by a Committee entrusted by the University with the task of examining such applications, and will be granted only in exceptional circumstances.

2. *Thesis writers are reminded that, if they have been engaged in contractual research, they may have already agreed to restrict access to their thesis until the terms of the contract have been fulfilled.*

High-pressure (HP), granulite-facies thrusting in a thick-skinned thrust system in the eastern Grenville Province, central Labrador.

by

Jason B. Krauss

A thesis submitted to the School of Graduate Studies
in partial fulfilment of the requirements for the degree of
Master of Science

Department of Earth Sciences,
Memorial University of Newfoundland

May 2002

St. John's Newfoundland

Abstract

In the eastern Grenville Province of central Labrador, the Grenvillian Grand Lake thrust system (GLTS) comprises part of a thick-skinned thrust system separating the allochthonous and parautochthonous Grenvillian terranes. North-northwest directed thrusting on the GLTS during the Grenvillian orogeny carried the Labradorian (1710-1600 Ma) rocks of the Cape Caribou River Allochthon (CCRA) and the overlying Mealy Mountains terrane (MMT), onto a footwall composed of similar aged granitoid gneisses of the Groswater Bay and Lake Melville Terranes (GBT and LMT). The CCRA is principally composed of an AMCG suite, with the GLTS comprising a basal shear zone about 1km thick characterized by mylonite and straight gneisses developed under granulite- and upper amphibolite-facies conditions. Lithologies in the GLTS include highly strained dioritic to granitic orthogneiss (straight gneiss) comprising alternating mafic and felsic layers consisting of a mineralogy composed of garnet, clinopyroxene, amphibole, plagioclase, quartz and minor orthopyroxene which locally defines the stretching lineation. The footwall rocks of the GBT and LMT were metamorphosed under upper amphibolite facies conditions during Labradorian orogenesis.

Field studies and published U-Pb data indicate that the extent of mylonitization and recrystallization induced by thrusting along the GLTS diminish rapidly upward into the allochthon and downward into the footwall rocks. U-Pb metamorphic ages within the CCRA and footwall rocks are Labradorian (1710-1600 Ma), whereas U-Pb metamorphic ages from the recrystallized rocks of the GLTS define two Grenvillian populations at 1040 and ~1010 Ma, which are correlated with the Ottawan and Rigolet orogenies respectively.

Detailed analysis of appropriate, low variance mineral assemblages within the GLTS and adjacent footwall and hangingwall rocks was carried out to determine the *P-T* conditions of thrusting during the Grenvillian orogenesis using the TWEEQU software. Resultant *P-T* estimates associated with Grenvillian thrusting in the GLTS yield a consistent grouping of ~875 ± 50°C and 14 kbar using garnet-clinopyroxene and garnet-amphibole thermobarometry on the porphyroblastic assemblage, and 700 ± 50°C and 6-9 kbar using

garnet-amphibole thermobarometry on the matrix assemblage, consistent with textural and mineralogical evidence of decompression. On the basis of core-rim *P-T* vectors in single grains it is concluded that non-synchronous closure of the geobarometric and geothermometric reactions occurred in some samples, and thus the highest *P-T* estimates are 'apparent peak' estimates that underestimate the true peak conditions. Although unquantified, the degree of underestimation of peak conditions is considered to be small on the basis of independent petrological considerations.

Detailed petrography has revealed a wide range of fabrics elements that are related to thrusting, but a precise link between the *P-T* estimates and the available U-Pb database is not currently possible. A tentative tectonic model for this part of the Grenville orogen involves formation of a crustal-scale orogenic wedge by thrust imbrication during the Ottawan orogeny (~1040 Ma), with development of high-pressure (HP) granulites (~875 °C and ~14 kbar) at the base of the wedge. The HP granulites were uplifted up a crustal-scale ramp and exhumed during both Ottawan (~ 1040 Ma) and Rigolet times (~1010-1000 Ma). Recrystallization in the GLTS during the Rigolet orogeny took place below the closure temperature for the Fe-Mg exchange geothermometers employed and must have been principally driven by ingress of H_2O and dynamic recrystallization. It is inferred that rapid uplift, exhumation and cooling of the orogenic wedge were facilitated by normal faulting at the top of the wedge, which brought the Mealy Mountains terrane, virtually un-metamorphosed during the Grenvillian orogenesis, into tectonic contact with the CCRA with the HP granulite-facies GLTS shear zone at its base.

This study points out the importance of integration of metamorphic petrology with geochronology in tectonic studies and emphasizes the significance of deformation as a mechanism to induce recrystallization and resetting of geothermobarometers and U-Pb systematics in dry metamorphic rocks.

Acknowledgements

Thanks must be given to the following people: Toby Rivers for being so patient and helpful while writing this manuscript, Jennifer Butt - the able bodied field assistant, the Newfoundland and Labrador Department of Mines "boys" at Otter Creek, Goose Bay, for all the gear, Bill Michelin of the town of Northwest River for the use of his "tilt" on Grand Lake after a bear ate our tents. Bruce Ryan, Richard Wardle and Gerry Kilfoil at the Geological Survey of Newfoundland and Labrador for all the help and discussion regarding many aspects of the field area. Tom Krogh for helping me understand geochronology much better, and discussions with Richard Cox greatly clarified many aspects of metamorphic petrology and the pitfalls of conventional geochronology. George Jenner for his help with geochemical aspects of the Northwest River and Mealy dykes. Much thanks towards Rick Soper in the Lapidary Lab at MUN for preparing all those polished thin sections. All the faculty and staff at Memorial University of Newfoundland that I had the good fortune of meeting and working with. I must especially thank all the wonderful people of Newfoundland and Labrador for their hospitality and humour towards CFA's like myself.

Support for this research was funded by NSERC funding to Toby Rivers and Memorial University of Newfoundland.

This thesis is dedicated to Rölph Ringstad, thanks for pointing me in the right direction. We all miss you. Ja you betcha !

Table of Contents

Chapter 2 Regional Geology

Chapter 3: Field Geology of the Goose Bay region

List of Tables

List of Figures

List of Abbreviations

Symbols for rock the forming minerals, after Kretz (1983)

Ab	albite
Act	actinolite
Alm	almandine
Aln	allanite
Am	amphibole
An	anorthite
Ann	annite
Ap	apatite
Bt	biotite
Cal	calcite
Cam	Ca amphibole
Chl	chlorite
Cpx	Ca clinopyroxene
Crn	corundum
Cum	cummingtonite
Di	diopside
Dol	dolomite
En	enstatite
Ep	epidote
Fa	fayalite
Fac	ferroactinolite
Fo	forsterite
Fpa	ferropargasite
Fs	ferrosilite
Fts	ferrotschermakite
Ftr	ferrotremolite
Grs	grossular
Grt	garnet
Hbl	hornblende
Hc	hercynite
Hd	hedenbergite
Hem	hematite
Ilm	ilmenite
Jd	jadeite
Kfs	K-feldspar
Ky	kyanite
Mag	magnetite
Me	meionite
Mnz	monazite
Ms	muscovite
Ol	olivine
Omp	omphacite
Opx	orthopyroxene
Or	orthoclase
Phl	phlogopite
Pl	plagioclase
Prg	pargasite
Prp	pyrope
Qtz	quartz
Rt	rutile
Scp	scapolite
Ser	sericite
Sil	sillimanite
Spl	spinel
Srp	serpentine
Tr	tremolite
Ts	tschermakite
Ttn	titanite
Ves	vesuvianite
Zrn	zircon

Chapter 1

Introduction

1.1 Introduction to the Study

The aim of this study is to determine the metamorphic pressure-temperature (*P-T*) history and conditions of thrusting in a major granulite-facies shear zone in a thick-skinned thrust system and to investigate the linkage between the estimated *P-T* conditions and the available uranium-lead (U-Pb) ages of metamorphism determined from accessory minerals. This general problem is of interest to a range of geoscientists, (petrologists, geochronologists, structural geologists and those working in tectonics) for several reasons including; uncertainties associated with *P-T* estimates from granulite-facies rocks, the nature of the link, if any, between recrystallization and therefore resetting in geothermobarometric and geochronological systems in high-grade rocks, and the relationship of macro- and micro-scale features to crustal scale tectonics.

1.2 Thick-Skinned thrust systems

Thick-skinned thrust systems, schematically shown in Figure 1-1, represent a class of thrust system in which tectonic transport is concentrated on one or a few major thrust or shear zones and the thrust slices may be up to 10 or more km thick. In such a setting, the interiors of the thrust slices may experience very limited internal deformation, especially if critical taper of the thrust wedge is maintained (e.g., Jamieson and Beaumont 1989) whereas

the bounding shear zones are typically relatively narrow zones of high shear strain (mylonites, straight gneisses). In such thrust systems, strain partitioning is extreme and recrystallization due to penetrative deformation is mainly restricted to the shear zones which separate the thrust slices. The shear zones thus afford the most appropriate sites for sampling in order to characterize the metamorphic conditions and timing of thrusting. In the case of thick-skinned thrusting of previously metamorphosed rocks, the rocks within the cores of the thick thrust slices or horses may retain the pre-thrusting metamorphic assemblages formed during the earlier metamorphic event, whereas the shear zones typically record the conditions of the superposed thrusting event. Examples of thick-skinned thrust systems where the strain is strongly partitioned within the bounding shear zones include the European Variscan belt (Fritz et al. 1996), the Jotun thrust sheet in Norway (Milnes and Koestler 1985), and the Grand Lake thrust system in the Goose Bay region of the eastern Grenville Province (Wardle and Ryan 1996).

1.3 Recrystallization in Shear Zones

Due to the extreme strain partitioning common in some thick-skinned thrust systems, a high concentration of strain is typical in the basal mylonitic shear zones. Temperature within these shear zones varies, but where the thrust slices are thick(~10 km thick or more), elevated temperatures are common because of the combined effects of the geothermal gradient, thermal relaxation and frictional heating (Pavlis 1986; Karabinos and Ketcham 1988; Royden 1993). Under these conditions of high strain and elevated P and T, minerals within the shear zones typically undergo variably pervasive recrystallization to reduce their

chemical and textural energies to a minimum under the imposed syn-thrusting, pressure-temperature-strain (P-T-ε) conditions. The extent to which the syn-thrusting conditions are recorded in the textures and chemical compositions of the shear zone mineral assemblage is largely a function of the intensity of the recrystallization accompanying shearing as well as the degree of annealing which may take place after shearing. The microstructural and mineralogical responses to recrystallization in a shear zone are described briefly below together with a discussion of the possible effects on geothermobarometric and geochronological systems.

1.3.1 Microstructural Response

Recrystallization in high strain zones usually involves grain size reduction thereby creating subgrains with a larger surface area to volume ratio than the pre-existing grains. There are many recognized deformation mechanisms of grain size reduction in mylonites, as discussed by Hobbs et al. (1976), Schmid (1983), and Williams et al. (1994), but the overall result is that the minerals tend to change their shapes and re-orientate their crystal lattices to accommodate the imposed strain. Depending on the amount of strain and subsequent annealing, the minerals in the mylonite or shear zone may display shape preferred orientation (SPO), or under more intense strains a lattice preferred orientation (LPO). In some shear zone rocks both SPO and LPO are preserved, for instance quartz with LPO occurring as rods or stringers in ultramylonite.

1.3.2 Mineralogical Response

Pervasive recrystallization of an existing mineral assemblage in a shear zone during thrusting typically erases any chemical zoning that may have been previously present in the minerals, thereby chemically resetting the assemblage to reflect the pressure and temperature conditions of thrusting. In many cases, this process goes to completion because, as discussed above, recrystallization usually involves grain size reduction, creating subgrains with a large surface area to volume ratio, thereby increasing the efficiency of grain boundary diffusion and re-equilibration. Smaller grains are more susceptible to thermal diffusion and complete chemical re-equilibration at high temperatures than larger grains and thus are more susceptible to continued re-equilibration at temperatures lower than the peak temperature. A second possible reason for enhanced recrystallization in mylonites or shear zones is that once the surface area to volume ratio is increased, shear zones can act as conduits for any intergranular fluid present. Such fluids may exchange ions with the country rock (metasomatism), or their effects may be limited to hydration or carbonation of the peak assemblage (e.g., retrogression of clinopyroxene to amphibole and the growth of retrograde carbonates).

1.3.3 Geochronological Response

Recrystallization of U-Pb bearing accessory phases (e.g., zircon and monazite) may involve the breakdown of existing grains or growth of new grains, either as new crystals or as rims on existing grains. In addition, it may involve resetting of the U-Pb systematics within existing grains. In the case of resetting of existing grains, radiogenic lead may be

partially to completely lost by diffusion through the deformed and/or partially metamict crystal lattice. In the case of new growth (e.g., of zircon) on existing grains, the new rims will have a different U-Pb isotopic signature from that of the core. Growth of new zircon either as rims or separate crystals, requires Zr to be released during recrystallization, possibly from the recrystallization of silicate phases such as pyroxenes within the shear zone.

In each of the above cases, the chemical zoning in accessory minerals deduced from cathodoluminescence (CL) or back-scattered electron (BSE) imagery shows that after recrystallization these phases display irregular zoning patterns possibly related to: (i) fracturing due to strain or α-damage with subsequent annealing (paleometamict zones), (ii) self diffusion or resorption and (iii) metamorphic recrystallization and overgrowths (Hanchar and Miller 1993; Zhu and O'Nions 1999). If fluids are present during fracturing, they may also remove mobile and even so-called "immobile" elements (e.g., Pan and Fleet 1996), causing severe chemical changes and production of new zircon and/or resetting of the old zircon. High-grade rocks that are essentially dry will likely respond to stress through grain size reduction and Pb loss. The response of accessory minerals such as zircon and monazite to strain may also depend on their petrographic location i.e., whether they are shielded in pressure shadows or within a stronger phase such as garnet, versus a location in the matrix where grain size reduction is prevalent. The shielded U-Pb phases typically record older ages than those within the matrix (e.g., Foster et al. 2000). From the above discussion it can be deduced that shielded crystals may retain their inherited U-Pb isotopic systematics whereas

those in recrystallized zones are likely tp record different U-Pb isotopic systematics which results in chemical and age zoning in those grains.

Closure temperatures (T_c) have been empirically estimated or measured for the U-Pb system in a range of minerals (e.g.,: zircon >1000°C - Mezger and Krogstad 1997, monazite ~725°C - Parrish 1990, titanite ~ 500-600°C - Cherniak 1993, rutile ~600°C - Cherniak 2000), although the extent to which these temperatures are valid in a high-strain setting such as a mylonite or shear zones remains questionable. It appears likely that the lattice strain induced by penetrative grain-size reduction in a mylonite zone could permit U or Pb diffusion at temperatures below the T_c.

1.3.4 Implications For Geothermobarometric and Geochronological Systems

Ideally, *P-T* determinations in high grade shear zones should be established utilizing mineral assemblages which define the syn-tectonic fabrics and do not show any evidence for disequilibrium. Microstructures in high grade metamorphic mafic tectonites that may be considered syn-tectonic include: mylonitic and straight gneiss fabrics, elongate crystals of e.g., orthopyroxene parallel to the stretching direction, growth of high *P-T* minerals e.g, clinopyroxene within the pressure shadows around garnet porphyroblast and snowball garnet porphyroblasts (e.g., Passchier and Truow 1998).

Several possible difficulties with selecting grains for *P-T* determinations may arise when dealing with high grade rocks such as granulites. It is reasonable to assume that the metamorphic conditions of a granulite-facies shear zone are typically recorded at the

maximum temperatures attained in the *P-T* path since these should be high enough to permit equilibration of cations between proximal minerals. Hence such assemblages should record the *P-T* conditions of shearing. However, there are commonly practical difficulties in obtaining these peak *P-T* (e.g., *P* at peak *T*) conditions which include the following: (i) Post peak resetting of the geothermometer and the geobarometer independently of each other. Typically the thermometer will tend to reset rather more readily than the barometer due to the relatively rapid rates of diffusion of similarly sized and charged cations used in exchange geothermobarometry compared to the more complex net transfer of ions and restructuring of mineral phases characteristic of most geobarometers. Furthermore, at the peak *P-T* conditions on a 'clockwise' *P-T* path, the pressure typically changes faster than the temperature thus preferentially slowing the rate of the net transfer reaction, whereas cation diffusion may continue for some time despite the "closure" of the barometer. In such cases, the intersection between the thermometer and barometer will provide a spurious *P-T* point which does not lie on the *P-T* path followed by the rock; (ii) Other possible problems involve resetting both of the geothermometer and geobarometer equally, yielding a *P-T* point on the *P-T* path that does not reflect the maximum T attained; and (iii) complete overprinting of the high-temperature assemblage during a post-peak lower grade metamorphic event which would also lead to unreasonable peak *P-T* estimates. These effects are schematically presented in Figure 1-2 where examples of i, ii and iii are shown on an idealized *P-T* path due to crustal thickening.

Figure 1-3 schematically shows the effects of recrystallization on zircons in a sample that has undergone variable degrees of strain and metamorphism. Zircon that did not undergo strain-induced recrystallization during thrusting or experienced only low temperatures during thrusting would not exhibit significant resetting of its U-Pb systematics and would thus lie on or near concordia for the pre-thrusting event (Figure 1-3a). In contrast, the U-Pb system in a zircon that has undergone intense strain and/or a high temperature thermal event might principally record the younger high-*T* /high strain event and the U-Pb system would be largely reset to the age of the high strain episode (Figure 1-3b). In between these extremes, partial Pb loss and/or growth of new rims on existing cores may result in partial resetting of the U-Pb systematics (Figure 1-3c), so that the analyses lie along a cord which joins the two intercepts, with the upper intercept being the age of intrusion for example, and the lower intercept being the age due to shearing.

1.4 Methodology

Investigation into crustal-scale thrusting in a shear zone and its adjacent footwall and hangingwall rocks begins with the discrimination of the syn-tectonic fabrics in the shear zone and the pre-tectonic fabrics present within the footwall and hangingwall rocks. Once the fabrics and mineralogy are identified, petrogenetic grids are used to constrain the possible *P-T* conditions that the assemblages records and suitable samples with equilibrium textures can be selected for the application of geothermobarometry to check against the petrogenetic grids. The electron microprobe is then used to establish coexisting mineral compositions and evaluate zoning, which provides constraints on the reaction history and allows the evaluation

of compositions that can be assumed to represent equilibrium. Such compositions can then be used for the application of geothermobarometry. Domainal equilibrium, in which parts of the rocks may not be fully recrystallized or did not reach chemical equilibrium during deformation whereas other parts did, is not uncommon. Once equilibrium fabrics and zoning profiles are established, analysis points inferred to represent equilibrium conditions are selected and *P-T* estimates for rocks from the shear zone, footwall and hangingwall may be obtained using geothermobarometry. However care must be taken to ensure that the *P-T* data are reliable and represent conditions on the *P-T* path. Methods have been proposed to obtain the peak metamorphic conditions of granulite facies rocks despite post peak cation diffusion, as schematically shown in Figure 1-2b. These methods are discussed by Bégin and Pattison (1994) who utilized a thermobarometer involving aluminium solubility, and Fitzsimons and Harley (1994) who discussed a correction factor applied to the Fe-Mg exchange thermometer. Frost and Chacko (1989) deescribed a different method which utilizes relict assemblages or "fossil thermometers" to obtain peak *P-T* conditions of granulite facies rocks.

Once the *P-T* estimates have been obtained it is essential to check if they are geologically reasonable. Mengel and Rivers (1991) have discussed the comparison and reactions inferred from petrogenetic grids with *P-T* estimates obtained from the same rocks. A similar methodology is applied in this study to estimate the *P-T* conditions of thrusting.

Special attention is paid to the microstructural setting of any U-Pb accessory phases present in the samples used for geothermobarometry. The samples were taken from as close as possible to the outcrops that were previously sampled for the U-Pb study so that the U-Pb

ages from the shear zone rocks may be correlated to specific textures and *P-T* conditions. However, in many cases, the accessory phases analysed for U-Pb ages were not characterized on the basis of their locations with respect to the shear zone or their petrographic setting but rather on their crystal quality e.g., clear gem-quality grains with specific morphologies which were interpreted as either metamorphic or igneous in origin. Furthermore, many of the zircon grains were not characterized with respect to their internal structures, such as chemical zoning, lattice defects, zones of annealing (paleometamict zones) etc. using CL, BSE, HF-etching and a basic petrographic microscope (Philippe et al. 1993 and Bussy et al. 1995). Thus these analyses are difficult to interpret with confidence even though the ages may be concordant and very precise. However, the accessory phases in several of these cases yielded mixed age results, reflecting partial recrystallization and/or analysis of a mixed population of partially reset older grains with or without rims and new grains. Linkage between textures, estimated *P-T* conditions and the U-Pb ages thus becomes more difficult to establish when fabrics, textures and mineralogies are not fully understood. Based on the fact that the U-Pb minerals were not discussed relative to textural setting in the published U-Pb studies from the field area, only a tentative linkage to the U-Pb ages can be made. Integrated studies including *in situ* dating methods are required to make direct links between fabrics, *P-T* conditions and U-Pb ages in these types of settings.

For the study at hand, *P-T* determinations are established in a field area where a crustal-scale, high-temperature shear zone is exposed. Particular attention is also paid to the textural development and setting of major minerals to determine if the texture of the rock can

be utilized as an indicator of the degree of U-Pb resetting. In order to carry out an evaluation of the role of strain on recrystallization, a starting point is a shear zone with two populations of metamorphic ages indicating variable resetting or growth of the U-Pb geochronometers (zircon, monazite titanite) during displacement in the shear zone. A shear zone with these properties occurs in the Grenville Province of central Labrador and is known as the Grand Lake thrust system.

1.5 Grand Lake Thrust System

The Grand Lake thrust system (GLTS), inferred to be part of a thick-skinned thrust system, provides an excellent site for a case study as the shear zone shows evidence for high-temperature deformation, in the form of syn-tectonic stable orthopyroxene crystals stretched parallel to the transport direction (Ryan et al. 1982, Wardle and Ash 1984), and there is a considerable database of U-Pb metamorphic ages already established. The approximately1 km thick Grenvillian shear zone is well exposed along the shores of Grand Lake. The footwall and hangingwall rocks typically preserve Labradorian (1710-1600 Ma) ages, whereas in proximity to and within the shear zone the rocks tend to yield Grenvillian ages (Philippe et al., 1993, Bussy et al., 1995). Moreover, the presence of monocyclic diabase dykes, the Northwest River dykes, in the hangingwall rocks enables accurate discrimination of the effects of Grenvillian deformation and metamorphism in the vicinity of the Grand lake thrust system.

The age of thrusting on the GLTS is well constrained, however no *P-T* conditions

have been obtained. The metamorphic grade is however, has been assumed to be granulite facies on the basis of the presence of orthopyroxene within mylonitic rocks of the GLTS (e.g., Ryan et al 1982; Wardle and Ash 1984). This study focusses primarily on the application of geothermobarometry and obtaining reliable peak P-T estimates for shearing in the GLTS in order to characterize the metamorphic history of the GLTS. These results are integrated with the published U-Pb dates.

1.5.1 Previous Work

The first systematic mapping of bedrock geology in the Goose Bay region at 1: 250,000 scale by Stevenson (1969) for the Geological Survey of Canada (GSC). Re-mapping at 1:100,00 and 1:50,000 scales by the Department of Mines and Energy (now the Geological Survey) of the Government of Newfoundland and Labrador was carried out by Ryan et al. (1982) and Wardle and Ash (1984 and 1986). Ryan et al. (1982) were the first to recognize the major shear zone demarcating the base of the Cape Caribou River thrust sheet, which was subsequently named the Cape Caribou River Allochthon. Further studies in the Goose Bay area include U-Pb sampling performed by Krogh (1986), Krogh and Heaman (1988), Philippe et al. (1993), Bussy et al. (1995), and detailed mapping and U-Pb work by Corrigan et al. (1997).

The most recent petrographic study on the shear zone was done by Best (1997), who petrographically characterized a small suite of samples from the Goose Bay area and attempted geothermobarometry on two samples, specifically from the footwall and within the shear zone. Results from that study suggested that temperatures ranged from 720 to

840°C with pressure estimates in the range of 12-14 kbar. These preliminary *P-T* results are in accord with granulite-facies conditions during thrusting along the GLTS.

1.5.2 Approach and Techniques

1.5.2.1 Sampling

For this study, two months in 1999 were spent mapping and sampling, utilizing the compiled map of Wardle et al. (1990a). The map was used in the field as a guide to choosing the best localities for sampling rocks from the shear zone and immediate footwall and hangingwall rocks. 196 field stations were established, and samples were collected for mineral assemblages, textures, structural (micro- and macro-) features, with the aim of establishing *P-T* conditions of thrusting. Samples were collected from most of the different lithological and structural units in the field area including: shear zone mylonites, footwall ortho and paragneiss, mafic dykes, ultramafic boudins and samples from different levels in the thrust stack.

1.5.2.2 Petrography and Petrology

The main thrust of the study is to characterize the petrography of the samples collected in the field for mineralogical assemblages, fabrics and various textures preserved in the rocks and to use this information to build a thermobarometric study. Laboratory work was conducted at Department of Earth Sciences at Memorial University of Newfoundland. Petrography was conducted on an Olympus petrographic microscope. Special attention was paid to metamorphic textures, especially equilibrium textures which might be appropriate for thermobarometry. Mineral compositions used in geothermobarometric calculations were

obtained using a Cameca SX-50 Microprobe with a LINK ED detector. Details of the operating conditions and standards used are given in Appendix C. *P-T* estimates were obtained using the thermodynamic data base of TWEEQU (Berman, 1991) and details of the method are given in Chapter 7. Whole rock X-Ray Fluorescence analyses of the diabase dykes were obtained using the ARL XRF at MUN. Details of the analytical procedure are given in Chapter 5.

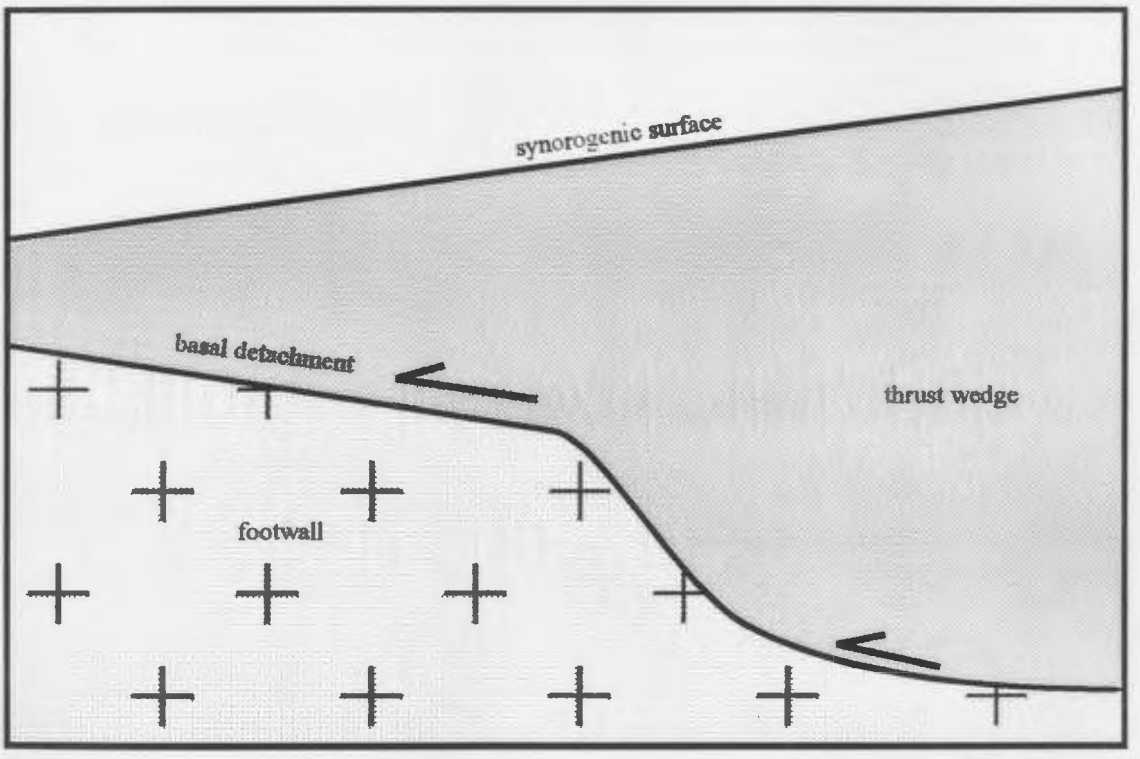

***Figure 1-1**: Schematic tectonic model displaying a thrust wedge with ramp and flat geometry.*

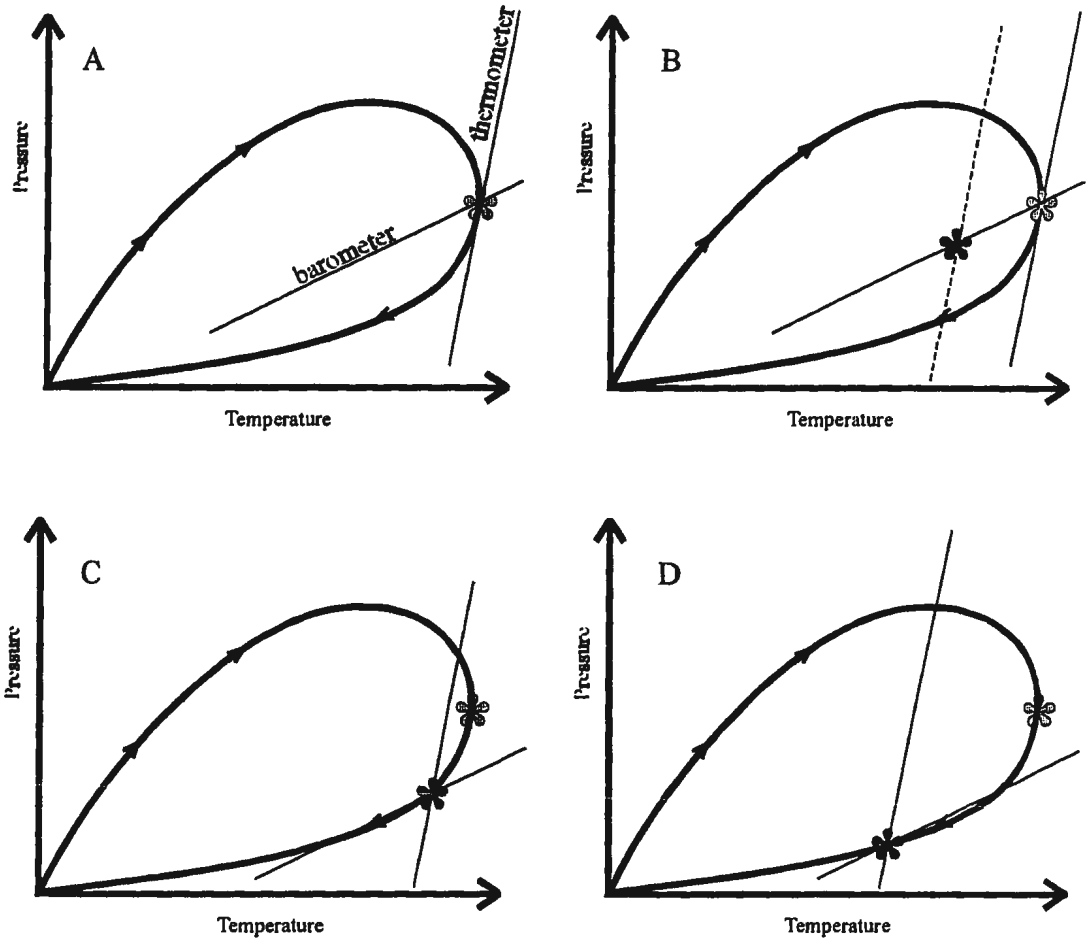

***Figure 1-2**: Idealized pressure-temperature (P-T) path displaying resetting of the thermometer and barometer of a high grade rock. (a) The peak T conditions that are ideally recorded by geothermobarometry. (b) The P-T estimate obtained from a rock in which the thermometer has continued to re-equilibrate thermally post the thermal peak of metamorphism (note the position of the barometer has not changed from the peak P). (c) The P-T point recorded assuming that both the thermometer and barometer continue to reset post peak T. (d) The P-T point recorded assuming that the composition of the minerals used in the thermometer and barometer continued to reset during retrogression along the P-T path.*

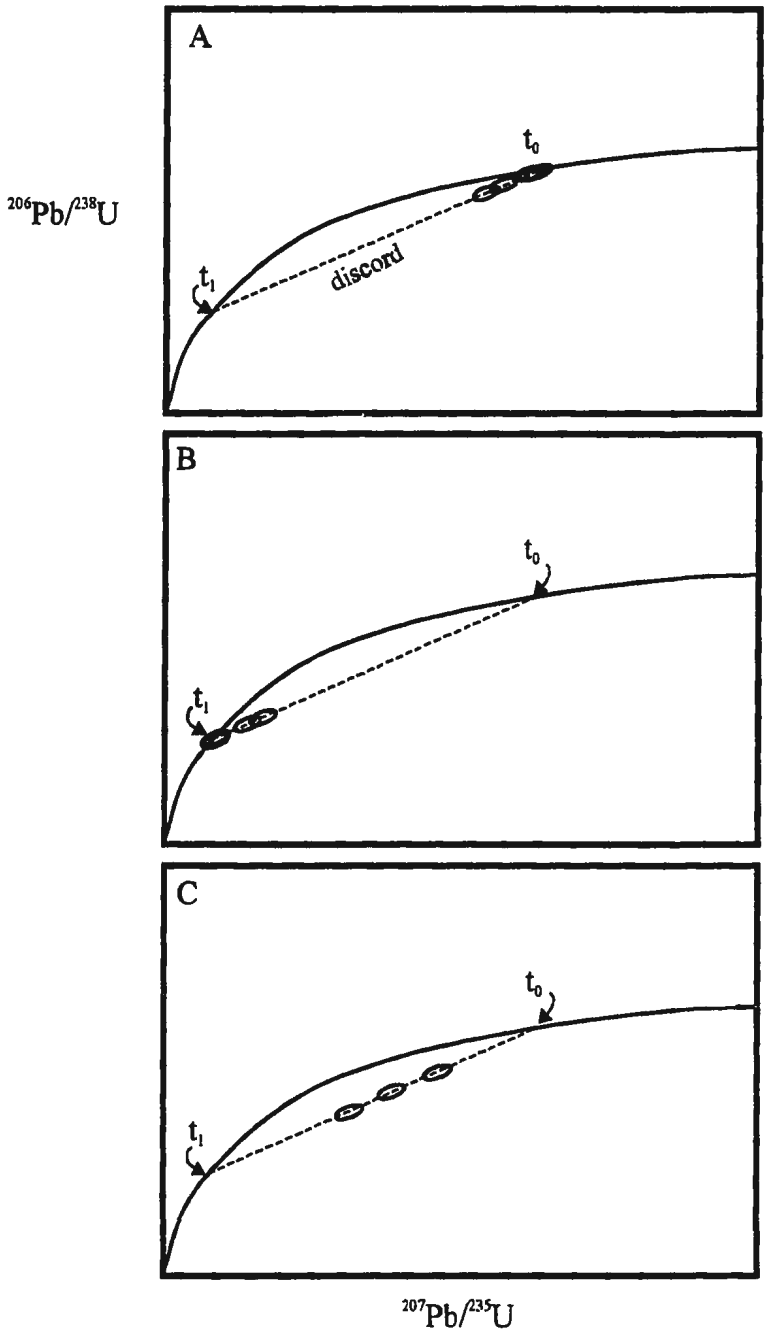

***Figure 1-3**: Schematic concordia diagrams displaying variable degrees of lead loss due to strain induced recrystallization or high grade metamorphism and new zircon growth. Figure (A) is the expected concordia plot for a rock that experienced no strain after intrusion. t_0 is the crystallization age for the magma and t_1 is the time of thrusting. (B) is the expected configuration for a rock which was completely recrystallized during a high-strain event at t_1. (C) is the expected configuration for a rock that experience partial lead loss through incomplete recrystallization of the U-Pb systematics and/or new growth as rims on old zircons during the event at t_1.*

Chapter 2

Regional Geology

2.1 Introduction

In order to provide a context for the geological setting of the Grand Lake thrust system, it is appropriate to review the geological history of the eastern Grenville Province. The pre-Grenvillian history is relevant to understanding the subsequent Grenvillian history because the Grenvillian orogenesis in Labrador mainly involved reworking of older Paleoproterozoic crust. Juvenile crustal additions immediately pre-dating the Grenvillian reworking constitute only a minor component of the orogen (e.g., Rivers et al. 1989, Gower 1996, Rivers 1997). Figure 2-1 shows the Grenvillian lithotectonic elements of the eastern Grenville Province. Figure 2-2 displays the area of interest at a larger scale and identifies the principal lithotectonic elements discussed in this chapter. The majority of these are composed of the Paleoproterozoic crust that formed in the interval ~1710-1600 Ma.

Terminology: the term 'terrane' as used in the literature of the Grenville Province and this study, does not imply connotations of an exotic origin. It is used in the sense of a fault or shear-zone bound area of metamorphic rocks that experienced a significantly different Grenvillian metamorphic history than adjacent terranes.

2.2 Late Paleoproterozoic Crustal Evolution

The late Paleoproterozoic (~1710-1600 Ma) was a period during which large volumes

of juvenile crust were formed on and/or subsequently accreted to the southeastern margin of Laurentia (Gower et al. 1992, Gower 1996). The period may be subdivided into an island arc and rifted backarc episode, a collisional orogenic event and a protracted period of post-tectonic magmatism that together span ~110 million years (Gower 1996). Figure 2-3, which schematically shows the current tectonic model for the late Paleoproterozoic crustal evolution of the Labrador orogen on the southeastern Laurentian margin, serves as a basis for the following discussion.

2.2.1 Backarc and Arc setting

Following the Makkovik-Penokean Orogeny on the southeastern margin of Laurentia at ~1900-1700 Ma (Culshaw et al. 2000), there was a tectonically quiescent period during which the protoliths of widespread metasedimentary gneisses were deposited in the area that subsequently became incorporated into the Labrador orogen of eastern Labrador. These metasediments, principally pelitic to semi-pelitic in composition with minor carbonate and quartzite layers and lenses, are inferred to have formed in a small ocean or backarc basin (Gower 1996). Figure 2-3a schematically displays the inferred configuration of the backarc basin during the period ~1710-1680 Ma. The source of the sediment is not well constrained, but available U-Pb ages of detrital zircons obtained from the metasedimentary gneisses show that the principal source was not the Archean craton of Laurentia, but rather juvenile Paleoproterozoic rocks from a coeval arc (Gower et al. 1992, Gower 1996). For instance, Krogh et al. (1996) documented the occurrence of xenocrystic zircons with ages at 2606, 1902, 1894 and 1746 Ma in supracrustal rocks of possible igneous origin. Rare magamtic

ages of 1734 and 1725 Ma associated with the ~1660 Ma juvenile arc rocks (Krogh et al. 1996) imply that the arc-related terranes also contain some older igneous rocks and sediments that possibly formed in a backarc basin environment, as schematically shown in Figure 2-3a. However, the extent of contributions from these and other sources has not been thoroughly evaluated.

2.2.2 The Labradorian Orogeny

Following sedimentation, the small ocean or backarc basin closed and a period of widespread magmatism and deformation ensued (Labradorian Orogeny, ~1680-1660 Ma). Penetrative deformation and imbrication of the juvenile Labradorian crust occurred during this time under metamorphic conditions ranging from greenschist to granulite facies. It is inferred that it was during this time interval that the Labradorian arc was accreted to the Laurentian margin (Rivers 1997) as shown in Figure 2-3b. Gower et al. (1992) and Gower (1996) have subdivided the magmatic events into three main episodes, namely: ~1677 Ma, ~1671 Ma and 1658-1649 Ma. The two older ages correspond mainly to calc-alkaline plutonism, which is inferred to have occurred above a north-dipping subduction zone under an island arc off the Laurentian margin (Figure 2-3 a and 2-3b; Gower et al. 1992, Connelly et al. 1995, Gower 1996). Examples of intrusive rocks of these ages include: the Susan River quartz diorite, 1672 +11/-10 Ma (Philippe et al. 1993); the Red Island hornblende-quartz diorite, 1671 ± 4 Ma; Sebaskatchu gneissic tonalite, 1677 +18/-11 Ma; Neveisik Island granodiorite, 1678 ± 6 Ma; and a banded migmatitic gneiss from the Mealy Mountains terrane with an inferred intrusive age of 1677 +16/-15 Ma (Schärer et al. 1986). Generally

the age of this calc-alkaline magmatism is older in the south and becomes younger towards the Trans-Labrador Batholith (TLB), which has been dated at ~1650 Ma (Gower 1996).

Other ages of magmatism such as 1664+14/-9 Ma and 1644+8/-6 Ma are reported by Scott et al. (1993) from within the LMT in the Gilbert River Belt on the east coast of Labrador. The ca. 1664 Ma age comes from a deformed rock that is interpreted to have undergone deformation during the Labradorian Orogeny (1680-1660 Ma) as the sample comes from a ductilely deformed granitic dyke that crosscuts amphibolite-facies mylonitic fabrics (Scott et al. 1993).

2.2.3 Trans-Labrador Batholith

The Trans-Labrador Batholith is a large, ~800 km long and 40 km wide, calc-alkaline batholith (Wardle et al. 1986) which intruded approximately along the present level of exposure of the suture between the Labradorian arc and Laurentian crust. The batholith lacks evidence of deformation related to the Labradorian Orogeny and is thus considered to post-Labradorian. Field evidence shows that the northern part of the batholith was emplaced into Laurentia (Wardle et al. 1986). The southern margin, in contrast, is strongly tectonized by thrusting inferred to have taken place during the Grenvillian Orogeny. Most models for the formation of the extensive batholith involve an Andean-style magmatic arc over a north-dipping subduction zone underneath the Laurentian margin (Figure 2-3c; Gower et al. 1992, Connelly et al. 1995, Gower 1996). The age of emplacement of the batholith and coeval felsic volcanic sequences (e.g., ca. 1652 Ma Blueberry Lake Group, James and Connelly 1995; 1649 ± 1 Ma Bruce River Group, Schärer et al. 1988) is consistent across its length at

~1650 ± 5 Ma (Wardle et al. 1986). This short-lived magmatic event is correlated with a short period of subduction of the backarc region as shown in Figure 2-3b and 2-3c.

2.2.4 Late Post-Labradorian Events

Following suturing of the Labradorian terranes to Laurentia and the emplacement of the TLB, post-tectonic magmatism, possibly in a backarc setting, included emplacement of anorthosite-mangerite-charnockite-granite (AMCG) suites such as the Mealy Mountains Intrusive Suite (1635 Ma, Emslie and Hunt 1990) and its northern component known as the Northwest River Anorthosite and the Dome Mountain suite (~1625 Ma, ~1631 Ma, Bussy et al. 1995; see Figure 2-3d). Granitoid plutons such as the 1632 +10/-9 Ma (Schärer et al. 1986) Double Mer granite in the Groswater Bay terrane were also emplaced within this time interval. In addition, Connelly et al. (1995) documented a late Labradorian partial melting event around 1636 Ma preserved in the Lac Joseph terrane (LJT), and Wardle et al. (1990a) have also documented late Labradorian deformation and metamorphism in the Goose Bay region at ~1620 Ma (1622 ± 6, Krogh and Heaman 1988; 1613 ± 40, Krogh 1986). Late Labradorian metamorphism and deformation have also been documented further east in the Rigolet area of the Lake Melville terrane (see formation of the precursor to the Rigolet thrust in Figure 2-3e) at 1619 +16/-14 Ma and 1610 ± 4 Ma (Corrigan et al. 2000). It appears that after about 1610 Ma the newly accreted Labradorian terranes stabilized, forming the southern extension of the Laurentian craton.

2.3 Mesoproterozoic Crustal Evolution

2.3.1 Early Mesoproterozoic Crustal Additions

The period immediately following the late Paleoproterozoic was one of relative magmatic quiescence for the whole of southeast Laurentia, as deduced from the lack of protolith ages between 1600-1530 Ma (Gower 1996). This quiescent period ended with the onset of voluminous magmatism and metamorphism associated with the Pinwarian Orogeny (~1530-1450 Ma). The magmatism is best characterized by the extensive granitoid plutonism in the Pinware terrane in southeast Labrador (see Figure 2-2, Gower 1996). The plutons are inferred to have been formed over a northward-dipping subduction zone that developed under a continental-magmatic arc under the Laurentian margin (Tucker and Gower 1994). U-Pb ages of intrusion for magmatic rocks within the Pinware terrane range from 1490 ± 7 to 1472 ± 3 Ma (Tucker and Gower 1994), and recently, magmatism of similar age has been shown to occur in the northern LMT, e.g., the Rigolet diorite, 1489 +2/-8 Ma, and the Wolfrey granite, 1474 +10/-7 Ma (Corrigan et al. 2000).

U-Pb ages for metamorphism associated with the Pinwarian Orogeny are limited in the eastern Grenville Province. Low grade metamorphism and imbrication of supracrustal and granitoid rocks of the eastern Wakeham group occurred at 1515 ± 30 Ma (T. Rivers, oral communication 2001) which supersedes previous estimations of the closure of the eastern Wakeham basin. Other metamorphic ages come from the Hart Jaune terrane (1469 ± 5 Ma, Scott and Hynes 1994), the Wakeham Supergroup (1495 ± 2 Ma, Clark and Machado 1994) and the Mealy Mountains terrane, where Krogh et al. (1996) dated tips of zircon from pegmatitic material in a boudin neck of a dyke that yielded ages of 1488 and 1491 Ma.

2.3.2 Middle Mesoproterozoic Crustal Additions

Near the end of the Pinwarian orogenesis (~1470 Ma), Gower and Tucker (1994) inferred that rifting, possibly in a backarc setting (Rivers 1997, Rivers and Corrigan 2000), led to a tensional tectonic environment within what is now the eastern Grenville Province and its northern foreland, which permitted the intrusion of a major mafic dyke swarm, known as the Shabogamo gabbro in western Labrador and Michael gabbro in eastern Labrador (Gower et al. 1990). The emplacement age of the Shabogamo and Michael gabbros is not well constrained, but is estimated to be between 1472-1426 Ma (Schärer et al. 1986,Connelly et al. 1995, Corrigan et al. 2000). The Shabogamo gabbro is confined to the Molson Lake and Gagnon terranes and the Michael Gabbro is similarly confined principally to the Groswater Bay terrane and the TLB, although a recent study by Corrigan et al. (2000) in the Rigolet area has also discovered its presence in the northern Lake Melville terrane.

Other Middle Mesoproterozoic magmatic activity of local importance to the Goose Bay area includes the small Arrowhead Lake mafic intrusion (Rb/Sr age of1307 ± 26 Ma, Fryer 1983) in the Groswater Bay terrane and the Upper North River syenite/granite in the Lake Melville terrane dated at 1296 +13/-12 Ma (Schärer et al. 1986).

2.3.3 Late-Middle Mesoproterozoic Crustal Additions

The olivine tholeiitic Mealy dykes intruded the Mealy Mountains terrane at 1250 ± 2 Ma (Hamilton and Emslie 1997). The Mealy dykes cross-cut all fabrics in their host rocks and were not affected by any other thermal or tectonic events until the onset of the Grenvillian orogenesis (see below). This dyke swarm, similar in age to the Sudbury dyke swarm in the western Grenville Province, and the Seal Lake sills in the northern part of the

Grenville Province of Labrador, is inferred to have intruded during upper crustal extension in a continental backarc setting (Rivers 1997, Rivers and Corrigan 2000).

In the Wakeham Supergroup, Martignole et al. (1994) documented granitoid magmatism during the interval of 1245-1239 ± 3Ma followed by emplacement of gabbros at ~1177 Ma. Deformation and coeval greenschist facies metamorphism are inferred to have occurred between the two magmatic events (Martignole et al. 1994). The Elzevirian orogeny 1230-1190 Ma (Gower 1996) followed this extensional event but its effects are localized in Labrador and they are not recognized in central Labrador. Much of the Laurentian crust in Labrador was subsequently stable until the onset of Grenvillian orogenesis.

2.4 Grenvillian Orogenesis

The onset of the Grenvillian orogenesis (~1190-980 Ma), as first proposed by Corrigan and Hanmer (1995), is interpreted from the change in the character of magmatism at ~1190 Ma. In the western Grenvill Province, calc-alkaline magmatism associated with the Elzevirian backarc gave way to A-type magmatism after 1190 Ma, which invlovled intrusion of voluminous AMCG suites after the closure of the back arc (Corrigan and Hanmer 1995). The Grenvillian orogenesis is characterized by extensive crustal thickening as a result of imbrication of large thrust slices and telescoping of the Laurentian margin (Rivers 1997). It involved at least three periods of northwest-directed crustal-scale thrusting and high-grade metamorphism, namely the Shawinigan orogeny at ~1190-1140 Ma, the Ottawan orogeny at ~1120-1020 Ma and the Rigolet orogeny at ~1010-980 Ma (Rivers 1997).

Deformation and metamorphism associated with each of the three orogenies is

unevenly distributed across the Grenville Province (Rivers 1997, Rivers et al. 2001). For instance the Shawinigan orogeny is well documented in western Grenville Province, whereas in the east, evidence for this orogeny is rare. On the basis of available evidence, the Ottawan orogeny was the most widespread of the three Grenvillian orogenies. It is characterized by thick-skinned thrusting and a coeval medium-pressure metamorphism throughout much of the Grenville Province, and a high-pressure belt in the northwestern part of the Grenville Province has recently been recognized (Rivers 1997;Rivers et al. 2002 in press). The Rigolet orogeny principally involved crustal thickening and associated metamorphism near the leading NW of the orogen (the Grenville Front) as the orogen advanced onto its foreland. In addition, it also locally involved reworking of shear zones first formed during the Ottawan orogeny in the interior of the orogen.

Subsequent to the several episodes of Grenvillian crustal thickening, orogenic collapse of the tectonically overthickened crust occurred by extensional faulting throughout much of the orogen (Rivers 1997), although no extensional shear zones have been mapped in central and eastern Labrador at the time of writing.

2.4.1 Grenvillian Lithotectonic Units of Eastern Labrador

The present day configuration of the lithotectonic units of the Grenville Province was assembled during the Grenvillian orogenesis. It was during this interval that the rocks of the Groswater Bay, Lake Melville and Mealy Mountains terranes (Figure 2-2) were variably reworked and the tectonic boundaries were established between them. The Grenvillian Parautochthonous belt (Figure 2-1) in the field area is composed of the Groswater Bay

terrane and the Grenvillian Allochthonous belt is made up of the Lake Melville and Mealy Mountains terranes, together with the Cape Caribou River Allochthon (Rivers et al. 1989)

2.4.1.1 Groswater Bay Terrane

The Groswater Bay terrane (GBT; Figure 2-2) is mainly composed of calc-alkaline migmatitic orthogneisses of granodioritic composition with subordinate inclusions of mafic-ultramafic pods that are cut by disrupted dykes of the Michael gabbro (Gower and Owen 1984). The rocks of the GBT are tectonically overridden by the Lake Melville and Wilson Lake terranes to the east and the west of the Goose Bay area respectively, and extend to the coast of Labrador in the east. The Trans-Labrador Batholith bounds the GBT to the north where the contact is ill-defined and may be either intrusive or tectonic (Gower 1996). The calc-alkaline orthogneisses ,which yield intrusive ages of 1671 ± 4 Ma and 1677 +18/-11 Ma (Schärer et al. 1986), were first deformed and metamorphosed to amphibolite facies during the Labradorian Orogeny ~1660 Ma (Gower 1996). Subsequent Grenvillian metamorphism and deformation, documented by widespread U-Pb titanite cooling ages at 990-970 Ma (e.g. Schärer et al. 1986), is associated with metamorphism in the GBT which varies from greenschist facies in the north to granulite facies in the south (Gower 1986). The Michael Gabbro best documents this change with individual dykes being recrystallized in the south but largely unaltered in the north of the GBT. Thrusts in the north of the GBT were much steeper dipping than those farther south (Gower 1986), with those in the south being accompanied by recumbent folding. The timing of Grenvillian high-grade metamorphism is not yet known as there are no zircon or monazite ages available from high grade assemblages.

2.4.1.2 Lake Melville Terrane

The Lake Melville terrane (LMT; Figure 2-2) is predominantly made up of migmatitic granodiorite to monzodiorite orthogneisses. The rocks of the LMT are similar to those in the GBT, but the LMT contains more supracrustal material and a greater amount of alkali feldspar megacrystic granitoids than the GBT (Gower 1996). Layered mafic intrusions are also a key feature of the LMT that appear to be more prominent along the northern edge of the terrane (Gower 1996). The age of intrusion determined from zircon from a granodiorite on Neveisik Island (in Lake Melville east) yields an upper intercept of 1678 ± 6 Ma and another sample from southeast LMT gives an age of 1677 +16/-15 (Schärer et al., 1986) indicating the Labradorian origin of these rocks.

Grenvillian deformation and metamorphism between in the LMT took place between1088 and 1013 Ma and involved a high-grade metamorphic event at ~1050 Ma (Mnz) that has been documented by Corrigan et al. (2000). Thrusting took place along the the Rigolet thrust at this time (Mnz age of 1047 ± 4 Ma Corrigan et al. 2000) reactivating the late-Labradorian shear zone that separates the LMT and the underlying GBT. The NE-SW, belt parallel structural grain of the northern LMT is defined by folds with oncreasingly tight hinge zones reflecting higher strain and a higher the metamorphic grade towards the leading edge of the terrane, where granulite-facies mineral assemblages form the mylonitic fabric in the Rigolet thrust zone (Corrigan et al. 2000).

2.4.1.3 Mealy Mountains Terrane and Cape Caribou River Allochthon

The northern part of the Mealy Mountains terrane (MMT) is dominated by the Mealy

Mountains Intrusive Suite (MMIS), an anorthosite-mangerite-charnockite-granite (AMCG) suite consisting of anorthosite, leucogabbroic, leucotroctolitic rocks and associated pyroxene-bearing granitoids (Emslie, 1976) that intrudes metasedimentary gneisses, orthogneisses and granitoid plutons. The rocks of the MMT are host to the 1250 ± 2 Ma (Hamilton and Emslie 1997) Mealy dykes. The MMT is bounded on its eastern flank by the Gilbert River Belt of the LMT. To the north much of the MMT is covered by drift and sediments associated with the Lake Melville Rift System and the contact with the Cape Caribou River Allochthon is unexposed.

Emslie and Hunt (1990) obtained emplacement ages for the MMIS at 1646 ± 2 Ma and 1635 +22/-8 Ma from pyroxene granitoids associated with the suite. Krogh et al. (1996) obtained ages from three samples of the host gneisses from the MMT. Two of the gneiss samples yielded possible igneous protolith ages of 1726, 1711 Ma, and the third sample yielded an array of slightly discordant single zircon ages of 2602, 1902, 1894, 1746 and 1717 Ma, all of which are interpreted to represent inherited ages from a mixed igneous-supracrustal sourece. The same gneiss sample also contains concordant metamorphic monazite at 1655 Ma. Another sample from a quartz monzonite within the MMT yielded intrusive ages at 1734 and 1725 Ma (Krogh et al. 1996). It is inferred from the above data that there was most likely a magmatic event ca. 1730 and a sediment source from the Superior, Churchill and Makkovik Provinces that supplied the detrital zircon which is now present as xenocrysts in the gneisses (e.g. Gower 1996).

Grenvillian deformation and metamorphism of the MMT is very minor (Gower

1996), and much of the MMT appears to have escaped Grenvillian reworking with only minor thermal disturbances recorded in the K-Ar and Ar-Ar systematics in the Mealy dykes (Reynolds 1989). In contrast, there is abundant evidence for northwest-directed thrusting of the Cape Caribou River Allochthon (CCRA) along the Grand Lake thrust system (GLTS; see below).

2.5 Lake Melville rift system

Following the uplift and erosion of the Grenville Orogen, Neoproterozoic rifting led to the formation of the Lake Melville graben system and other grabens and half grabens in central and eastern Labrador (Gower 1986). Late Neoproterozoic (ca. ~615 Ma; Bdl age from the Long range dykes, Kamo et al. 1989) clastic sediments known as the Double Mer Formation fill in the grabens and half grabens (Gower 1986). Uplift structures are preserved in the Grenvillian basement as brittle deformation features, such as brittle faults and shear zones with greenschist-facies mineralogy and slickensides.

2.6 Lithotectonic Elements of the Goose Bay Region

The study area, located in central Labrador approximately 100 km south of the Grenville Front at the western end of Lake Melville (Figure 2-2), encompasses rocks of the Cape Caribou River Allochthon (CCRA), the Groswater Bay terrane (GBT), the Lake Melville terrane (LMT), and the Neoproterozoic Lake Melville Rift System. The major Grenvillian tectonic boundaries in the area include the Grand Lake thrust system and the Rigolet thrust which is a part of the Allochthon Boundary Thrust (ABT) system (Rivers et

al. 1989). Figure 2-4 is a geological map of the field area with available U-Pb ages of metamorphism, magmatism and deformation. Field descriptions of these units are discussed in the following chapter.

2.6.1 Groswater Bay terrane

In the Goose Bay area, two main elements comprising the GBT include; 1) granodiorite gneisses containing rafts of kyanite-bearing metasediments and minor mafic-ultramafic pods, and 2) the Susan River quartz diorite. These two units were emplaced before or during the Labradorian Orogeny. For instance, much of the gneissic fabric in rocks of the GBT in the study area was developed during the Labradorian Orogeny as documented by migmatitic orthogneiss yielding metamorphic zircon ages of 1659 ± 8 Ma and a poorly constrained upper intercept at 1656 +74/-69 Ma (Mnz) for the paragneiss (Philippe et al. 1993). The mafic-ultramafic pods included in the gneisses have not been directly dated but are inferred to be part of the juvenile arc rocks which were incorporated during the Labradorian Orogeny. The Susan River quartz diorite (SRQD) was emplaced at 1672 +11/-10 Ma (Zrn; Philippe et al. 1993) comparable to the age of the granodiorite gneisses elsewhere in the GBT (ca. 1671).

Grenvillian reworking of the GBT took place during both the Ottawan and Rigolet orogenies as a result of thrusting of the CCRA over the GBT. Evidence for Ottawan metamorphism in the GBT is based on the U-Pb 1038 ± 2 Ma monazite age from the GLTS (Philippe et al. 1993). However, Rigolet ages are more common in the GBT for example, paragneiss in the vicinity of the GLTS has yielded monazite U-Pb ages of1005 ± 2 Ma and

metamorphism is documented by the growth of titanite at ca. 990 Ma (Philippe et al. 1993). Schärer et al. (1986) have also noted the apparent lack of penetrative Ottawan metamorphism elsewhere in the GBT. The extent of Grenvillian deformation and metamorphism appears to be concentrated in the GLTS with minor thermal disturbances away from major shear zones in the terrane.

The volumetrically small Arrowhead Lake intrusion, in the western part of the field area, emplaced at 1307 ± 28 Ma (Fryer 1983), was characterized by Ryan et al. (1982) as a two pyroxene bearing gabbro, with coronas of garnet surrounding pyroxenes, the latter presumably being a Grenvillian feature. The Rb-Sr whole rock age (~1307 Ma) for this intrusion does not appear to have been affected by Grenvillian thermal events despite the growth of titanite at ~994 Ma in the host gneisses (Philippe et al. 1993).

2.6.2 Lake Melville terrane

In the Goose Bay area, the granodiorite to diorite gneisses of the LMT formed during the Labradorian Orogeny are bounded on their northern margin by the Rigolet thrust and the Grand Lake thrust system. Protolith ages for the gneisses in the LMT are undated, but are presumed to be similar to magmatic zircon ages found to the east of the field area at ~1677 Ma. The migmatitic to banded gneisses in the LMT are cut by a suite of diabase dikes, called the Northwest River dykes, that has been tentatively inferred to be part of the 1250 ±2 Ma (Hamilton and Emslie 1997) Mealy dykes found in the Mealy Mountains terrane. In the southern part of the field area, a syn-tectonic pegmatite dyke in the LMT yields an age of 1613 ± 40 Ma (Zrn; Krogh 1986) which is inferred to represent the timing of thrust

movement along the Labradorian precursor to the Rigolet thrust (e.g. Corrigan et al. 2000).

The Grenvillian reworking of the rocks of the LMT involved thick-skinned thrusting and associated high-grade metamorphism. The Rigolet thrust is interpreted to be a reactivated post Labradorian shear zone (see above) along which thrusting occurred during the Ottawan Orogeny (Corrigan et al. 2000). Evidence for reworking in the field area comes from a syntectonic pegmatite in the south part of the field area with growth of monazite at 1044 ± 4 Ma (Krogh 1986) inferred to represent the timing of continued thrusting along the Rigolet thrust. Further east the Rigolet thrust preserves evidence for Ottawan thrusting events at 1088 and 1046 Ma in a shear zone formed during the late Labradorian orogeny (Corrigan et al. 2000). Other Grenvillian features found in the LMT of the Goose Bay area include leucosome formation in a mildly foliated quartz diorite at 1013 +5/-8 Ma (Zrn; Philippe et al. 1993). This unit is inferred to be part of the SQRD (Wardle et al. 1990a) on the basis of rock type, although no protolith age has been obtained.

2.6.3 Cape Caribou River Allochthon

The Cape Caribou River Allochthon (CCRA) has been inferred to be the northern continuation of the MMT (Wardel et al. 1990a). A similar assemblage of rocks to that found in the MMIS occurs in the CCRA, where the Northwest River Anorthosite grades into a leucogabbro, which intrudes an "amphibolite and local mafic granulite layer" (Wardle et al 1990a; this unit is hereafter referred to as the recrystallized gabbro-diorite layer in this study). These units are underlain by pyroxene-bearing granitoid gneisses (locally charnockitic), which is intruded by the Dome Mountain suite. The lowest structural unit of the CCRA

comprises granitoid basal mylonites.

The crystallization age of the massive Northwest River anorthosite (to leucogabbro) body in the CCRA is 1625 ± 6 Ma, and it intrudes host rocks of the Dome Mountain suite 1631 ± 2 Ma, 1626 ± 2 Ma, 1636 ± 3 Ma and 1660 ± 3 Ma host rocks of the "recrystallized gabbro-diorite layer" (Bussy et al. 1995). The ~1630 Ma ages from the Dome Mountain suite at are similar to the ages of the pyroxene granitoids (1645-1630 Ma) in the MMIS (Emslie and Hunt 1990).

The available evidence suggests that the CCRA was thrust northwest in two major pulses of Grenvillian deformation. U-Pb ages of 1038 ± 2 Ma (Philippe et al. 1993) from the GLTS are inferred to date the time that the CCRA overrode the Rigolet thrust. The second northwest-directed thrusting event occurred during the early Rigolet orogeny at 1016 +7/-3 Ma (Bussy et al. 1995) and 1005 ± 2 Ma (Philippe et al. 1993). The effects of Grenvillian thrusting are principally concentrated within and adjacent to the shear zone. The metamorphic grade during thrusting was granulite facies on the basis of the stability of orthopyroxene which defines the mineral lineation within the shear zone rocks (Ryan et al. 1982, Wardle et al. 1990a).

2.7 Summary

During the Grenvillian orogenesis, late Paleoproterozoic and Mesoproterozoic units of the Goose Bay area were heterogeneously reworked by polyphase northwest-directed thrusting and associated high-grade metamorphism in the shear zones (Wardle et al. 1990a).

The Cape Caribou River Allochthon, the Lake Melville and Groswater Bay terranes were all involved in the northwest-directed deformation episodes. Figure 2-5 schematically shows the major map patterns of the lithotectonic units of the Goose Bay region. This figure shows the concentration of Grenvillian ages in the GLTS and the dominant Paleoproterozoic ages in the footwall and hangingwall rocks. It is inferred from the map pattern and the available U-Pb ages that the CCRA was thrust northward during the Ottawan Orogeny coeval with the LMT overriding the GBT along a reactivated (~1630 Ma) Rigolet thrust at ~1040 Ma. During the Rigolet Orogeny further displacement of the CCRA along the GLTS at ~1010 ±10 Ma occurred, whereas the Rigolet thrust remained inactive after the Ottawan orogeny. Similar evidence for an Ottawan pulse along the Rigolet thrust in the Rigolet area is documented by Corrigan et al. (2000) who obtained 1088-1040 Ma ages for thrusting along a shear zone originally formed during the late Labradorian (~1610 Ma).

Following thrusting during the Rigolet orogeny, a cooling age for titanite at 994 Ma (Philippe et al. 1993) is thought to represent uplift or exhumation and cooling after tectonism (e.g., Gower 1996). The deformation episode that resulted in the open folding of the allochthon about a NW-SE trending axis to its present synformal shape is also assumed to be a late Grenvillian feature (Wardle et al. 1990a).

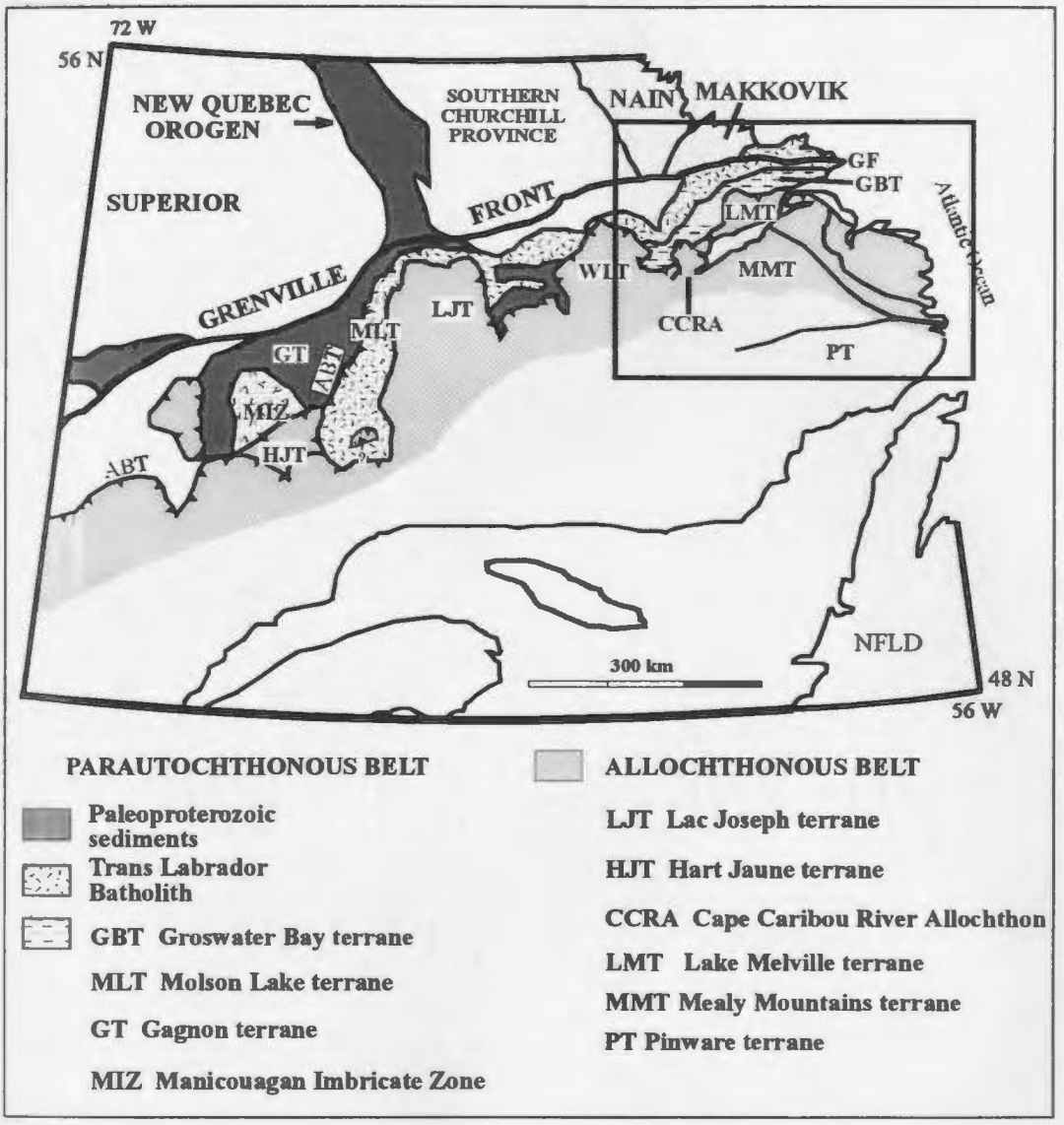

***Figure** 2-1: Tectonic elements of the eastern Grenville Province (modified after Rivers and Chown, 1986). Note the location of the Allochthon Boundary thrust (ABT) across the Grenville Province. The box indicates the location of Figure 2-2.*

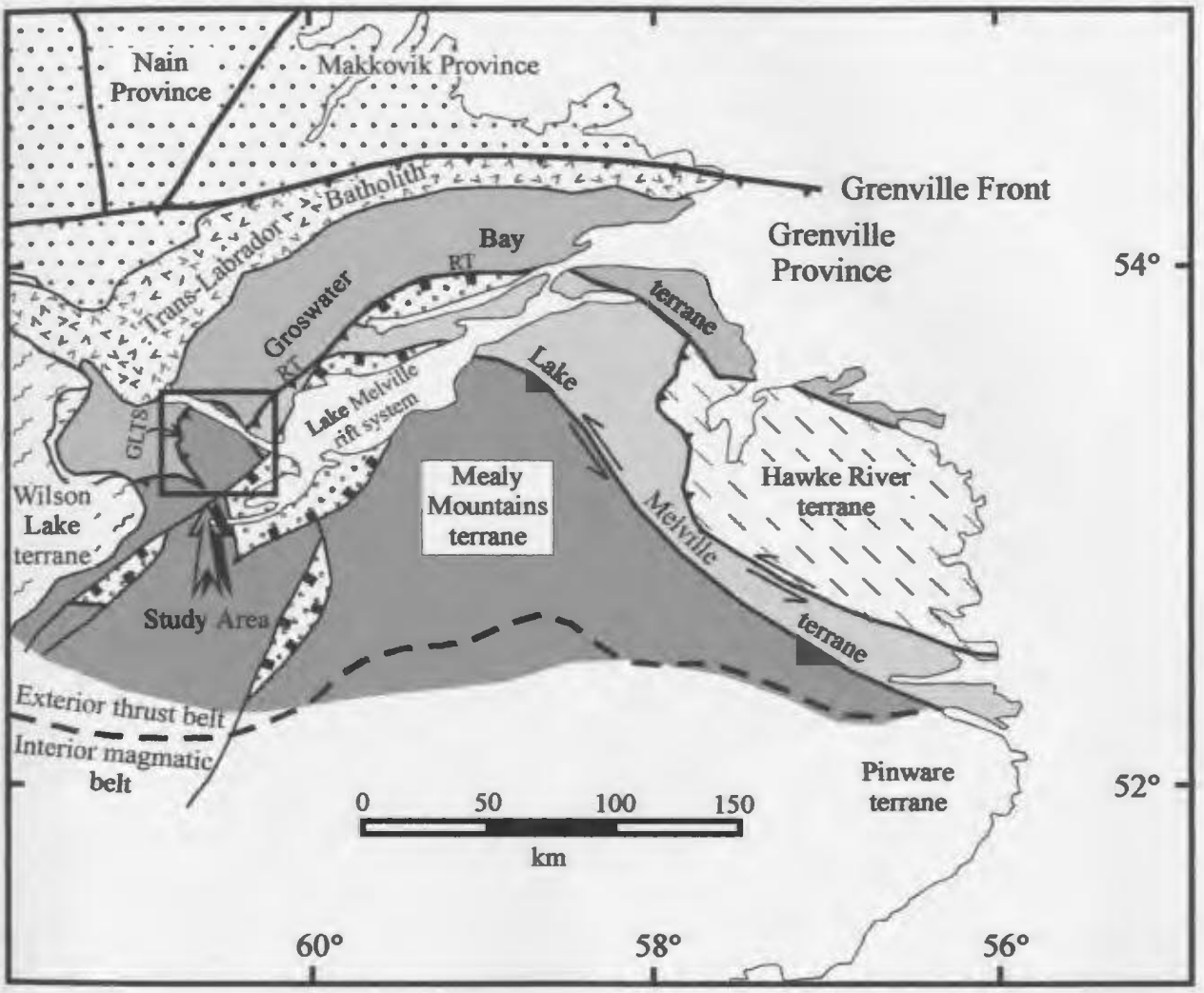

***Figure 2-2**: Major structural divisions and Grenvillian terranes in the eastern Grenville Province. Location of the Goose Bay region (Figure 2-4) is shown by the box. Diagram is after Wardle and Ryan (1996). GLTS-Grand Lake thrust system; RT-Rigolet thrust.*

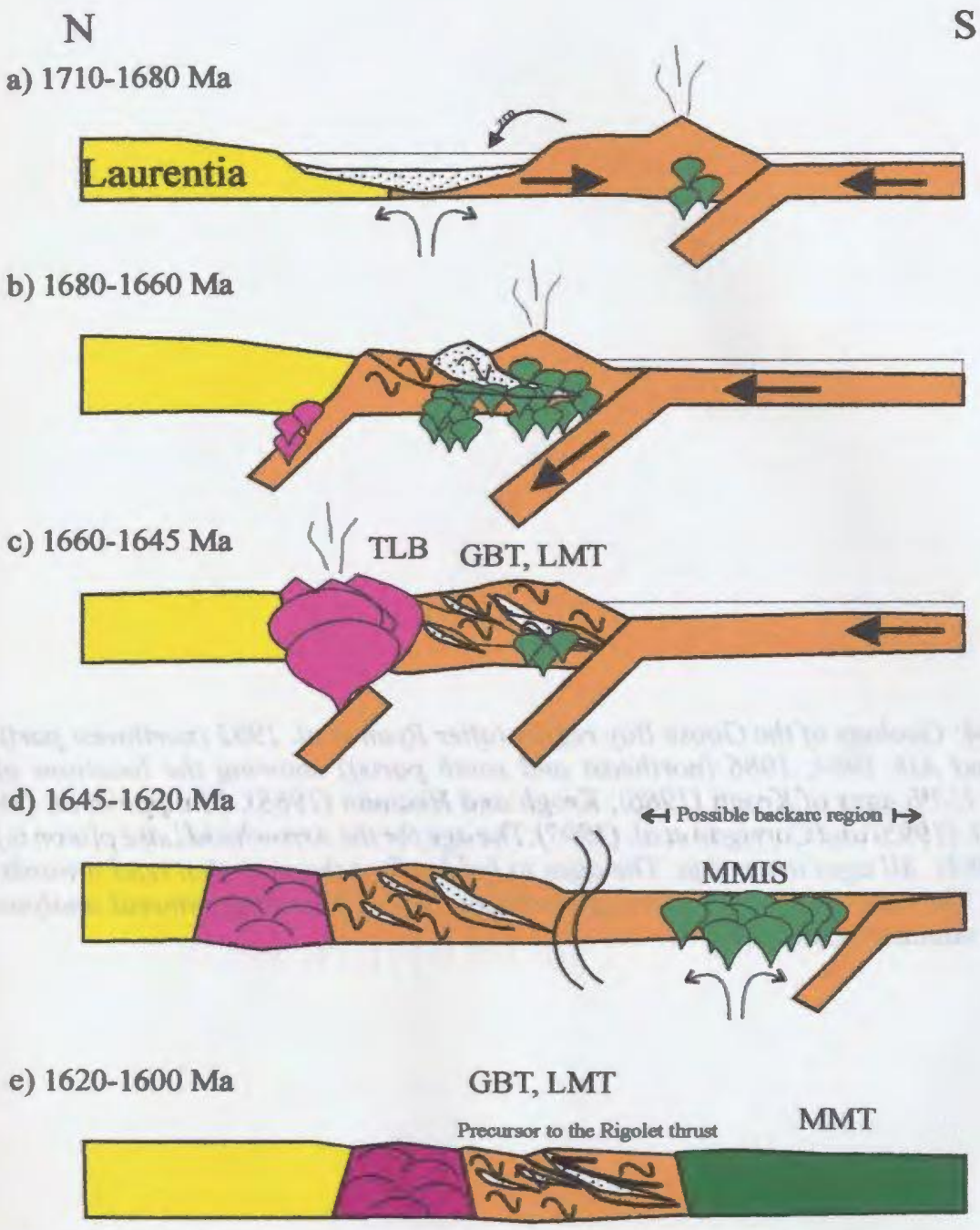

***Figure 2-3**: Schematic representation of the current tectonic model for the evolution of Labradorian terranes during the late Paleoproterozoic. Constructed from the data presented in Gower (1996) and Corrigan et al. (2000). a) configuration of the backarc basin between the calc-alkaline arc and the Laurentian margin. b) and the onset of the Labradorian Orogeny with continued magmatism under both the arc terrane and the Laurentian margin. c) emplacement of the TLB into the Laurentian margin and continued deformation in the arc terranes. d) emplacement of MMIS AMCG suites in a backarc setting. e) magmatic quiescent period with continued deformation and the formation of the precursor to the Rigolet thrust.*

***Figure 2-4**: Geology of the Goose Bay region (after Ryan et al. 1982 (northwest part) and Wardle and Ash 1984, 1986 (northeast and south parts)) showing the locations of the available U-Pb ages of Krogh (1986), Krogh and Heaman (1988), Philippe et al. (1993), Bussy et al. (1995) and Corrigan et al. (1997). The age for the Arrowhead Lake pluton is from Fryer (1983). All ages are in Ma. The ages in bold reflect the ages that tend towards that intercept. The letters following each age indicate the U-Pb bearing mineral analysed (z; zircon, m; monazite, t; titanite)*

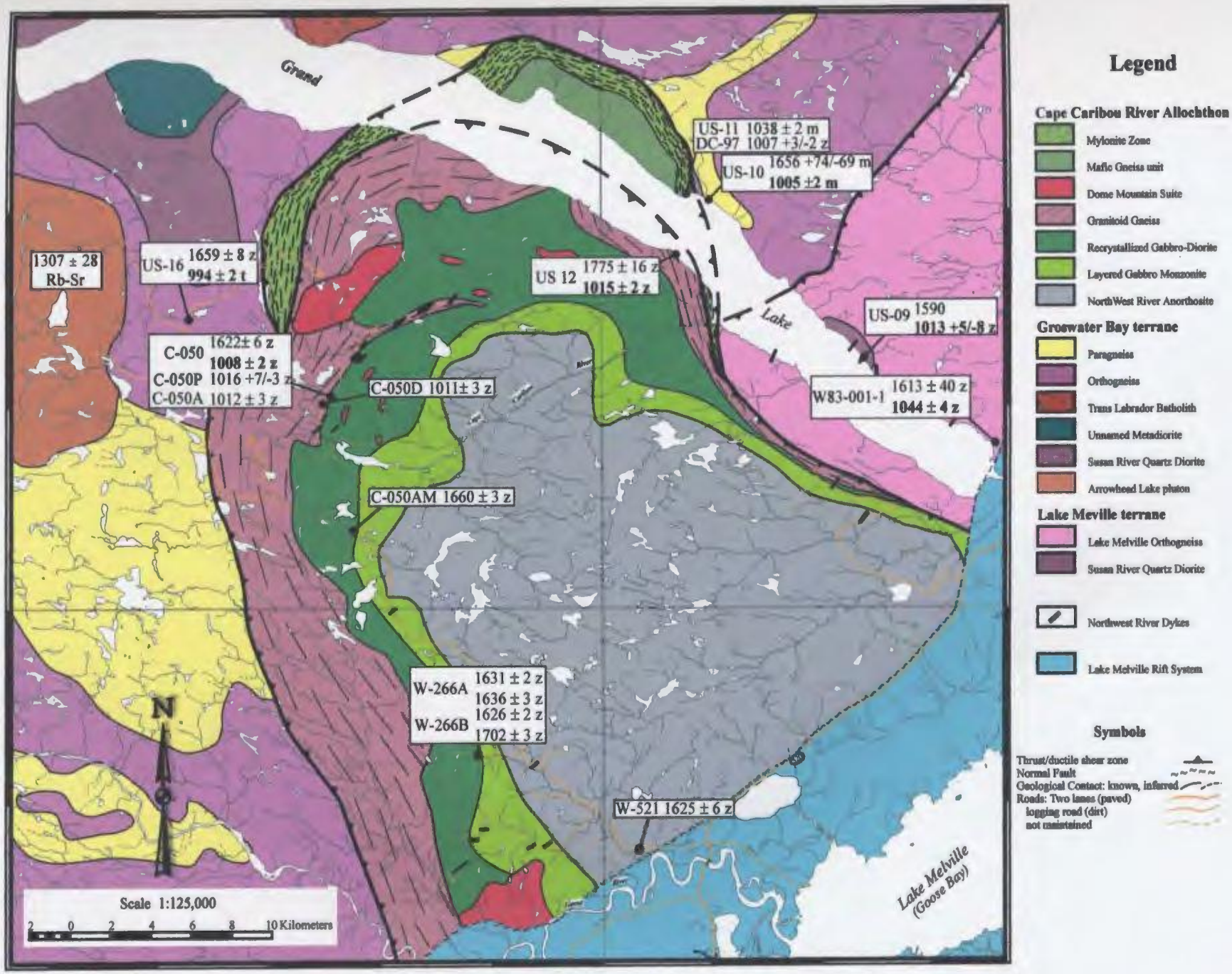
Grand
Lake
US-11 1038 ± 2 m
DC-97 1007 +3/-2 z
US-10 1656 +74/-69 m
1005 ±2 m
US-09 1590
1013 +5/-8 z
US 12 1775 ± 16 z
1015 ± 2 z
US-16 1659 ± 8 z
994 ± 2 t
1307 ± 28
Rb-Sr
C-050 1622± 6 z
1008 ± 2 z
C-050P 1016 +7/-3 z
C-050A 1012 ± 3 z
C-050D 1011± 3 z
W83-001-1 1613 ± 40 z
1044 ± 4 z
C-050AM 1660 ± 3 z
W-266A 1631 ± 2 z
1636 ± 3 z
W-266B 1626 ± 2 z
1702 ± 3 z
W-521 1625 ± 6 z
Lake Melville
(Goose Bay)
N
Scale 1:125,000
2 0 2 4 6 8 10 Kilometers
Legend
Cape Caribou River Allochthon
Mylonite Zone
Mafic Gneiss unit
Dome Mountain Suite
Granitoid Gneiss
Recrystallized Gabbro-Diorite
Layered Gabbro Monzonite
NorthWest River Anorthosite
Groswater Bay terrane
Paragneiss
Orthogneiss
Trans Labrador Batholith
Unnamed Metadiorite
Susan River Quartz Diorite
Arrowhead Lake pluton
Lake Melville terrane
Lake Melville Orthogneiss
Susan River Quartz Diorite
Northwest River Dykes
Lake Melville Rift System
Symbols
Thrust/ductile shear zone
Normal Fault
Geological Contact: known, inferred
Roads: Two lanes (paved)
logging road (dirt)
not maintained

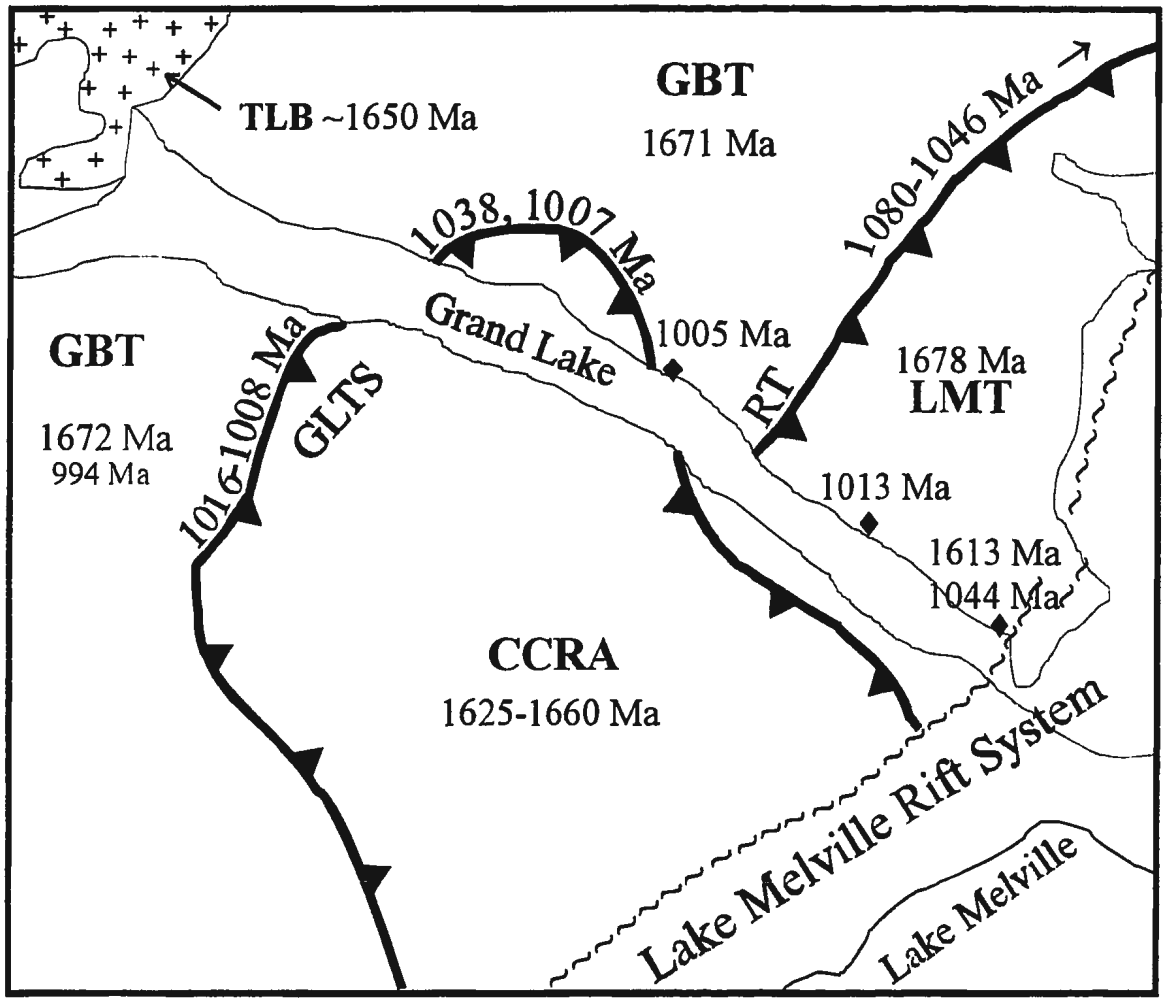

Figure 2-5: *Schematic map showing the major tectonic boundaries and lithotectonic units of the Goose Bay area. Note the concentration of Grenvillian ages at the GLTS similar to that shown in Figure 2-4. See text for discussion. TLB, Trans-Labrador Batholith; GBT, Groswater Bay terrane; LMT, Lake Melville terrane; CCRA, Cape Caribou River Allochthon; GLTS, Grand lake thrust system; RT, Rigolet thrust.*

Chapter 3

Field Geology of the Goose Bay region

3.1 Introduction

The 1:100,000 scale geological map of the Goose Bay region by Ryan et al. (1982) (northwestern part) and Wardle and Ash (1984, 1986) (northeastern and southern parts respectively), was used to guide sampling of the Grand Lake thrust system in the field and to record the locations of samples selected for petrographic analysis and geothermobarometry. Access to the outcrops was by boat on Grand Lake and by 4-wheel drive vehicle on the logging roads. The best outcrop exposure in the area is on the lake shore and along road cuts. Elsewhere, the area is largely covered by marshes, glacial drift or old growth forest and outcrop is patchy. However, some inland outcrop near the Cape Caribou River is largely vegetation-free due to a large forest fire in 1989.

Two months were spent in the field with a field assistant during the summer of 1999. Much of the time was devoted to the outcrops on the shores of Grand Lake where half of the field stations are located and where a cross-section of the shear zone, and the hangingwall and footwall rocks are well exposed. The remaining stations are located on the extensive and locally overgrown logging roads north of the town of Goose Bay. Where possible, station density was increased in proximity to the shear zone in order to record changes in structure and metamorphic mineralogy related to the thrust. Samples were also taken at localities where U-Pb dating had previously been performed by Krogh (1986), Krogh and Heaman

(1988), Phillipe et al. (1993), Bussy et al. (1995) and Corrigan et al. (1997). In this case the aim was to evaluate the petrographic setting of dated samples and attempt to link age determinations and *P-T* estimates (Chapter 8). At some stations, however, sampling was not possible due to the smooth glacially polished outcrop surfaces.

3.2 Lithologies in the Study Area

The lithologies in the study area are broadly grouped into three major Grenvillian lithotectonic units, namely: i) the Groswater Bay terrane (GBT), ii) the Lake Melville terrane (LMT), and iii) the Cape Caribou River Allochthon (CCRA) which is the northern extension of the Mealy Mountains terrane (MMT). These terranes are stacked, with the LMT overlying the GBT along the Rigolet thrust (RT) and the Cape Caribou River Allochthon together with its basal shear zone, the Grand Lake Thrust System (GLTS) overlying both the LMT and GBT (Figure 3-1).

3.2.1 Groswater Bay Terrane

In the study area, the Groswater Bay terrane (GBT) is mainly composed of granitic-granodioritic orthogneiss, which is host to packages of pelitic and calc-silicate paragneiss and mafic to ultramafic enclaves. The orthogneiss is intruded by the Arrowhead Lake pluton in the northwest part of the field area (Figure 3-1).

3.2.1.1 Granitic to Granodioritic Orthogneiss

The orthogneiss unit is principally composed of grey-weathering migmatitic granodioritic to granitic gneisses. The gneissic fabric is well developed where hornblende

defines the mineral elongation lineation together with subordinate feldspars, quartz and scapolite. This gneissic fabric is crosscut at high angles by many alkali feldspar-plagioclase-quartz-biotite pegmatites between 5 cm and 5 m thick with the thicker pegmatites containing alkali feldspar crystals up to 50 cm in diameter.

The mineralogy of the orthogneiss is fairly consistent in the field area, being composed of the assemblage: hornblende-plagioclase-alkali feldspar-quartz - garnet ± biotite ± epidote ± scapolite ± clinopyroxene. Garnet is ubiquitous, but clinopyroxene is only found in the high strain orthogneiss near the contact with the overlying CCRA.

The contact between the orthogneiss and the paragneiss unit (see below) is commonly a highly tectonized zone as shown in Figure 3-2, where the mylonitic orthogneiss with a planar straight gneissic fabric is juxtaposed against the paragneiss unit with a discontinuous migmatitic layering deformed into SW-plunging folds. This relationship between the units is common and has been observed at many localities in the field area, although locally the contact is obscured by pegmatites intruded along the boundary between orthogneiss and paragneiss. The original nature of the contact between the orthogneisses and the paragneiss is not known.

3.2.1.2 Pelitic and Calc-silicate Paragneiss

Minor discontinuous belts of supracrustal rocks within the field area are largely composed of kyanite ± sillimanite and alkali feldspar bearing migmatitic paragneiss with the complete compositional range spanning semipelite to pelite with minor calcareous layers or lenses. A Ky-Sil isograd is has been defined in the field area, with Ky being present in the north and Sil farther south. Ky and Sil coexist over a distance of ~10 metres. Green kyanite

blades, ~5-10 mm in length, lie within the foliation planes but are not generally aligned parallel to the L_s fabric defined by quartz and feldspar rodding. Sillimanite, where present, occurs as fibrous knots or as fine prisms lying within the foliation planes and is similarly not aligned parallel to quartz-feldspar lineation. The paragneiss unit on the shores of Grand Lake contains the mineral assemblage garnet-alkali feldspar-biotite-kyanite-quartz with local post-peak sillimanite and muscovite. Samples collected by Ryan et al. (1982) from the paragneiss on the west side of the field area have a similar assemblage except that muscovite rather than K-feldspar is present as part of the main assemblage though sillimanite is still inferred to be a post peak phase.

The mineralogy of the calc-silicate layers consists of garnet-clinopyroxene-carbonate-epidote-quartz-titanite ± olivine. Calc-silicate to carbonate lenses commonly have wispy terminations in cross section and a dome and basin style structure in plan view (Figure 3-3). The calc-silicates, although strongly deformed, do not generally preserve penetrative fabrics, presumably due to post-tectonic annealing. Volumetrically small alkali feldspar-bearing pegmatites, which are associated with the calcareous units, intrude along contacts between the calcareous units and the metapelites. The forest-green pods in Figure 3-3 are principally composed of clinopyroxene with rims of amphibole against the pegmatite. This texture is interpreted to represent hydration of clinopyroxene-bearing calc-silicates by fluids from the pegmatite. A fluid is also assumed to have contributed to the local hydrous retrogression of the host paragneiss. At some locations, the pelite grades into a semipelite and then into calcareous layers. This compositional variation is inferred to reflect the original sedimentary layering of the protolith, although it has been strongly modified during metamorphism.

3.2.1.3 Mafic-Ultramafic Rocks

Kyanite paragneiss is locally observed to host a dark green, friable, amphibole-rich layered unit composed of cummingtonite-orthopyroxene-spinel-plagioclase±garnet which grades across strike into a rock composed of euhedral garnet, hornblende and plagioclase. This mafic-ultramafic unit also occurs as boudins and pods throughout the NTS map sheet 13F/10 (see Ryan et al. 1982). These pods are inferred to have been tectonically incorporated into the paragneiss during thrusting and imbrication of the juvenile island arc sequence during the Labradorian Orogeny.

3.2.1.4 Arrowhead Lake pluton

The Arrowhead Lake pluton (Rb/Sr isochron age of 1307±26, Fryer 1983) in the northwest part of the field area forms a distinct unit in the GBT. This oval composite intrusion, which is approximately 6-8 km wide and 11-12 km long, is hosted by GBT orthogneisses, comprises gabbronorite, pyroxene-bearing monzonite and granite. The Arrowhead Lake pluton is weakly deformed indicating that it mainly escaped penetrative Grenvillian tectonism. The nature of the contact with the orthogneisses was not observed due to the lack of outcrop and heavy vegetation.

3.2.2 Lake Melville terrane

The LMT is predominantly made up of granodioritic to dioritic gneisses. Minor mafic to ultramafic enclaves are hosted within these gneisses. In addition, the LMT is host to mafic dykes which are part of the Northwest River dyke suite, and are discussed below in section 3.2.4.

3.2.2.1 Granodioritic to Dioritic Orthogneiss

The orange-yellow to black-grey weathering migmatitic granodioritic to dioritic orthogneiss have a layered appearance due to alternating mafic and felsic layers. The orthogneiss of the LMT are cut by alkali feldspar-quartz-plagioclase-biotite pegmatites that may comprise up to 50% of the outcrop exposure. Some of the pegmatitic dykes contain allanite crystals up to 2 cm in diameter with radiating fractures.

The mineralogy of the granodioritic to dioritic gneiss is predominantly plagioclase-hornblende-quartz-alkali feldspar ± garnet ± clinopyroxene ± orthopyroxene. Hornblende is the most abundant mafic mineral in the orthogneiss, whereas garnet is principally a local phase together with the pyroxenes.

Contrasting with the migmatitic and high strain LMT orthogneiss, is a grey to orange-yellow weathering, variably foliated quartz diorite unit containing mafic enclaves (Figure 3-4). Mildly deformed portions of the quartz diorite grade into much more highly strained mylonitic portions which bound the low strain zone to the north and south. The unfoliated quartz diorite is reported by Philippe et al. (1993) to contain leucosomes, implying static metamorphism at high temperatures, although no evidence of migmatization was observed in the studied outcrops.

3.2.2.2 Mafic Rocks

The orthogneiss, excluding the quartz diorite, is host to mafic and ultramafic pods, such as hornblendite pods which occur as large outcroppings or a series of smaller pods within an outcrop. These mainly amphibole-rich pods may contain up to 15% plagioclase feldspar locally. Foliation present within these pods is generally parallel to the regional

Grenvillian foliation, although locally an older fabric may still be preserved, as in a 10-20cm wide ultramafic lens containing the assemblage serpentine-biotite-orthopyroxene. These mafic and ultramafic pods probably have similar origins to those described above in the GBT.

3.2.3 Cape Caribou River Allochthon

The CCRA is made up of massive anorthosite (Northwest River Anorthosite), associated gabbroic rocks and pyroxene-bearing granitoids. This lithological assemblage comprises an anorthosite-mangerite-charnockite-granite (AMCG) suite, possibly part of the Mealy Mountains Intrusive Suite (MMIS) in the adjacent MMT. The Northwest River Anorthosite occurs at the present day top of the thrust stack comprising the CCRA and is underlain by gabbronoritic rocks. The recrystallized gabbro-diorite unit occurs in the middle of the thrust stack and is underlain by gneissic granitoids that make up the lower portions of the allochthon with a locally charnockitic basal mylonite forming part of the GLTS, together with mafic straight gneisses elsewhere. Pyroxene-bearing granitoid rocks, known as the Dome Mountain Suite are possibly part of the AMCG suite, and intrude throughout the allochthon (see Figure 3-1) except in some parts of the basal mylonite and anorthosite.

3.2.3.1 Anorthosite and Gabbronorite

Anorthosite and gabbronorite of the Northwest River body preserve a variety of igneous textures such as gabbroic patches with ophitic textures, igneous lamination and layering defined by the preferred orientation of mafic phases, and orthopyroxene megacrysts. Penetrative metamorphic fabrics are not present, although the units have undergone static

recrystallization marked by the presence of garnet in some of the gabbronoritic rocks.

The anorthosite weathers grey to white and fresh surfaces are medium grey to dark grey-purple in colour. Crystals of plagioclase feldspar range in size from a few millimeters up to 20 cm and display labradorescence at some outcrops. The anorthosite massif is composed of several intrusions distinguished by their variable percentages of mafic minerals and differences in the colour and textures. For instance, one body of the anorthosite displays ophitic textures in 4-6 cm wide gabbroic patches (Figure 3-5), whereas in another body, orthopyroxene occurs as megacrysts up to 50 cm in long dimension. The large orthopyroxene megacrysts are restricted to parts of the anorthosite that have undergone extensive subsolidus recrystallization, as indicated by grain boundary adjustments and kink banding preserved in the larger plagioclase and pyroxene crystals. Commonly where orthopyroxene is present as megacrysts in anorthosite and in gabbronorite, it is rimmed or pseudomorphed by hydrous minerals in coronas (Figure 3-6). Minor parts of the anorthosite bodies are composed of nelsonite (apatite-magnetite rock) and granophyric (alkali feldspar and quartz) intergrowths which are inferred to be last melt pockets of liquid to crystallize in the pluton. The 1625 ± 6 Ma U-Pb age (Bussy et al. 1995) for the anorthosite was determined from zircon in one of these pockets.

3.2.3.2 Recrystallized Gabbro-Diorite Unit

The rocks in the recrystallized gabbro-diorite unit (amphibolite and local mafic granulite unit of Wardle et al. 1990a) are mainly gabbroic, dioritic-monzodioritic in composition and contain the metamorphic mineral assemblage plagioclase-hornblende-clinopyroxene ± alkali feldspar ± orthopyroxene ± garnet. The rocks are generally weakly

layered and contain local leucosome patches near the base of the unit. Some outcrops display ductile deformation characteristics. On the basis of the age of the pyroxene-bearing granitoids (~1630 Ma) and the ductilely deformed gneisses (1660 ± 3 Ma; both ages from Bussy et al. 1995) the ductile deformation episode is inferred to be Labradorian. This unit is not well exposed and all information is constrained from the few available outcrops and U-Pb data.

3.2.3.3 Basal Granitoid

Structurally beneath the recrystallized gabbro-diorite unit is granitoid gneiss that forms the basal unit of the allochthon. The gneiss is generally granodioritic, granitic or tonalitic in composition (locally charnockite, charno-enderbite and enderbite respectively) containing the mineral assemblage plagioclase-alkali feldspar-quartz-hornblende-biotite-garnet ± orthopyroxene ± clinopyroxene ± scapolite.

The best exposure of the basal granitoid gneisses is found on Cape Caribou, Grand Lake, where cliffs rise upwards of ~250 m from the lake, and display gneisses and highly deformed pegmatitic material. Layers of amphibolite present within the rock face contain the mineralogy hornblende-plagioclase-clinopyroxene-garnet ± orthopyroxene.

At Cape Caribou, a relatively little deformed mafic unit inferred to be a tectonic inclusion in the basal gneiss, is composed of plagioclase-hornblende-garnet-clinopyroxene-orthopyroxene and contains large euhedral porphyroblasts of garnet up to 3-10 cm in diameter (see Figure 3-7). The foliation wraps around the garnets implying pre-tectonic growth of garnet. This same unit also is host to patchy leucosomes containing orthopyroxene and plagioclase implying high temperature melting under nearly static conditions.

3.2.3.4 Basal Mylonite

The granitoid gneiss unit (see above) is characterized at its base by a basal mylonite composed of high strain granitoid gneiss and layered straight gneisses along the shores of Grand Lake. The best outcrops of the mylonite zone are found directly across from Cape Caribou on a rounded point (Big Point; Figure 3-1) where there is nearly 100% exposure. The mylonites are composed of alternating layers of mafic and felsic rock that weather black and buff-tan respectively. Mafic layers contain the mineral assemblage hornblende-plagioclase-garnet±clinopyroxene±orthopyroxene, whereas the felsic layers contain plagioclase- alkali feldspar- quartz - garnet ± hornblende ± biotite ± orthopyroxene ± clinopyroxene. The width of the mafic layers ranges up to 10 cm and remains constant across the outcrop exposure yielding the aspect of straight gneisses. All the shear zone rocks are studded with garnet ranging in size from a few millimeters up to 10 cm crystals or aggregates (Figure 3-8). The mylonitic foliation wraps around the larger porphyroblasts of garnet, implying pre-tectonic growth of those porphyroblasts. The foliation surfaces display well formed quartz and feldspar rods which are inferred to define the thrusting direction. Within the shear zone, orientations of both the foliation and mineral elongation lineation are fairly constant.

The straight gneisses grade structurally upward into the "layered mafic unit" interpreted by Wardle and Ash (1984) to form a high strain base to the layered gabbros and gabbronorite of the Northwest River Anorthosite. The "layered mafic unit" is here interpreted to represent lesser strained straight gneiss that displays alternating gabbroic and granitic

(locally charnockitic) layers (Figure 3-9) similar to the underlying straight gneisses and is henceforth referred to as the mafic gneiss unit. Based on this interpretation, the entire package of rocks on the north side of Grand Lake is considered to be composed of straight gneiss with the more highly strained portions forming the base of the allochthon and the shear zone.

Outcrops of the basal mylonite on the southern shore of Grand Lake near the nose of the thrust consist of pyroxene-bearing mylonitic granitoid rocks with the assemblage orthopyroxene-clinopyroxene-garnet-plagioclase-quartz-alkali feldspar. Further inland, a recently exposed outcrop along a woods roads also located at the nose of the thrust displays granitoid straight gneisses that also contain hornblende porphyroclasts, similar to those on the lake shore. This locality was one of the few observed where the kinematic indicators unequivocally indicate top-to-the-north (i.e., thrust) sense of shear on the GLTS.

3.2.3.5 Dome Mountain Suite

The Dome Mountain Suite (~1630 Ma, Bussy et al. 1995), which ranges in composition from orthopyroxene monzonite (mangerite) to granite (Ryan et al. 1982), includes several bodies that intrude the recrystallized gabbro-diorite unit as well as the basal granitoid gneisses. One small granite body discovered on a woods road preserves highly deformed intrusive contacts with the recrystallized gabbro-diorite layer whereas the centre of the stock is not deformed. This relationship is similar to that reported by Ryan et al. (1982) for other granitoid bodies within the CCRA. Other granitoid intrusions related to the Dome Mountain Suite occur as sheet-like intrusions into the recrystallized gabbro-diorite layer and as intermixed pyroxene granitoid and gabbroic rocks (Wardle and Ash 1986).

3.2.4 Northwest River dykes

The CCRA and the LMT are host to the diabase Northwest River dykes which are inferred to be correlative with the 1250 ± 2 Ma (Hamilton and Emslie 1997) Mealy dykes found in the MMT to the south. The dykes cross-cut Labradorian fabrics in both the LMT and CCRA but are variably metamorphosed and deformed depending on their proximity to the basal mylonite.

Northwest River dykes occur in all units of the CCRA. In the Goose Bay region, they trend ~220° ± 20°, their intrusive nature is easily recognizable and observed dykes vary from 1 or 2 m up to 60 m wide. Ryan et al. (1982) noted that the dykes become more strained and the metamorphic mineralogy becomes increasingly coarse grained towards the present day nose (i.e., base) of the allochthon, and they also pointed out peculiar garnet veining seen in some of the dykes at this locality (Figure 3-10). Dykes found further south tend to retain more igneous textures with a variable metamorphic overprint depending on proximity to the mylonite zone.

Northwest River dykes also occur in the LMT in the Goose Bay area and probably also ~200 kilometres farther east in the LMT near Rigolet, where Corrigan et al. (2000) reported dykes with similar crosscutting relationships that they interpreted as part of the Mealy swarm. In the Goose Bay area, these amphibolitized diabase dykes also trend approximately 220° and range in thickness from 10 to 60 cm. The mineralogy of the dykes changes from hornblende-plagioclase±garnet ± orthopyroxene ± clinopyroxene in the south

to hornblende-plagioclase-garnet-quartz in the north. In the southern portions of the LMT, the dykes crosscut Labradorian fabrics and retain original intrusive characteristics such as chilled margins. In the north of the LMT, the dykes are completely amphibolitized and become progressively stretched, boudinaged and rotated into the prevailing Grenvillian foliation.

One dyke, approximately 60 cm wide, is preserved in a glacially polished outcrop and displays changes in the metamorphic mineralogy across the width of the dyke. At the margins of the dyke the mineralogy is hornblende-plagioclase±garnet, whereas in the core the grain size is coarser and the mineral assemblage is hornblende-clinopyroxene-orthopyroxene-garnet-plagioclase. This is interpreted to reflect an episode of retrogression along the margins that post dated the formation of the high grade metamorphic assemblage.

On account of their importance wit respect to possible correlations between the LMT, MMT and the CCRA, and because of their potential as marker units for Grenvillian deformation and metamorphism, the chemistry and petrology of the Northwest River dykes and their relationships to the Mealy dykes are discussed in greater detail in Chapter 5.

3.3 Summary

It is commonly difficult to distinguish between Labradorian and Grenvillian fabrics and metamorphic mineral assemblages in the Goose Bay area, especially in the footwall rocks. Overall, it appears that the effects of the Labradorian Orogeny in the GBT and LMT are more widespread than the localized Grenvillian deformation, which occurs principally at the base of the CCRA and in adjacent footwall rocks. The Grand Lake thrust system is

inferred to be a strictly Grenvillian feature and not a reworked Labradorian shear zone such as the Rigolet thrust (Corrigan et al. 2000) as fabrics of the basal mylonite crosscut Labradorian fabrics or rework the Labradorian foliation into the prevailing Grenvillian fabric. These observations suggest that it is possible to distinguish Labradorian from Grenvillian fabrics locally, although metamorphic assemblages related to those deformation episodes may not always be readily discernible. The presence of the Northwest River dykes in the LMT and CCRA provides an excellent marker for Labradorian versus Grenvillian metamorphic mineral assemblages in the upper parts of the thrust stack and near the shear zone. It is concluded that with careful observation, sampling and petrographic analysis of the fabrics and mineral assemblages and using the available information for U-Pb ages, it should be possible to delineate Labradorian and Grenvillian deformation and metamorphism in the rocks of the Goose Bay area.

Figure 3-1: Geological map of the Goose Bay region (after Ryan et al. 1982 (northwest part) and Wardle and Ash 1984, 1986 (northeast and south parts)).

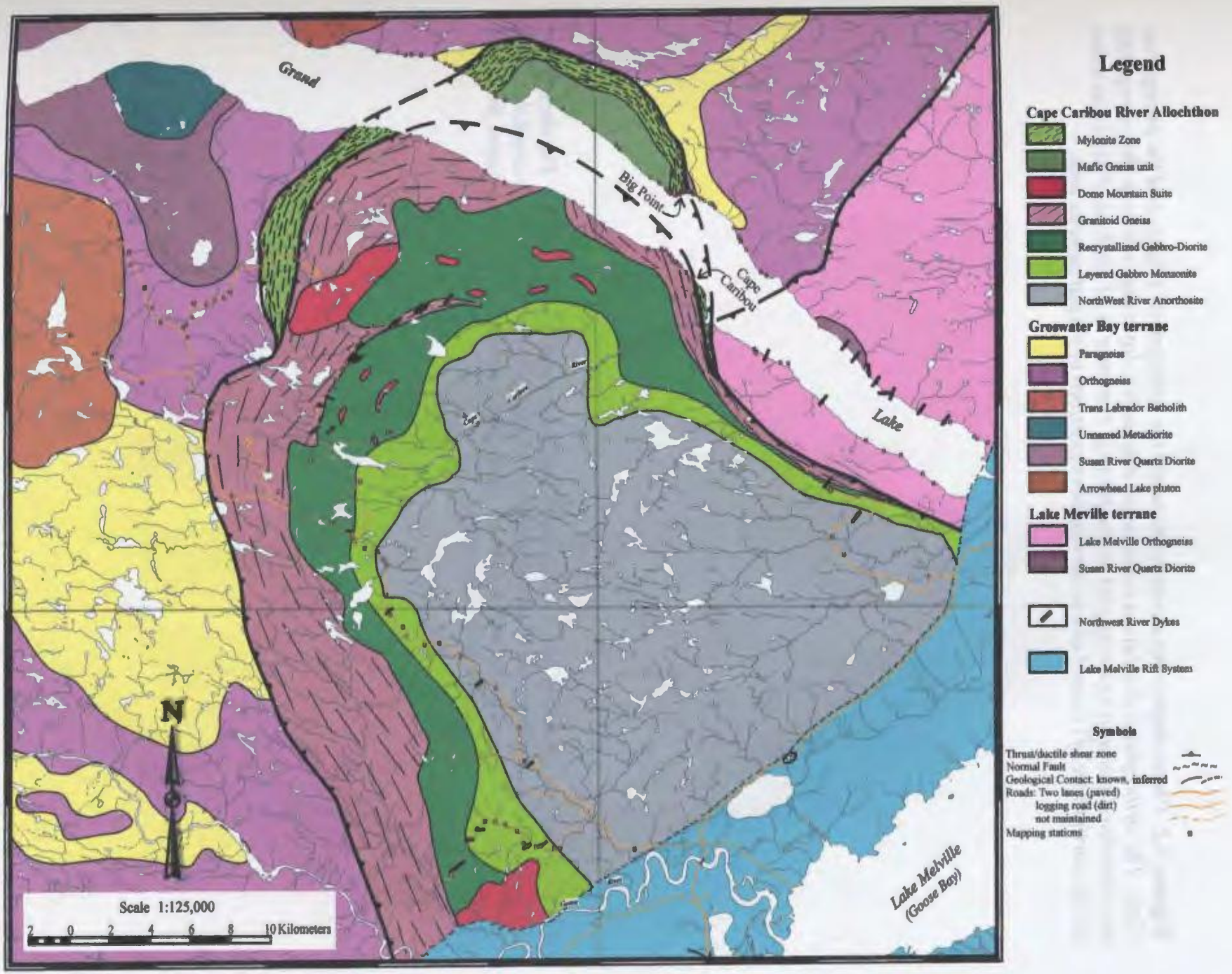
Grand
Big Point
Cape Caribou
Lake
Lake Melville (Goose Bay)
N
Scale 1:125,000
2 0 2 4 6 8 10 Kilometers
Legend
Cape Caribou River Allochthon
Mylonite Zone
Mafic Gneiss unit
Dome Mountain Suite
Granitoid Gneiss
Recrystallized Gabbro-Diorite
Layered Gabbro Monzonite
NorthWest River Anorthosite
Groswater Bay terrane
Paragneiss
Orthogneiss
Trans Labrador Batholith
Unnamed Metadiorite
Susan River Quartz Diorite
Arrowhead Lake pluton
Lake Melville terrane
Lake Melville Orthogneiss
Susan River Quartz Diorite
Northwest River Dykes
Lake Melville Rift System
Symbols
Thrust/ductile shear zone
Normal Fault
Geological Contact: known, inferred
Roads: Two lanes (paved)
logging road (dirt)
not maintained
Mapping stations

***Figure 3-2**: Photo displaying a contact between the orthogneiss (right) and the paragneiss (left). The orthogneiss displays a continuous migmatitic layering, whereas the paragneiss displays discontinuous layering and minor folding. Hammer is 41 cm long. Photo was taken on the north shore of Grand Lake in the southern portions of the paragneiss unit.*

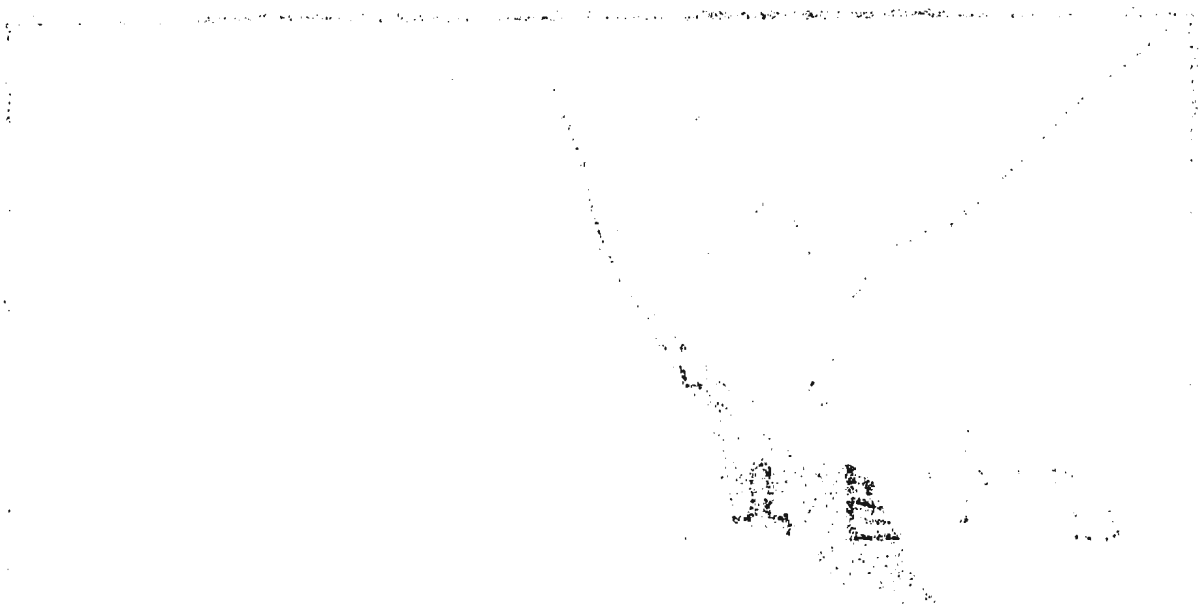

***Figure 3-3**: Photograph of calc-silicate rocks in contact with ky-paragneiss. The dark green pods are primarily composed of clinopyroxene. The pods are retrogressed to amphibolite at their margins due to interaction of fluids from the pegmatite. Photo is taken from the paragneiss unit 200 m south of the shear zone.*

3-2

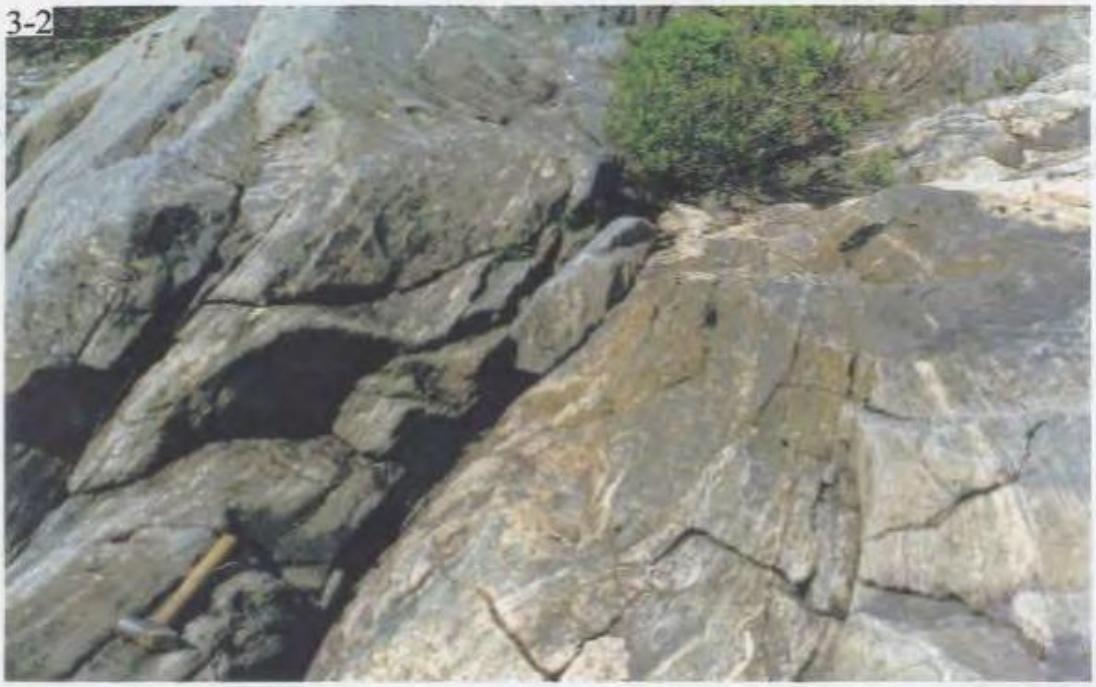

3-3

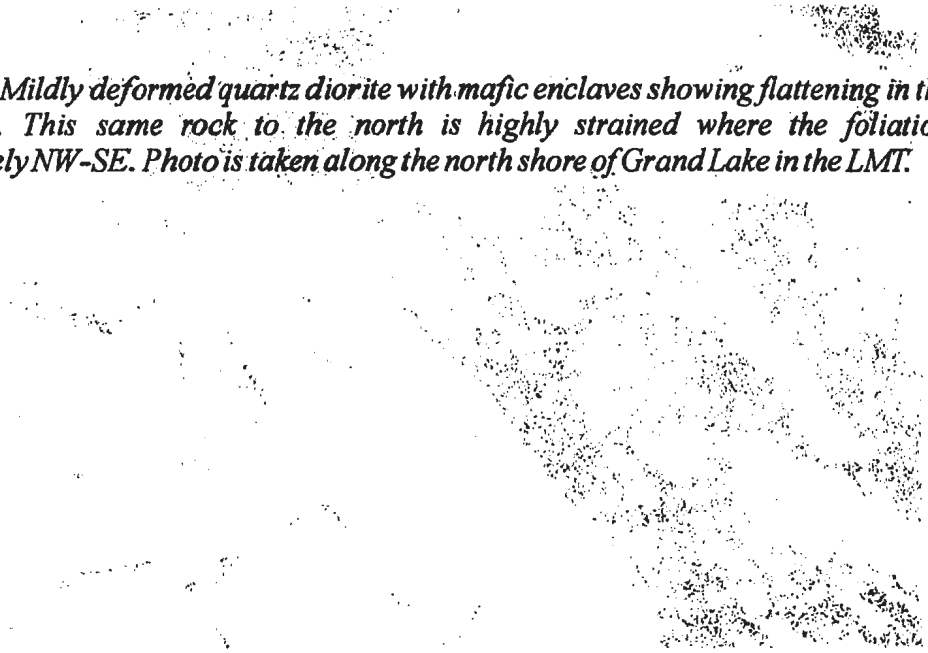

***Figure 3-4**: Mildly deformed quartz diorite with mafic enclaves showing flattening in the E-W foliation. This same rock to the north is highly strained where the foliation is approximately NW-SE. Photo is taken along the north shore of Grand Lake in the LMT.*

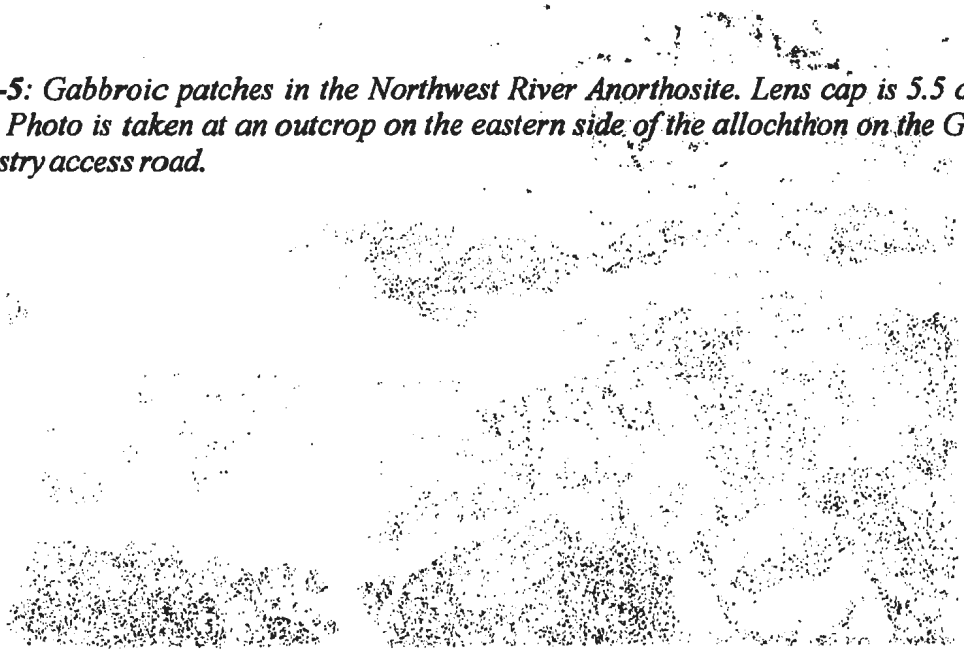

***Figure 3-5**: Gabbroic patches in the Northwest River Anorthosite. Lens cap is 5.5 cm in diameter. Photo is taken at an outcrop on the eastern side of the allochthon on the Grand Lake forestry access road.*

3-4

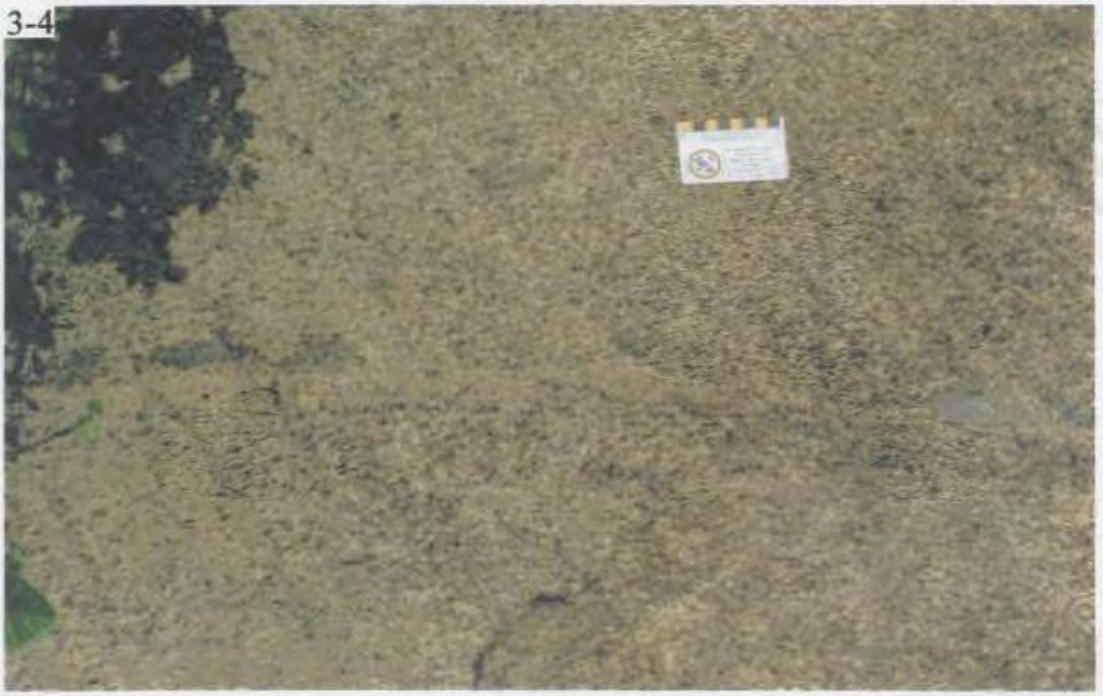

3-5

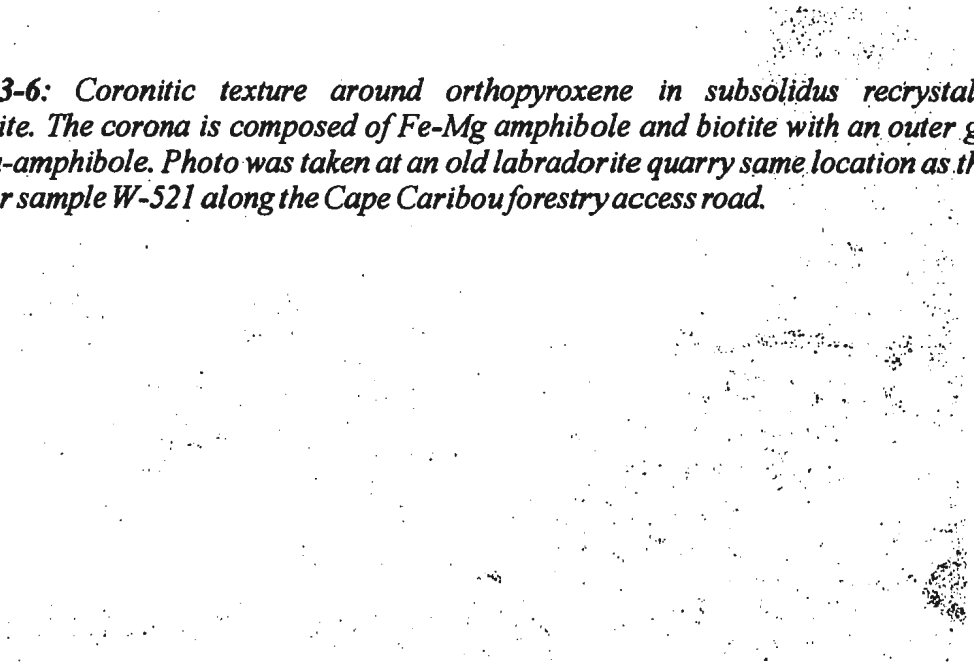

Figure 3-6: *Coronitic texture around orthopyroxene in subsolidus recrystallized anorthosite. The corona is composed of Fe-Mg amphibole and biotite with an outer green rim of Ca-amphibole. Photo was taken at an old labradorite quarry same location as the U-Pb age for sample W-521 along the Cape Caribou forestry access road.*

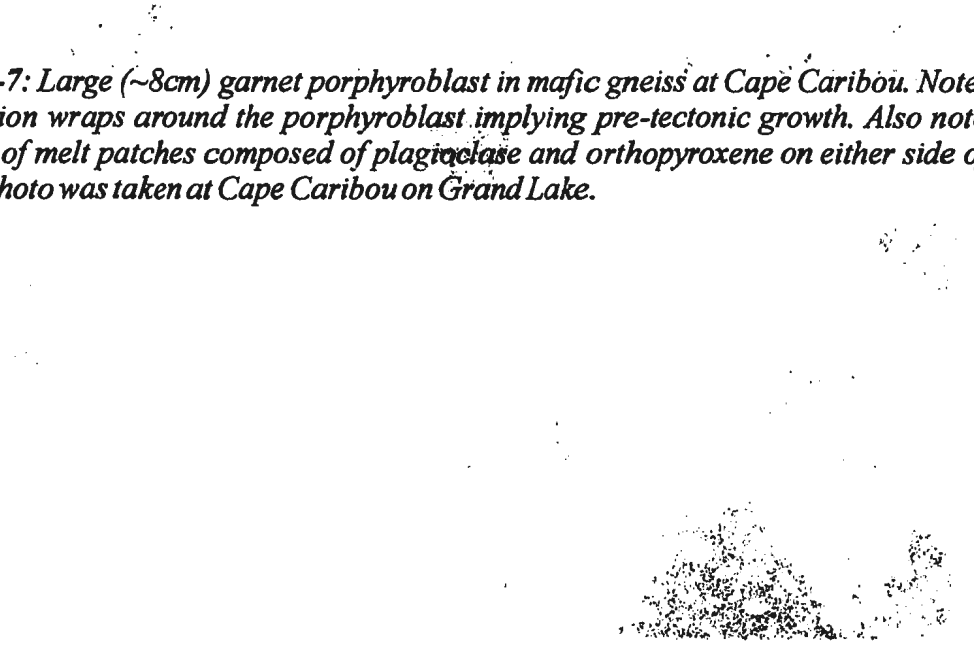

Figure 3-7: *Large (~8cm) garnet porphyroblast in mafic gneiss at Cape Caribou. Note that the foliation wraps around the porphyroblast implying pre-tectonic growth. Also note the presence of melt patches composed of plagioclase and orthopyroxene on either side of the garnet. Photo was taken at Cape Caribou on Grand Lake.*

3-6

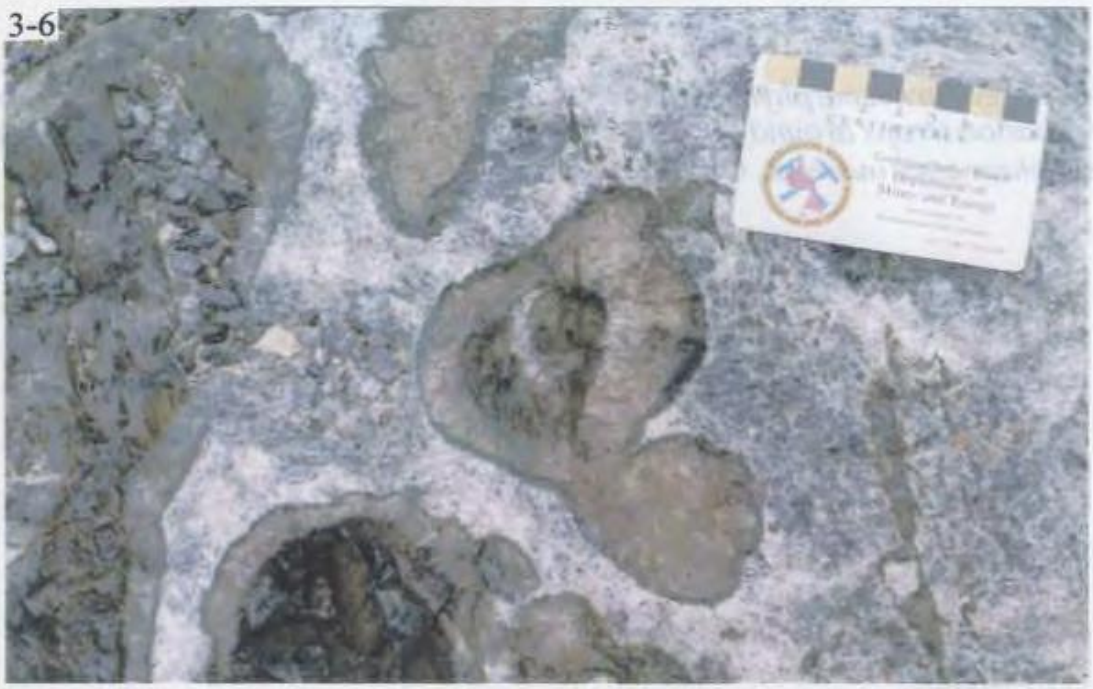

3-7

***Figure 3-8**: Large garnet porphyroblast in straight gneiss of the mylonite zone. Note how the mylonitic foliation wraps around garnet implying pre-tectonic growth. Photo was taken at the northern shear zone outcrops, Grand Lake.*

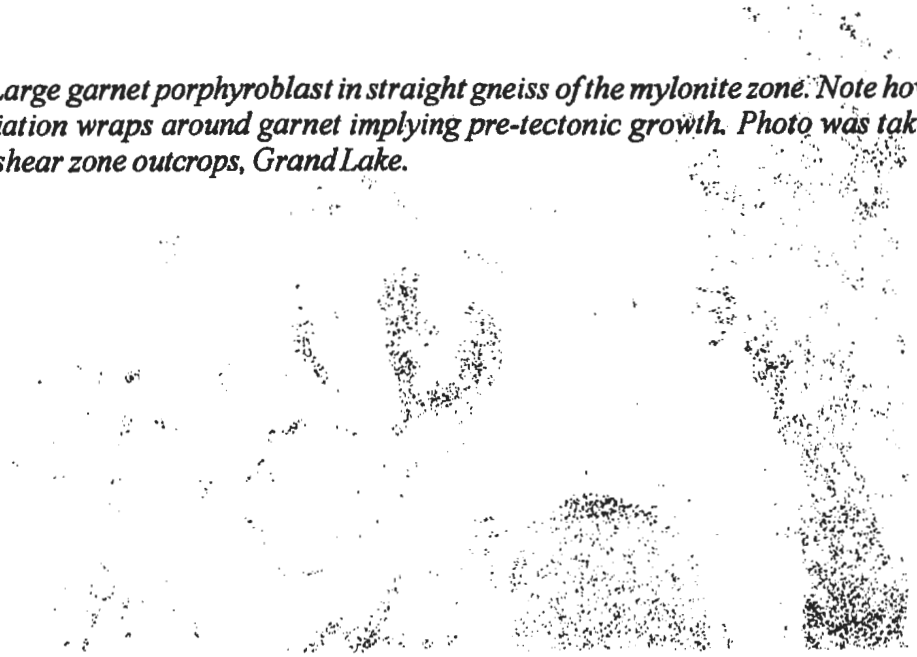

***Figure 3-9**: Tectonic layering preserved in the mafic gneiss unit. Photo was taken from an outcrop 50 m north of the straight gneisses of the shear zone on Grand Lake.*

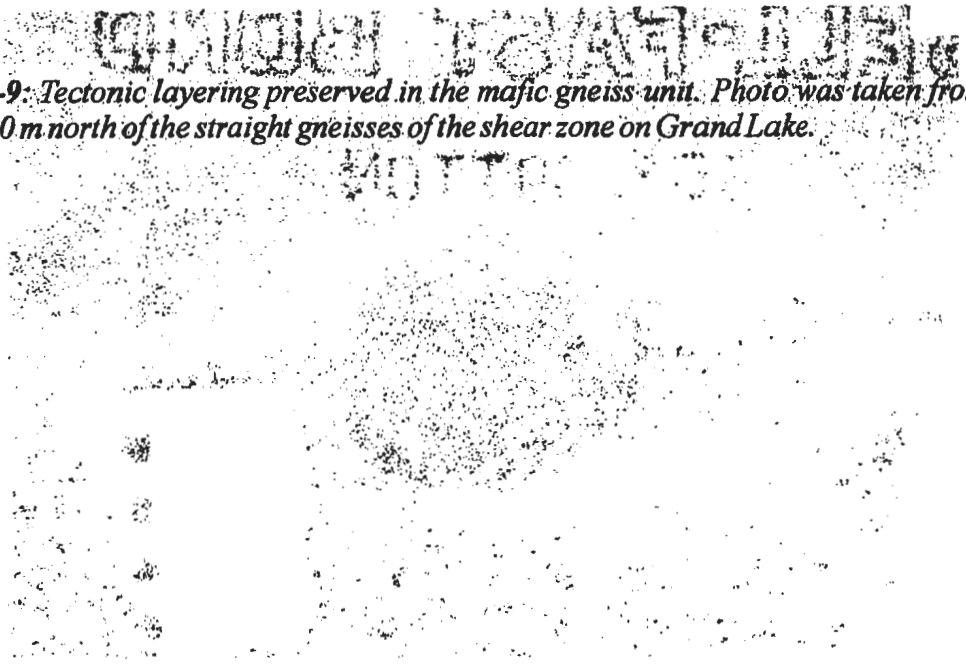

3-8

3-9

***Figure 3-10**: Northwest River dyke in the CCRA preserving igneous features such as chilled margin and plagioclase phenocrysts. The host rock is a two pyroxene garnet granulite and the dyke is a two pyroxene and amphibole bearing granulite. The veins in the dyke are principally composed of garnet and clinopyroxene. Photo was taken along the Cape Caribou forestry access roads at the same location as U-Pb sample C-050 AM.*

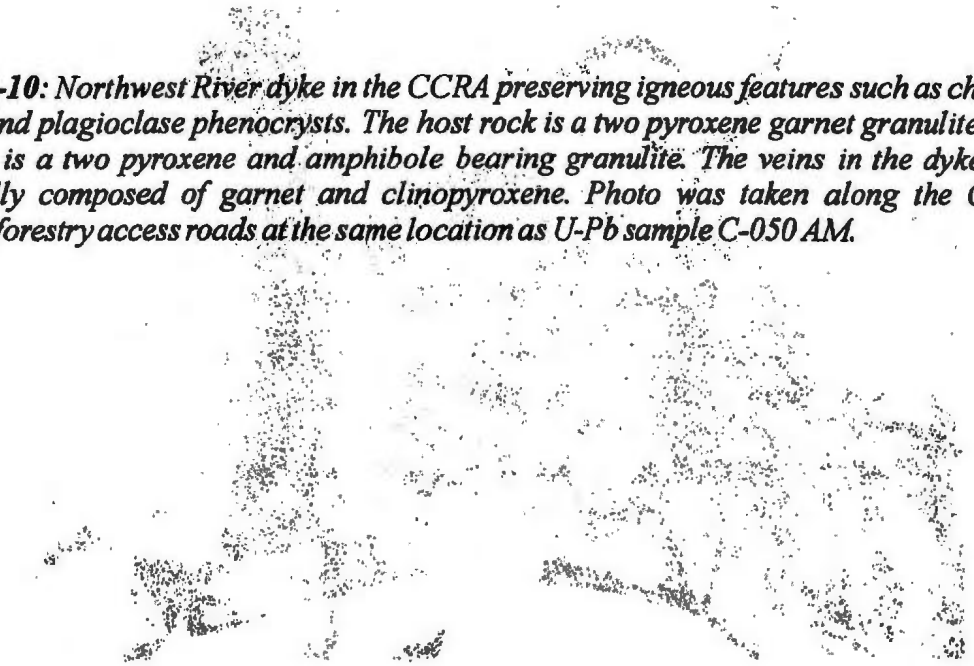

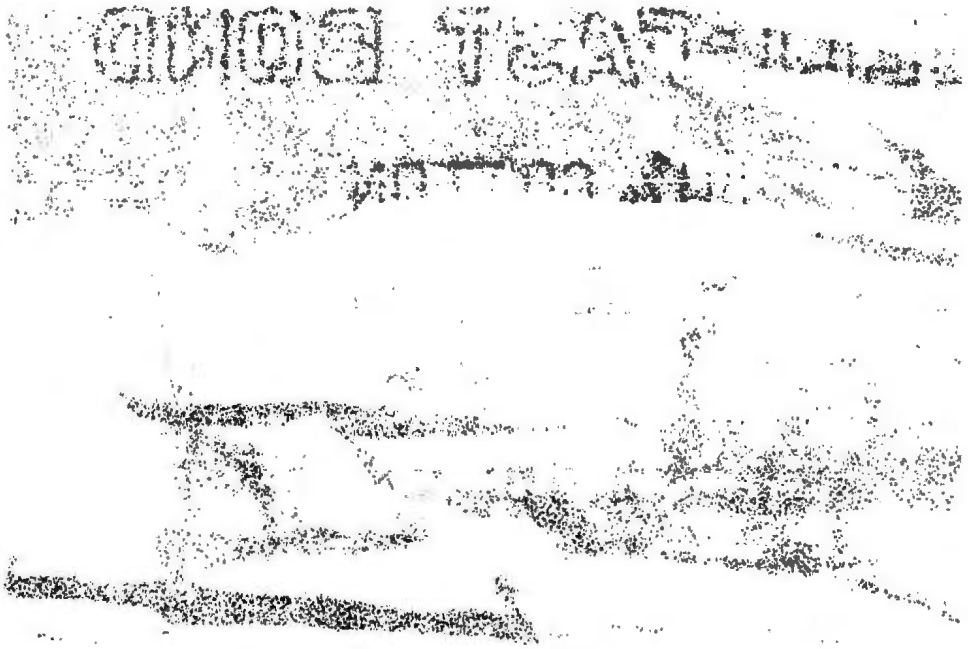

3-10


CENTIMETRES
Geological Survey Branch
Department of
Mines and Energy

Chapter 4

Structural Overview of the Grand Lake thrust system

4.1 The Grand Lake thrust system

As discussed in previous chapters, the Grand Lake thrust system (GLTS) at the base of the Cape Caribou River Allochthon is inferred to be part of a thick-skinned thrust system. The GLTS is characterized by the presence of strongly lineated straight gneiss and local zones with mylonitic to ultramylonitic fabrics (Ryan et al. 1982; Wardle and Ash 1984, 1986; this study). The best exposures of the GLTS are on the shores of Grand Lake, where it is characterized by syntectonic, granulite-facies assemblages in the shear zone that grade into amphibolite-facies assemblages in the adjacent footwall and hangingwall rocks (Ryan et al. 1982; Wardle et al. 1990a). The following discussion principally concerns the mesoscopic scale fabrics associated with the GLTS.

4.1.1 High Strain Textures in the GLTS

Based on field studies of Ryan et al. (1982), Wardle and Ash (1984, 1986) and this study, strain-induced heterogeneous recrystallization associated with the GLTS is principally restricted to the ~1 km thick shear zone at the base of the CCRA. The shear zone rocks are largely composed of straight gneisses with alternating layers of mafic and felsic composition. Mafic layers are typically composed of Grt-Cpx-Pl-Hbl-Opx±Qtz, whereas the felsic layers

are composed of Pl-Qtz-Grt-Cpx-Opx-Hbl. This difference in mineralogy resulted in a difference in strain response, and hence microstructures in the mafic and felsic layers. In particular, the stretching lineation (L_s) is generally better developed in the felsic layers as a result of subgrain formation in feldspar and ribbon development in quartz along with the stretched orthopyroxene grains. However, clinopyroxene, amphibole and orthopyroxene in mafic layers also locally define the L_s fabric. In general, the temperature of the formation of quartz ribbons is estimated to be > 400 to 700 °C, plagioclase is known to undergo dislocation climb and recovery at T > 500 °C and dislocation glide and/or stacking faults form in orthopyroxene at T > 700 °C (Passchier and Trouw 1998), compatible with preliminary *P-T* data for the GLTS (Best 1997). Thus all these features point to a high temperature (> 650 °C) of deformation in the GLTS.

Outcrops in the shear zone generally lack unambiguous kinematic indicators, although from the few rare examples observed, the sense of shearing is top toward the north-northwest, compatible with observations of Wardle and Ryan (1996). For example, one outcrop that lies within the nose of the thrust displays centimetre-scale sigma (σ) style asymmetrical porphyroblasts of amphibole as schematically depicted in Figure 4-1. The sparsity of kinematic indicators is attributed to the very high strain in the GLTS during thrusting, and the subsequent annealing that occurred as a consequence of the elevated strain energy and temperature.

On the basis of grain size, two populations of garnet can be seen in the straight gneiss outcrops. One population is characterized by large (1-6 cm diameter) euhedral to subhedral

crystals (Figure 3-8), whereas garnet in the other population are much smaller and subhedral to anhedral. The shear zone foliation wraps around both populations of porphyroblasts. Timing of growth of the larger porphyroblasts is not directly known but it is assumed to predate the most strongly developed fabrics, that on the basis of available U-Pb monazite ages from the GLTS (e.g., 1038 ± 2 Ma, Philippe et al. 1993), are thought to have formed during the Ottawan orogeny. Further discussion of relating fabrics to U-Pb ages can be found in Chapter 8.

Discontinuities in the straight gneiss layering were observed at several localities in the shear zone. They define structural ramps in the thrust system. They were observed in outcrops that are orientated perpendicular and sub-parallel to the inferred transport direction, indicating the existence of both frontal and lateral ramps. The ramp angles are typically less than 20° and the ramps merge with the shear zone fabric within 2-10 m (e.g., Figure 4-2a). The ramps are generally <1-2 m in structural height. Figure 4-2b displays the inferred structural configuration of the ramp in Figure 4-2a. Mylonitic to ultramylonitic fabrics locally define planar discontinuities in the straight gneiss layering (Figure 4-3a) and these are inferred to represent the latest stage of thrust development. Figure 4-3b schematically displays an interpretation of the structure shown in Figure 4-3a. It is inferred that during thrusting, fault propagation advanced into the footwall as the thrust wedge thickened and the shear zone widened. The gentle angles and low structural height of these ramps are consistent with high total strain and the inferred high temperature of deformation and consequent low ductility in the straight gneiss.

Evidence for penetrative ductile deformation associated with the GLTS diminishes away from the shear zone into the adjacent footwall and hangingwall rocks. For instance, in proximity to the contact with the GLTS, the orthogneisses of the GBT are fine grained and contain porphyroclasts of garnet and hornblende that are finer grained than those farther away from the contact. Furthermore, the foliation and lineation within the vicinity of the shear zone are heterogeneously re-orientated into the prevailing foliation direction of the GLTS as shown in Figure 4-4. Deformation in the hangingwall rocks also diminishes away from the shear zone as displayed by the monocyclic Northwest River dykes, which are recrystallized to amphibolite (Pl-Cam) and granulite-facies (Opx-Cpx-Pl-Cam±Grt) granoblastic assemblages near the GLTS but commonly retain relict igneous textures higher up in the thrust stack.

Within the footwall rocks, local mylonitic fabrics are preserved as 5-30 cm wide high strain zones, as shown in Figure 4-5. Garnet commonly occurs as porphyroclasts in these zones of grain size reduction. In Figure 4-5, from the GBT footwall, the mylonitic fabric is subparallel to the older pre-shearing fabric, whereas footwall rocks in the LMT may display two distinct fabrics at high angles to each other (Figure 4-6). Krogh (1986) obtained zircons from a foliated granitoid sheet orientated parallel to the Grenvillian shear zone fabric in the southern portion of the LMT on Grand Lake that yielded a lower intercept age of 1044 ± 4 Ma and an upper intercept age of 1613 ± 40 Ma. The inferred Ottawan fabric is preserved as discrete 10-50 cm wide mylonite zones that crosscut older Labradorian fabrics (Figure 4-7). The trend of these shear zones is subparallel to that of the transport direction at ~165°. This

Ottawan lower intercept age is similar to ages of ~1038 Ma determined from the shear zone by Philippe et al. (1993) and ca. 1050 Ma determined for the Rigolet thrust in the LMT farther east (Corrigan et al. 2000).

Fabrics in the GLTS shear zone are inferred to be principally Grenvillian given that Labradorian ages are rare. The footwall and hangingwall rocks however, may also contain Labradorian fabrics, in addition to variably penetrative Grenvillian fabrics. The variability of Grenvillian and pre-Grenvillian fabrics should be kept in mind when discussion of pretectonic fabrics or identification of fabrics arises in the following sections.

4.1.2 Structural Analysis

Structural measurements of mineral stretching lineations, metamorphic foliations and locally igneous laminations were made at most stations in the field. Measurements of foliations were performed to constrain the attitudes of folds of all scales, from outcrop scale features (~10 m) to the large structure that defines the overall synformal shape of the allochthon. Analysis of these data helsp to distinguish the effects of pre-, syn and post Grenvillian tectonism.

4.1.2.1 Stretching Lineation (L_s)

Lower hemisphere equal-area stereographic projections of L_s from the GLTS (Figure 4-8a) yield a spread of orientations with a predominant NW-SE trend and a well defined mean plunge and trend of 25°→165, which is interpreted to represent the direction of thrusting of the CCRA. The spread of the data in Figure 4-8a and 4-8b is interpreted to be

in part the result of synthrusting lateral ramping and/or open post emplacement folding of the allochthon about an axis subparallel to the L_s. The presence of open dome and basin style interference patterns and open folds within the footwall and hangingwall rocks also contribute to the scatter in the plot.

4.1.2.2 Foliation

The lower hemisphere equal-area projection of poles to foliation in the GLTS is shown in Figure 4-9 in which poles from the east and west limbs and the hinge area are distinguished. There is some scatter in the orientations, but there is a clear segregation of poles from the different parts of the fold, implying an overall synformal shape. The scatter may be caused by either the open folding event and/or may be related to the presence of lateral or frontal ramps, as noted above. If the large scale fold were cylindrical the poles from the limbs and the hinge zone would tend to fall on a great circle (π-girdle), whereas if the fold were conical the poles would define a small circle. However, the data fulfill neither criterion very precisely. It is tentatively concluded from the data that the GLTS is folded into an irregular conical fold with a gently plunging fold axis tending to the southeast parallel to the L_s.

Much smaller folds, such as a 10-20 m antiform-synform pair with a fold axis of 17°→265 were observed in the LMT. This fold axis is nearly perpendicular to the mean mineral lineation of 25°→165 reported above. The time of formation of the open antiform-synform pairs and the dome and basin structures is not well constrained.

4.2 Cross sections

Several cross-sections through the GLTS and CCRA are presented in this section in order to define the geometry of the allochthon. The locations of the cross-sections are shown in Figure 4-10.

4.2.1 NE-SW Cross-section

A NE-SW cross-section drawn through the centre of the allochthon parallel to the transport direction was presented by Wardle et al. (1990a) and is reproduced here slightly modified as Figure 4-11. It clearly displays the inferred shallow dips of the GLTS and the CCRA but the scale used does not allow the basal mylonite or the smaller granitoid sheets related to the Dome Mountain suite to be shown. The layering in the units is inferred to be parallel to the GLTS, and the thickness of the Northwest River Anorthosite is inferred to increase towards the contact with the Neoproterozoic Lake Melville Rift system, which truncates the southern edge of the allochthon. Based on the mapping of Wardle and Ash (1984, 1986), geophysical modelling of Ash (1985) and the aeromagnetic map of the Goose Bay region, the cross-section displays the inferred continuation of the layered CCRA at some level below the erosion surface to the southeast. The only major modification to the figure of Wardle et al. (1990a) made in this study is the extension of the trace of the GLTS to the contact with the Lake Melville graben.

4.2.2 A-A' North shore Grand Lake

Figure 4-12 is a NE-SW trending cross-section along part of the northeast shore of

Grand Lake, subparallel to the cross-section in Figure 4-11. This section is drawn through an area of good exposure where structural measurements from the densely spaced stations can be accurately projected onto the cross section. Due to the nature of the thrust itself and the general southeast dip of foliations in both the allochthon and the underlying parautochthonous terranes, it is not possible to project data from the south side of the lake into the section.

Assumptions/constraints used in drawing this figure include: 1) the mylonite zone at the base of the allochthon is assumed to be of constant thickness across the length of the section; 2) the maximum thickness of the overlying mafic gneiss unit cannot be constrained since the full thickness of this unit is not exposed; 3) the mafic gneiss unit and underlying basal mylonite are restricted to the northeast part of the allochthon and are assumed to be separated from the structurally higher parts of the allochthon by a thrust located under Grand Lake (Wardle and Ash 1984; Wardle et al. 1990a; this study); 4) in the footwall beneath the leading edge of the allochthon, an upright fold pair is present in the orthogneiss of the GBT. These folds are inferred to be related to thrusting of the CCRA, as are other E-W trending structures present in the GBT to the east of the field area (Gower 1986).

Three features are immediately apparent from this cross-section. Firstly, the GLTS truncates the Rigolet thrust in its footwall, implying that the latter is the older structure. This relationship is comparable with ages of ~1045 Ma for the Rigolet thrust farther east (Corrigan et al. 2000) and with the available determination of ca.1010 Ma for the GLTS (Philippe et al. 1993, Corrigan et al. 1997). Secondly, considerable structural relief of the basal shear zone is apparent, which cuts topographically both up and down in the direction

of tectonic transport. However, it is not clear whether this is an original feature or is a result of subsequent folding. Thirdly, there are at least two important thrust systems at the base of the allochthon with the mylonite and the mafic gneiss unit sandwiched between them and excised from the southwest limits of the cross-section.

4.2.3 B-B' Perpendicular to Mean Lineation

Vertical cross section B-B' (Figure 4-13) is drawn perpendicular to the mean of the stretching lineation. This section displays the asymmetrical synformal shape of the allochthon with the western flank of the allochthon being principally composed of the granitoid straight gneisses that pinch out on the eastern flank where the mafic gneiss unit outcrops. The form of the lens-shaped granitoid sheets of the Dome Mountain suite is schematic. These bodies have strongly foliated contacts with relatively unfoliated cores (Ryan et al. 1982, this study).

4.3 Conclusions

On the basis of geological, structural and geochronological data, the Cape Caribou River Allochthon (CCRA) was thrust northward along the GLTS during both the Ottawan (~1040 Ma) and the Rigolet (~1010 Ma) orogenies. Penetrative deformation related to Grenvillian thrusting was principally restricted to the shear zone leaving much of the adjacent thrust stack and footwall rock with only a minor imprint of Grenvillian tectonism. Shearing took place under granulite-facies conditions based on the local presence of lineated orthopyroxene lying in the shear fabric of the GLTS. The stretching lineation in quartzo-

feldspathic rocks and sparse kinematic indicators yield a transport direction of top towards the northwest (i.e., thrust) sense of displacement.

As briefly discussed above, the tectonic grain in the LMT and GBT is E-W, whereas it is principally N-S in the CCRA. A similar tend is found farther east in Labrador where Grenvillian allochthonous terranes exhibit curvilinear N-S trends whereas the footwall rocks maintain an E-W tectonic grain (Gower 1986). The E-W grain present in the footwall rocks has the following two implications for Grenvillian thrusting. Firstly, heterogeneous shearing in thrust planes may have had minor lateral or frontal ramps to overcome which may be the cause for the observed discontinuities in the shear zone. Secondly, the allochthon was probably folded following Rigolet thrusting into an open upright non-cylindrical synform, although structural evidence for this remains unequivocal.

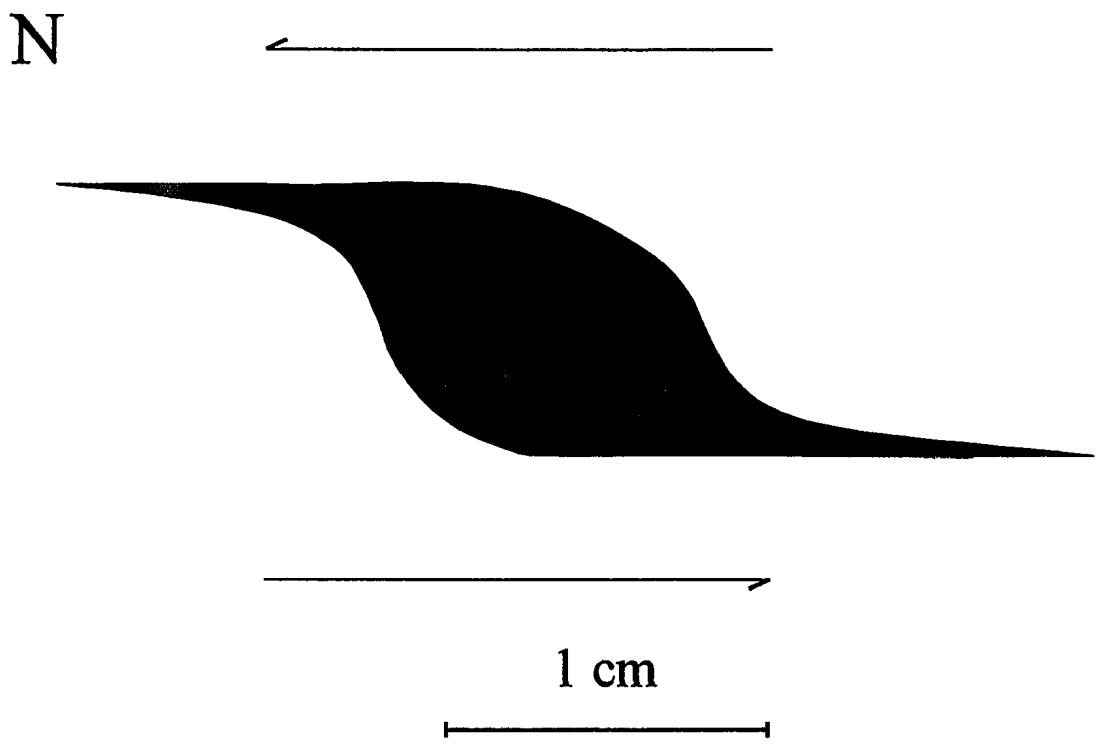

***Figure 4-1**: Schematic representation of a syntectonic σ shaped hornblende in the GLTS displaying an asymmetrical stair stepping shape indicating top to the north sense of shear. View perpendicular to lineation and foliation.*

***Figure 4-2a**: Lateral ramp in the straight gneisses view towards the north approximately parallel to L_x. The ramp angle is 15°. Note that the mylonitic foliations above and below the ramp are parallel at the left. This photo was taken at Big Point, Grand Lake.*

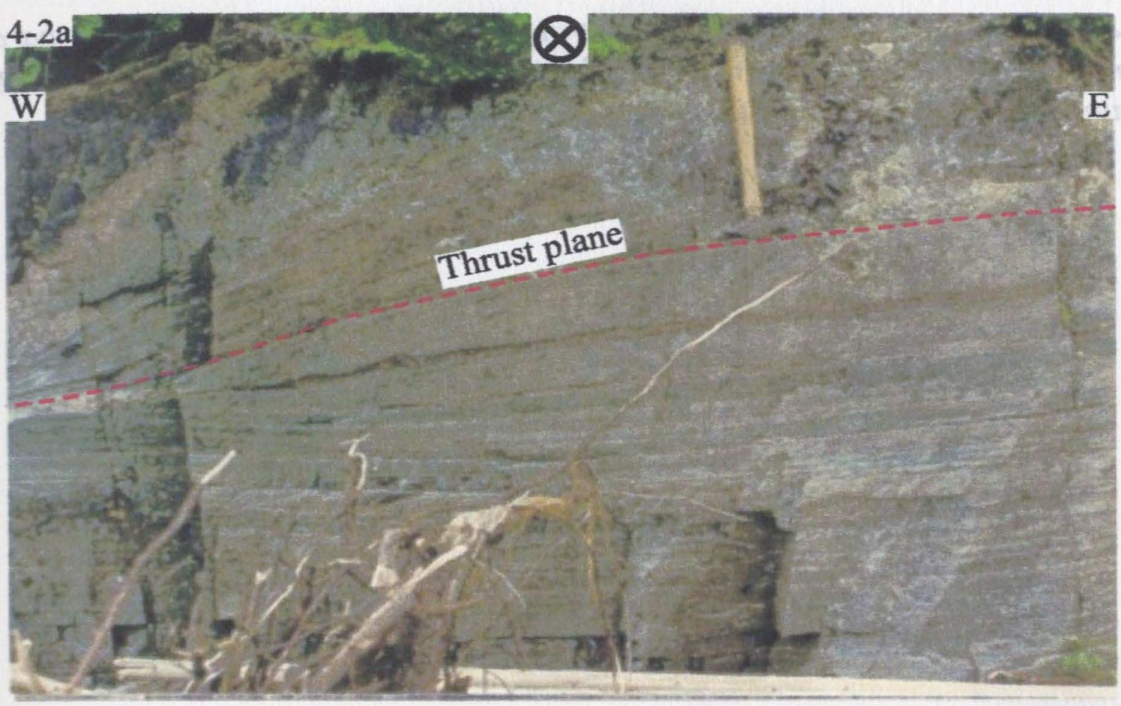

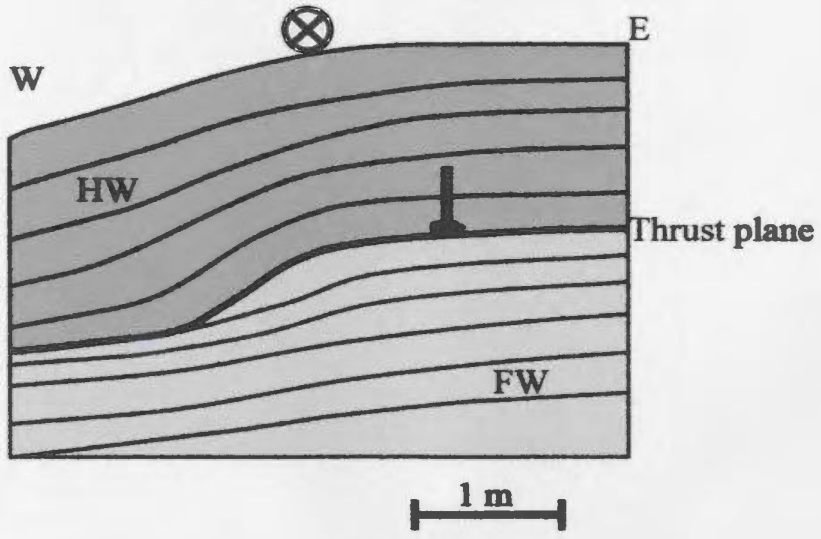

***Figure 4-2b**: Schematic diagram showing relationship of hangingwall mylonitic foliation to footwall foliation and the presence of a lateral ramp where the hammer lays on the thrust plane defined by the thick black line. Drawn from Figure 4-2a. Looking north, parallel to L_x in the direction of tectonic transport.*

***Figure 4-3a**: Close up of a lateral ramp in straight gneiss view is approximately parallel to L_r. The ramp angle is 20°. Note the ultramylonitic fabrics at the base of the ramp implying broadening of the thrust system. Photo taken at Big Point, Grand Lake.*

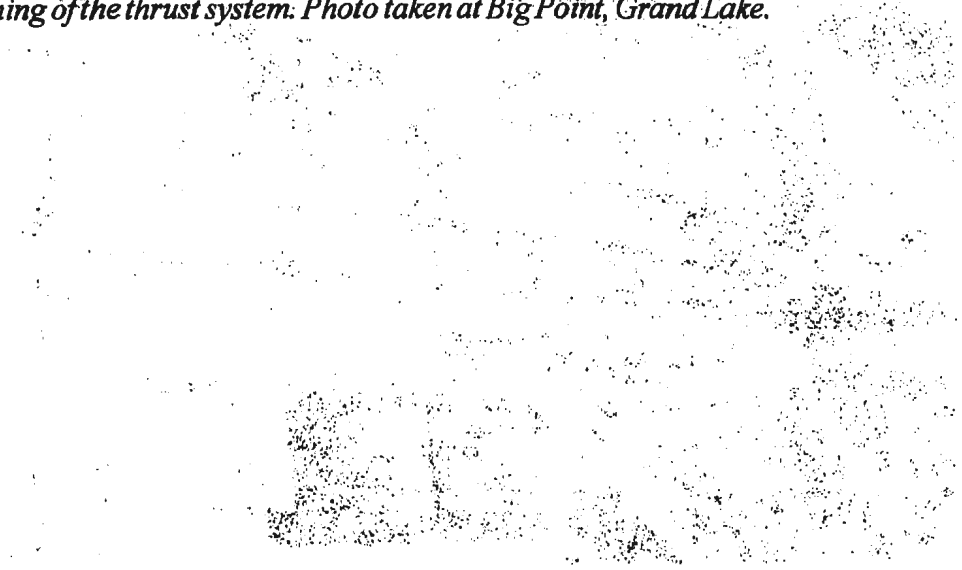

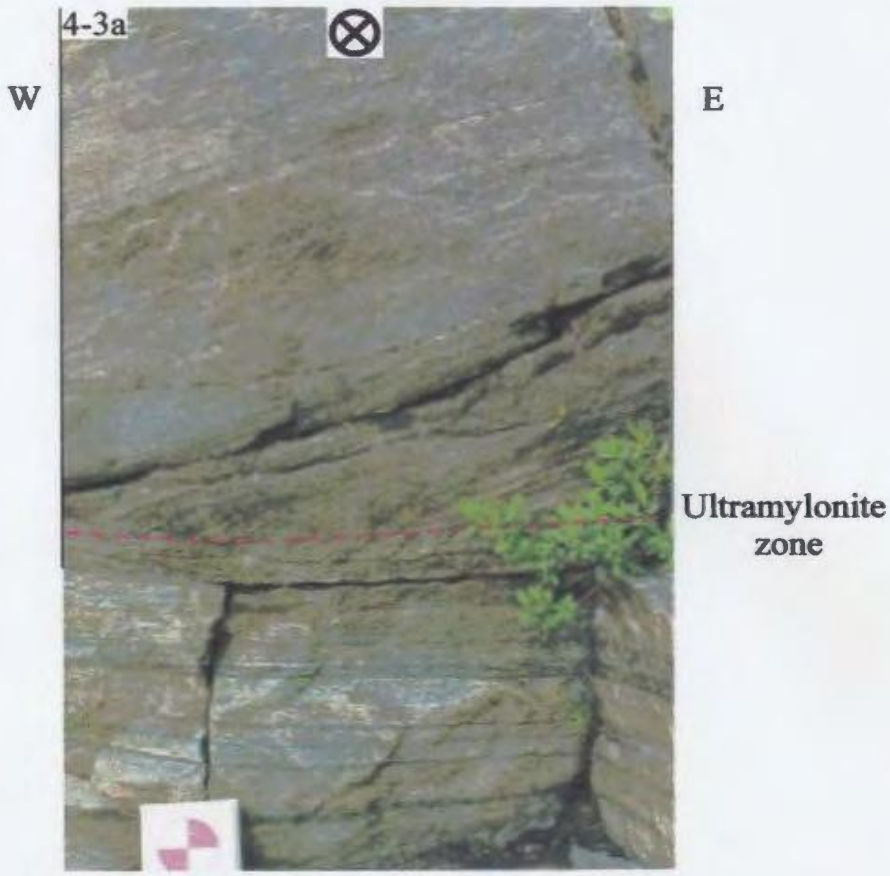

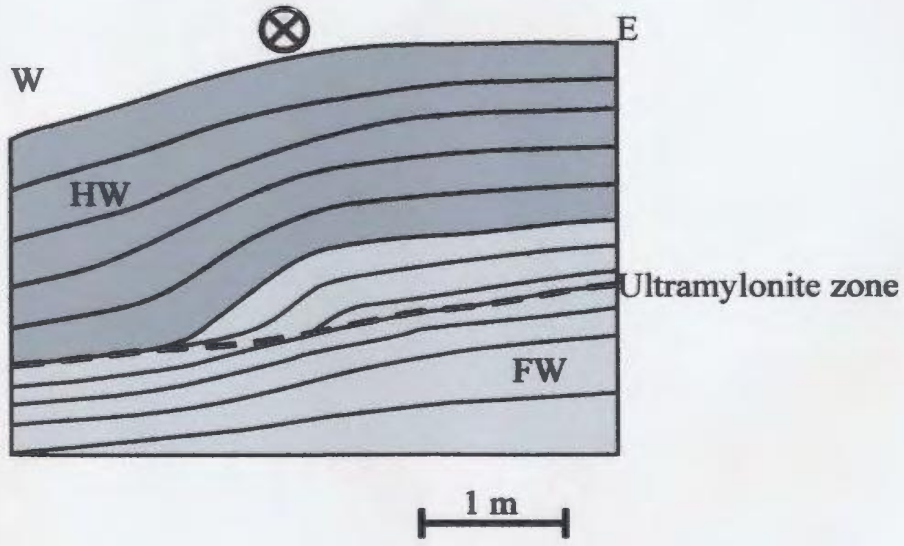

***Figure 4-3b**: Schematic diagram showing the configuration of the discontinuity in Figure 4-3. Note that the mylonite forms by lateral propagation of the thrust system. Looking north.*

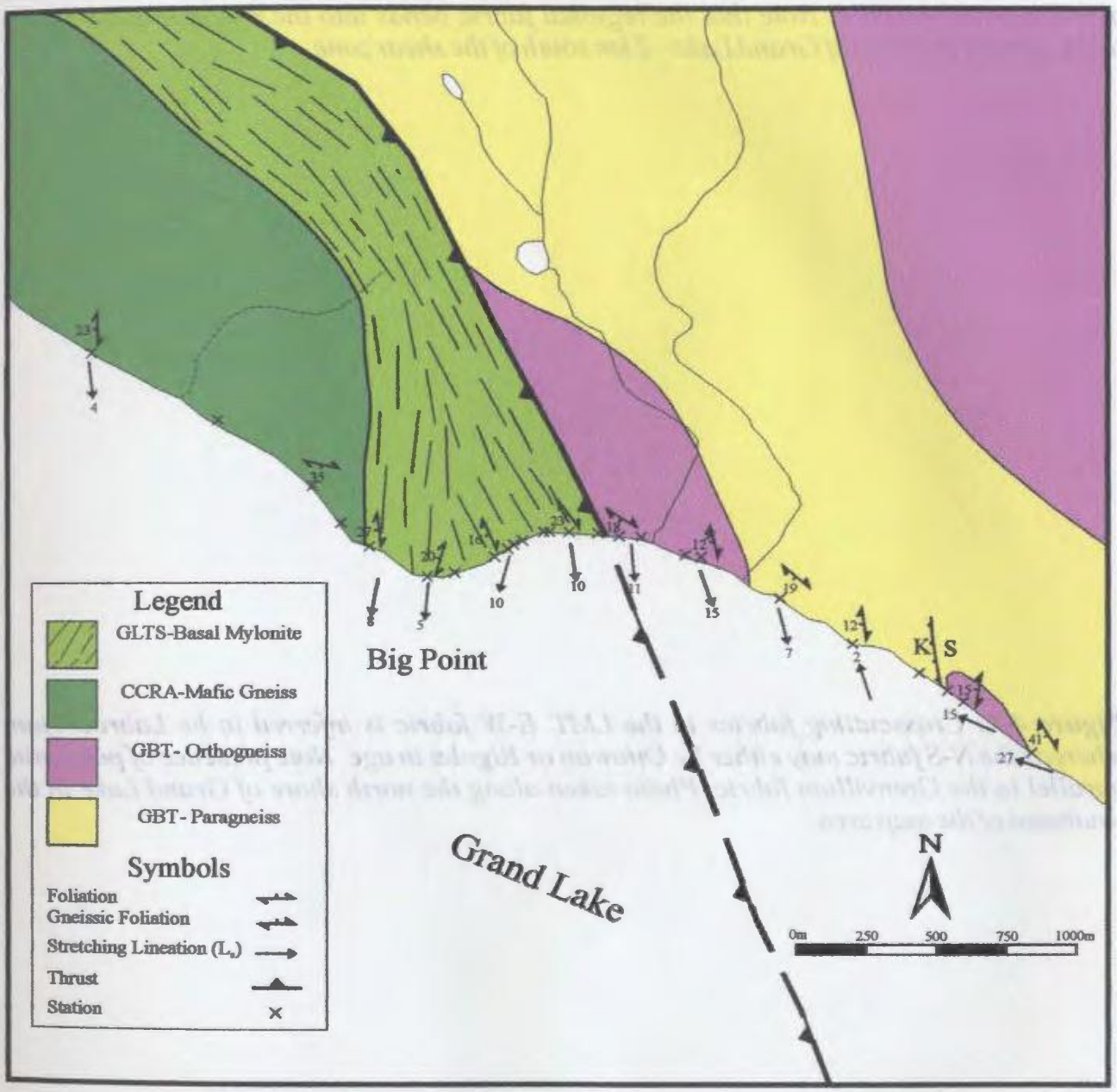

***Figure 4-4**: Enlargement of part of Figure 3-1 showing details of the shear zone exposed at Big Point. Note the variable orientation of the foliation in the footwall suggesting that it was heterogeneously reworked during emplacement of the CCRA. The range of orientations of the L_s is characteristic of the GLTS.*

***Figure 4-5**: Photo of a thin mylonite zone (centimetre grid for scale) preserved in the orthogneiss of the GBT. Note that the regional fabric bends into the mylonite zone. Photo taken along the shores of Grand Lake ~2 km south of the shear zone.*

***Figure 4-6**: Crosscutting fabrics in the LMT. E-W fabric is inferred to be Labradorian, whereas the N-S fabric may either be Ottawan or Rigolet in age. Note presence of pegmatite parallel to the Grenvillian fabric. Photo taken along the north shore of Grand Lake in the southeast of the map area.*

4-5

4-6

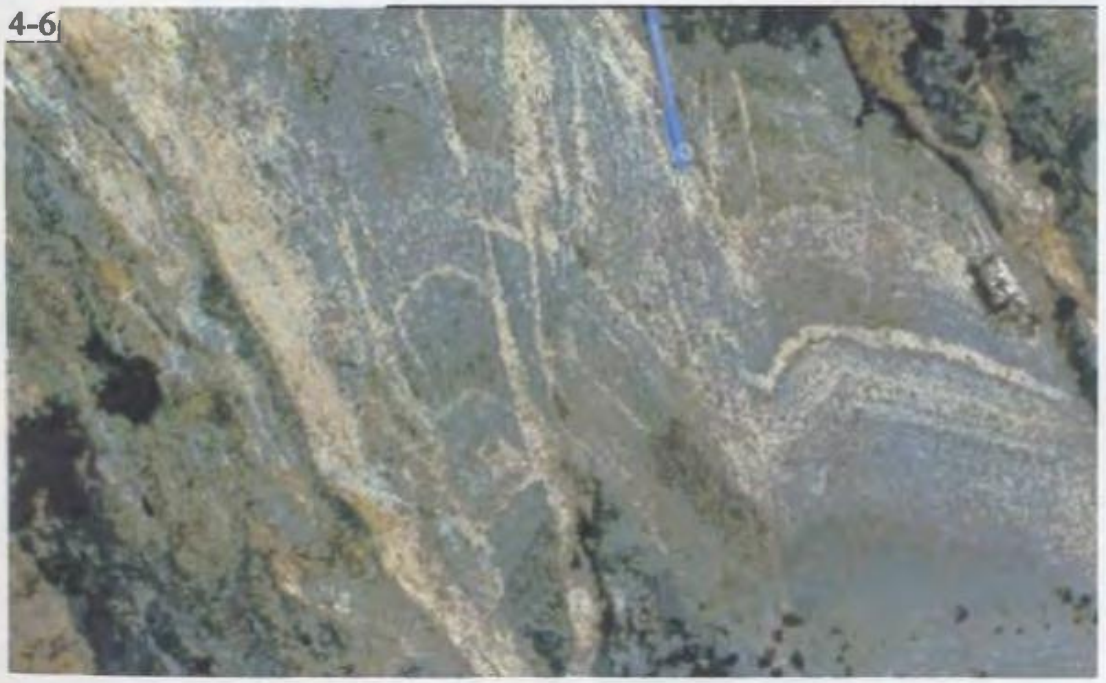

***Figure 4-7**: Cross-cutting shear zone fabric in the LMT. Similar to Figure 4-6, E-W fabric is inferred to be Labradorian and N-S fabric is inferred to be Grenvillian and has been dated at ~1044 Ma (Krogh 1986). Note also the presence of porphyroclasts of disaggregated pegmatite parallel to the Ottawan fabric (compare to Figure 4-6).*

4-7

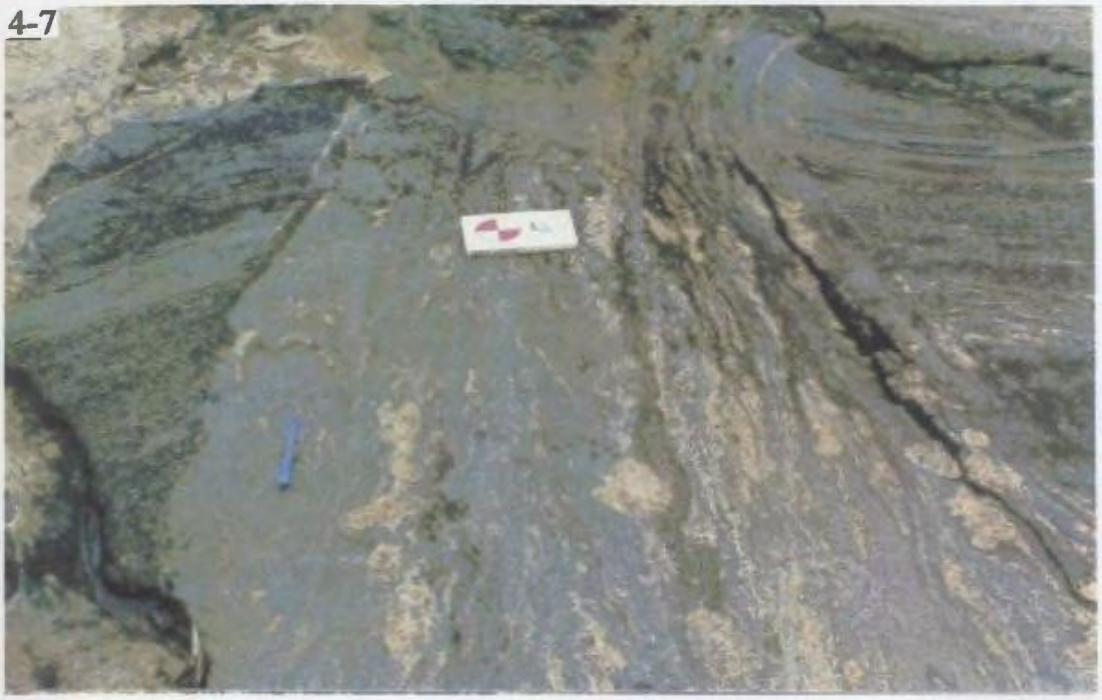

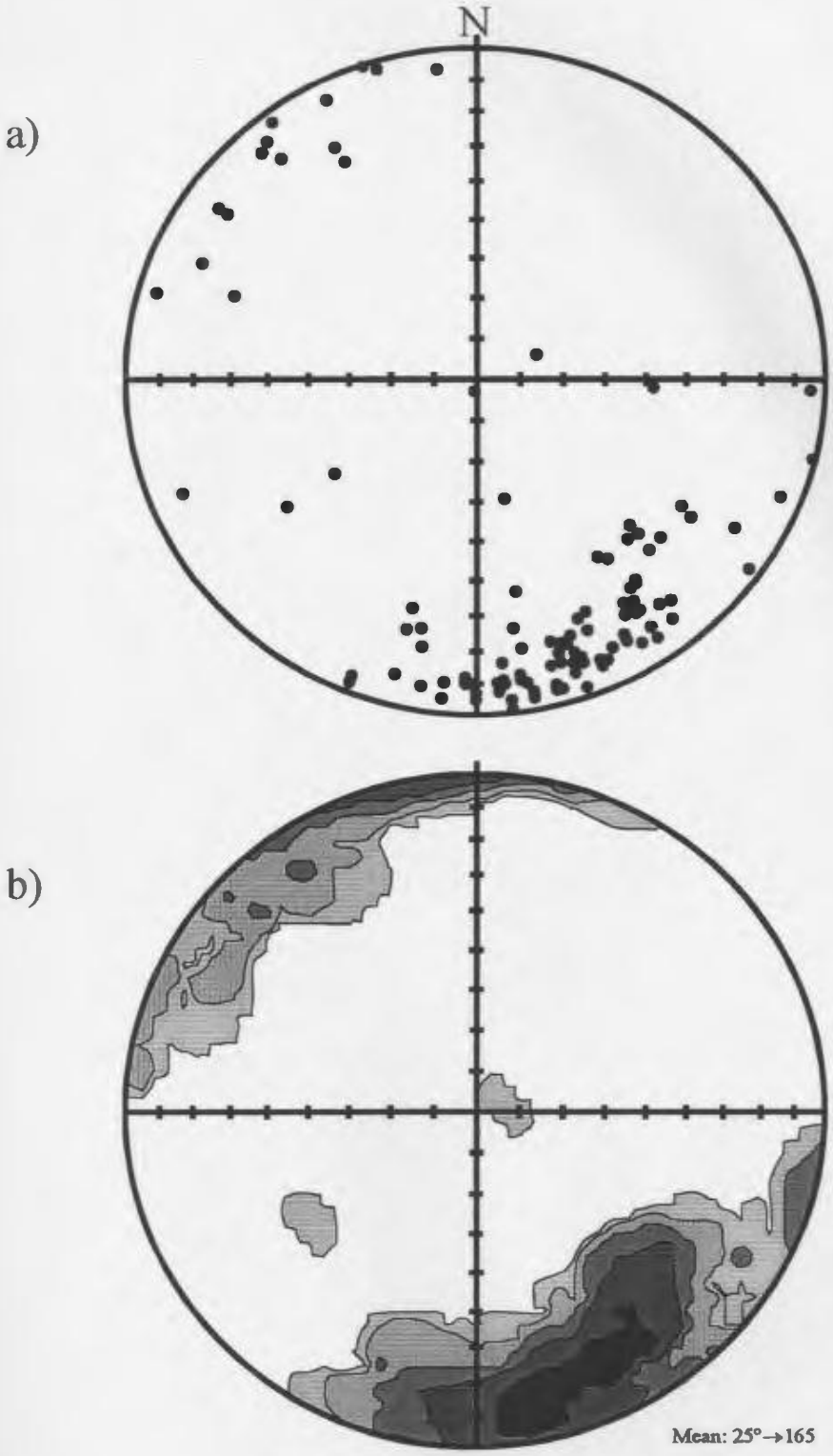

***Figure 4-8**: Lower hemisphere equal-area stereoprojections of stretching lineation data from the Goose Bay area. a) displays the individual data points and b) shows the same data contoured. The calculated mean L_x is 25°→165.*

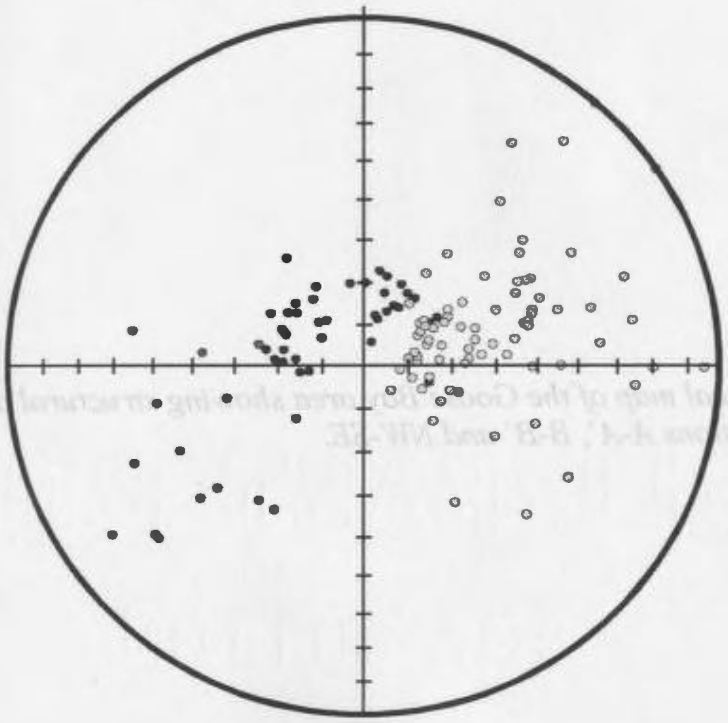

***Figure 4-9**: Lower-hemisphere equal-area stereoprojection of poles to the planes of foliation from the Goose Bay area. Dark grey dots are from the west limb of the synform, light grey dots are from the east limb and black dots are from the hinge. See text for discussion.*

***Figure 4-10**: Geological map of the Goose Bay area showing structural data and the locations of cross-sections A-A', B-B' and NW-SE.*

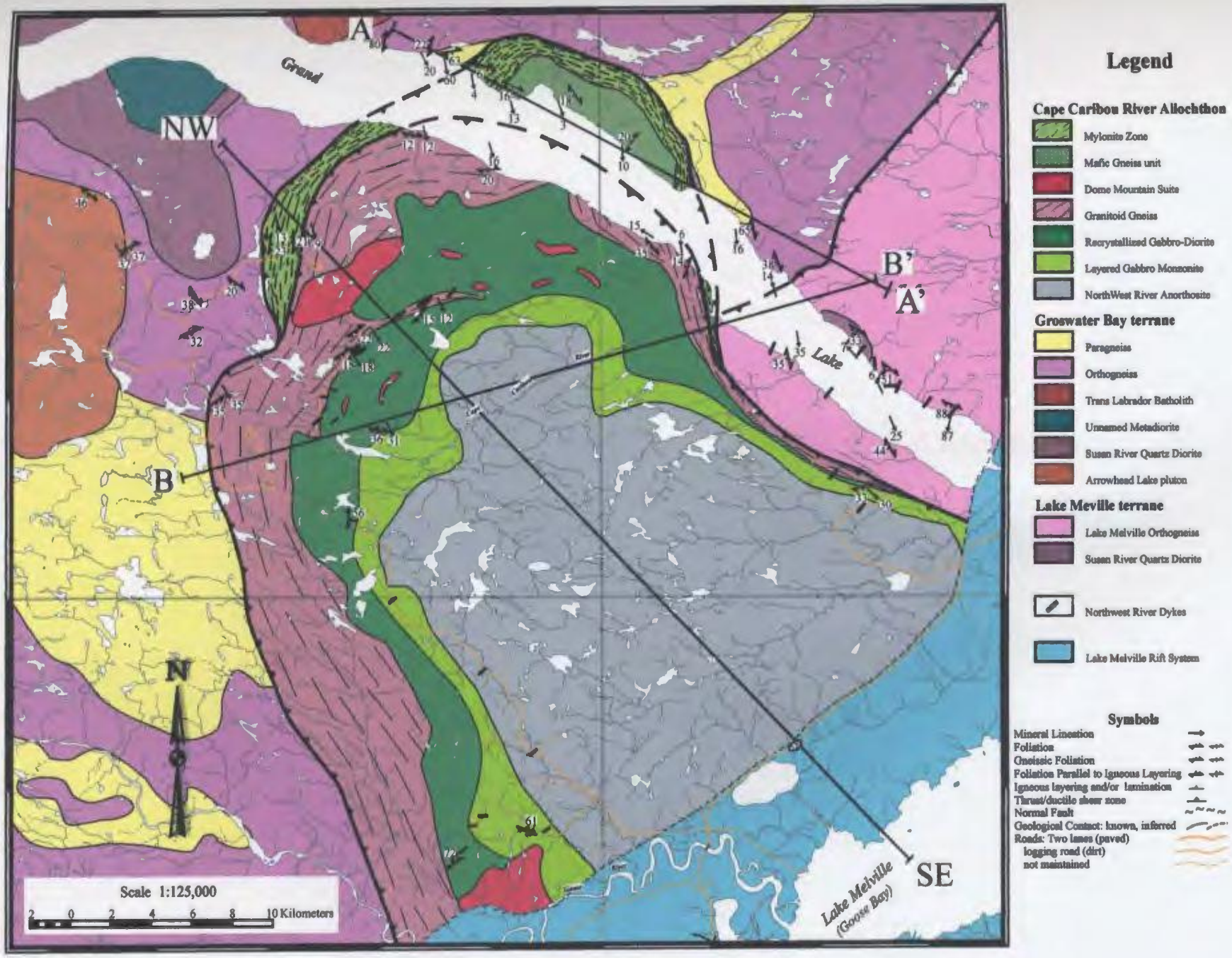
A
A'
B
B'
NW
SE
Grand
Lake
Lake Melville
(Goose Bay)
N
Scale 1:125,000
2 0 2 4 6 8 10 Kilometers
Legend
Cape Caribou River Allochthon
Mylonite Zone
Mafic Gneiss unit
Dome Mountain Suite
Granitoid Gneiss
Recrystallized Gabbro-Diorite
Layered Gabbro Monzonite
NorthWest River Anorthosite
Groswater Bay terrane
Paragneiss
Orthogneiss
Trans Labrador Batholith
Unnamed Metadiorite
Susan River Quartz Diorite
Arrowhead Lake pluton
Lake Meville terrane
Lake Melville Orthogneiss
Susan River Quartz Diorite
Northwest River Dykes
Lake Melville Rift System
Symbols
Mineral Lineation
Foliation
Gneissic Foliation
Foliation Parallel to Igneous Layering
Igneous layering and/or lamination
Thrust/ductile shear zone
Normal Fault
Geological Contact: known, inferred
Roads: Two lanes (paved)
logging road (dirt)
not maintained

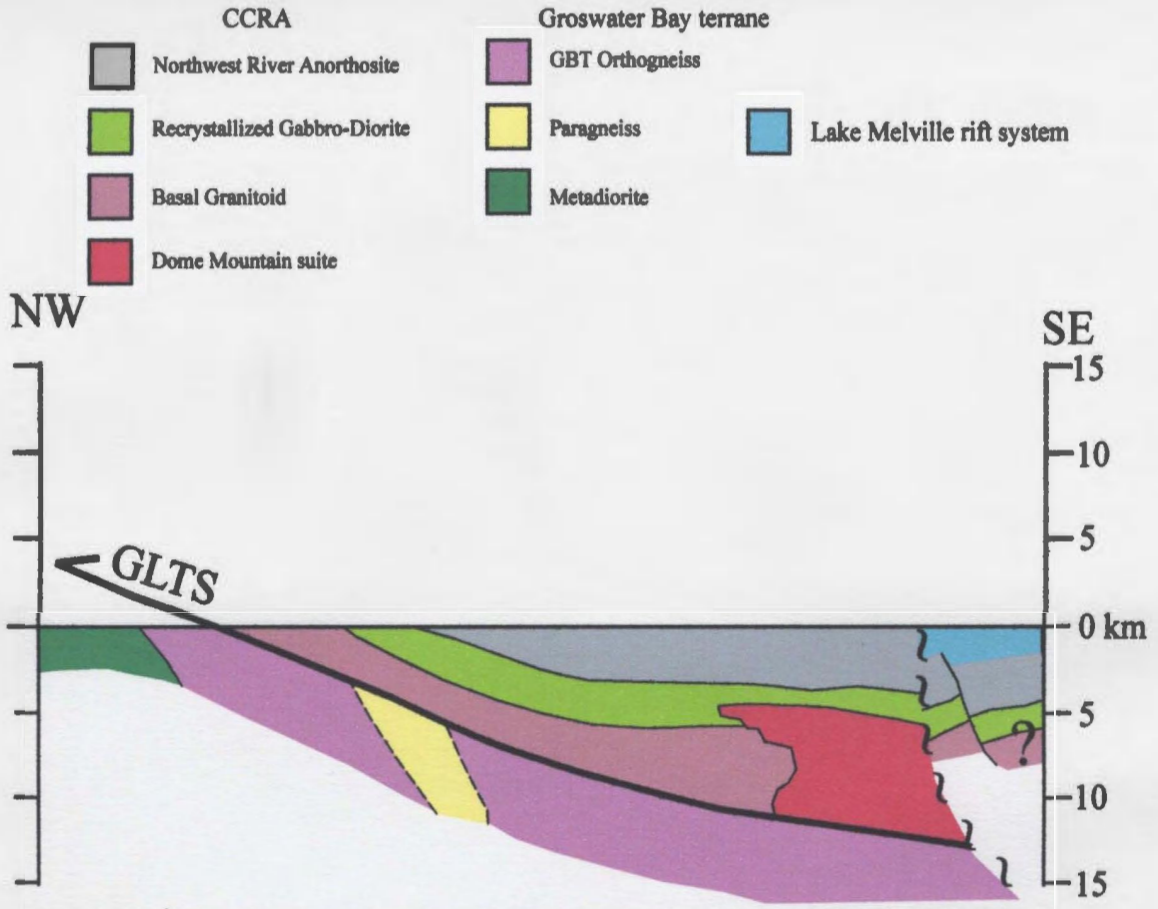

***Figure 4-11**: Cross section through the core of the Cape Caribou River Allochthon drawn parallel to the direction of the mean elongation lineation. Modified after Wardle et al. (1990a). See text for discussion.*

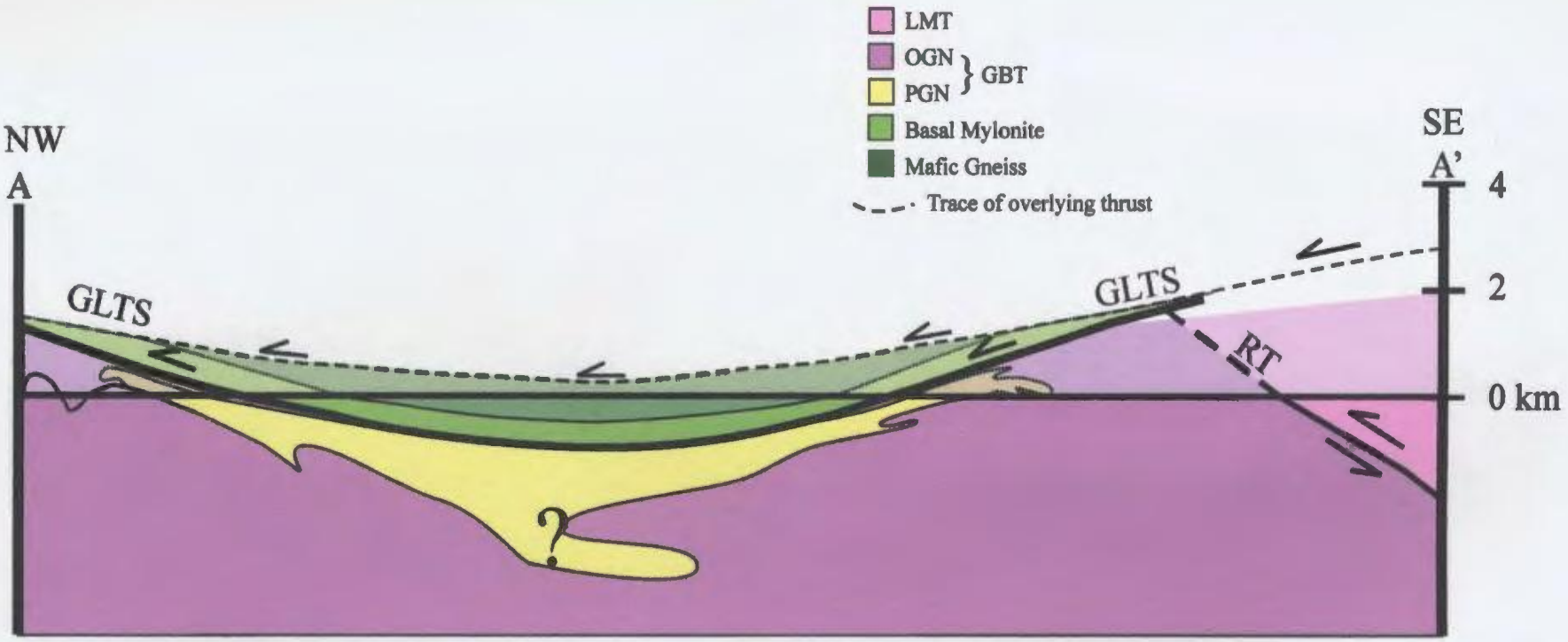

***Figure 4-12**: Cross-section drawn through the shear zone exposed on the northern shore of Grand Lake. The overlying units of the CCRA cannot be projected onto the section because of the lack of lines of projection (e.g., cylindrical folds) and the thickness of the units do not remain constant. Scale is 1:125,000, no vertical exaggeration. RT: Rigolet thrust, GLTS: Grand Lake thrust system.*

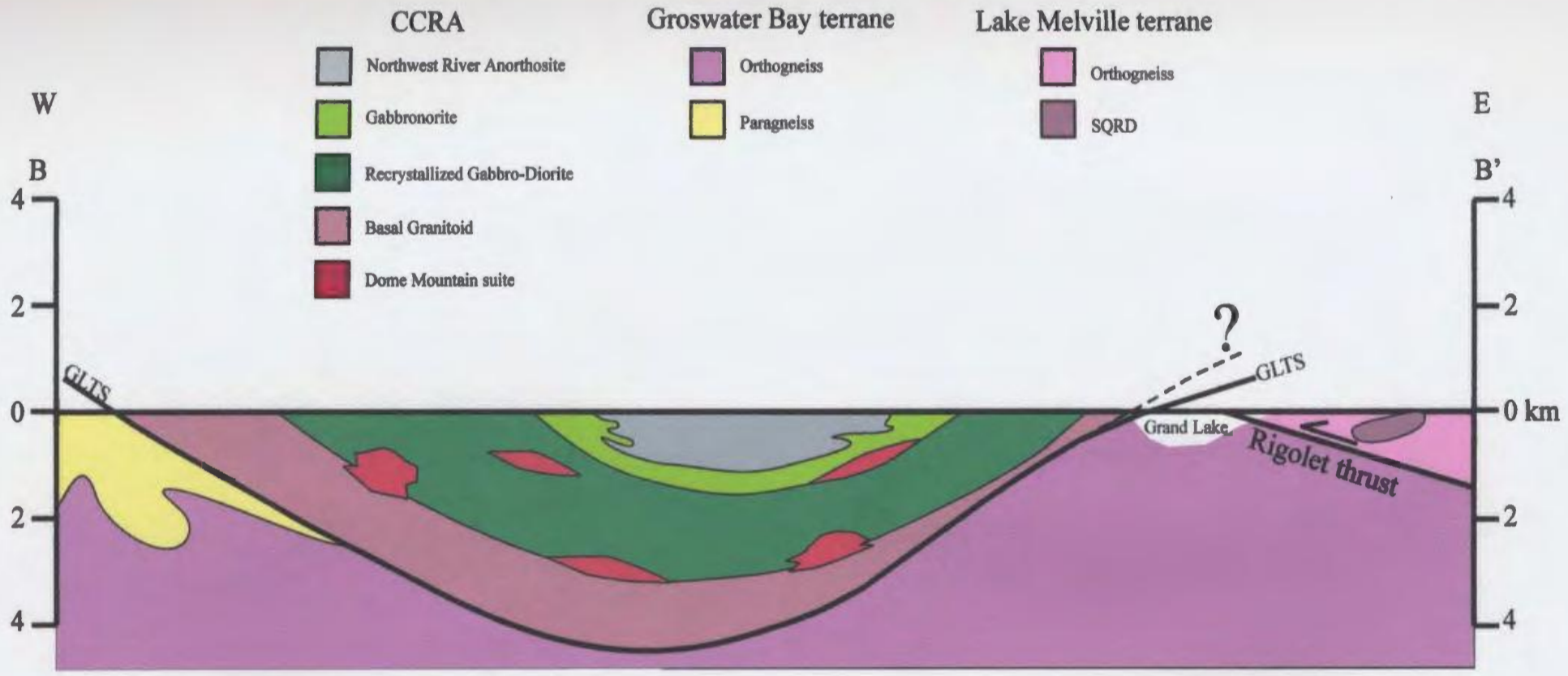

Figure 4-13: *Cross-section perpendicular to the mean stretching lineation, looking north up thrust direction, showing the asymmetrical synformal shape of the allochthon. Scale is 1:125,000, no vertical exaggeration. SQRD: Susan River quartz diorite*

Chapter 5

The Northwest River Dykes

5.1 Introduction

The Northwest River dykes, first described by Ryan et al. (1982) and subsequently by Wardle and Ash (1984, 1986), are a minor but important component of the Cape Caribou River Allochthon (CCRA) and the Lake Melville terrane (LMT). They have a special significane for this study, as in contrast to theor host rocks, they are inferred to be monocyclic (see Below) and thus should provide a clear record of Grenvillain metamorphism and deformation.

The Northwest River dykes outcrop in all levels of the CCRA and also occur in the LMT along the shores of Grand Lake. The dykes crosscut Labradorian fabrics and many retain igneous features such as chilled margins, plagioclase phenocrysts and igneous fabrics. Others were deformed in Grenvillian high strain zones or underwent a static Grenvillian metamorphic overprint (Wardle and Ash 1984, 1986; this study). The Northwest River dykes have not been precisely dated. Their age is constrained from field relations to be late to post Labradorian and pre-Grenvillian. Wardle et al. (1990a) postulated that the most likely correlatable dyke suite was the Mealy dykes in the Mealy Mountains terrane (MMT) described by Emslie (1976). Based on the field descriptions of the Mealy dykes (Emslie 1976; Emslie et al. 1984) and the Northwest River dykes (Wardle and Ash 1984, 1986; this

study), it is clear that the two suites have a similar northeast trend and also share many other field characteristics (see below). The locations of the Mealy dykes and Northwest River dykes are shown in Figure 5-1, and the common trend is apparent. Recent field studies by Corrigan et al. (2000) in the LMT in the Rigolet area have also documented dykes with similar characteristics to the Northwest River dykes in the LMT near Goose Bay which they also correlated with the Mealy dykes.

Although the Northwest River dykes in the CCRA and the LMT have not been directly dated, the Mealy dykes have been dated using K/Ar, Ar/Ar, Rb/Sr and more recently U-Pb system. These ages are summarized in Table 5-1. The currently accepted time of emplacement of the Mealy dykes is given by the U-Pb baddeleyite age of 1250 ± 2 Ma (Hamilton and Emslie 1997). Attempts to date the emplacement age of the Northwest River dykes have not been successful. Bussy et al. (1995) obtained a U-Pb age of 1011 ± 3 Ma that is interpreted to be the age of metamorphic zircon growth (Table 5-1). In the remainder of this chapter, the textural and chemical evidence for correlation of the Mealy dykes and the Northwest River dyke swarms is evaluated.

Sample	*Age (Ma)*	*Method*	*Reference*	*Interpretation*
EC75-149	955 ± 27	K-Ar (Bt)	Emslie et al. 1984	1
EC75-35	964 ± 21	K-Ar (Bt)	Emslie et al. 1984	1
P7-098	1078 ± 48	K-Ar (WR)	Gittins 1972	2
P7-099	1123 ± 50	K-Ar (Bt)	Gittins 1972	2
16R	1215 ± 10	Ar-Ar (Hbl)	Reynolds 1989	3
FA-744804	1222 ± 101	K-Ar (WR)	Fahrig and Loveridge 1981	3
18R	1230 ± 8	Ar-Ar (Hbl)	Reynolds 1989	3
-	1250 ± 2	U-Pb (Bdl)	Hamilton and Emslie 1997	4
7 samples	1380 ± 54	Rb-Sr (WR)	Emslie et al. 1984	5
C-050D	1011 ± 3	U-Pb (Zrn)	Bussy et al. 1995	6

***Table 5-1**: Summary of ages for the Mealy and Northwest River dykes. Interpretation of age data: 1 = post metamorphic cooling age; 2 = excess argon?; 3 = post intrusion cooling age; 4 = U-Pb age of intrusion; 5 = Rb-Sr errorchron; 6 = U-Pb age of metamorphism. Uncertainties for Reynolds data are 1σ, all others are 2σ. Abbreviations in brackets: Bt=analysis only on biotite; WR=whole rock analysis; Hbl=analysis only on hornblende: Zrn = zircon: Bdl = baddeleyite.*

5.2 Petrography of the dyke suites

5.2.1 Mealy Dykes

Emslie et al. (1984) described the Mealy dykes as mainly subophitic olivine diabase with microphenocrysts of olivine, clinopyroxene, orthopyroxene and plagioclase. Olivine is usually fresh and may have igneous reaction rims of orthopyroxene indicating that the peritectic reaction took place on cooling. Plagioclase is normally zoned and charged with fine-grained Fe-Ti oxides. Clinopyroxene and/or orthopyroxene form the intercumulate phases and may contain many fine-grained inclusions of Fe-Ti oxides. Amphibole occurs as narrow rims on clinopyroxene in few samples. Biotite is present also in the dykes but is

notably a late crystallizing phase. Accessory phases present in the Mealy dykes include apatite, magnetite, ilmenite and rare dark green spinel. Pyroxene charged with inclusions of Fe-Ti oxides locally replaces olivine, which may also have rims of pyroxene.

Many of the Mealy dykes in the MMIS are not metamorphosed as no reaction between plagioclase and olivine is reported (Emslie, 1976) despite some minor thermal resetting (see Table 5-1). Chilled margins are preserved in dykes that are 1cm to 60m wide.. The dykes are typically fine-grained but may contain rare phenocrysts of plagioclase readily visible on the outcrop scale and the thicker dykes may contain pegmatitic patches in their cores.

5.2.2 Northwest River Dykes

Most of the dykes are found within the CCRA but a few dykes also outcrop on the shores of Grand Lake in the Lake Melville terrane. The following sections include brief petrographic of the dykes occurring in the LMT and CCRA, with those within the CCRA being discussed with respect to their location within the allochthon and the metamorphism of the host rocks.

5.2.2.1 Lake Melville terrane

Northwest River dykes in the LMT are principally composed of the assemblage hornblende-biotite-plagioclase-quartz±garnet±orthopyroxene±clinopyroxene with tremolite and calcite occurring as retrograde phases. Accessory phases include magnetite-ilmenite, apatite and zircon. All of the dykes in the LMT have been recrystallized to metamorphic assemblages and a mild foliation is present in some samples. The overall grade of the dyke

samples is amphibolite facies (Opx generally not present) with remnants of an earlier two-pyroxene granulite-facies event with local melt patches.

5.2.2.2 Cape Caribou River Allochthon

The dykes sampled from the lower parts of the CCRA, including the recrystallized gabbro-diorite facies layer and the basal gneiss unit are variably deformed and recrystallized, containing the metamorphic assemblage hornblende-plagioclase-garnet±clinopyroxene ±orthopyroxene ±quartz with Fe-Ti oxides and apatite as accessory phases. All of the dykes are fine-grained and may preserve plagioclase "phenocrysts" which on inspection under the microscope are generally resolved as recrystallized plagioclase aggregates. However, rare examples of relict plagioclase may be found in thin section. These crystals still partially maintain the original lath shapes, twinning and zoning but contain fine-grained spinel inclusions that occur along oscillatory zoning domains that are likely a result of changing melt composition during dyke emplacement. In more pervasively recrystallized examples, plagioclase consists of untwinned, polygonal shaped subgrains that may be normal zoned.

The Northwest River dykes that occur in the upper parts of the allochthon tend to be less strongly deformed and retain more of their igneous textures with a variable static metamorphic overprint. The igneous assemblage includes plagioclase-orthopyroxene-clinopyroxene±olivine and Fe-Ti oxides, with the effects of metamorphism being recorded as coronitic textures. Metamorphic minerals that overprint the igneous assemblage include orthopyroxene-clinopyroxene-biotite-amphibole-plagioclase ± garnet.

Igneous textures preserved in this part of the suite include ophitic to subophitic textures with randomly oriented grains and aggregates of spinel charged, lath-shaped

plagioclase phenocrysts enveloped in pyroxene. As mentioned above the presence of spinel inclusions in plagioclase is inferred to be an igneous feature. Where deformation and hydration were pervasive, the pyroxenes are largely replaced by amphibole. Despite metamorphic recrystallization, relict igneous textures remain readily visible under the microscope and in hand specimen.

In summary, deformation of the Northwest River dykes correlates closely with the inferred Grenvillian strain in the host rocks, being greater in the basal, high-strain part of the allochthon and diminishing up-section away from the GLTS. Metamorphic recrystallization is likewise very variable, but there is evidence that some of the dykes have undergone a granulite-facies event that led to reactions between olivine (and/or pyroxene) and plagioclase to form pyroxene and garnet assemblages, and there is also local evidence for partial melting in the form of tonalitic leucosomes. Later hydration led to the formation of amphibolite-facies assemblages in some of the dykes. Nonetheless, despite its heterogeneous distribution, there is no doubt that the dykes preserve evidence for a high-grade, presumably Grenvillian, metamorphic event and that they were penetratively deformed in the vicinity of the GLTS.

5.3 Geochemistry

Whole rock geochemistry of fifteen samples of the Mealy dykes was published in Emslie et al. (1984) and extended trace element data for the Mealy dykes were provided by Ashwal et al. (1986). In order to compare the Northwest River dykes with published analyses of the Mealy dykes, whole rock geochemical analyses of the Northwest River dykes was performed at the XRF facilities in the Earth Sciences Department, Memorial University of

Newfoundland.

Samples were first pulverized in the crushing facilities at MUN. A mixture of the powdered sample (5.00 g) and phenolic resin (0.70 g) (BRP-5933 Bakelite phenolic resin) was mixed thoroughly for 3-5 minutes for homogeneity. This mixture was then pressed into a Herzog pellet press for 5 seconds at 20 tons. The resulting pellets were then baked at 200°C for 15 minutes. XRF-elemental analysis was carried out on a Fisons/ARL 8420+ sequential wavelength dispersive X-ray spectrometer. Detection limits on pressed pellets range from 0.7 ppm (Nb) to 41 ppm (Ce) with an approximate precision around 0.2% to 3.1%. Analytical results are given in the appendix.

5.3.1 Results

5.3.1.1 Major Element Geochemistry

The Northwest River dykes have been variably metamorphosed during the Grenvillian orogenesis and subsequently their major element chemistry cannot be assumed to have been completely unaffected during metamorphism. Alkalis including Na_2O, K_2O and CaO may have been mobilized during metamorphism and are thus unreliable for use in discriminatory geochemical plots derived from the major oxide data. Comparisons of the remaining available major oxide data between the Northwest River dykes and the Mealy dykes are presented in Figure 5-2. Major differences are evident in the SiO_2 and Al_2O_3 wt% contents, with the Mealy Dykes being more enriched in these oxides. This difference may be explained by plagioclase accumulation, which would be consistent with observations of phenocrysts of plagioclase within both dykes suites. However, average Ca and Na contents

of the two suites overlap, which is not compatible with significant differential accumulation.

Figures 5-3a and 5-3b display the tholeiitic character of the dyke suite, which appears especially pronounced in Figure 5-3b. The data for the Mealy and Northwest River dykes fall well within the tholeiite field. The few outliers (122, 177a and 75-35) are assumed to represent hybrid compositions formed by contamination during intrusion. Special attention was paid to the data for these samples in later plots. The significance of the Nb values for the dykes displayed in Figures 5-3a and 5-3b is explained below.

Major element plots, although useful for basalt discrimination, cannot conclusively prove an association so additional plots using trace elements are presented. The relative immobility of certain trace elements during metamorphism provides more confidence in the comparison.

5.3.1.2 Trace Element Geochemistry

Concentrations of trace elements, especially relatively immobile elements such as the rare earth elements (REE), Sc, Y, Th, Zr, Hf, Ti, Nb, Ta and P, should not have been radically altered during metamorphism and therefore should reflect the true nature of the igneous 'provenance' for the suites. Applying this assumption to the Northwest River dykes, plots in Figures 5-4 to 5-6 involve the immobile trace elements and the ratio of FeO*/MgO where all iron is calculated as FeO (= FeO*). Scatter in these types of diagrams is mainly due to fractionation within the dyke suite. Due to the limitations associated with the Mealy Dyke data, some of the plots do not fully represent the Mealy suite. Figure 5-4a displays the subalkaline nature of the Northwest River dykes and Figure 5-4b displays the tendency of the Northwest River dykes to plot in the volcanic arc basalt field. Data for the Mealy dykes are

based on three samples and which are plotted as a field. The Mealy dykes are more enriched in Y (Figure 5-5) but have comparable Zr and Ti abundances. The Mealy dykes show scatter in the Y data for the suite whereas the Mealy dykes form a group in the within-plate basalt field. Gower et al. (1990) assumed the variability in Y values was a function of dyke magmatism progressively farther from the cratonic margin and reflected progressively younger magmatism towards the north. The data for the Northwest River dykes data from the CCRA cluster within the within-plate basalt field, and overlap with some of the Mealy dykes. However the spread of Y concentrations for the Mealy dykes is very large suggesting local contamination and/or an analytical problem.

In all of the diagrams involving the trace elements, symbols or fields are used to discriminate between sub-suites within the Northwest River dyke suite. Subdivisions of the Northwest River dyke data are based upon sorted Nb ranges (<10 ppm, 10-15 ppm, >15 ppm) which allow for the distinction of sub-suite fractionation trends within the entire suite. The high Nb group is further sorted into moderately high Nb (15-20 ppm) and high Nb (>20 ppm) to show the extent of fractionation in the sub-suites. Linear trends extrapolated from the scatter are consistent for these groupings across plots of FeO*/MgO versus P_2O_5, Nb, Y and Zr shown in Figures 5-6a to5-6d. The same trends are also readily extrapolated in Figures 5-6e to 5-6g. Note the linear trends within the subgroups of the data, especially within the middle Nb range (10-15 ppm). It is from these linear trends within the subgroups that individual fractionation trends can be seen and the differentiation of the whole suite into minor sub-suites may be made. These within-suite fractionation trends are inferred to be related to differing ages of intrusion from a single magmatic source. The more fractionated

samples (Nb >15 ppm) are inferred to be the youngest intrusions, whereas low Nb dykes are the most primitive are thus inferred to be the oldest in the suite. Without complete trace element data for the Mealy dykes, similar fractionation trends and sub-suite discriminations are not possible.

Note that some of these groupings based on Nb values also hold in major element plots (Figures 5-3a and 5-3b). Figure 5-3b specifically shows a linear trend and groupings of similar Nb ranges which shows that Ti fractionation must have been related to Nb fractionation and possibly also to fractionation of other trace elements such as Y.

The trace element list for the Mealy dykes is limited and thus limits the geochemical comparison between the dyke suites so no other definitive trace element plots can be produced. Despite these limitations, the available geochemical data are not incompatible with the interpretation of Wardle and Ash (1986) that the dyke suites are parts of the same dyke swarm. The consistency of linear trends and groupings in the plots support this conclusion.

5.4 Discussion

Without available igneous U-Pb ages for the Northwest River dykes, lithological, petrological and geochemical comparisons between the Northwest River and Mealy dyke suites and their host rocks are the only means to test the affinity of the two suites. Possible correlation between the Labradorian Northwest River Anorthosite and the MMIS has been discussed by Wardle et al. (1990a) who concluded that they were not compatible with a physical linkage at ~1640 Ma. Correlation of the Mealy and Northwest River dykes would imply that the physical link was retained until at least 1250 Ma, with the separation into two

terranes occurring during the Grenvillian orogenesis. In the study area, the age of the Northwest River dykes is principally constrained by field relationships which show that the dykes crosscut Labradorian fabrics and the evidence that they underwent Grenvillian metamorphism (discussed above and also sample C-050D of Bussy et al. 1995, Table 5-1). Additional evidence for linking the two suites comes from their similar SW trends, which in the case of the Northwest River suite is preserved despite significant burial and tectonic transport. Finally, as discussed above, the two suites appear to have essentially similar major and trave element geochemistry, despite a few minor differences.

In conclusion, the fabrics and mineral assemblages indicate that the Northwest River dykes are monocyclic with respect to Grenvillian metamorphism, and their trends and geochemistry support a common origin with the Mealy dykes. Although further work, including an in-depth analysis of trace elements from a larger sample population and precise U-Pb age dating, are required to fully establish the affinity of the two dyke suites, the available evidence all points to their common origin. Thus, until such work is done, the Northwest River dykes should be assumed to be the correlative with the Mealy dykes and thus to have been emplaced into the CCRA and LMT at ca.1250 Ma.

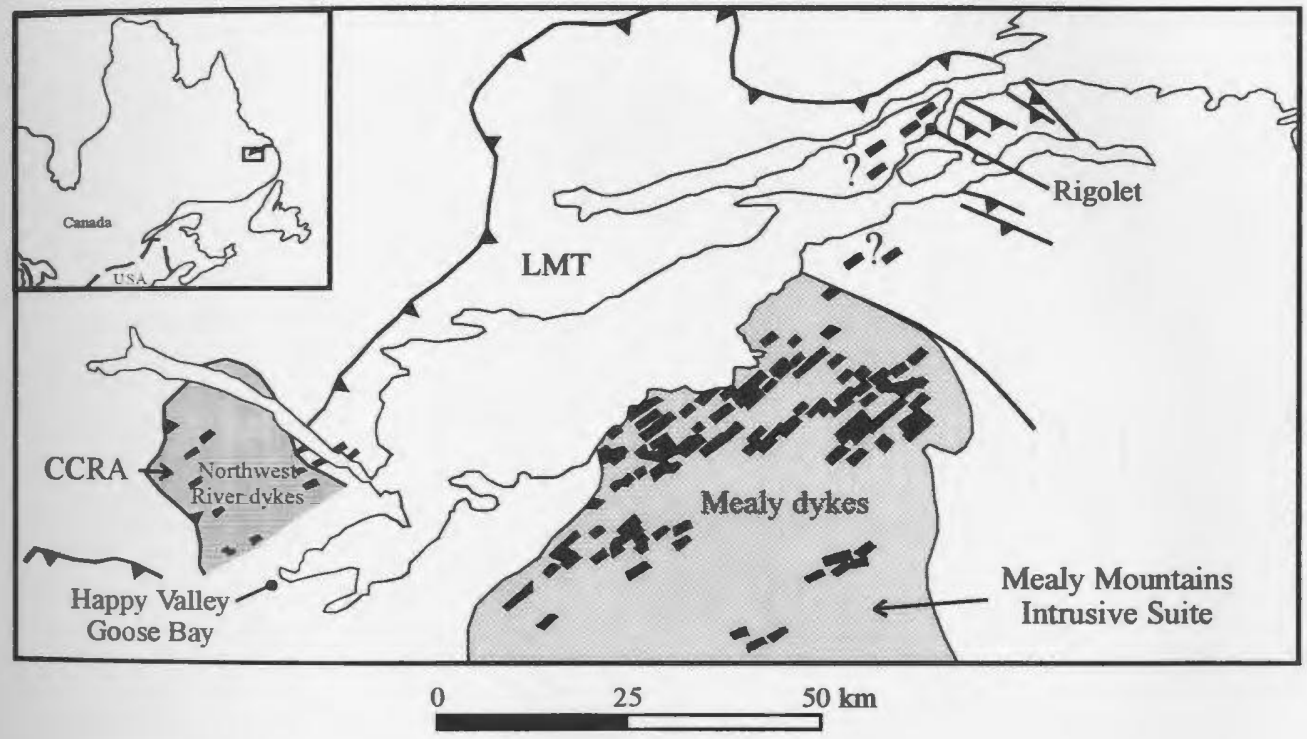

***Figure 5-1**: Distribution of the Mealy and Northwest River dykes. Note the presence of the dykes in the Lake Melville terrane in the west near the CCRA and in the east near the hamlet of Rigolet. The question marks regarding the Mealy dykes in the Rigolet area refer to the data of Corrigan et al. (2000) who do not discuss field relationships of this dyke swarm and the orientations of the dykes are not known. Diagram modified after Gower et al. 1990.*

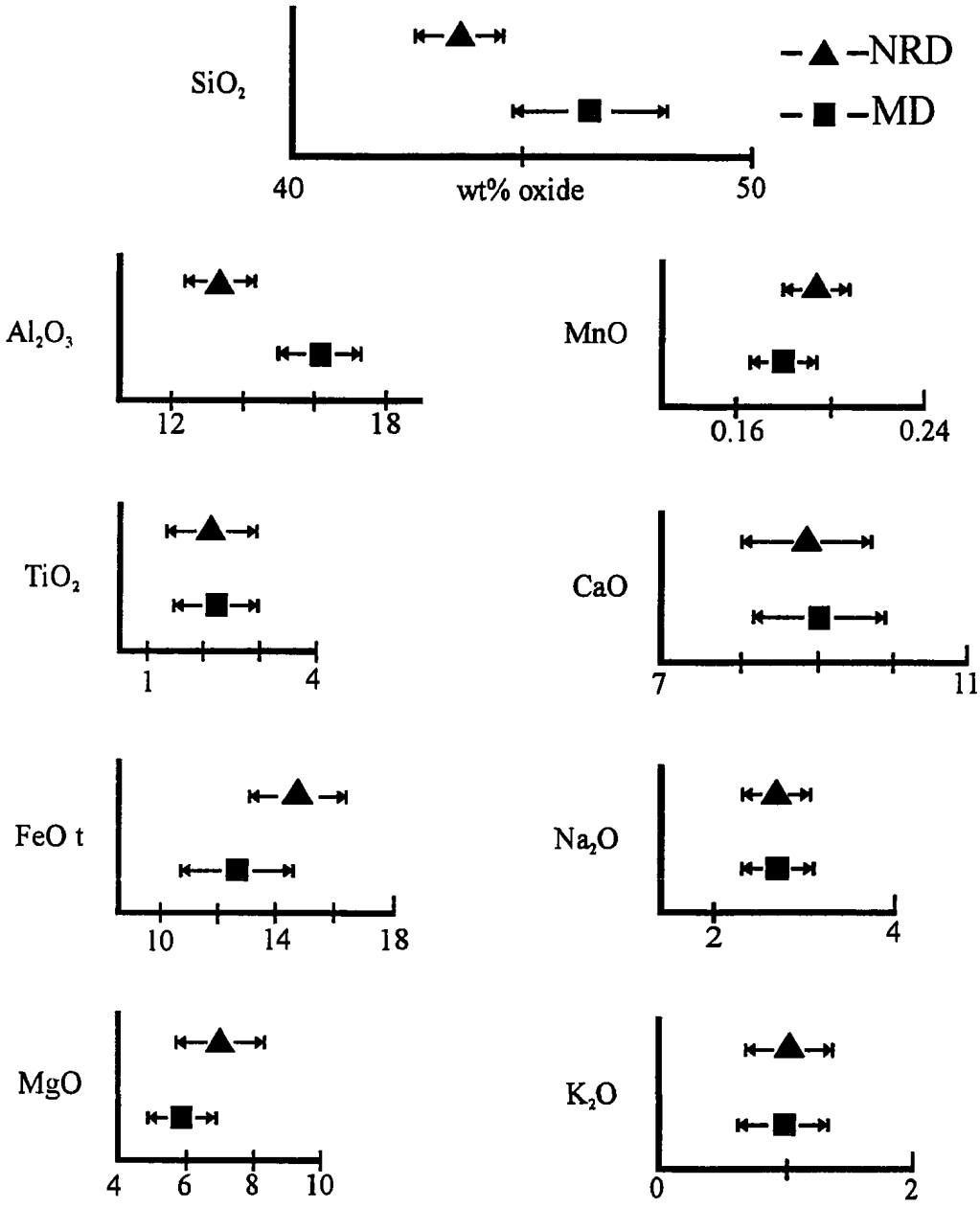

***Figure 5-2**: Comparison plots of the mean compositions and 1 σ standard deviations of the major oxides for the Northwest River (NRD) and Mealy dykes (MD). FeO t = FeO+Fe_2O_3.*

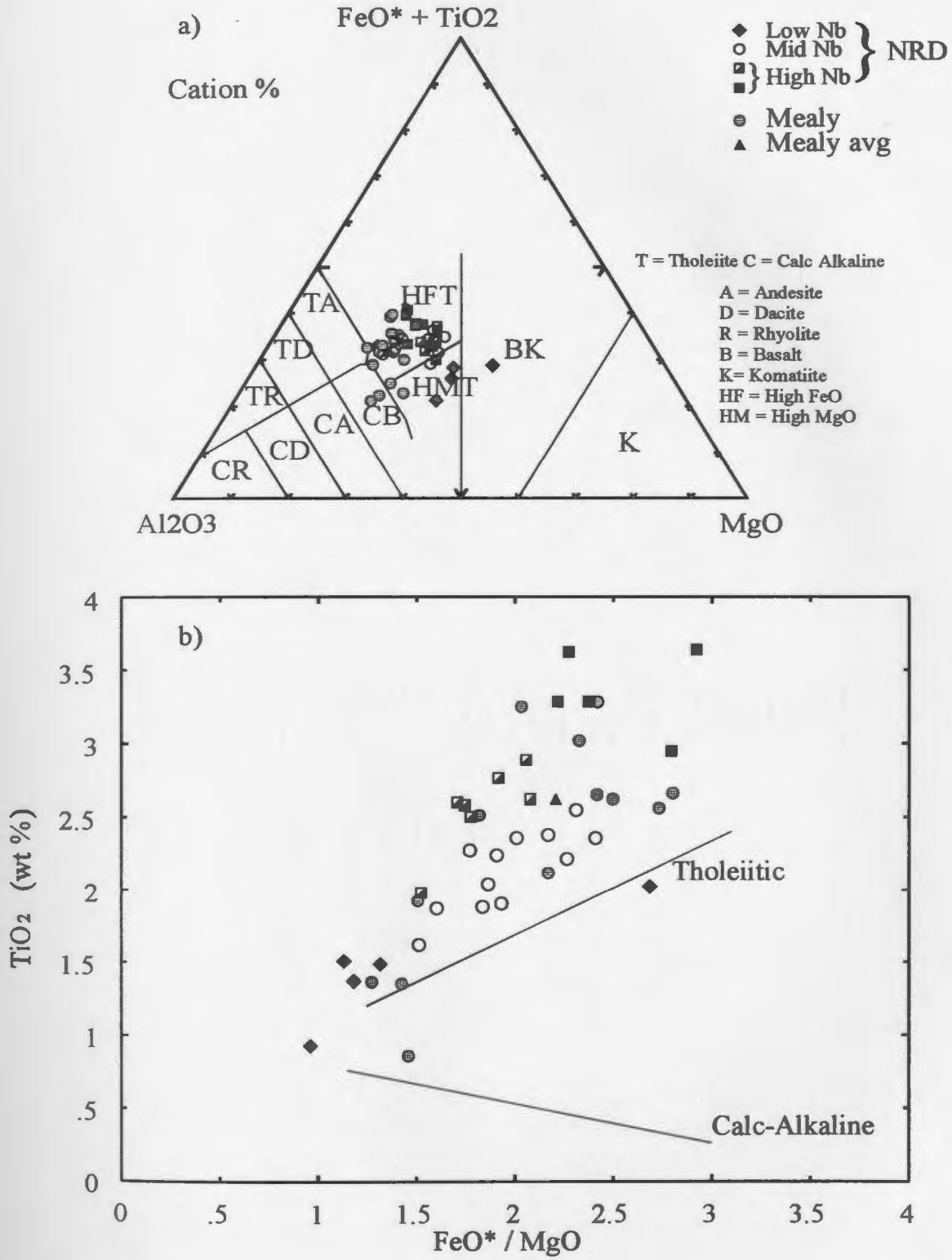

***Figure 5-3**: Major element diagrams for the Mealy and Northwest River dykes see text for discussion. a) Diagram displaying the high Mg-Fe tholeiitic character for the dyke suites, after Jensen (1976). b) Diagram displaying the tholeiitic character of the dyke suites after Miyashiro (1974).*

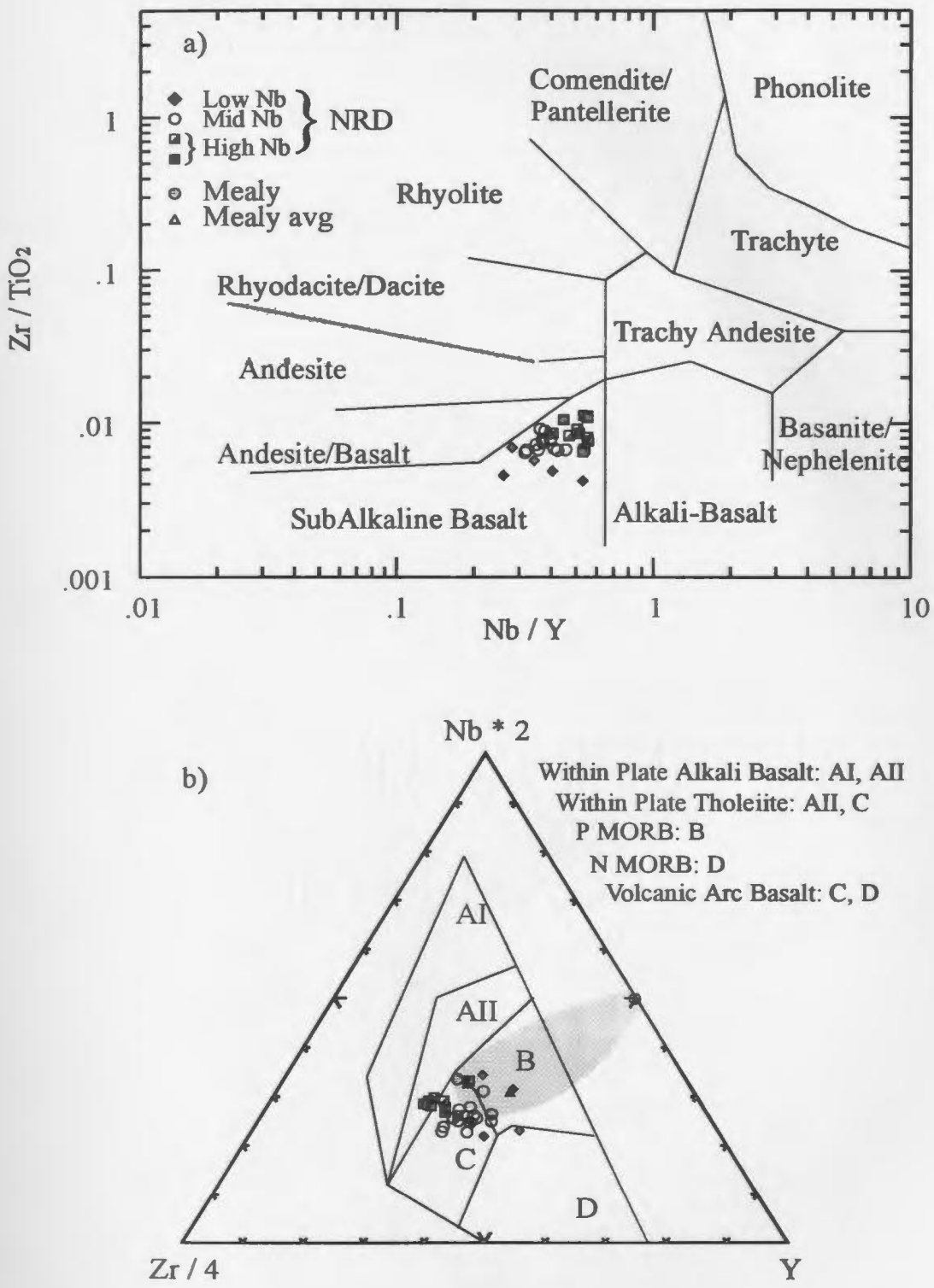

***Figure 5-4**: a) Trace element diagram displaying the subalkaline basalt nature of the dyke suites; after Winchester and Floyd (1977). b) Diagram for tectonic distinction of basalts showing the volcanic arc signature of the dyke suites; after Meschede (1986). The shaded area shows where the extent of the Mealy dyke data must lay based on available data.*

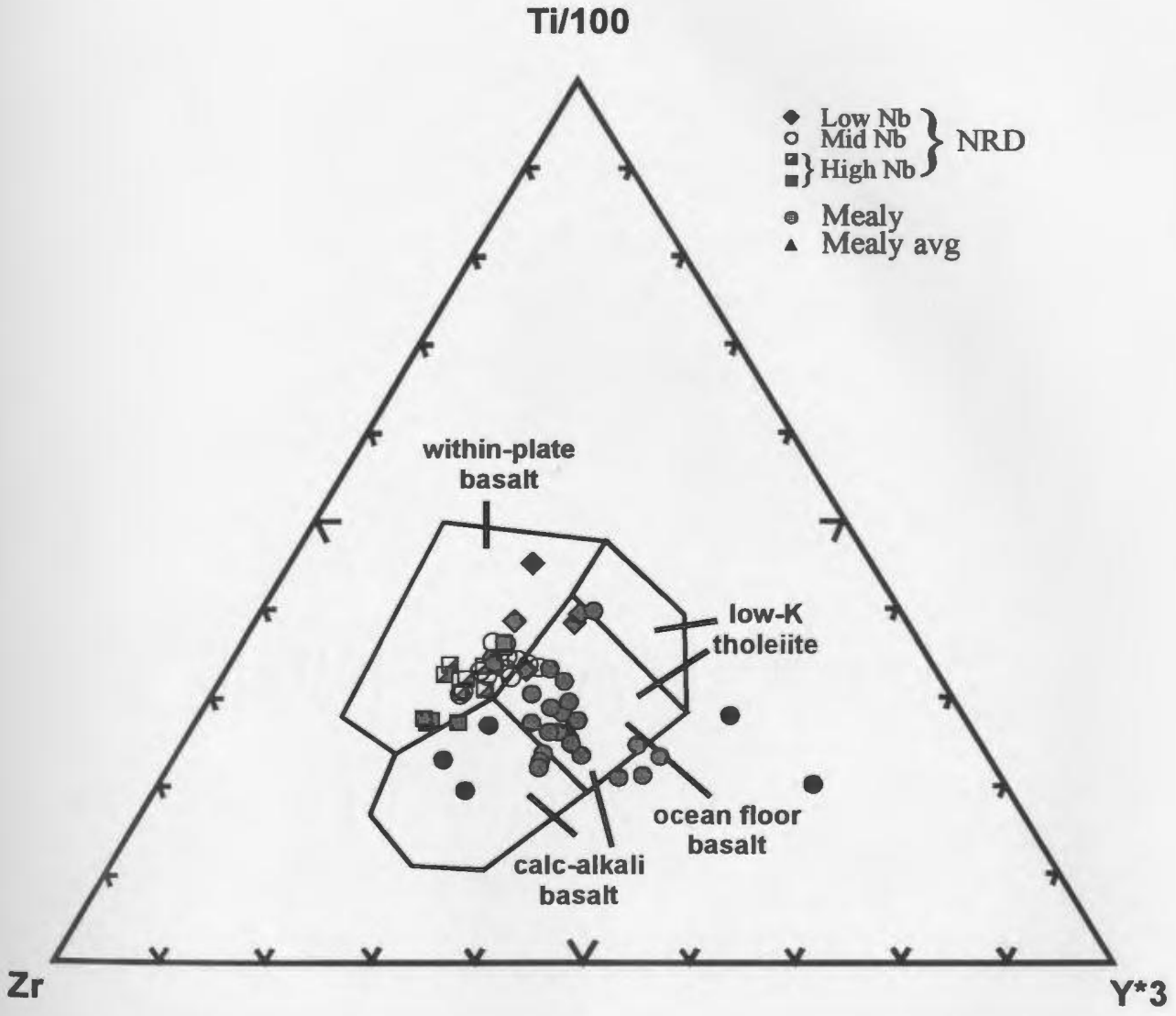

***Figure 5-5**: Within plate basalt discrimination diagram after Pierce and Cann (1973). Y values for the Mealy dykes were taken from Figure 7 of Gower et al. (1990).*

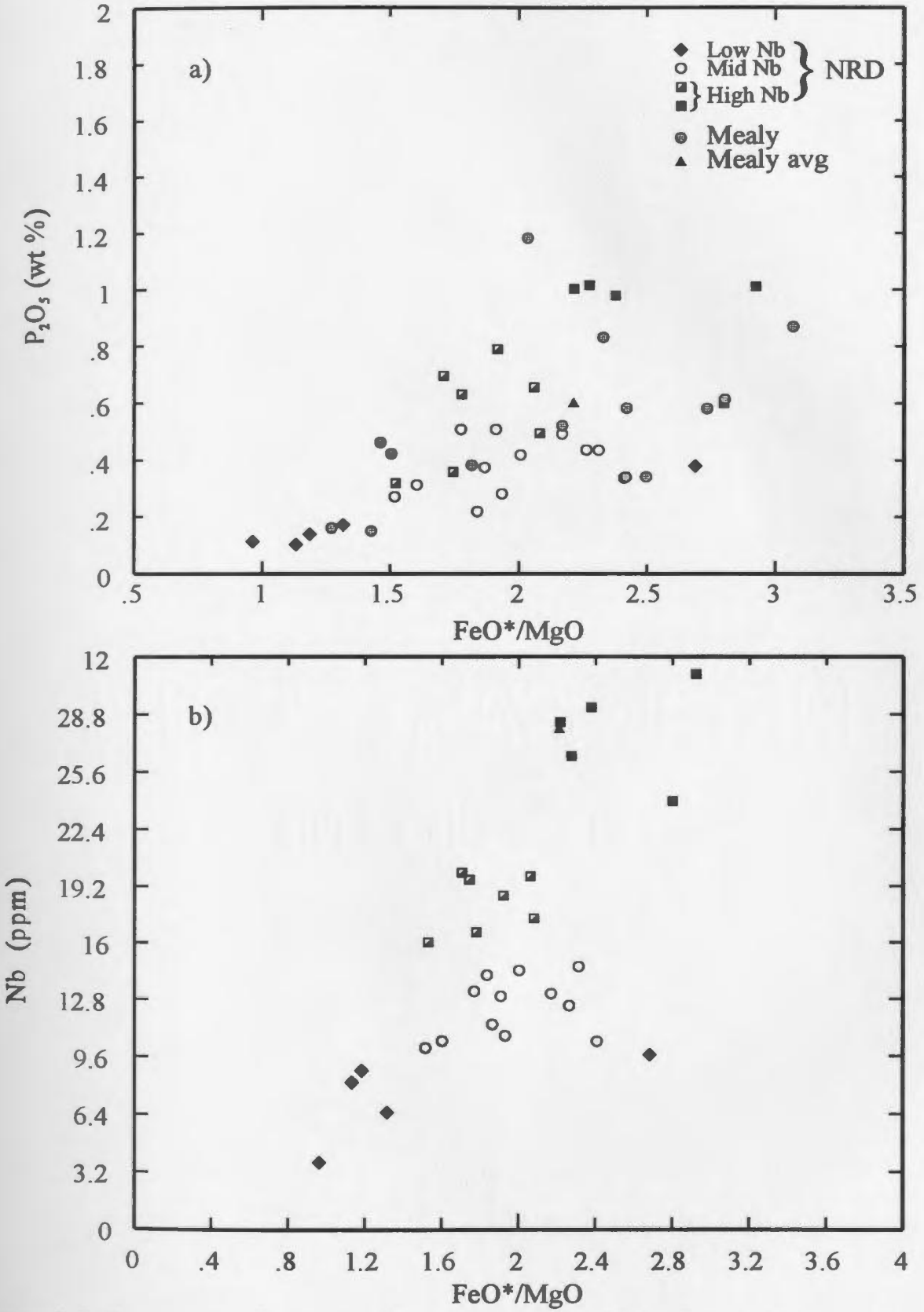

***Figure 5-6**: Comparison diagrams of trace elements displaying fractionation trends based on Nb ppm ranges. See text for discussion.*

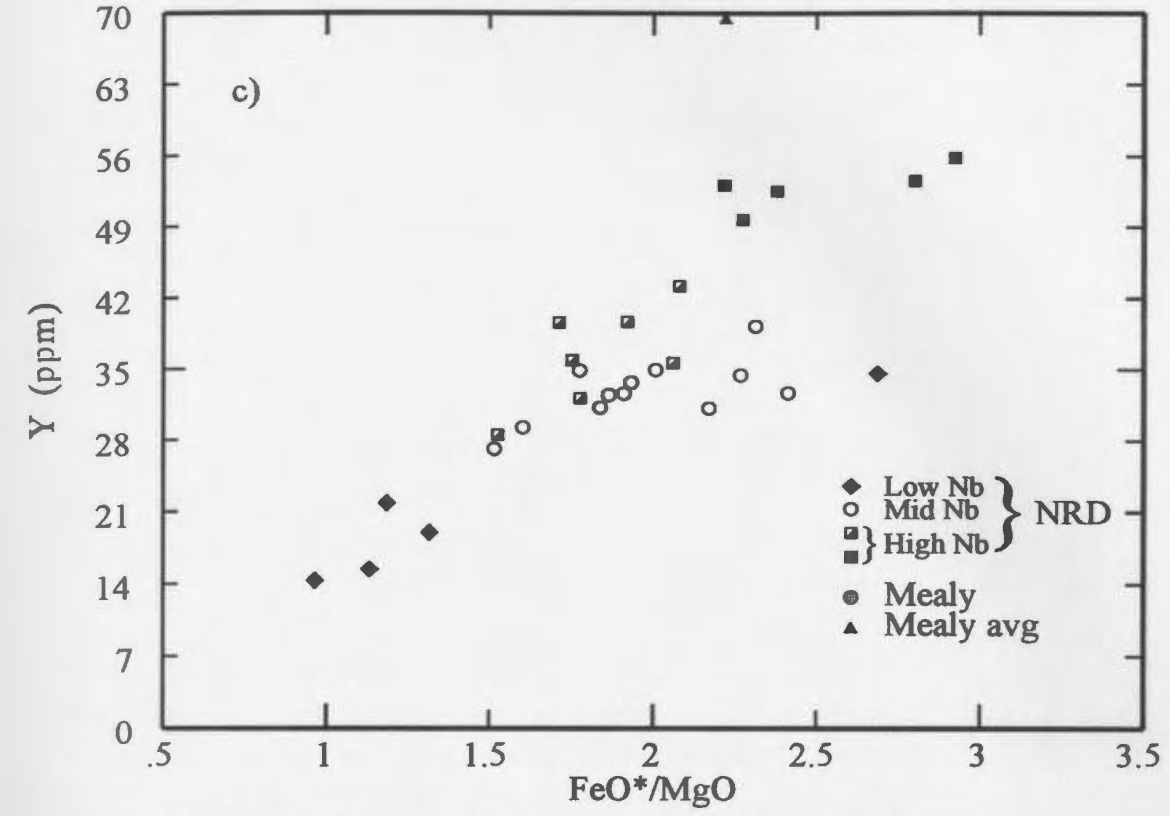

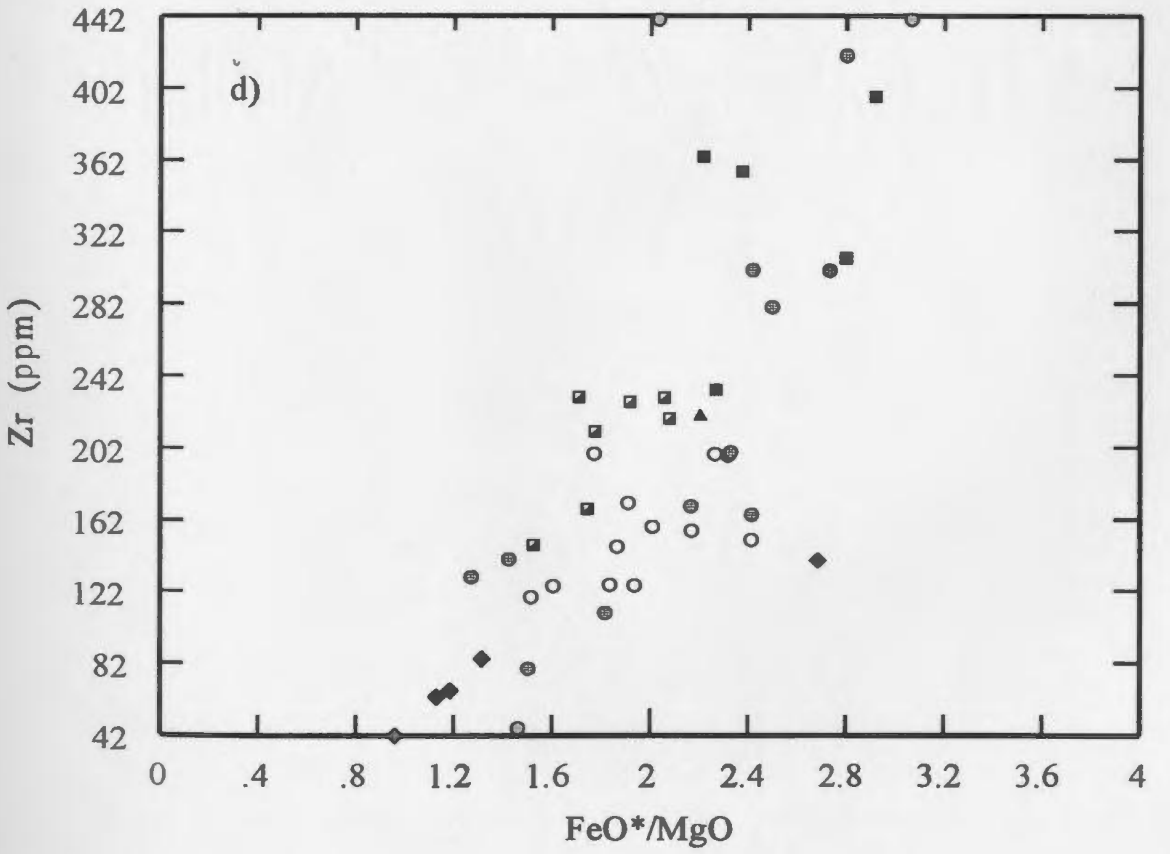

***Figure 5-6**: continued.*

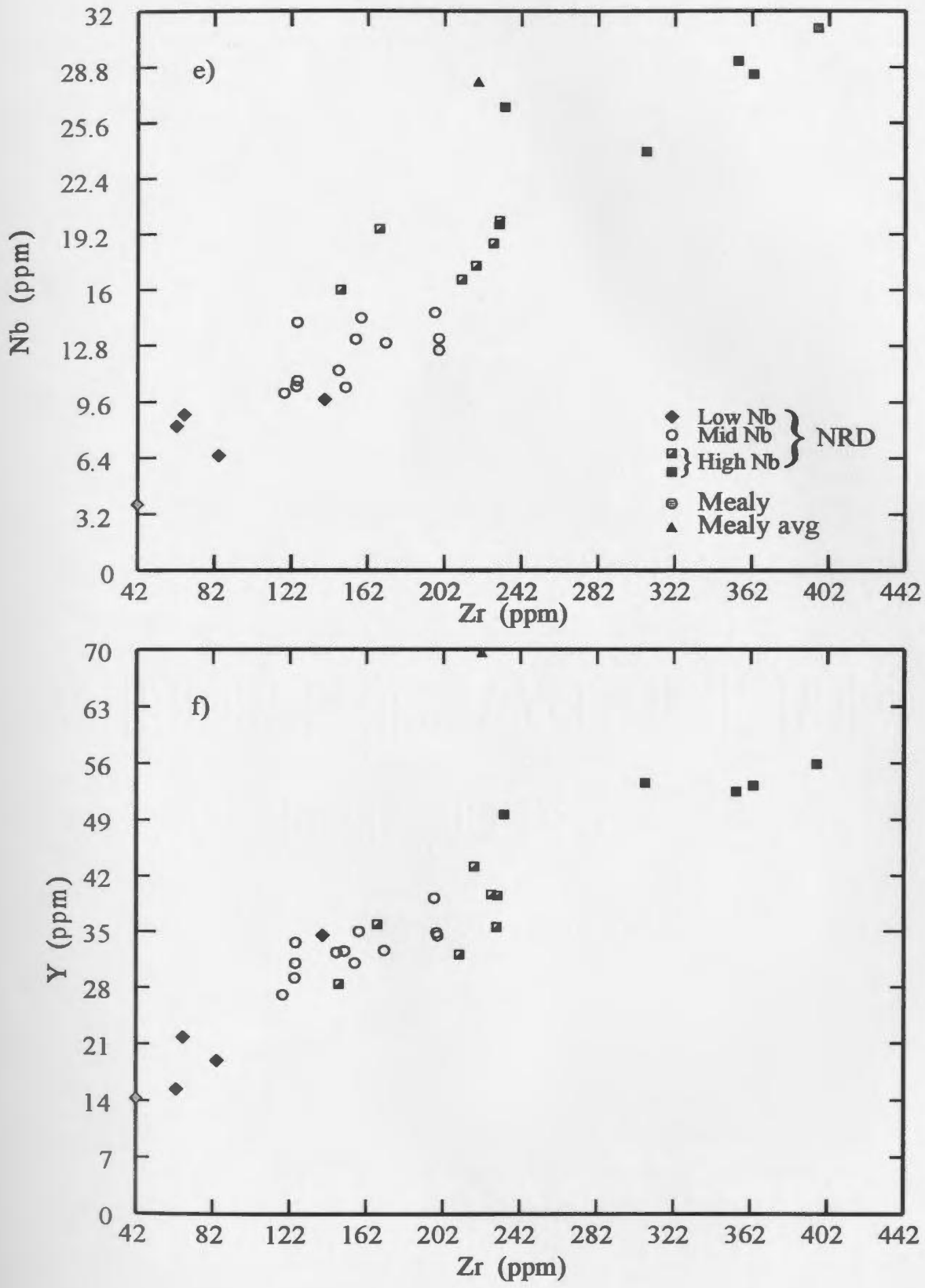

***Figure 5-6**: continued.*

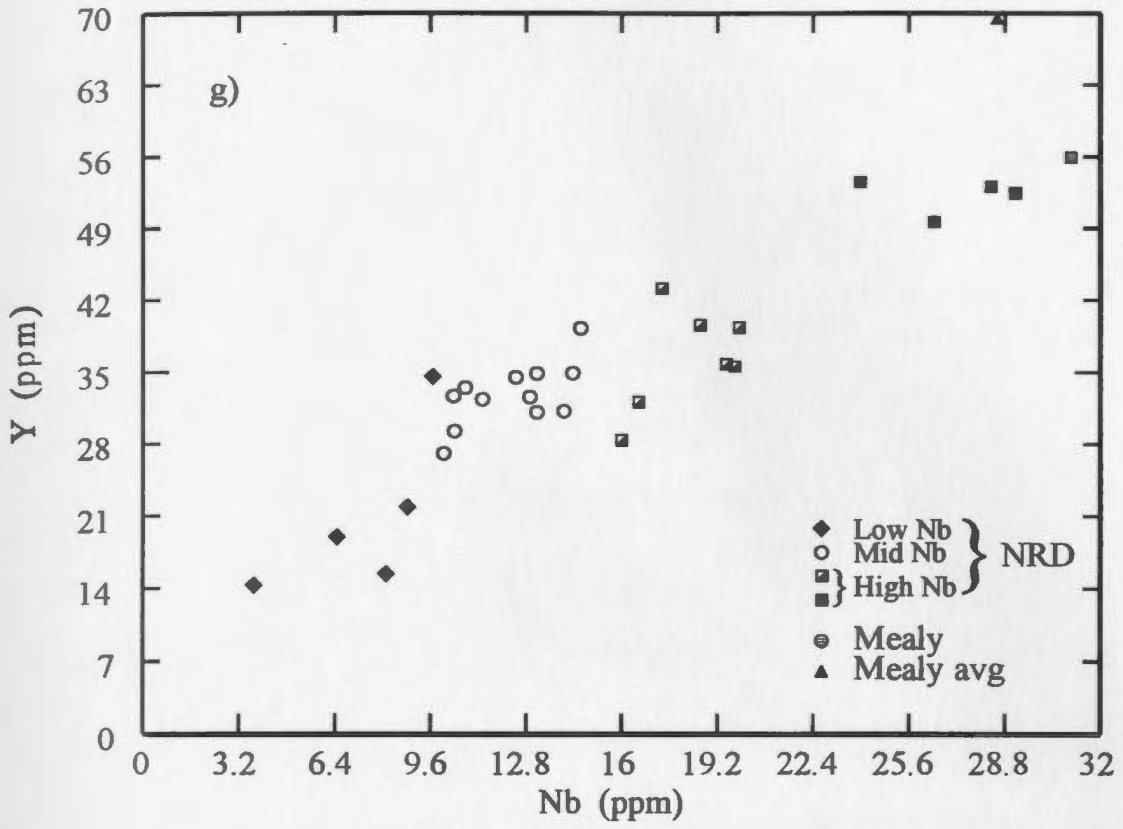

***Figure 5-6**: continued.*

Chapter 6

Metamorphism I:

Petrography and Mineral Reactions

6.1 Introduction

The results of petrographic analysis of fabrics, textures and reaction relationships in the shear zone of the GLTS, and adjacent footwall and hangingwall rocks are described in this chapter. Samples of the shear zone rocks were collected in the field in order to characterize the Grenvillian (Ottawan and/or Rigolet) effects associated with thrusting at the mineral scale and these results are contrasted with those from samples in the hangingwall and footwall of the shear zone that carry Labradorian and/or Ottawan signatures. Thin sections of the shear zone rocks were examined for fabric information related to the relative timing of deformation and mineral growth and also for evidence of reaction relationships that could be used to infer the direction of metamorphic reactions and/or would be suitable for quantitative geothermobarometry. Shear zone samples are characterized by syntectonic fabrics and a strong stretching lineation (L_s) that is inferred to mark the local transport direction (see Chapter 4). Thin sections of samples with L_s fabrics were cut parallel to stretching lineation and perpendicular to the shear zone foliation. In addition some orientated samples were collected for kinematic analysis of the microstructures.

In the following sections, the mineral assemblages, reaction textures and important microstructural features of the GBT, LMT, CCRA, the Northwest River dykes and the basal mylonitic rocks are described. Petrogenetic grids are also applied to the peak assemblages of appropriate rock types to qualitatively estimate the metamorphic conditions achieved by the rocks. A complete table of the samples and mineral assemblages may be found in Appendix B. All mineral abbreviations are after Kretz (1983).

6.2 Groswater Bay terrane

The Groswater Bay terrane (GBT) consists of orthogneisses that are host to rafts of paragneiss and boudinaged mafic-ultramafic units. The orthogneiss is also intruded by the Arrowhead Lake pluton in the northwest part of the field area.

6.2.1 Orthogneiss

The main assemblage in the orthogneiss is away from the GLTS shear zone is Hbl-Bt-Pl-Kfs-Qtz±Grt±Scp±Cpx. Accessory phases present are Ap, Zrn, Aln, opaques and Ttn. Retrograde phases include Chl, Cal, Ser, Ms, Ep and Cam.

The tectonic fabric in the unit is defined by the preferred orientation of Hbl-Bt-Pl-Qtz- Scp and Cpx where present, implying upper amphibolite to local granulite facies conditions. The fabric wraps around Hbl-Pl and Grt-Scp aggregates and porphyroblasts.

Scp, based on its optical properties is enriched in the calcium carbonate end-member meionite (Me). It occurs in Pl-rich layers in association with Qtz and Cal as shown in Figure 6-1, suggesting that it may have formed by the reaction:

$$5An + Grs + 2CO_2 = 2Me + Qtz \quad [R1]$$

(Baker and Newton 1995). Small, clear Zrn crystals are commonly associated with Scp, suggesting that the formation of Zrn may also be associated with the flux of CO_2-rich fluids.

Porphyroblasts of Grt which have Qtz inclusions in the cores vary in grain size from a few mm up to 1cm in diameter. Some Grt is anhedral and clearly resorbed (see below) whereas other Grt crystals retain subhedral to euhedral forms.

Cam was observed to occur in two textural associations in thin section. The texturally earlier Cam principally consists of large grains up to 1 cm in size which are enclosed in the main foliation. The later Cam occurs as partial replacement of garnet and locally Cpx and is clearly a retrograde phase.

With increasing proximity to the GLTS shear zone Cpx becomes a common foliation-forming phase in the assemblage. The addition of Cpx to the assemblage can be explained by the generalized reaction:

$$Hbl + Pl + Qtz = Grt + Cpx + H_2O \quad [R2]$$

This reaction has a steep negative slope in *P-T* space (Pattison in press; see below) where the product assemblage occurs on the high-temperature side, implying that there was an increase in temperature towards the GLTS.

Cpx and Grt show evidence of reaction to produce appreciable quantities of secondary Cam and Pl, through a reversal of R2 above:

$$Grt + Cpx + H_20 = Hbl + Pl + Qtz \quad [R2]$$

It appears that retrogression may have gone to completion in some rocks based on the limited amount of Cpx remaining in the orthogneiss. Resorbed Grt is also characterized by the growth of secondary Bt, Pl and Qtz by the reaction:

$$Grs + 2Prp + 2Kfs + 2H_2O = 2Phl + 3An + 3Qtz \quad [R3]$$

This reaction is very common in the orthogneiss and results in fingers of Bt surrounded by Pl embaying grain boundaries of garnet (Figure 6-2). The reaction has a steep negative slope in *P-T* space (Spear et al. 1999, Fig 5) with the product assemblage on the low temperature side.

6.2.2 Paragneiss

Paragneiss units sampled along Grand Lake comprise migmatitic pelitic gneisses and calc-silicate pods (described below). The pelitic paragneiss has the assemblage Grt-Bt-Ky-Kfs-Pl-Qtz ± Ep with retrograde (or post peak) Sil and Ms. Accessory phases include Ap, Fe-Ti oxides, Zrn, Mnz, ± Aln. This assemblage does not change with increasing proximity to the GLTS shear zone, but migmatite zones become stretched out into thin Kfs-Pl-rich zones with lattice preferred orientated Qtz.

Migmatite zones, in order of crystal abundance, contain the assemblage Kfs-Qtz-Pl-Ky-Bt implying upper amphibolite conditions. Boudinaged granitic veins are wrapped by stringers of Qtz and aligned Bt and Ky + Qtz (Figure 6-3). These migmatite zones are inferred to have formed during the dehydration of Ms following the reaction (see Figure 6-4):

$$Ms + Pl = Kfs + Al_2Si0_5 + L \quad [R4]$$

Ky is rarely found in the migmatite zones and is either at the fringes of the leucosomes or in the melanosomes. Elongated grains of Ky in the matrix are generally subparallel to the foliation, although in rare cases crosscut the foliation. Some Ky grains can be found clustering around Fe-Ti oxides implying that Ky growth was chemically linked to the oxides implying the breakdown of an Fe-Al rich phase (sapphirine? spinel?). These blades are rounded and subhedral to anhedral in shape and are partially replaced by Ms at grain boundaries and cleavage planes.

Ky is the principal aluminosilicate phase in the pelitic rocks along the shores of Grand Lake although a Ky-Sil isograd has been located in the more southern portions of the outcrops of the paragneiss (Wardle and Ash 1984). The Ky-Sil isograd is primarily based on the lack of Ky in the south part. Primary Sil was not observed in any samples from the study area (primary Sil is taken in this text as crystals produced through dehydration reactions rather than retrograde Sil formed during retrogression, see below). Some very fine prismatic crystals that are very pale yellow in plane light and first order grey in cross polarized light were originally inferred to be Sil, but with microprobe analysis were determined to be Ap.

Outside of the migmatite zones the matrix assemblage is Grt-Ky-Bt-Kfs-Pl-Qtz±Ep. The foliation is defined by the preferred orientation of Ky, Bt and Qtz and wraps around porphyroblasts of Grt. Porphyroblasts of Grt vary in size from a few mm up to 1 cm in diameter and have inclusions of all the other phases including Zrn-Mnz.

Ep is present in few samples obtained from paragneiss units closest to the shear zone of the GLTS. Ep, which occurs as resorbed, 1-3 mm diameter crystals, does not appear to be a late retrograde phase but rather part of the peak matrix assemblage. The stability of Ep is inferred to reflect an increase in pressure towards the shear zone shown in CKNASH reactions, where Zo (or Ep) occurs on the high pressure side of many reactions (see Figure 9-18 of Spear 1993) especially under preliminary *P-T* conditions in the range 12-14 kbar and 720-840 °C, as preliminarily estimated by Best (1997). This assumed increase in pressure in the paragneiss is similar to the change of the mineral assemblage of the orthogneiss adjacent to the GLTS (see above).

The source of the fluids responsible for post-peak hydration and/or decompression reactions is inferred to have been stored in the melt and was released during cooling (Spear et al. 1999). For example, Grt is resorbed by either R3 above or a variation involving either the production or reaction of an aluminosilicate (Figure 6-5):

$$Grs + 3Prp + 3Kfs + H_2O = 3Phl + 3An + Al_2Si0_5 + 5Qtz \quad [R3a]$$

Both reactions 3 and 3a have negative steep slopes in *P-T* space suggesting that the metapelites must have surpassed this reaction on the prograde *P-T* path and came back on the retrograde path. The peak *P-T* conditions achieved by the paragneiss based on the reactions and textures observed is discussed further below in section 6.6.1.

Retrograde/post-peak Sil and Ms are found along brittle fractures present in many rocks of the paragneiss (Figure 6-6). Sil does not appear to replace Ky as it occurs generally within Ms and Bt. Bundles of Sil needles are principally restricted to foliation planes although the orientation of the bundles may not be parallel to the elongation lineation. This

implies that the growth of Sil did not occur during penetrative metamorphism and is more likely to have grown principally within the confines of the foliation planes where fluids migrated during cooling of the rocks.

Calc-silicate rocks associated with the Ky-paragneisses typically contain the assemblage Grt-Ep-Cpx-Cal-Qtz. Ttn, Ap and sometimes Zrn are the accessory phases present. Samples of marble collected by Best (1997) are from within the same outcrop localities and contain the different assemblage of Dol-(Cal)-Cpx-Cam-Srp (pseudomorphs of Ol) and Ves. Accessory phases included in the samples are Qtz-Chl-Bt and Fe-Ti oxides.

Carbonate present in samples of the calc-silicate is either Cal or Dol although based on the mineral assemblages it is assumed that most is Dol occurring interstitially between Ep, Grt and Cpx.

Cpx (Di-Hd) in the marbles form large rounded to irregular shaped crystals and contain inclusions of Ttn and Ap. The crystals typically display mild pleochroism from pale yellow to pale green similar to Cam though the crystals lack the typical amphibole cleavage. Most Cpx grains are found in association with Grt and Ep, though Ep appears to be reacting with Grt and Cpx (see below).

Crystals of Grt, orange-yellow in plane light suggesting that they are andradite-rich, occur sporadically throughout the calc-silicate samples. Grt occurs as subidiomorphic to anhedral aggregates and contains inclusions of Ttn, Ep and Cpx. Grt is commonly associated with Cpx and where next to Ep, the Ep showing diffusional zoning (see below) with Grt due to Al $\leftrightarrows Fe^{3+}$ exchange.

Ep forms large granoblastic grains which may have inclusions of Grt-Cal-Tr-Ttn. Grains of Ep display the common pale yellow pleochroism to more intense yellow where in contact with Grt which is inferred to be related to higher iron contents in Ep adjacent to Grt. Where the cores of Ep are Fe^{3+}-poor (pale yellow pleochroism) and the rims are Fe^{3+}-rich (or Al-poor, more intense yellow pleochroism) this zoning relationship is correlated to an initial prograde metamorphism followed by a retrograde event (Deer et al. 1992). Based on the textures from most of the collected samples, Grt and Cpx grew at the expense of Ep via the reaction:

$$6Cal + 11Qtz + Dol + 2Ep = 3Grs + Di + 7CO_2 + H_2O \quad [R5]$$

Ep, Grt and Cpx form an intergrowth involving Qtz (Figure 6-7) whereas other samples lack Ep and Qtz in certain zones implying either Ep instability or local changes in bulk composition.

Ep may also be found as inclusions in anhedral Grt or as small secondary crystals forming at Qtz-Grt grain boundaries (Figure 6-8), which is inferred to represent destabilisation of Grt with the production of Ep from the andradite component during retrograde fluid influx or decompression.

6.2.3 Mafic-Ultramafic rocks

The mafic-ultramafic rocks are spatially associated with the paragneiss units on the northern shore of Grand Lake and on the western flank of the allochthon (Ryan et al. 1982). The mineral assemblage is variable. For instance, in a mafic-ultramafic pod north of the GLTS the mineralogy varies on the outcrop scale from Cam-Opx-Fe-Ti oxides-Spl±Grt near

the paragneiss contact grading to Grt-Hbl-Cpx-Pl further away. A similar sequence is found south of the GLTS on the lake shore.

The minerals of the mafic ultramafic pods do not show any preferred orientation and are generally granoblastic, except for one sample that contains Cam with a shape preferred orientation parallel to the mild foliation.

Granoblastic Cam grains in the ultramafic rocks display very pale green pleochroism. The Cam crystals are optically positive, with maximum birefringence of second order red with a maximum inclined extinction angle of ~15°, indicating that the amphibole may be Cum. These amphibole grains coexist with pale-pink pleochroic Opx crystals that display mild Srp alteration along cleavage planes and crystal edges. In another sample with a similar assemblage, Opx crystals may be poikiloblastic with Cam inclusions and are unaffected by any retrograde effects.

In the mafic rocks, Cam, determined to be of a Hbl composition, is stable with Grt, Cpx and Pl. Grt occurs as subhedral to amorphous aggregates that have inclusions of Ap-Qtz-Rt-Cpx-Pl and opaques. Subhedral grains of Cpx exhibit patchy extinction and minor Cam replacement at grain boundaries and cleavage planes.

Fe-Ti oxides are present in all sections and may display exsolution of Ilm from Hem or vice-versa. Most grains are anhedral but some of the smaller grains occur as euhedral squares implying that some of the Fe-Ti oxides may be Hem.

Ttn and Rt may be spatially associated with Fe-Ti oxides either as moats or single grains growing from grain boundaries (Figure 6-9). Rt and Ttn may also be found as individual grains as inclusions in Cpx, Grt, Cam and Pl. Where Fe-Ti oxides and Rt are in

contact with Pl or Cpx, Ttn forms rims around those minerals through the reaction:

Fe-Ti oxide or Rt + Ca in Pl = Ttn + less calcic Pl? + Hem [R6]

The presence of Ttn after Fe-Ti oxides is inferred to represent retrogression from granulite facies assemblages (Mengel and Rivers 1991) though the slope of this reaction is not known.

6.2.4 Arrowhead Lake pluton

The Arrowhead Lake pluton ranges in composition from gabbronorite to monzodiorite to Cpx-bearing alkali feldspar granite. Three samples were collected from this pluton and each sample contains a different assemblage and is thus described separately below.

From near the edge of the pluton, an undeformed Cpx-bearing alkali feldspar granite was sampled containing the assemblage Cpx-Cam-Grt-Kfs-Qtz-Pl-Bt. This sample contains excellent examples of mesoperthite where the grain size of Kfs varies from a few mm up to 10 mm in diameter, and where each grain contains exsolved Pl. Some grains in contact with Pl may display myrmekite textures. Anhedral grains of a sodic clinopyroxene (Agt based on optical properties) contain exsolution lamellae of Opx (partly replaced by Cam). Those same grains are commonly surrounded by a moat of Pl or by exsolved Ab where hosted in Kfs. This suggests that the pluton cooled slowly allowing exsolution in the pyroxene and feldspars. Later Grenvillian metamorphism resulted in Grt and sodic-amphibole after Cpx and Pl through the general reaction:

$$Agt + Pl + H_2O = Grt + Na\text{-}Am \quad [R7]$$

The second sample was obtained from an undeformed, but recrystallized meta-gabbronorite that contains the mineral assemblage Grt-Cam-Pl-Ttn-Fe-Ti oxides with Rt, Aln and Ap as accessory phases. Grt is anhedral to subhedral and contains inclusions of Cam, Ttn, Rt and Pl. Inclusions of Cam occur as small (≤2 mm) anhedral grains to euhedral rhombs in contrast to Cam in the matrix which forms large (> 5 mm) anhedral grains. Symplectites formed between Fe-Ti oxides and Cam (Figure 6-10) replace former Ttn. Grt and matrix Cam are commonly present near Ttn although Grt may be separated from Ttn by Pl. Ttn may also be partially replaced by the symplectite surrounded by sericitized Pl. The reaction, based on these textures is inferred to be:

$$Fts + 4Ttn + 2Alm = 4An + 4Ilm + 3Ftr \quad [R8]$$

The sample from near the centre of the pluton is a mildly foliated diorite-monzondiorite which contains the assemblage Grt-Opx-Cpx-Bt-Pl-Kfs with accessory Ttn, Rt, Ap and Fe-Ti oxides. Grains of Bt define the mild foliation along with Cpx and Opx, although some pyroxene grains may crosscut the fabric. Opx is either being replaced by Bt or is hydrated at rims and fractures. Cpx is relatively fresh whereas anhedral grains of Grt show resorption by Pl and Bt through R3:

$$Grs + 2Prp + 2Kfs + 2H_2O = 2Phl + 3An + 3Qtz \quad [R3]$$

6.3 Lake Melville terrane

The granodiorite to diorite gneisses of the LMT are intruded by many granitic

pegmatite dykes and are host to minor amounts of mafic and ultramafic boudins. The LMT is also host to the Northwest River dykes which are discussed under 6.5.

6.3.1 Orthogneiss

The main assemblage present in the orthogneiss of the LMT is Opx-Cpx-Cam-Bt-Pl-Qtz±Grt±Kfs with accessory Ap-opaques-Zrn±Ttn±Rt and retrograde Cal-Cam-Ep-Ser. Depending on the location of the sample, the fabric changes from granoblastic textures in the south to foliated in proximity of the shear zone (Rigolet thrust and/or GLTS). Cam together with Bt, Cpx and Opx define the foliation in the gneiss. The presence of Opx in the samples along with Cpx and Hbl implies that the rocks of the LMT reached granulite-facies conditions.

Two distinct varieties of Cam occur in the rocks of the LMT based on optical properties. The first variety consists of crystals of 3mm up to 10 mm in size that define the fabric, where present, and display the typical tan to forest green pleochroism of Hbl. The second variety is clearly a retrograde amphibole forming rims around pyroxene and partially replaces Hbl. It displays aqua blue-green to pale tan pleochroism with second to third order birefringence. This variety is commonly associated with carbonate and retrograde Ep after Pl. Its composition is unknown.

Cpx and Opx are present in most samples in the LMT where Opx is fairly common, although it is usually retrogressed. Often both pyroxenes are partially retrogressed to Cam although Opx is more often partially replaced by Bt. Where pyroxenes are present they are

stable with Cam (see above) implying that the two-pyroxene plus amphibole assemblage formed under granulite-facies conditions.

Grt is rare but where present it may be found in several textural settings. It may occur as 2-5 mm in diameter subhedral to euhedral grains that contain inclusions of Cpx-Pl-Cam-Qtz. Larger grains may be amorphous or "skeletal" with variable grain size from a few mm up to 10 mm and contain varying quantities of Cpx-Pl-Cam-Qtz inclusions. Grt is restricted to particular zones within a sample implying domainal equilibrium or chemical domains in which garnet may be produced. Typically these zones are enclosed in a matrix composed of Opx, Cpx, Pl and Hbl (Figure 6-11) implying the general reaction:

$$Opx + Pl = Cpx + Grt + Qtz \quad [R9]$$

where the Grt-Cpx zones are forming at the expense of the two-pyroxene plus Cam granulite facies assemblage. This reaction defines the low pressure boundary between medium pressure granulites and the high-pressure granulite subfacies (Pattison in press). The transition has a low slope in *P-T* space with the products occurring on the high pressure side of the reaction. Implications of this reaction are further discussed below in section 6.6.

6.3.2 Mafic Rocks

Two mafic-ultramafic samples in the LMT were collected from the rocks along the shores of Grand Lake. The hornblendite is composed of Cam-Pl-Bt with accessory Ap and Zrn. The ultramafic rock is principally composed of Srp-En-Tr-Bt-opaque.

The hornblendite pod is rich in Cam with little more than 5% composed of Pl. Cam is randomly orientated and may contain inclusions of Bt and opaques. Grains exhibit tan to

grass-green pleochroism in plane light and sweeping to patchy extinction in cross polarized light. Pl crystals, which are interstitial between the Cam crystals, may retain lamellar twinning and are partially saussuritized and/or sericitized.

Srp, in the ultramafic sample, comprises near half of the thin section where the grains are aligned parallel to the mild foliation present in the section. Zones of Srp are inferred to replace Ol-rich layers that were present prior to retrograde metamorphism. Srp replaces most of the other phases in the rock except Bt. It also invades other phases including rounded En and Tr grains in fractures, cleavage planes and at grain boundaries.

Bt based on its optical properties in plane polarized light is the Mg end-member Phl. It may be kink banded, curved or intricately deformed with opaques and defines the mild foliation present in the sample.

6.4 Cape Caribou River Allochthon

The following descriptions of the rocks of the CCRA begin at the structural top of the thrust stack and work towards the basal granitoid gneisses, the mafic gneiss unit and the basal mylonite. The Northwest River dykes also occur in the CCRA but are discussed in 6.5. The reader is reminded here that samples from the lowest parts of the allochthon contain a stronger Grenvillian metamorphic overprint than those from farther up in the thrust stack. The Dome Mountain suite is not included in the following discussion since it was not sampled.

6.4.1 Northwest River Anorthosite

The anorthosite is principally composed of Pl and may locally contain megacrystic Opx. The anorthosite is also host to subordinate nelsonite (Mag-Ilm Ap) pods and gabbroic patches. The massive anorthosite does not generally show evidence of deformation or metamorphism although evidence of fluid infiltration may be found as variable retrogression of primary igneous phases.

Pl crystals range in size (depending on the body) from 10 to 50 cm to much smaller laths only a few centimeters long. Pl may exhibit recrystallization features such as subgrain formation, grain boundary adjustments. These features are regarded as part of a subsolidus process which took place during cooling of intrusion. The crystals are typically twinned and may be normal zoned. Dustings of spinel are also present in varying amounts within the feldspars.

Opx in the anorthosite varies in grain size from megacrystic 10-50 cm crystals to fine grained 0.5-1 cm grains that commonly display exsolution lamellae. Some of the larger crystals are kink banded possibly as a result of igneous emplacement processes. Depending on the location within the anorthosite unit, Opx may be surrounded or completely pseudomorphed by coronas of hydrous minerals including Cum, Tr and Bt. For example, from core to rim, the assemblage is Opx→Cum→Tr→Bt→Pl where Pl and Opx are the primary igneous phases (Butt 2000, see Figure 3-6).

Nelsonite pods in the anorthosite display coronas of Bt and Grt around Mag-Ilm grains formed by the reaction:

$$(\text{Mag-Ilm}) + \text{Pl} + \text{Kfs} + H_2O = \text{Alm} + \text{Grs} + \text{Ann} \quad [\text{R10}]$$

The production of these coronas is inferred to be a Grenvillian feature as Emslie (1976) does not report any coronas in the anorthosite of the MMIS (Mealy Mountain intrusive suite). The timing of the fluid flow through the CCRA is not constrained although it is presumed to be Grenvillian. Low temperature geochronology (e.g., Ar/Ar systematics in Bt) are required to confirm this interpretation.

Two samples of leuco-gabbronoritic rocks from the anorthosite pluton contain the assemblage Pl-Opx-Cpx-Cam-Bt±Grt with accessory opaques and Zrn. One sample contains primary Opx with minor Cam rims whereas Cpx is completely pseudomorphed by Cam that retains exsolution lamellae of the host pyroxene. Crystals of Pl contain micron scale inclusions of euhedral Cam near the contacts with larger Cam that are replacing pyroxene. Pl in these zones also preserves a myrmekitic or wormy texture inferred to have been produced by local thermal activity or fluids related to the retrogression of pyroxene.

The other sample contains Opx partially replaced by Bt and knots of Grt between Bt and Pl phenocrysts. Opx is also partially replaced by coronas of Cam and Bt similar to that discussed above in the anorthosite. Sericitized, lamellar twinned, Pl grains preserve twin gliding and kink bands, though these features are inferred to be a subsolidus recrystallization common to the anorthosite pluton.

6.4.2 Gabbronorite

Samples from the gabbronorite on the southeastern flank comprise granoblastic Opx±Cpx-Cam-Pl assemblage with accessory Bt-Ap-Fe-Ti oxide-Zrn. Opx is hydrated at

rims and in fractures and partially retrogressed to Cam similar to retrogression of Cpx. The lack of any prevalent foliation in these samples implies that the shear zone must have localized much of the strain as these samples come from less than 1km (map distance) from the assumed location of the shear zone in that area.

Samples from the west- northwest part of the allochthon are recrystallized with the main assemblage in these rocks consisting of Cam-Bt-Pl-Qtz±Cpx with accessory phases including Fe-Ti oxides-Ap-Zrn. One sample from this area contains an inferred primary igneous mineralogy of Opx-Cpx-Pl which is partly replaced by coronas of Grt-Cam-Bt (Figure 6-12). Opx and Cpx are inferred to be the products of the breakdown of Ol and plagioclase via the reaction:

$$Ol + An = (Fe\text{-}Mg)Cpx + Opx + Spl \quad [R11]$$

The corona structure, from a core of Opx to relict igneous plagioclase laths, is Opx→Cpx→Pl_2→Grt→Pl_1 where Pl_2 is metamorphic feldspar and Pl_1 is the igneous xenocryst which often retains its lath shape and fine dusting of spinel inclusions. This texture is similar to that reported by Indares and Dunning (1997) who characterized the formation of the garnet coronas through the reaction:

$$3(Fe\text{-}Mg)Cpx + 3An = 2Grs + (Fe\text{-}Mg)Grt + 2Qtz \quad [R12]$$

Grt shows the presence of fine grained low relief inclusions that are inferred to be Qtz, supporting the operation of this reaction. Another Grt type, together with Bt, is growing from Fe-Ti oxides and Pl to form Bt and Grt rims around the oxides, similar to the texture in the nelsonite pods of the anorthosite. Grt may also be found partially pseudomorphing xenocrysts of Pl, implying operation of the An breakdown reaction.

6.4.3 Recrystallized Gabbro-Diorite

Samples collected from the recrystallized gabbro-diorite layer consist of variably foliated metamorphosed mafic rocks containing the assemblage Opx-Cpx-Hbl-Pl in the gabbroic rocks and Grt-Bt-Pl-Kfs±Qtz in the diorite to monzodiorite samples where both rock types may contain the accessory minerals; Ap-Zrn-Fe-Ti oxide ±Aln±Ttn.

Depending on the degree of strain preserved in the sample, Opx, Cpx and Cam may define the imposed foliation. Opx may be intergrown with Cpx or vice-versa in more highly strained gabbronoritic rocks (Figure 6-13). This texture is inferred to be the result of deformation of Opx that contained Cpx exsolution lamellae that were deformed to form individual subgrains in the host Opx. Opx is variably hydrated at rims, fractures and cleavage planes and is also partially replaced by Cam together with Cpx. It is inferred that the two-pyroxene plus amphibole assemblage (moderate pressure granulite facies)was stable during deformation but was retrogressed subsequently.

In the diorite to monzodiorite samples, Grt is partially replaced by Bt and Pl and contains inclusions of Bt, Pl, Ap and Qtz. Inclusions of Bt are orientated perpendicular to the matrix foliation defined by Cam and Bt. This implies that Grt and Bt were stable together before penetrative deformation. Bt in certain zones of the and in inclusions in Grt is completely retrogressed to Chl. This fluid influx is inferred to be post metamorphism and deformation. Bt appears to be the only mineral to have undergone hydration.

6.4.4 Basal Granitoid Gneiss

Samples from this unit were taken throughout the field area although the majority of

were collected along the south shore of Grand Lake at Cape Caribou. The gneisses at Cape Caribou and north of the cape are tonalites to diorites whereas the remaining samples from the woods roads are more granodioritic to granitic in composition.

The rocks that outcrop at Cape Caribou contain the assemblage Grt-Opx-Cpx-Cam-Bt-Pl±Qtz±Scp with accessory opaque-Ap-Zrn±Spl and retrograde Cal-Ep-Ser. These samples are gneissic with a shape preferred orientated (SPO) crystals of Opx-Cpx-Bt-Cam defining the foliation, implying upper amphibolite to granulite facies conditions during thrusting although some of the samples are locally retrogressed to amphibolite facies.

Both Cpx and Opx show evidence for retrogression with Opx displaying partial Bt replacement at grain boundaries and Cpx being rimmed by Cam. Cam also occurs as part of the peak assemblage with pyroxene as 5 mm up to 10 mm crystals that define the foliation and contain inclusions of Opx or Cpx.

Where Grt porphyroblasts are present the foliation wraps around them implying pretectonic growth, although textures preserved in some samples indicate that later Grt growth overgrew this wrapping fabric, so that the inclusions are aligned to the external foliation (Figure 6-14).

Micro-scale shear zones (referred to here as microshear zones) also wrap around Grt porphyroblasts and locally may also cross cut earlier fabrics defined by Opx, Cpx, Cam and Bt. In one example, Opx defines the foliation and is crosscut by microshear zones which produce microboudinage of Opx in late C-S fabrics (Figure 6-15).

Samples that preserve the inferred peak assemblage (Grt-Opx-Cpx-Pl-Cam±Qtz) exhibit the following general reactions:

$$Hbl + Pl + Qtz = Grt + Cpx + H_20 \quad [R2]$$

and

$$Opx + Pl = Cpx + Grt + Qtz \quad [R9]$$

These reactions indicate an increase in pressure locally (Figure 6-16) whereas, as mentioned above, other samples are retrogressed through decompression and hydration reactions. These samples contain Hbl replacing Cpx or just Hbl, inferred to have formed by complete retrogression of Cpx. One sample of these amphibole-rich rocks contains scapolite, produced through the general reaction:

$$Pl + CO_2 = Scp + Qtz \quad [R13]$$

This reaction implies that a CO_2-bearing fluid was present during retrogression. Other samples do not contain Scp, although evidence of retrogression is present by the hydration of feldspar to produce Ser, Ep and Cal.

The rocks of the basal granitoid gneiss, which are more typically granitic in composition, contain the assemblage Grt-Bt-Cam-Pl-Kfs-Qtz with accessory opaque-Ap-Zrn-Aln±Ttn and retrograde Cal-Ms-Ser-Chl. The foliation in these samples is defined by the SPO crystals of Cam-Bt and LPO ribbons of Qtz, inferred to have formed under upper-amphibolite facies conditions.

Porphyroblasts of Grt with inclusions of Bt-Pl-Qtz-Ap±Cam, are wrapped by the foliation implying pre-tectonic growth. These same Grt porphyroblasts are heavily resorbed

via decompression and fluid ingression to produce secondary Bt, Pl and Qtz through R3, common to all granitic rocks in the field area:

$$Grs + 2Prp + 2Kfs + 2H_2O = 2Phl + 3An + 3Qtz \quad [R3]$$

6.4.5 Mafic Gneiss Unit and the Basal Mylonite

The mafic gneiss unit and the basal mylonite are inferred to be derived from the same protolith, though the basal mylonite is more highly strained and the contact between these subunits is gradational. The mafic gneiss unit is principally layered mafic rocks with alternating mafic and felsic layers similar to the basal mylonite.

The mineralogical assemblage of the mafic gneiss unit is Opx-Cpx-Grt-Cam-Bt-Pl-Scp±Qtz±Kfs, accessory Ap-Zrn-opaque ± Rt and retrograde Ser-Cal and Cam. The gneissic fabric is defined by the shape preferred orientation of Opx-Cpx-Cam±Scp crystals and stringers of Qtz. In more highly strained portions in some of the samples (e.g., felsic layers) Opx may be stretched and boudinaged in the prevailing foliation (see below). This implies that the rocks of the mafic gneiss unit were deformed under granulite-facies conditions.

Where Grt is present the foliation wraps around those porphyroblasts implying pre-tectonic growth. Grt generally occurs as ~5mm subhedral crystals although one sample preserves three varieties based on morphology. The first textural type occurs as 5-10 mm anhedral crystals containing inclusions of Cpx-Opx-Pl-Qtz-Scp-Bt and opaque. The second and third varieties are similar in morphology though the second type contains inclusions of Qtz and Cpx and the third are generally absent of inclusions. These varieties of Grt are inferred to reflect minor differences in composition and fluid activity between layers.

Many of the crystals of Cpx and Opx have undergone subgrain formation and grain boundary adjustments during shearing. Cpx is encroached at grain boundaries by secondary Cam whereas Opx is partially replaced by late Bt. Some larger Cpx grains still preserve exsolution lamellae despite grain boundary adjustments (Figure 6-17).

Scp is present in most samples from this unit. It is generally associated with Cam and/or Pl and defines possible fluid conduits in which Scp was formed. In one sample it is included in Grt and defines the foliation in the matrix, implying that Scp was growing at near peak conditions and was stable along with Grt and Opx. Scp is assumed to have formed through R1 (see section 6.6.4) at high temperatures where CO_2 bearing fluids were present during thrusting.

The basal mylonite, briefly discussed in Chapters 3 and 4, consists of alternating layers of mafic and felsic straight gneiss which outcrops on the north shore of Grand Lake. The mafic layers are principally composed of the assemblage Grt-Opx-Cpx-Hbl-Bt-Pl±Qtz±Scp±Kfs with accessory Ap-opaque-Zrn-Aln±Ttn and retrograde Cam-Cal-Ser. The felsic layers contain Pl-Qtz-Grt-Opx-Cpx-Bt-Kfs±Scp±Hbl with accessory Ap-Zrn-opaque±Ttn. SPO of Cpx, Opx and Cam crystals define the mylonitic foliation in the mafic layers and together with ribbon Qtz in the felsic layers suggesting granulite-facies conditions during thrusting. The straight gneiss however, preserves local amphibolite facies assemblages in mafic layers that acted as fluid pathways late in the stages of thrusting.

A common feature to all the samples from the straight gneiss is a pervasive fracture system orientated perpendicular to the foliation which crosscut porphyroblasts of Grt and

other rigid crystals including Cpx, Opx and Cam. These tensile fractures are interpreted to represent an anisotropic response to brittle horizontal extension during uplift (e.g., Ji et al. 1997) and cooling of the allochthon.

Grt is present in all samples collected from the straight gneisses. The morphology of Grt varies from sample to sample where subhedral to anhedral grains vary in size from 2mm to1cm in diameter. They may be inclusion-free, contain minor amounts of inclusions (Cpx-Pl-Qtz-Ap-Hbl) or may be skeletal with inclusions of Qtz and/or Cpx. In many samples, two populations may be present where one population locally is heavily resorbed (see below) and is wrapped by mylonitic fabric and the second is euhedral to subhedral grains that show no evidence for retrogression inferred to be part of a later fabric associated with late Cam (growth during amphibolitization).

Resorbed crystals of Grt can be characterized by the generalized cooling-decompression reaction:

$$Grt + Cpx + H_20 = Hbl + Pl + Qtz \quad [R2]$$

as shown in Figure 6-18, or by the production of secondary Bt and Pl by:

$$Grs + 2Prp + 2Kfs + 2H_2O = 2Phl + 3An + 3Qtz \quad [R1]$$

Retrograde assemblages are localized in the shear zone where garnets from samples preserve variable evidence for retrogression through the above reactions.

As discussed above, Cpx and sometimes Opx are present in the samples where they define the mylonitic foliation. Opx has typical pale pink to grey-green pleochroism, is usually hydrated at rims and fractures and is locally partially replaced by Bt. Opx grains are

commonly stretched and locally micro-boudinaged in the mylonitic foliation and lesser strained crystals may display sweeping extinction and minor subgrain formation. Grains of Opx occur in both mafic and felsic layers although some samples have Opx restricted to Qtz-Pl layers and Cpx only in mafic layers.

Cpx with pale green pleochroism typically occurs as small granoblastic grains inferred to be the result of complete subgrain formation. Less strained grains may preserve grain boundary adjustments (core and mantle type where the cores may retain exsolution lamellae) in either mafic or felsic layers. Cpx is commonly associated with Grt as inclusions or in the matrix forming in the pressure shadows around garnet (Figure 6-19). Commonly Cpx shows variable amounts of replacement by secondary Cam principally by hydration of Cpx or by decompression of Grt-Cpx assemblages to produce secondary Cam via R2 above (also see Figure 6-18).

Cam, having tan to green pleochroism, may occurs in two distinct textural varieties. The first is a texturally older Cam that was stable with Cpx and Grt at peak metamorphic conditions, whereas the second, as discussed above, occurs as replacement of Cpx or Grt-Cpx. The texturally older Cam usually defines and is also wrapped by the mylonitic foliation.

Pl grains vary in size from 1mm up to 5mm where larger grains are generally exhibiting a SPO and smaller grains presumably formed by subgrain formation also show a SPO and also show LPO in many samples (Figure 6-20). Matrix Pl crystals have grain boundaries that are ragged or seriate and typically display patchy extinction, whereas in pressure shadows of resorbed Grt, Pl crystals generally show little evidence for deformation.

Scp grains are generally inclusion free and are commonly found in association with

Cam. In few samples, Opx and Scp occur together in the mylonitic foliation (Figure 6-21) implying the stability of the two phases at high temperatures possibly through the reaction:

$$4Di + 2Prp + 4An + 2CO_2 = 5En + 2Me \quad [R14]$$

Yoshino and Satish-Kumar (2001) attributed the stability of Opx and Scp to this reaction together with the absence of Cpx in Opx-Scp zones in metabasite rocks.

6.5 Northwest River dykes

The mineralogy of Northwest River dykes was mentioned briefly in Chapter 5. This section includes a more detailed description of the mineralogy and fabrics including metamorphic characteristics and coronitic textures of the dykes that outcrop in the LMT and the CCRA.

6.5.1 Northwest River dykes in the LMT

The dykes in the Lake Melville terrane are variably recrystallized to metamorphic assemblages that include Opx-Cpx-Hbl-Bt-Pl-Qtz±Grt with accessory Fe-Ti oxides-Ap-Zrn± Aln±Rt. Retrograde phases present include Cal and Act-Tr. Most samples are not penetratively deformed and display a granoblastic fabric. Typically one pyroxene or both may be found with Pl and Cam. Despite late Cam rimming Cpx and partial replacement of Opx by Bt, the two-pyroxene plus Cam assemblage typical of low-medium pressure granulite-facies rocks that is observed in many samples.

Tan to dark-green/brown pleochroic Cam is a ubiquitous phase within the dykes of the LMT. Where a foliation is present, amphibole defines that foliation. Cam may be granoblastic, most commonly anhedral, simple twinned and equigranular. Some grains exhibit slight zonation and may contain inclusions of opaques, Qtz, Bt and Ap. One rock contains knots of Cam presumed to pseudomorph Grt and Cpx porphyroblasts (Figure 6-22) through decompression from a higher grade assemblage through the general reaction:

$$Grt + Cpx + H_2O = Hbl + Pl + Qtz \quad [R2]$$

This reaction is inferred to have gone to completion based on the lack of both Grt and Cpx. The Cam may be poikiloblastic and/or zoned, and may contain inclusions of Qtz and a yet undetermined high relief mineral (possibly another Cam based on the morphology and pleochroism).

Grt is found within a few of the dykes (see Appendix B) and where present, it is apparently not in textural equilibrium with Cam. Commonly anhedral and resorbed, Grt may contain inclusions of Hbl-Bt-Pl-Qtz and Grt rich in amoebal Qtz inclusions (Figure 6-23) may also occur.

Opx is hydrated at grain boundaries and in fractures and Cpx is partially retrogressed to Cam. Figure 6-24 shows the assemblage composed of Opx, Cpx, Pl and Cam. Based in this texture it is inferred that the Northwest River dykes in the LMT must have attained granulite facies conditions. The assemblage is partially retrogressed taking place during either post peak fluid infiltration or amphibolite facies metamorphism.

6.5.2 Northwest River dykes in the CCRA

Dykes from the CCRA differ from those in the LMT as they are variably recrystallized to metamorphic assemblages depending on their proximity to the shear zone. Dykes found in the lowest structural part of the allochthon are typically completely recrystallized whereas those in the higher levels of the thrust stack preserve igneous textures. Those dykes in the lowest structural parts allochthon near the northern exposure of the GLTS contain the mineral assemblage Cam-Cpx-Opx-Grt-Pl-Bt±Qtz and accessory phases including opaque phases (Fe-Ti oxides and Ccp), Ap, Zrn ±Rt. Scp and Cal form part of a retrograde assemblage.

Cam with inclusions of Fe-Ti oxides and Bt occurs as equigranular subhedral to anhedral grains that exhibit typical "Hbl" pleochroism with simple twins common in the larger porphyroblastic grains. Cam may be found in two textural varieties. The first variety is inferred to represent part of an earlier Cam-bearing granulite-facies assemblage whereas the second variety is found as replacement of Opx, Cpx and or Grt and is unambiguously part of a later retrograde overprint.

Where present, Opx occurs as anhedral grains displaying the typical pale pink to colourless pleochroism. In some samples, grains seem to be in local equilibrium with Cam whereas in other samples, Cam is replacing Opx or Opx may be hydrated and/or replaced by Bt.

Anhedral grains of Cpx display the usual characteristic pale-green body colour in plane polarized light. Some grains may preserve exsolution lamellae indicating relatively

slow cooling period after growth or recrystallization of Cpx. Most grains are variably altered to an Cam that is inferred to have formed during a retrograde event.

Grt occurs as aggregates of small subhedral grains with inclusions of Cpx, Opx, Hbl, Bt, Fe-Ti oxides, Pl and Qtz. Anhedral crystals of Grt may contain inclusions of Qtz, Pl and pyroxene in a skeletal texture that is inferred to be the result of fast porphyroblastic growth. Commonly this skeletal Grt occurs with euhedral inclusion-free Grt, but the relationship between the two textural types is not known.

Pl crystals, displaying patchy extinction, deformation twins and subgrain formation, occur as equigranular grains displaying triple point junctions that may be normally zoned in proximity to another Ca-bearing mineral such as Grt or Cam. Pl "phenocrysts" shown in Figure 3-10, occur as recrystallized Pl aggregates in a rock with no discernable fabric implying static metamorphic recrystallization. There are a few relic Pl phenocrysts still present in a few samples (Figure 6-25, e.g., they retain their original igneous morphology), and the grains are normally zoned and display carlsbad and albite twinning.

Qtz is rare in the dykes and is only associated with reactions involving Grt.

Veins present in certain dykes such as the one shown in Figure 3-10, are principally composed of Cpx with Grt with minor Cam, Qtz and Pl (Figure 6-26). The morphology of the Cpx in these veins is anhedral and commonly equigranular. Some grains are partially replaced by Cam. Grt morphology in these veins is subhedral to anhedral skeletal types. Inclusions in Grt include Cpx, Pl, Hbl, Rt and locally Qtz. Cal may also be found in the veins implying that the growth of Grt and Cpx was directly related CO_2 bearing fluids during

metamorphism. The reaction to produce Grt and Cpx is

$$Hbl + Pl + Qtz + CO_2 = Grt + Cpx + H_2O + Cal \quad [R2a]$$

The presence of CO_2 as a reactant resulted in the local activity of H_2O to decrease (see below) allowing this reaction to occur.

The dykes from the structurally higher levels of the thrust stack typically contain igneous mineralogy and textures variably overprinted by metamorphic assemblages. The dykes commonly display cumulate textures where Pl laths are randomly orientated. The paragenetic sequence of crystal growth may still be inferred despite the nearly complete reaction of Cpx and Opx (+ Ol?) to Cam, Bt and/or secondary (metamorphic) Opx and Cpx. The igneous assemblage, based on the least recrystallized samples, is Opx-Cpx-Pl-Cam-Spl±Ol with accessory Ap-Zrn and Fe-Ti oxide.

Pl is the most abundant mineral and generally the least recrystallized. Pl is commonly lath shaped with carlsbad and albite twinning present in most crystals. The laths range in size from 5mm to 10 mm long and sometimes form agglomerations in radiating patterns. In samples that are more recrystallized, grain boundaries are seriate and resorbed. Normal zoning is present in all of the crystals and some crystals preserve oscillatory zoning enhanced by fine grained Spl inclusions. All of the Pl crystals are variably charged with Spl inclusions that typically occur in the cores of those crystals.

Only in one sample are un-recrystallized igneous Cpx and Opx found. Both pyroxenes occur as interstitial phases charged with fine-grained opaque inclusions and exsolved Rt orientated to crystallographic planes.

Fresh Ol was observed in one sample. It is not zoned and is rimmed by Opx produced via the reaction of Ol with silica. Similar Ol-Opx textures are reported by Emslie et al. (1984) for the Mealy dykes. Ol also has undergone a reaction with Pl to produce magnificent kelyphytic textures in this sample (Figure 6-27, see below).

Forest green Spl occurs mainly with Fe-Ti oxides in the same section with Ol and primary Ccp and Fe-Ti oxides. Oxides rarely show exsolution lamellae and are generally anhedral.

Recrystallized phases assumed to have been produced during the Grenvillian orogenic cycle include Opx-Cpx-Cam-Bt-Grt. These phases generally formed *in situ* and may form part of corona structures present through static metamorphism of many of the dykes in the CCRA. Corona structures are described below in section 6.5.3

Both Opx and Cpx are present in most sections. Opx and Cpx commonly occur as aggregates of small grains that locally form moats or coronas around other pyroxenes (e.g., Cpx coronas around Opx and vice versa). Pseudomorphs of Ol are replaced by Opx and opaques via the oxidation reaction:

$$Ol = Opx + Mag \quad [R15]$$

A distinctive feature of this reaction is the fine grained needle-like opaques concentrated at

the cores of the pseudomorphed Ol (Figure 6-28). In most cases, Cpx and Opx are replaced partially by Cam. Few samples contain Opx intergrown with Fe-Ti oxides which form radial patterns in the interstices between plagioclase laths (Figure 6-29).

Cam is by far the most abundant hydrous Fe-Mg mineral in the dykes. The modal abundance of Cam differs from sample to sample. It is generally pleochroic tan to green and fine grained. It is usually found in corona structures along with fine-grained inclusions of Spl and also as pseudomorphs of Cpx.

Bt is commonly associated with the Fe-Ti oxides where Bt usually forms part of a corona structure with Cam or Grt. Grain size of Bt depends mainly on location within the corona structures. It either occurs as large grains surrounding opaques (5mm in diameter), or as fine grains intergrown with Grt.

Grt occurs as small subhedral grains in coronas or forms part of a symplectite with a clear low relief, low birefringent phase (Kfs?). Widths and morphologies of Grt coronas vary from sample to sample.

6.5.3 Characterization of Corona Structures

Corona structures are subdivided into three types based on whether the central phase in the core is 1) Fe-Ti oxide, 2) Cpx or Opx or 3) Ol or pseudomorphed Ol (Opx + Mag) with phenocrysts or recrystallized plagioclase forming the outer part of the corona in each type.

Type 1

Coronas involving Fe-Ti oxides are the most common type present in the suite (see Figure 6-27). Commonly Bt and Cam form the major constituents of the corona with local Grt. Where garnet is present, it may contain inclusions of Bt and or Cam or may be intergrown with a yet undetermined mineral (Kfs or Cpx?).

Type 2

Coronas involving recrystallized, and sometimes relic, Opx and Cpx may have local Grt coronas. Relic Opx and Cpx may be rimmed by recrystallized Opx and Cpx, apparently derived either from the relict crystal or via a reaction involving the pyroxene and the surrounding Pl. In these varieties, Grt coronas are found. The widths of the Grt coronas vary between and in the samples.

Relic igneous Opx and Cpx are more commonly rimmed with Cam than Grt however. Figure 6-26 shows the general texture of a recrystallized pyroxene core with Cam corona although Opx and/or Cpx does not generally contain as many Fe-Ti oxide inclusions in this type of corona. Where Grt is present it may be in direct contact with Cpx and/or Opx or there may be a thin rim of Bt and or Cam separating the two phases.

Type 3

Coronas involving Ol or Ol pseudomorphs composed of Opx and Mag (see Figures 6-27 and 6-28) are present in a few samples. This corona type is characterized by kelyphytic coronas involving the general corona structure consisting of Ol (or Opx+Mag) →Opx→Cam±Spl→Pl. The timing of Ol replacement/oxidation is uncertain. It may have taken

place during the Grenvillian orogeny, but formation during late stages of emplacement at ~1250 Ma cannot be ruled out. Emslie et al. (1984) reported that Ol pseudomorphs are "rare" in samples from the Mealy Dykes to the south. Kelyphytic coronas are assumed to have formed during Grenvillian metamorphism as no such textures are reported in Mealy Dyke samples.

6.6 Discussion

Peak metamorphic conditions for the rocks of the shear zone footwall and hangingwall rocks may be estimated with the use of petrogenetic grids based on the peak mineral assemblage and reactions and textures discussed above. Two grids were introduced to show the reactions as they appear in *P-T* space and these grids may now be used to constrain the metamorphic conditions achieved by the rocks in the Goose Bay area. The two grids are used include the NaKFMASH system for pelitic rocks (after Spear et al. 1999) and the CFMASH grid for metabasite rocks (after Pattison in press). Metamorphic facies for metabasite rocks are shown in Figure 6-30 where the amphibolite-granulite-eclogite facies *P-T* fields are defined. Important to note is the granulite facies in this study is defined by the presence of Opx. There is however, a transitional *P-T* field where Opx and Hbl may coexist separating the granulite and amphibolite facies. Figure 6-30 also shows the Opx-free domains where the high-pressure (HP) granulite subfacies occurs (Pattison in press). Figure 6-31 shows the CFMASH grid with the general reactions which define the boundaries between amphibolite granulite and HP granulite facies.

6.6.1 Metamorphism of the Footwall Rocks

The peak assemblage for the orthogneiss of the GBT (Grt-Cam-Bt-Pl-Kfs-Qtz) is not diagnostic of either amphibolite or granulite metamorphic facies, however based on the local presence of reaction R2 (Hbl + Pl + Qtz = Grt + Cpx + L) adjacent to the shear zone, suggests that the GBT orthogneiss achieved the metamorphic conditions up to the lower boundary of the transition to the HP granulite facies assemblage (Grt-Cpx-Pl).

The LMT orthogneiss peak assemblage (Opx-Cpx-Hbl-Pl±Grt) suggests that these mafic rocks achieved moderate pressure granulite facies conditions (Figure 6-30). Some rocks from the LMT mafic orthogneiss also preserve evidence of reaction R9 (Opx + Pl = Grt + Cpx + Qtz) which suggests that these rocks achieved the lower boundary for the transition into HP granulite facies conditions (Figure 6-31).

The paragneiss assemblage suggests that the footwall rocks achieved pressures greater than the Ky-Sil transition and surpassed the melting reaction Ms + Pl = Ky + Kfs + L (~700 °C) to produce the leucosomes in the paragneiss (as shown on Figure 6-32) and also must have surpassed the Bt melting reaction Bt + Ky = Grt + Kfs + L for this reaction to be observed in reverse in the paragneiss. The lack of Opx in the assemblage suggests that the reaction Bt + Grt = Opx + Ky + L was not achieved during peak metamorphism, placing an upper temperature limit for peak metamorphism at < 875 °C (in the Ky field). The minimum pressure is constrained by Ky in the assemblage. Thus assemblages in paragneiss record conditions within the *P-T* field shown on Figure 6-32 at >8-11 kbar and 700-875 °C.

6.6.2 Metamorphism of the Hangingwall Rocks

The rocks in the upper sections of the thrust stack (Northwest River anorthosite and underlying gabbronoritic rocks) do not contain evidence for penetrative fabrics and Grenvillian metamorphic assemblages (Grenvillian metamorphism largely limited to static coronas in mafic rocks), whereas the recrystallized gabbro-diorite unit and granitoid gneisses at the base of the CCRA are inferred to be composed of Grenvillian metamorphic assemblages. The Northwest River dykes contain only Grenvillian metamorphic assemblages and thus the dykes can be used to accurately gauge the effects of Grenvillian metamorphism in the CCRA. The Northwest River dykes generally preserve the two-pyroxene plus amphibole (Opx-Cpx-Hbl-Pl) assemblage or may locally have the peak assemblage Grt-Cpx-Cam-Pl-Qtz (Figure 6-30). Grt-Cpx-Cal veining present in the Northwest River dykes is inferred to have been the result of the breakdown of amphibole to produce garnet and clinopyroxene in the presence of a CO_2-bearing fluid. The presence of the Grt-Cpx veins is assumed not to be the result of an increase in pressure or temperature but rather is a function of fluid composition and activity. The general reaction to produce the Grt-Cpx veins is R2a ($Cam + Pl + Qtz + CO_2 = Grt + Cpx + H_2O \pm Cal$), shown in Figure 6-33 along with other reactions pertinent to the metabasites of the field area. The reactions all assume that the activity of water is one and thus the invariant point lies at the point marked i_1 on Figure 6-33. If CO_2 was present during metamorphism and mixed with H_2O, then the activity of H_2O decreases according to the amount of CO_2 present. All the reactions in the CFMASH system include a fluid except the [Hbl] reaction and thus the invariant point, and the remaining reactions ([Opx], [Cpx], [Grt], [Pl]), slide along the projection of this reaction (reaction [L])

to a point (i_1') reflecting the decreased activity of H_2O in the system. Thus this reaction is primarily the result of fluid composition and activity and not changing *P-T* conditions during peak metamorphism.

6.6.3 Metamorphism of the GLTS

The rocks from the shear zone of the GLTS vary in inferred peak assemblage based on the assumed rock composition e.g., granitoid to diorite compositions. Peak assemblages from the GLTS vary from Grt-Cpx-Pl (Grt-Cpx-Pl±Hbl) to Grt-Cpx-Opx-Pl±Hbl and others contain the lower pressure peak assemblage Cpx-Hbl-Pl±Grt and Opx-Cpx Pl (Figure6-30). A few rocks contain two peak assemblages such as Grt-Cpx-Hbl-Pl and Opx-Cpx-Hbl-Pl and Grt-Cpx-Opx-Pl and Grt-Cpx-Pl±Hbl. These assemblages, based on Figure 6-30, occur at the transition from amphibolite facies to Opx-free domain and the transition from granulite facies to the lower boundary of the Opx-free domain. It is inferred that the variation in the peak assemblage in the GLTS is due to the variation bulk composition of the investigated rocks and the activity of H_2O in the GLTS. The stability of Cam in the peak assemblage of some rocks implies that fluid was present during metamorphism. Scp, also present in many assemblages from the shear zone, implies that CO_2-bearing fluids were present during high temperature ductile shearing in the GLTS thus affecting the location of the invariant point in the CFMASH system as discussed above.

Thus the rocks of the GLTS are inferred to have attained granulite facies conditions with the presence of local the Opx-free HP granulite facies assemblage (Grt-Cpx-Pl± Hbl or

Qtz) in compositional domains in the rocks. The next chapter will quantify the *P-T* estimates when geothermobarometry is applied to select samples from the study area.

6.6.4 Reaction Summary

$5An + Grs + 2CO_2 = 2Me + Qtz$ [R1]

$Grt + Cpx + H_20 = Hbl + Pl + Qtz$ [R2]

$Hbl + Pl + Qtz + CO_2 = Grt + Cpx + H_2O + Cal$ [R2a]

$Grs + 2Prp + 2Kfs + 2H_2O = 2Phl + 3An + 3Qtz$ [R3]

$Grs + 3Prp + 3Kfs + H_2O = 3Phl + 3An + Al_2Si0_5 + 5Qtz$ [R3a]

$Ms + Pl = Kfs + Al_2SiO_5 + H_20$ [R4]

$6Cal + 11Qtz + Dol + 2Ep = 3Grt + Di + 7CO_2 + H_20$ [R5]

Fe-Ti oxide or Rt + Ca in Pl = Ttn + less Calcic Pl + Hem [R6]

$Agt + Pl + H_2O = Grt + Na\text{-}Am$ [R7]

$Fts + 4Ttn + 2Alm = 4An + 4Ilm + Ftr$ [R8]

$Opx + Pl = Cpx + Grt + Qtz$ [R9]

$(Mag\text{-}Ilm) + Pl + Kfs + H_2O = Alm + Grs + Ann$ [R10]

$Ol + An = (Fe\text{-}Mg)\ Cpx + Opx + Spl$ [R11]

$3(Fe\text{-}Mg)\ Cpx + 3An = 2Grs + (Fe\text{-}Mg)\ Grt + 2Qtz$ [R12]

$Pl + CO_2 = Scp + Qtz$ [R13]

$4Di + 2Prp + 4An + 2CO_2 = 5En + 2Me$ [R14]

$Ol = Opx + Mag$ [R15]

***Figure 6-1**: Scapolite-quartz-plagioclase in granodiorite gneiss. XPL Sample JK-99-023 For all photomicrographs PPL = plane polarized light; XPL = cross polarized light.*

***Figure 6-2**: Secondary biotite, plagioclase and quartz after garnet and alkali feldspar in orthogneiss from the GBT. PPL Sample JK-99-021*

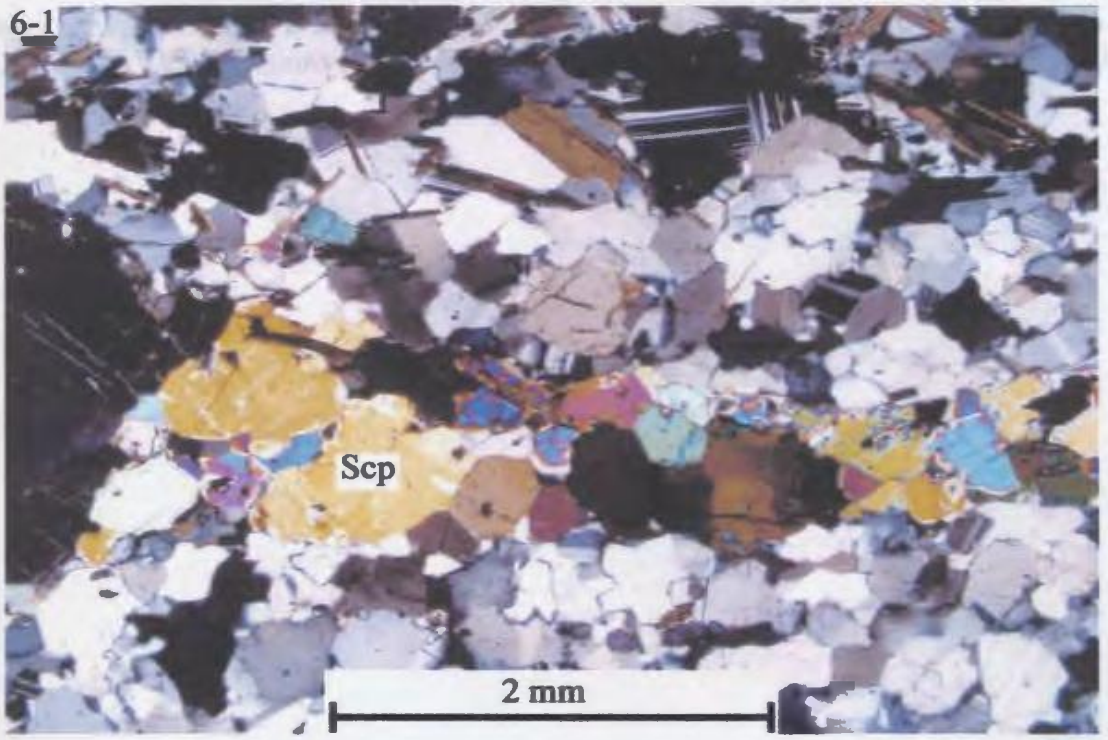
6-1
Scp
2 mm

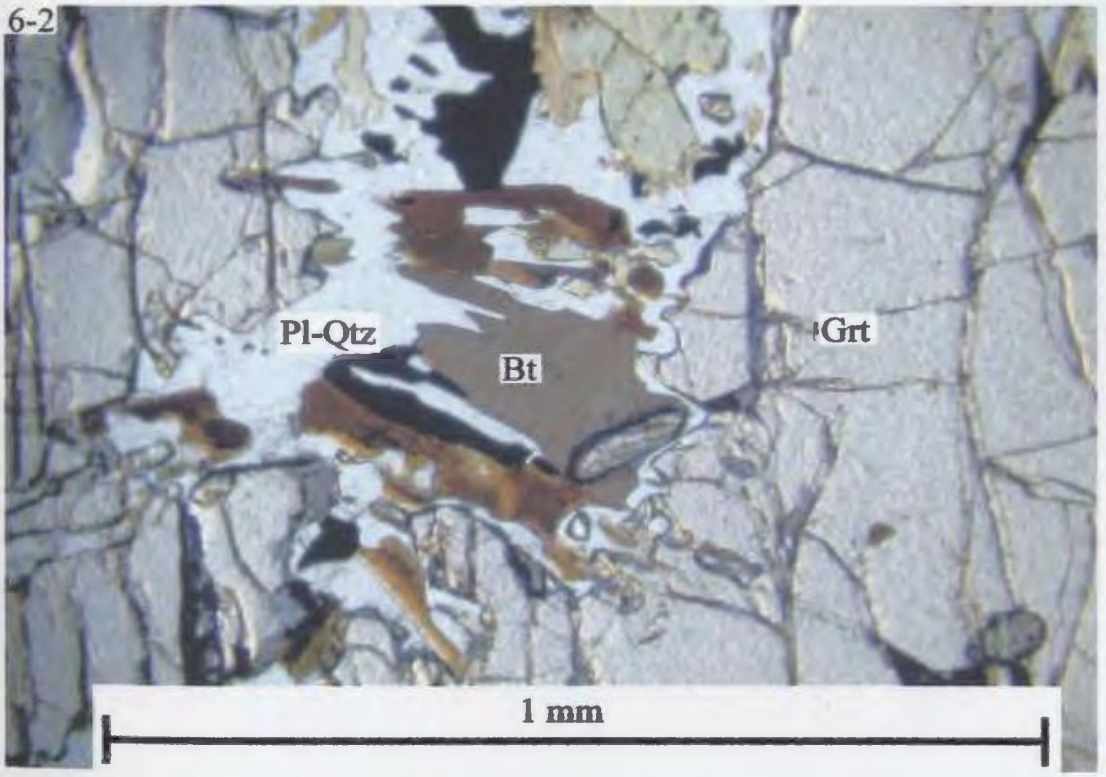
6-2
Pl-Qtz
Bt
Grt
1 mm

***Figure 6-3**: Preferred orientation of kyanite and biotite around a migmatitic lens composed of alkali feldspar, plagioclase and quartz in paragneiss from the GBT. PPL Sample JK-99-002*

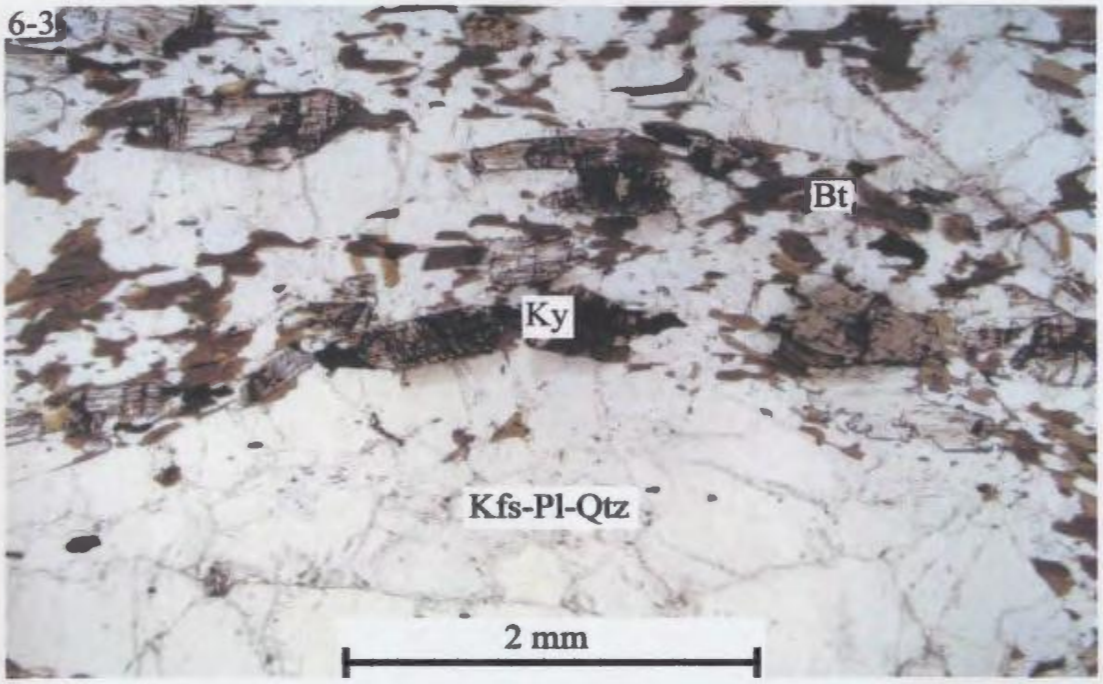
6-3
Bt
Ky
Kfs-Pl-Qtz
2 mm

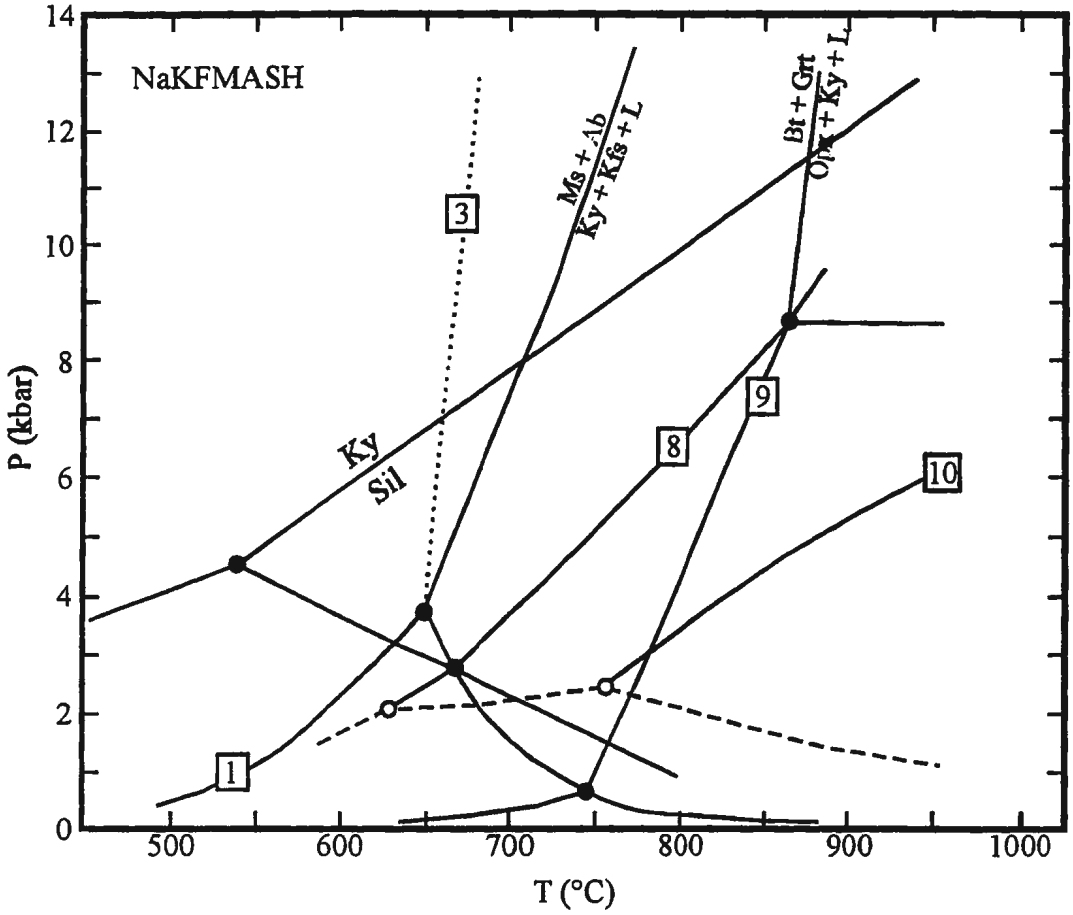

Reactions

1: Ms + Ab = Als + Kfs + V
3: Ms + Ab + V = Als + L
8: Bt + Als = Grt + Crd + L
9: Bt + Grt = Opx + Crd + L
10: Grt + Sil = Spl + Crd

***Figure 6-4**: Petrogenetic grid for the NaKFMASH system (after Spear et al 1999) showing the melting reaction Ms + Ab = Kfs + Als + L. Als= aluminosilicate.*

***Figure 6-5**: Heavily resorbed garnet that is being replaced by secondary biotite, plagioclase and quartz in paragneiss from the GBT PPL. Sample JK-99-001*

6-5

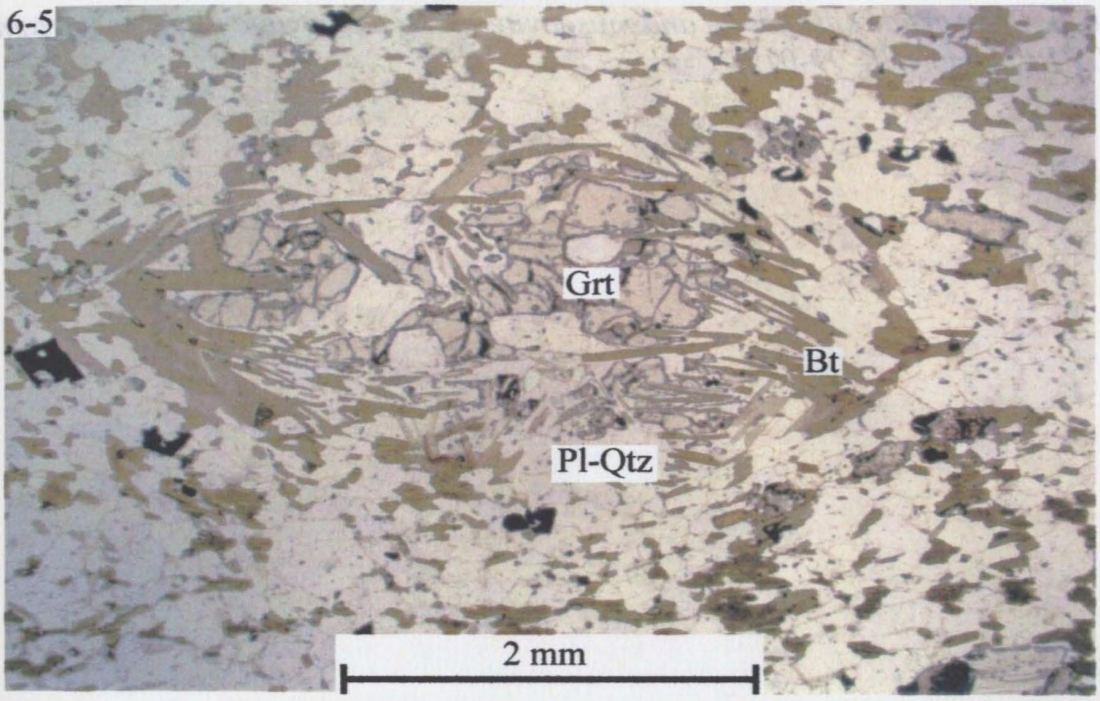

***Figure 6-6**: Retrograde sillimanite and muscovite along a cleavage plane in paragneiss of the GBT. PPL Sample JK-99-019*

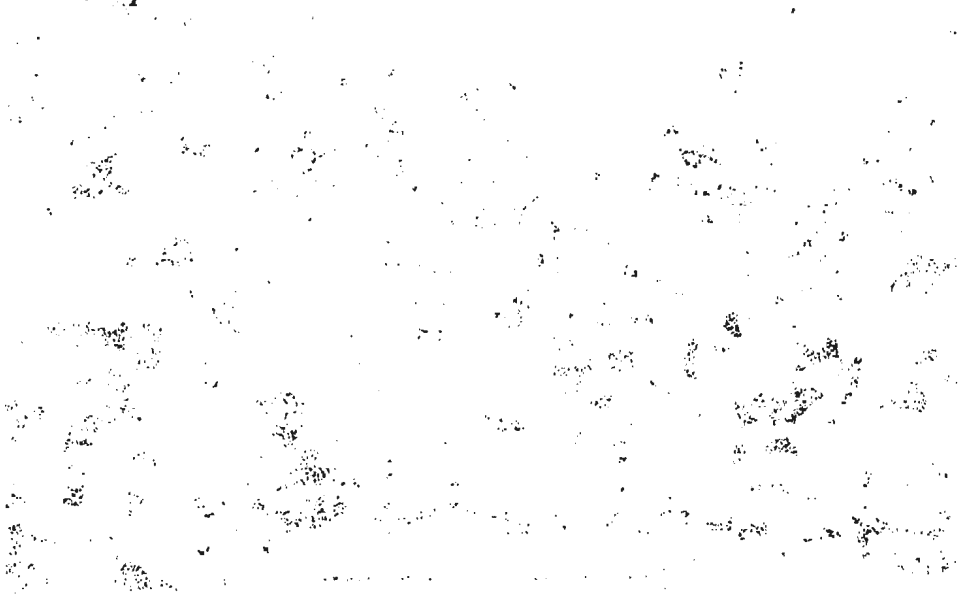

***Figure 6-7**: Calc-silicate sample (JK-99-024a) from the GBT displaying a symplectite reaction involving Grt-Cpx-Ep-Qtz. Note the zoning (yellow fringes) in epidote crystals next to garnet implying post peak metamorphism cation diffusion. PPL.*

6-6

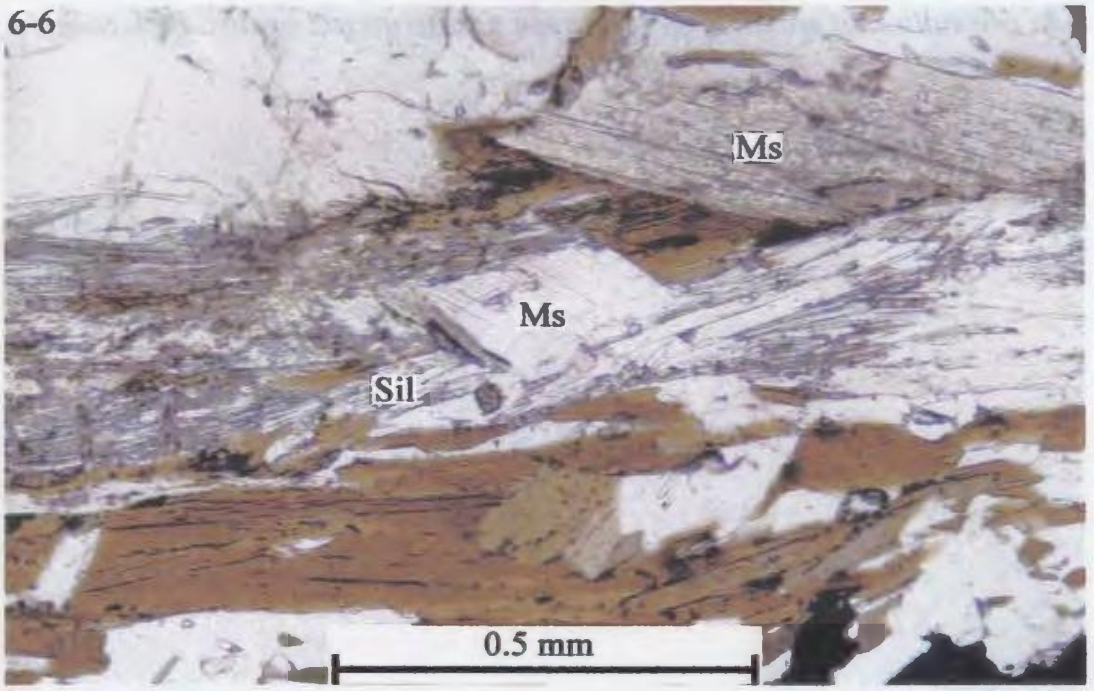

6-7

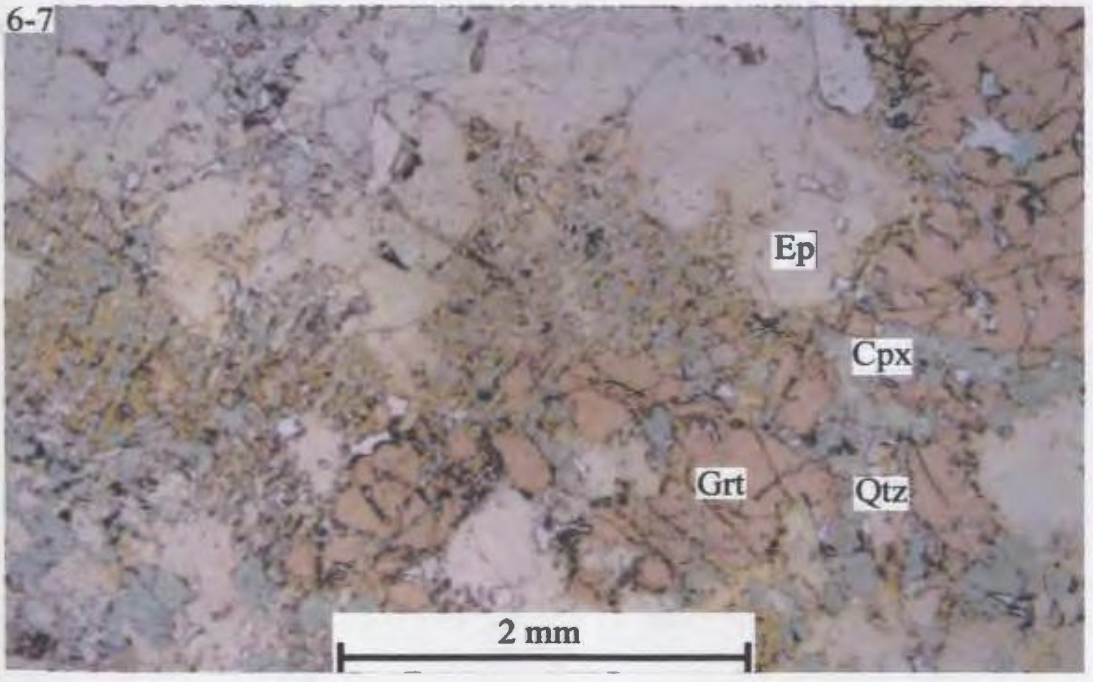

***Figure 6-8**: Formation of epidote rim on garnet next to quartz grains. PPL Sample JK-99-024a*

***Figure 6-9**: Retrograde reaction involving Ti-bearing phases (ilmneite-rutile) to produce titanite in a mafic rock from the GBT. PPL Sample JK-99-079c*

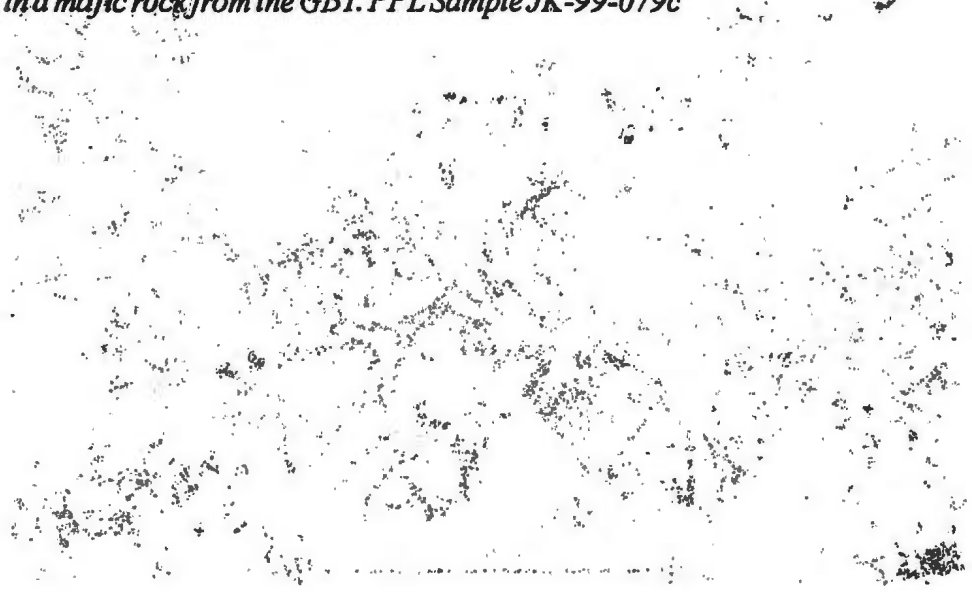

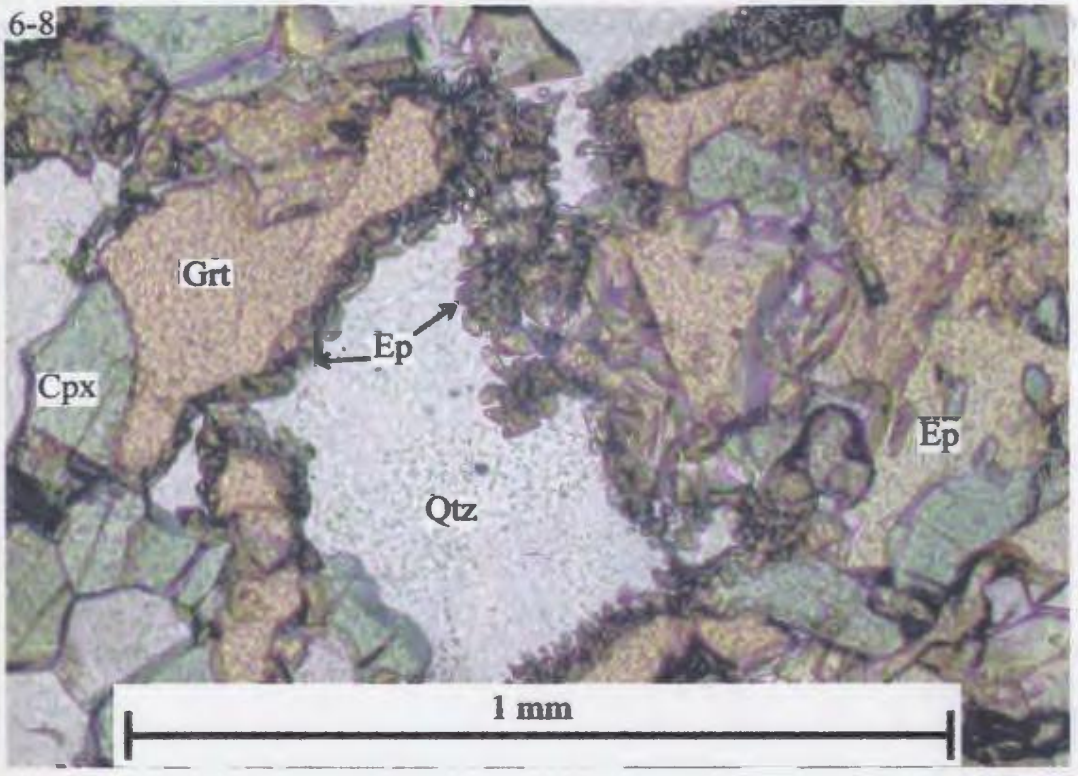
6-8
Grt
Ep
Cpx
Ep
Qtz
1 mm

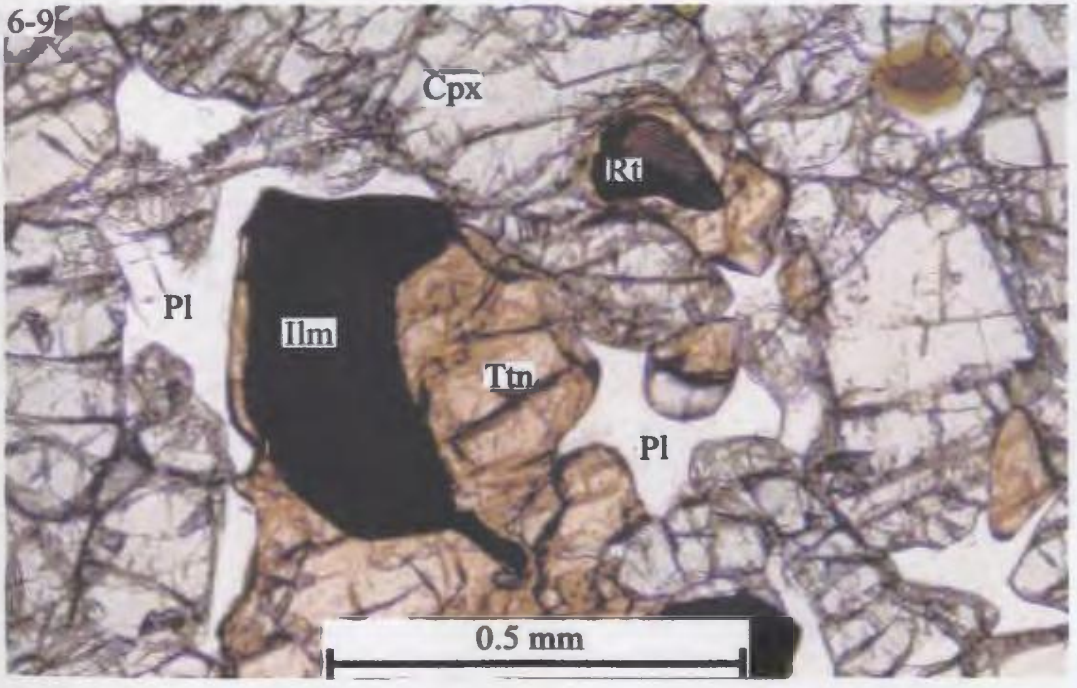
6-9
Cpx
Rt
Pl
Ilm
Ttn
Pl
0.5 mm

***Figure 6-10**: Reaction producing a symplectite of amphibole and Fe-Ti oxide and secondary plagioclase after garnet and titanite in the Arrowhead Lake Pluton. PPL Sample JK-99-102*

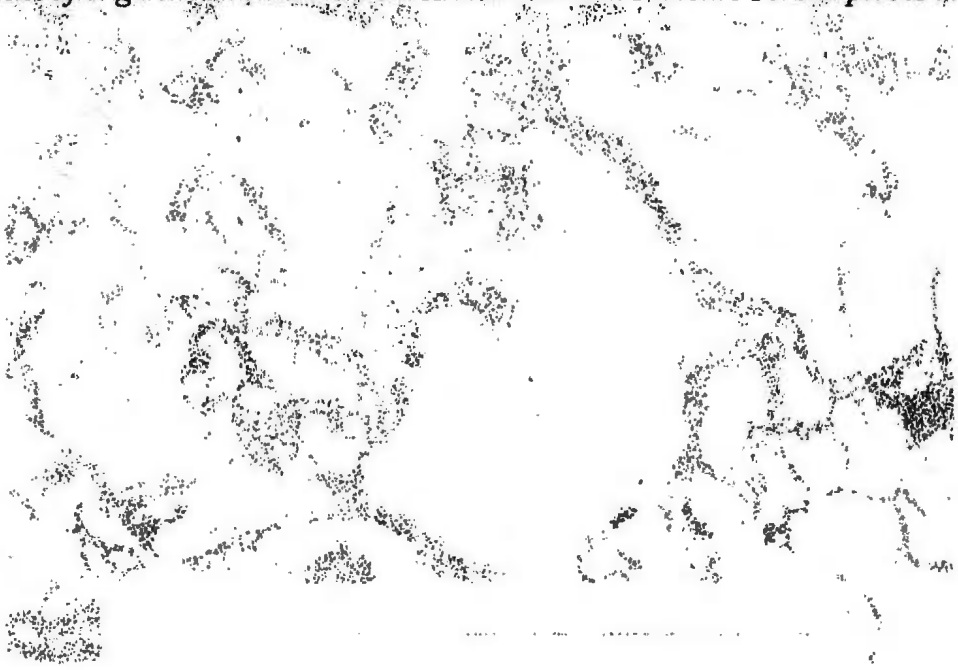

***Figure 6-11**: Domainal equilibrium in mafic gneiss from the LMT. Top part of photo is composed of Grt-Cpx-Pl±Cam whereas the bottom part is Opx-Cam-Pl. Note the lack of orthopyroxene in the upper part. PPL Sample JK-99-054*

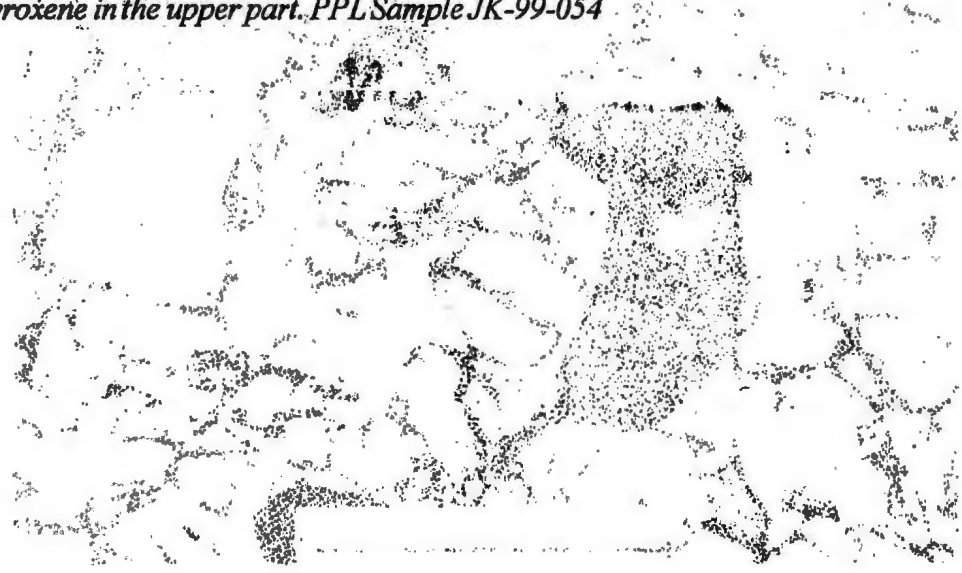

6-10

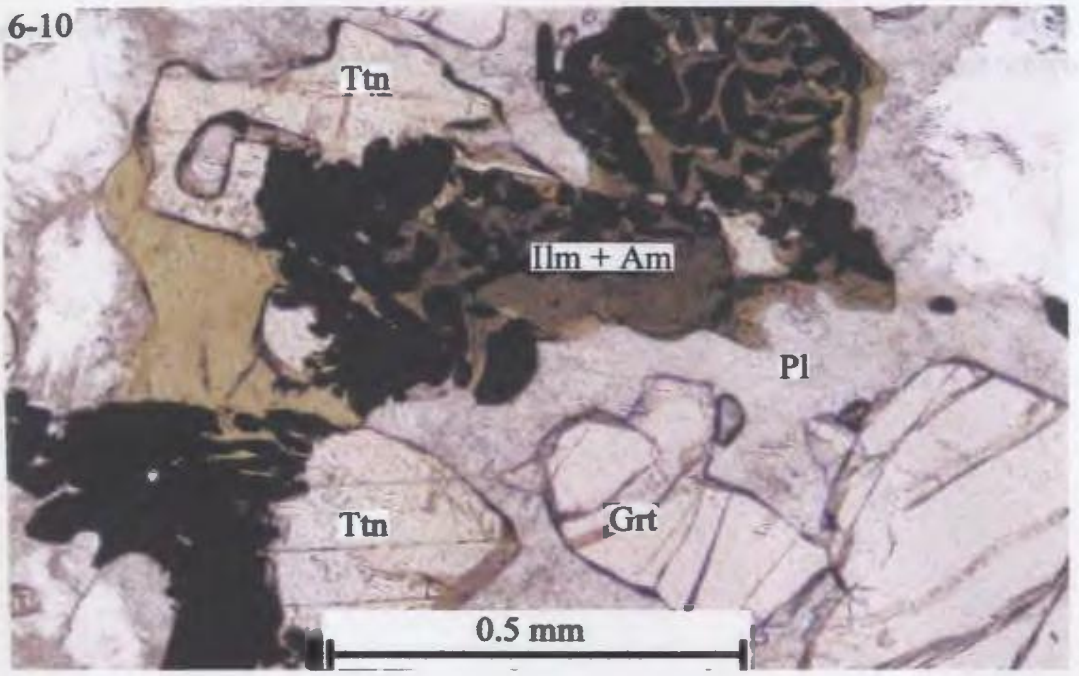

6-11

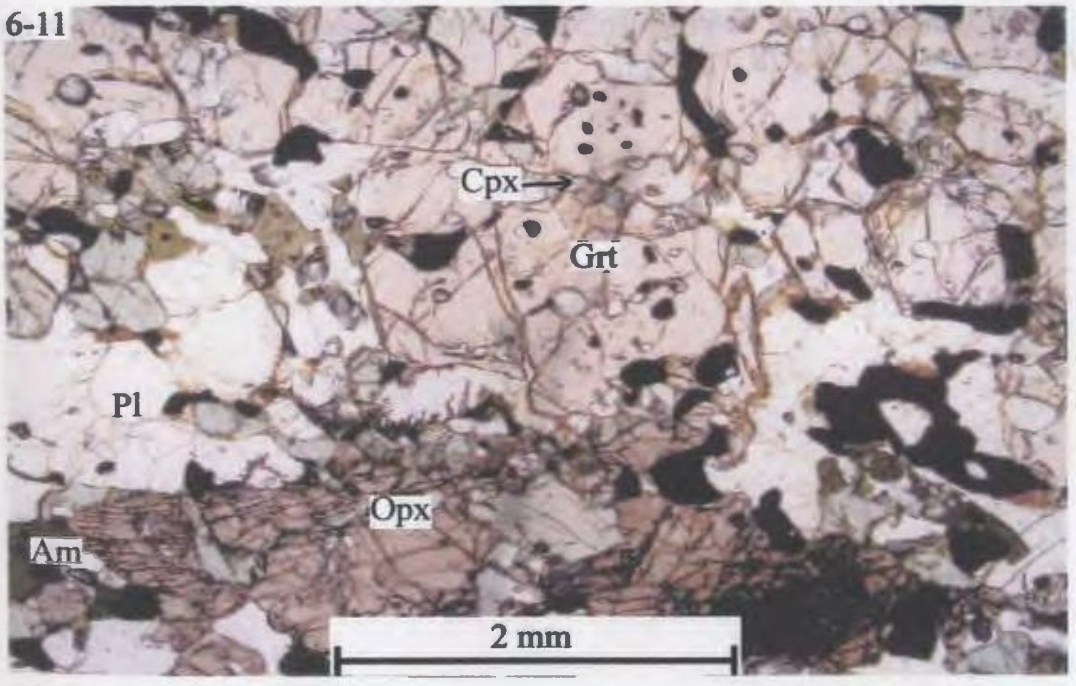

Figure 6-12: *Corona texture in a gabbroic rock with Opx→Cpx→Pl_2→Grt→Pl_1, where Pl_2 is metamorphic feldspar and Pl_1 is relict igneous feldspar. PPL Sample JK-99-151*

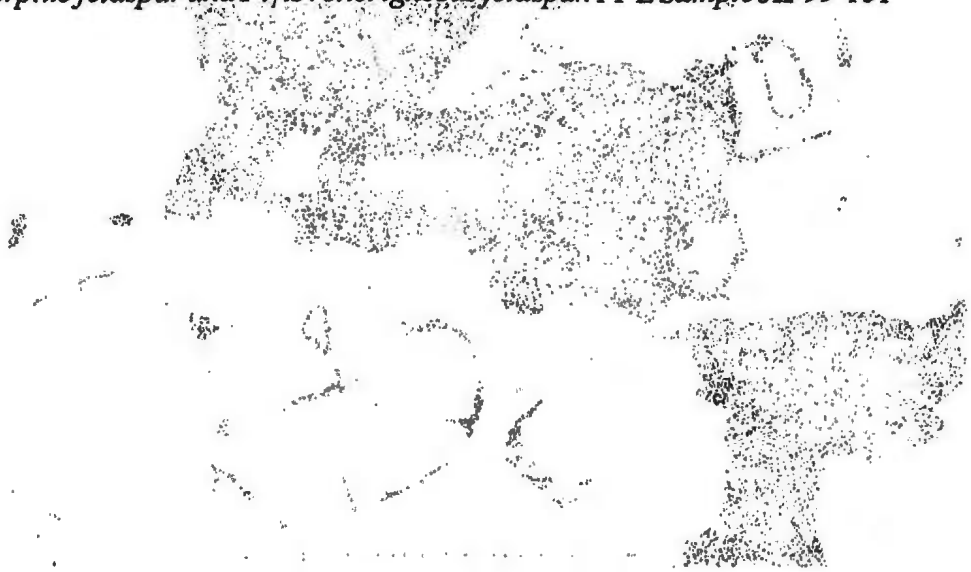

Figure 6-13: *Clinopyroxene intergrown with orthopyroxene in a high strain gabbroic gneiss. PPL Sample JK-99-128*

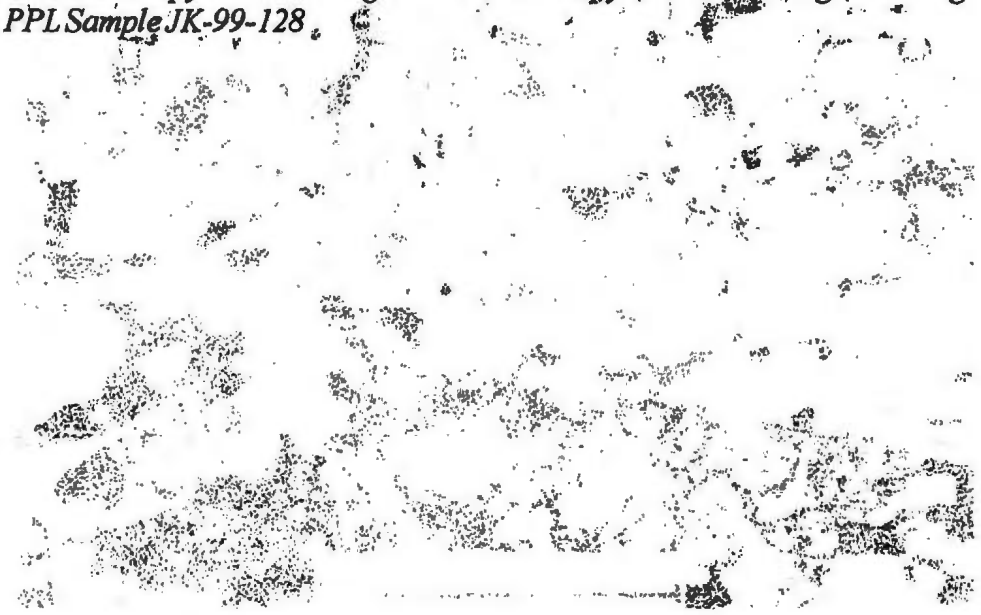

6-12

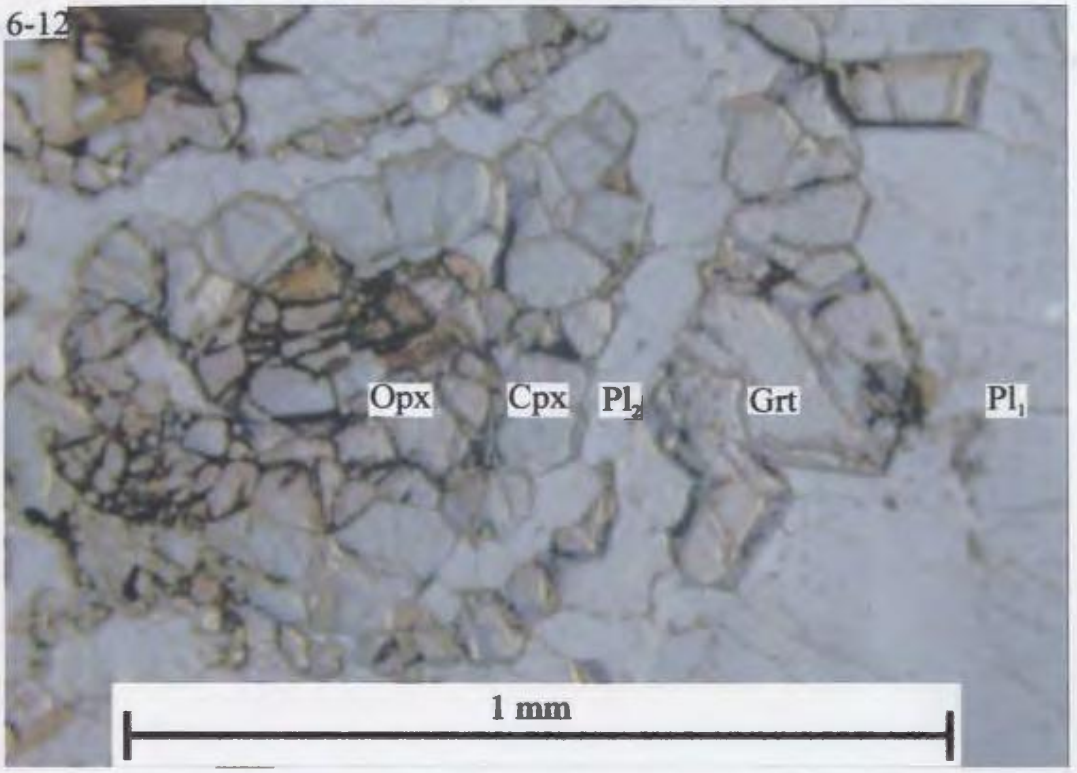

6-13

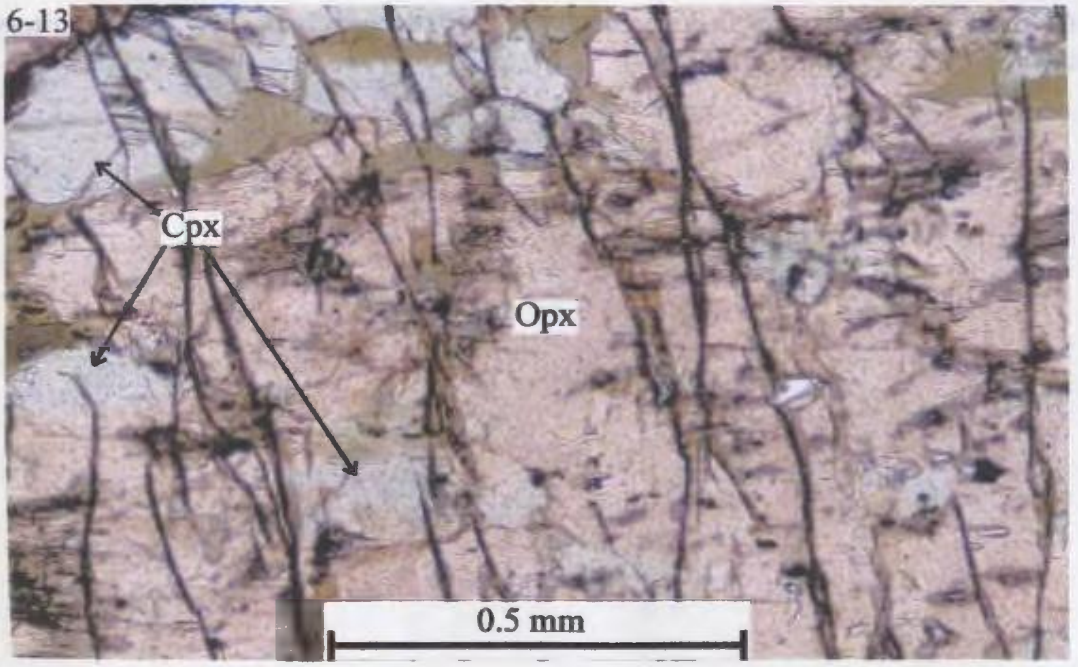

***Figure 6-14**: Syntectonic garnet growing on a resorbed host garnet with unorientated inclusions from the gneiss at Cape Caribou. PPL Sample JK-99-059.*

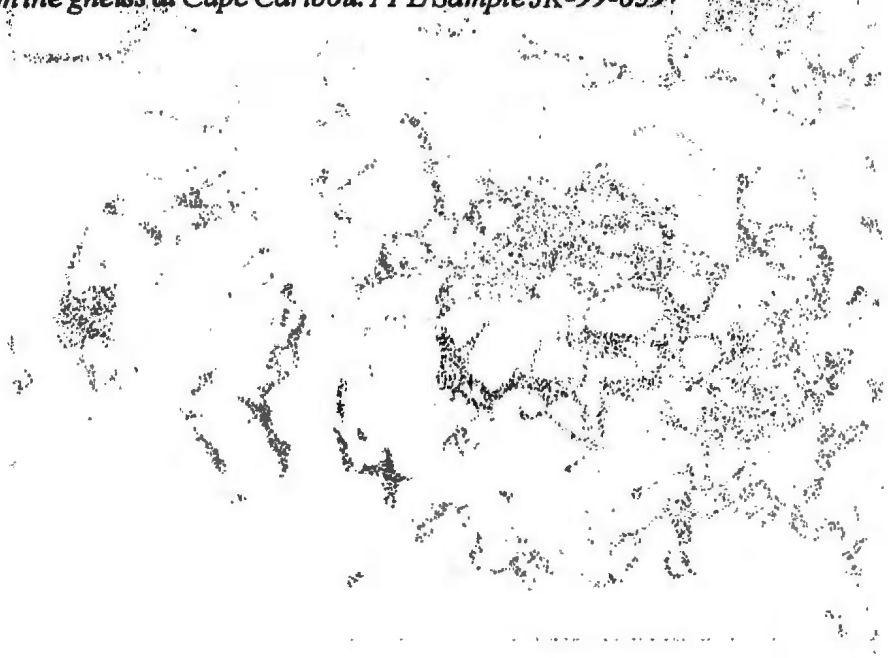

***Figure 6-15**: Microshear zones in a C-S texture that crosscuts orthopyroxene in gneiss from Cape Caribou. PPL Sample JK-99-059*

6-14

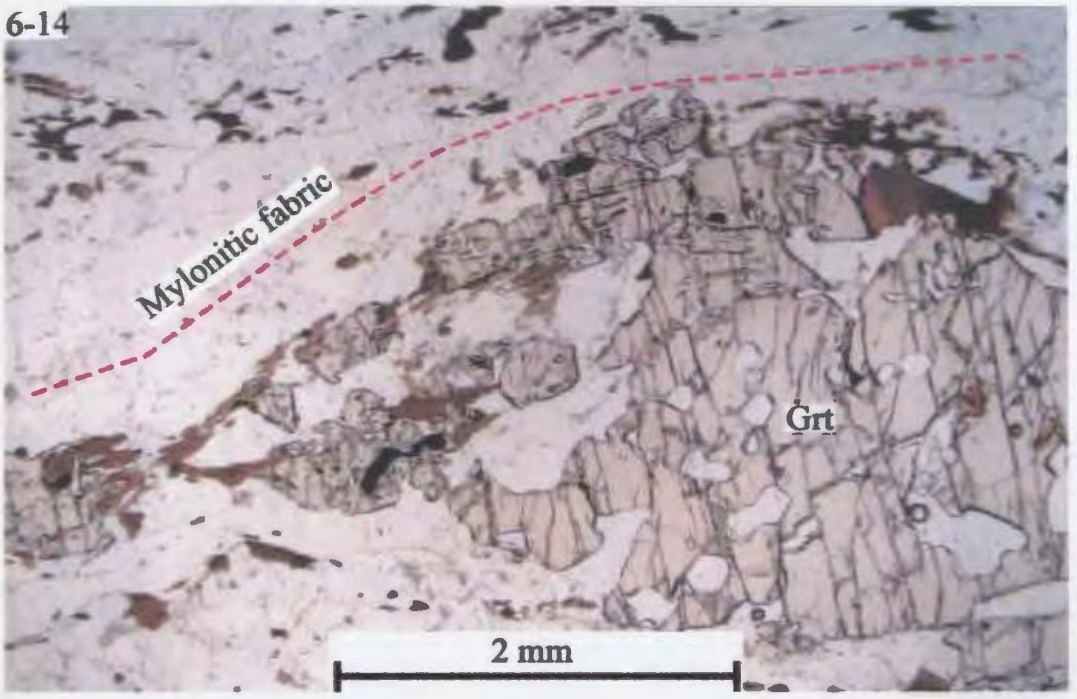

6-15

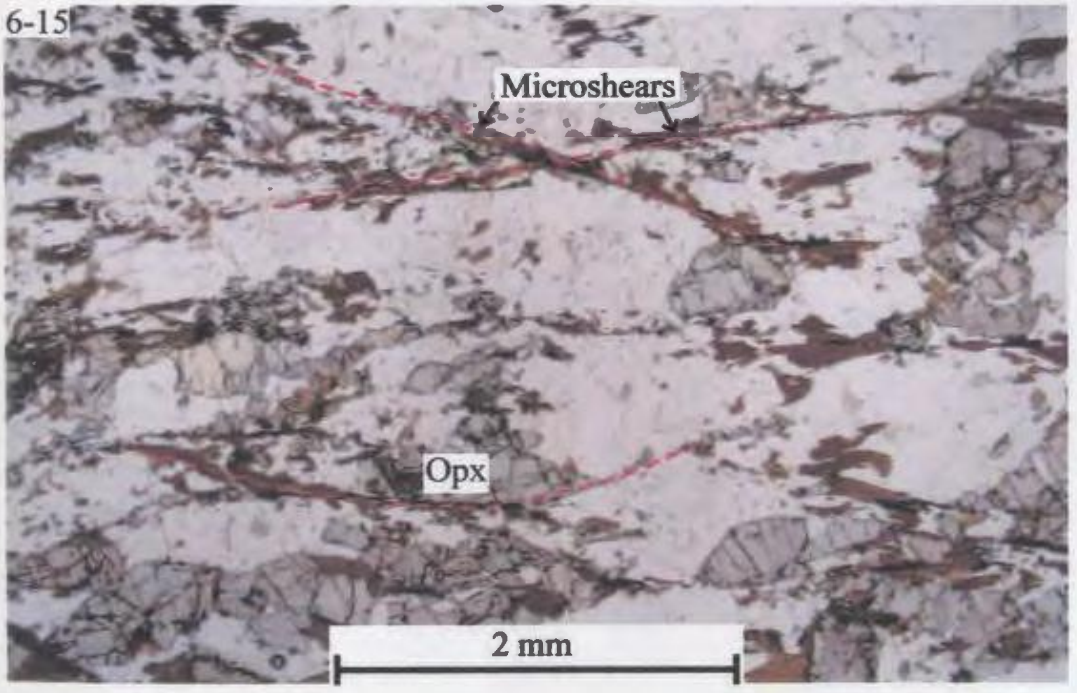

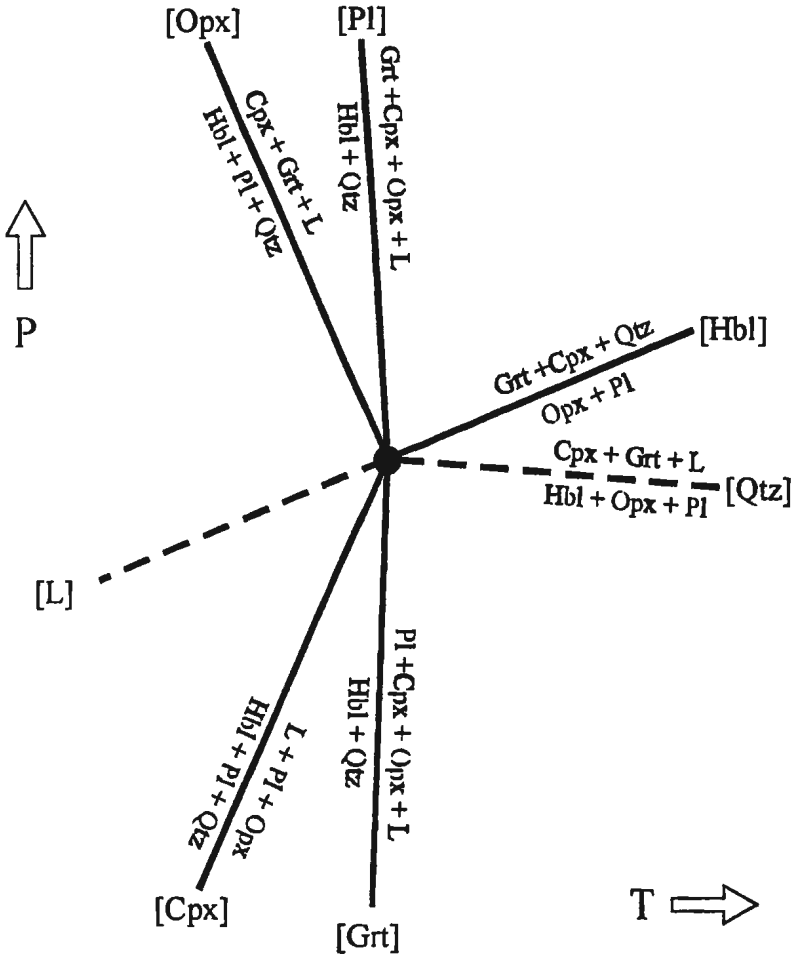

***Figure 6-16**: Phase equilibria in the CaO-MgO-(FeO)-Al_2O_3-SiO_2 (CMASH or CFASH) system after Pattison (in press) assuming the presence of quartz.*

***Figure 6-17**: Clinopyroxene grain displaying exsolution lamellae and grain boundary adjustments in mylonitic gneiss. PPL Sample JK-99-090*

6-17

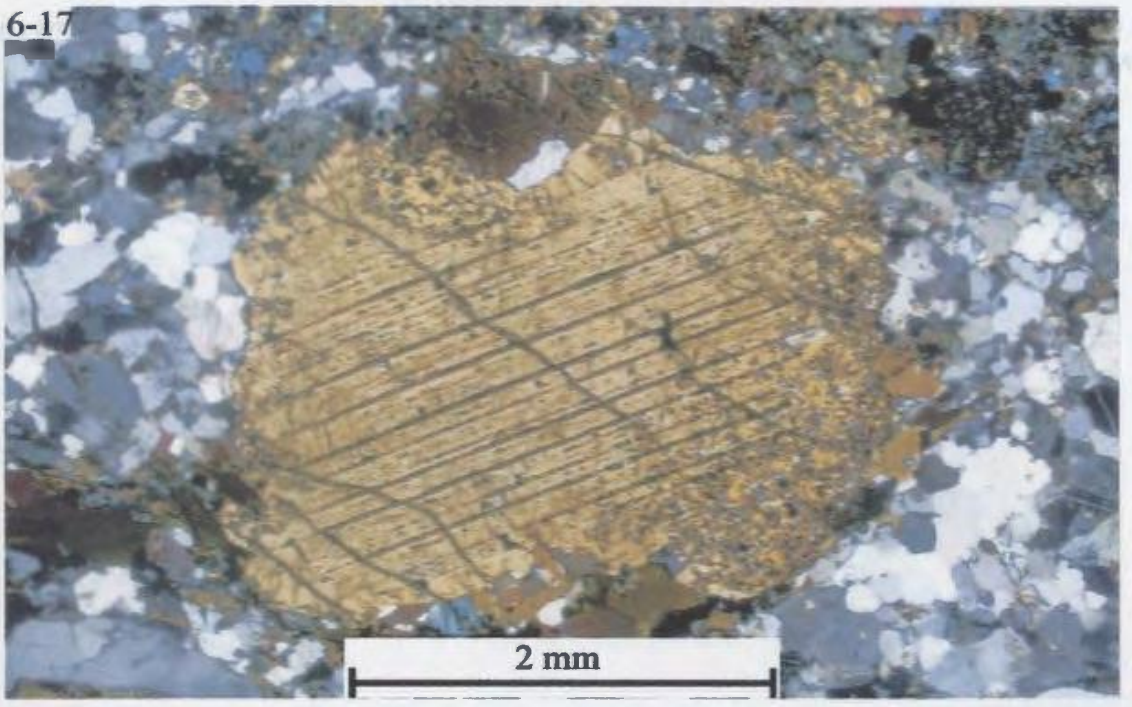

***Figure 6-18**: Calcic amphibole, plagioclase and quartz after garnet and clinopyroxene in mafic gneiss. PPL Sample JK-99-086*

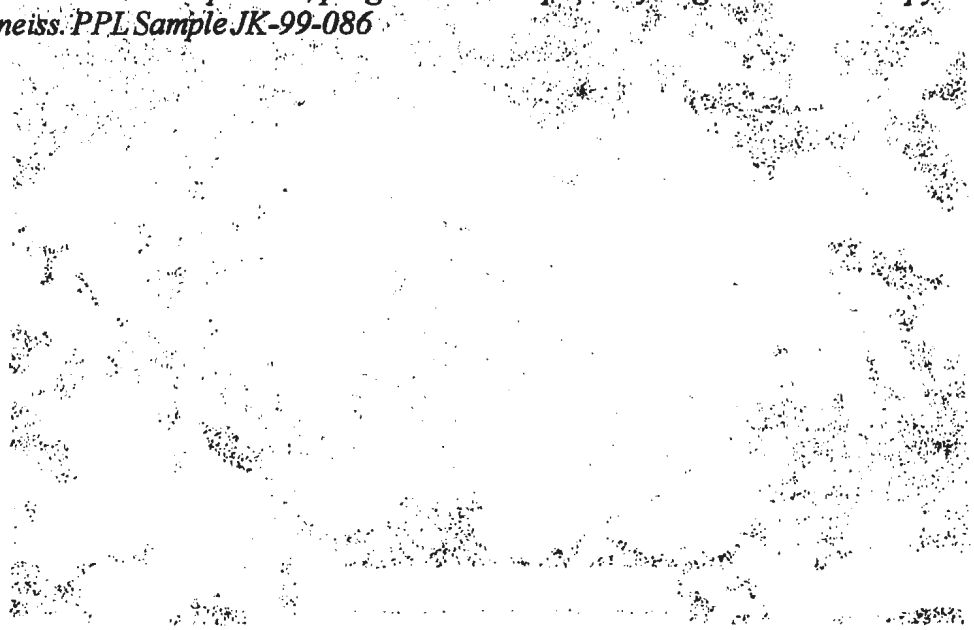

***Figure 6-19**: Clinopyroxene in the pressure shadow of garnet in mylonitic gneiss. PPL Sample JK-99-090*

6-18

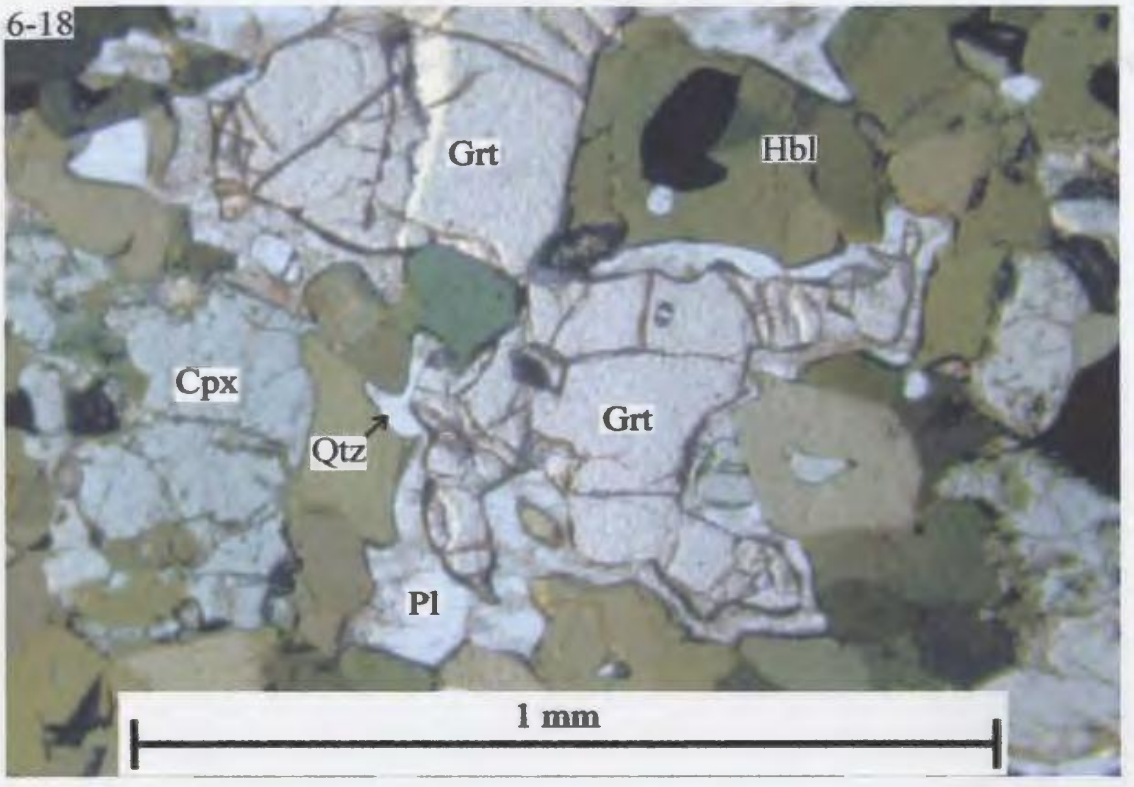

6-19

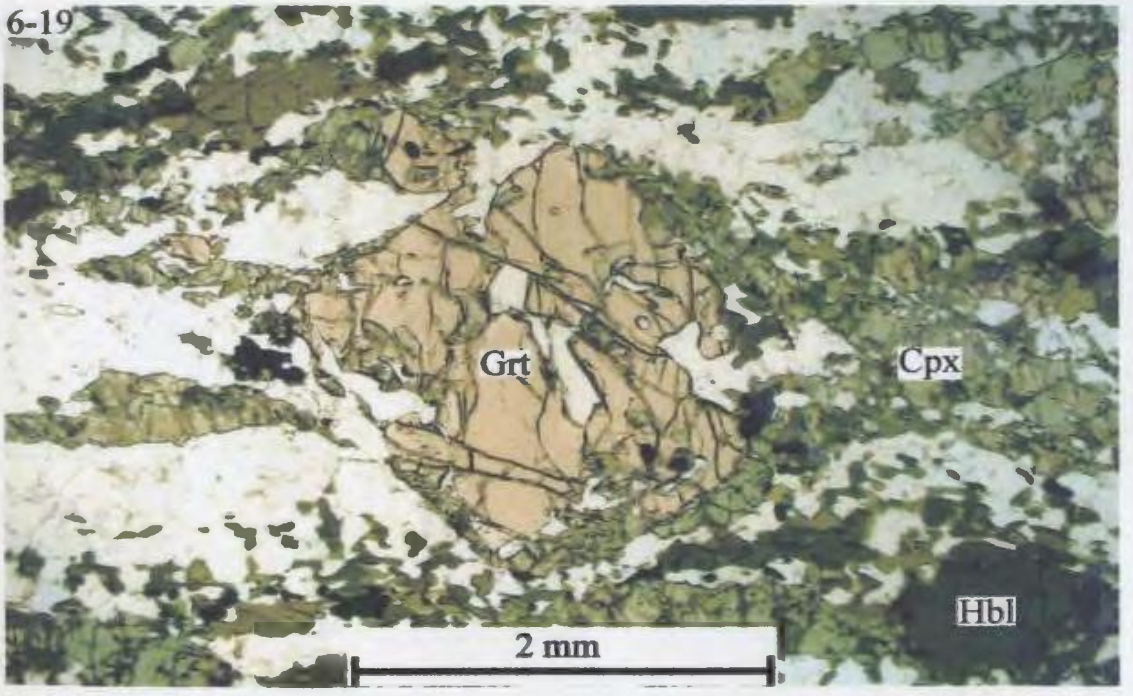

Figure 6-20: *Shape preferred and lattice preferred orientation of quartz ribbons and feldspar in mylonite. XPL + quartz plate. Sample JK-99-015*

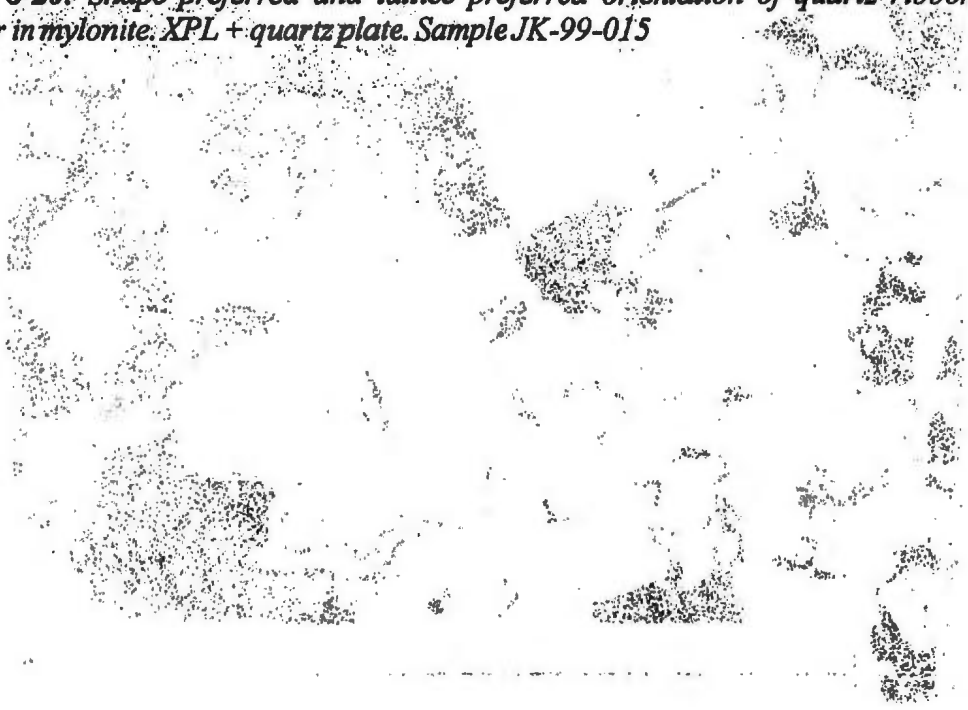

Figure 6-21: *Stable scapolite and orthopyroxene coexisting in mylonite. XPL Sample JK-99-028*

6-20

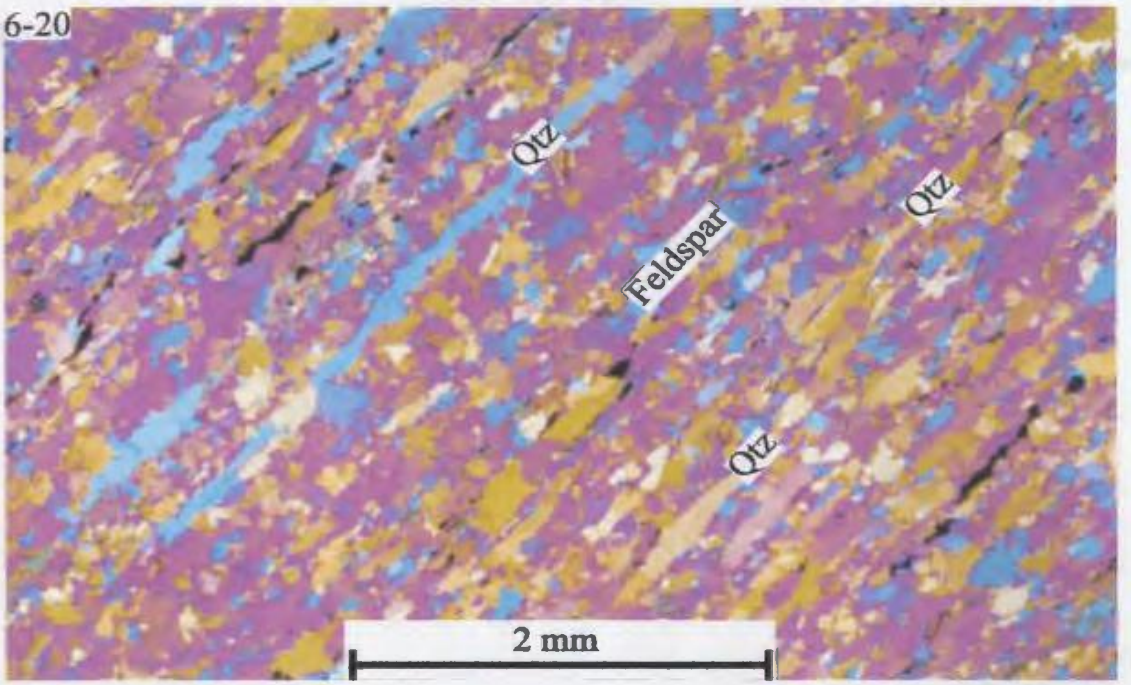

6-21

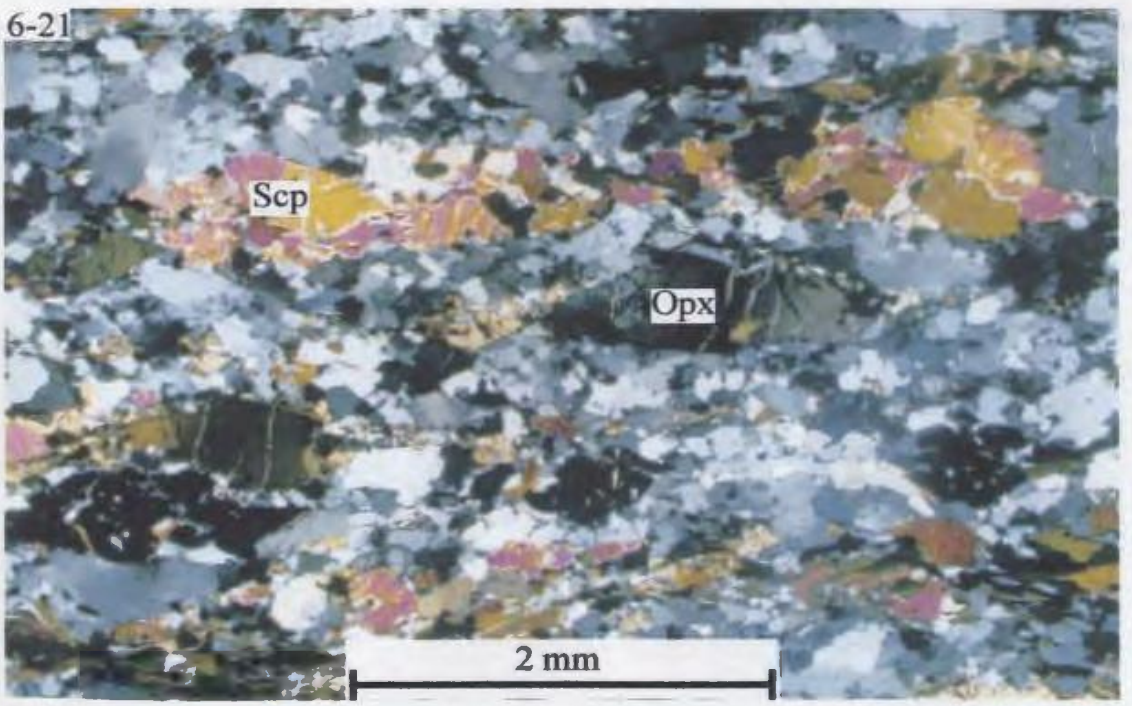

***Figure 6-22**: Knot of retrograde amphibole, plagioclase and quartz in metamorphosed Northwest River dyke. PPL Sample JK-99-037a*

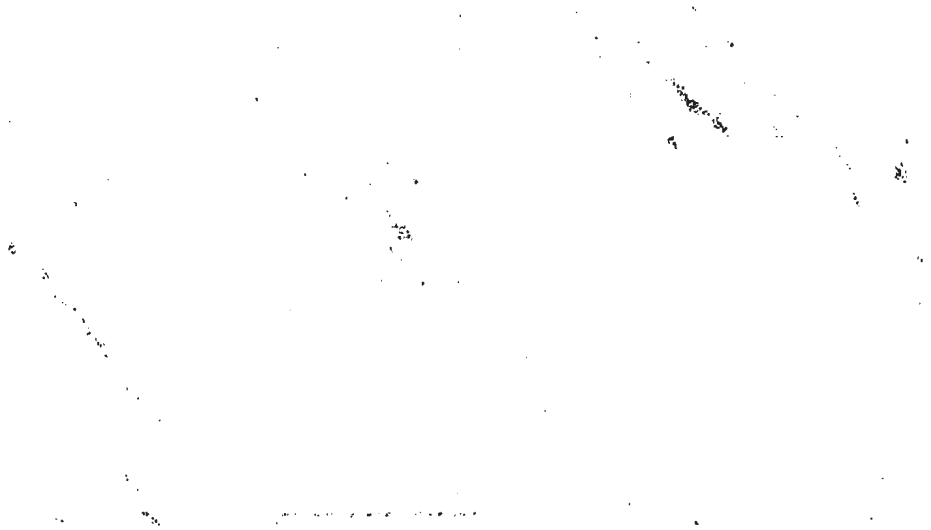

***Figure 6-23**: Garnet with ameobal quartz inclusions in a plagioclase, amphibole ± quartz matrix. PPL Northwest River dyke Sample JK-99-056*

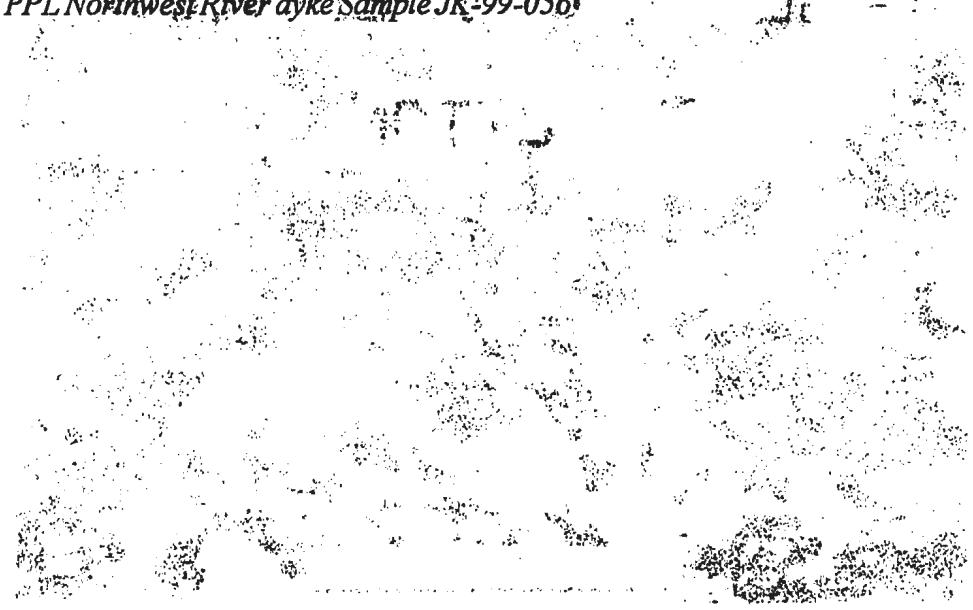

6-22

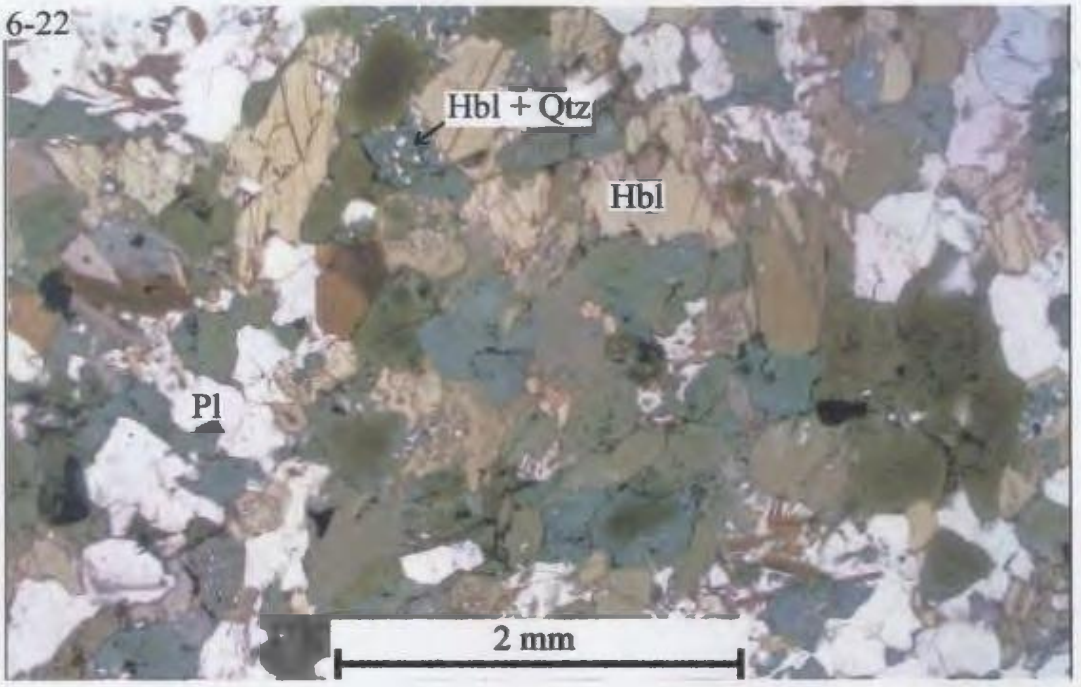

6-23

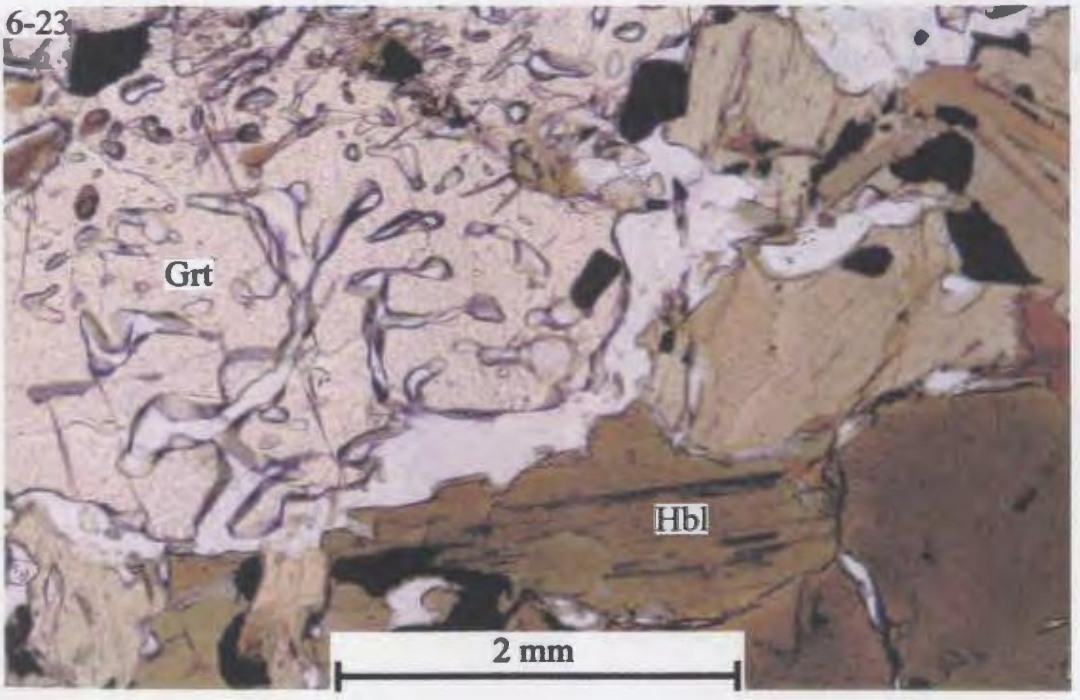

***Figure 6-24**: Partially retrogressed orthopyroxene and clinopyroxene in a plagioclase-amphibole matrix. PPL Northwest River dyke Sample JK-99-041a*

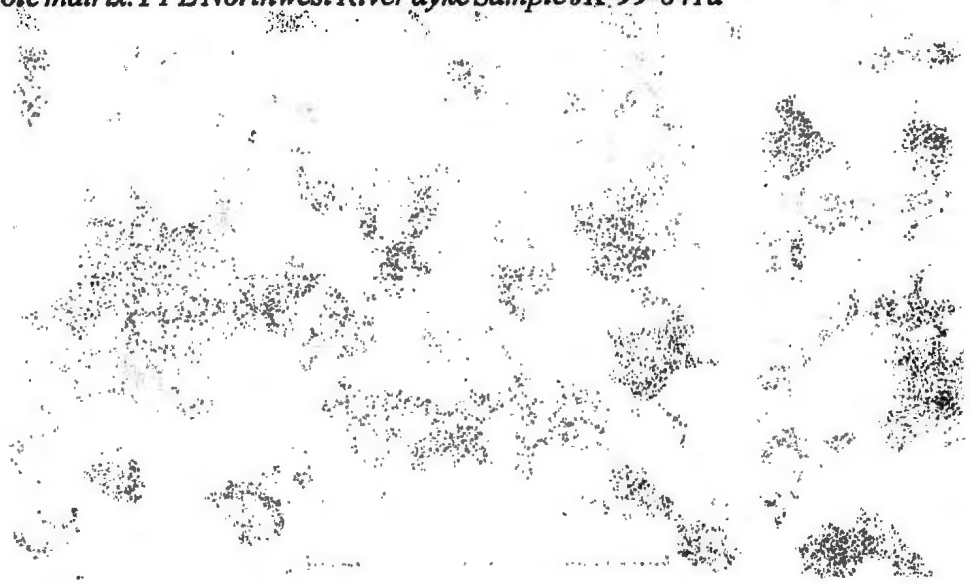

***Figure 6-25**: Relic plagioclase lath in a granoblastic Northwest River dyke. Note the presence of granoblastic feldspar. XPL Sample JK-99-122-1*

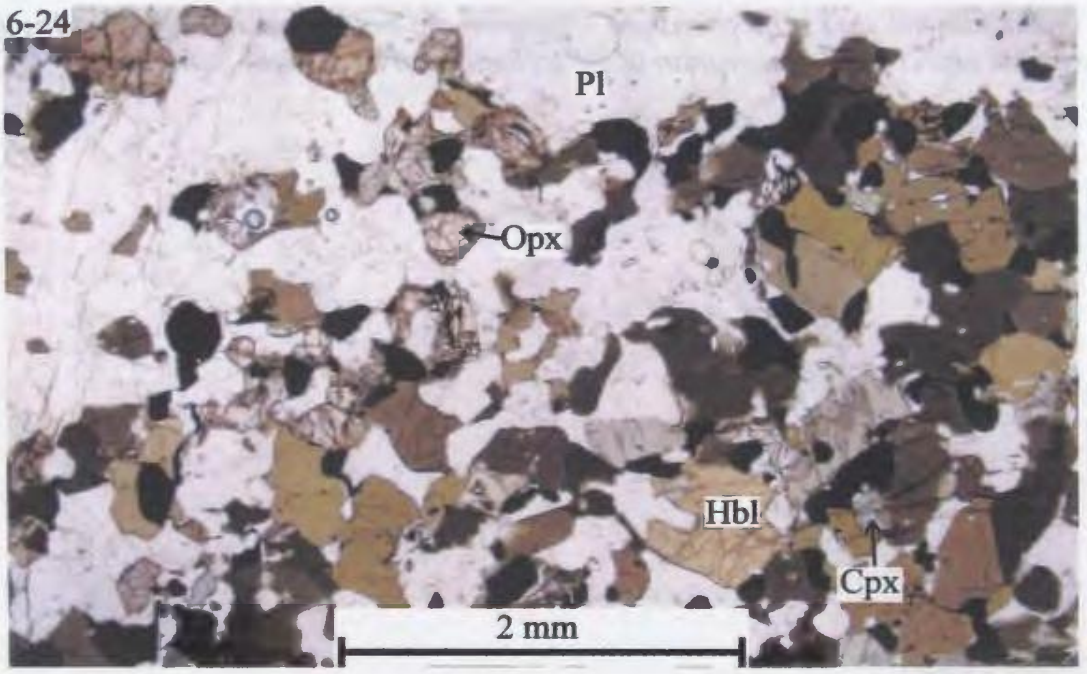
6-24
Pl
Opx
Hbl
Cpx
2 mm

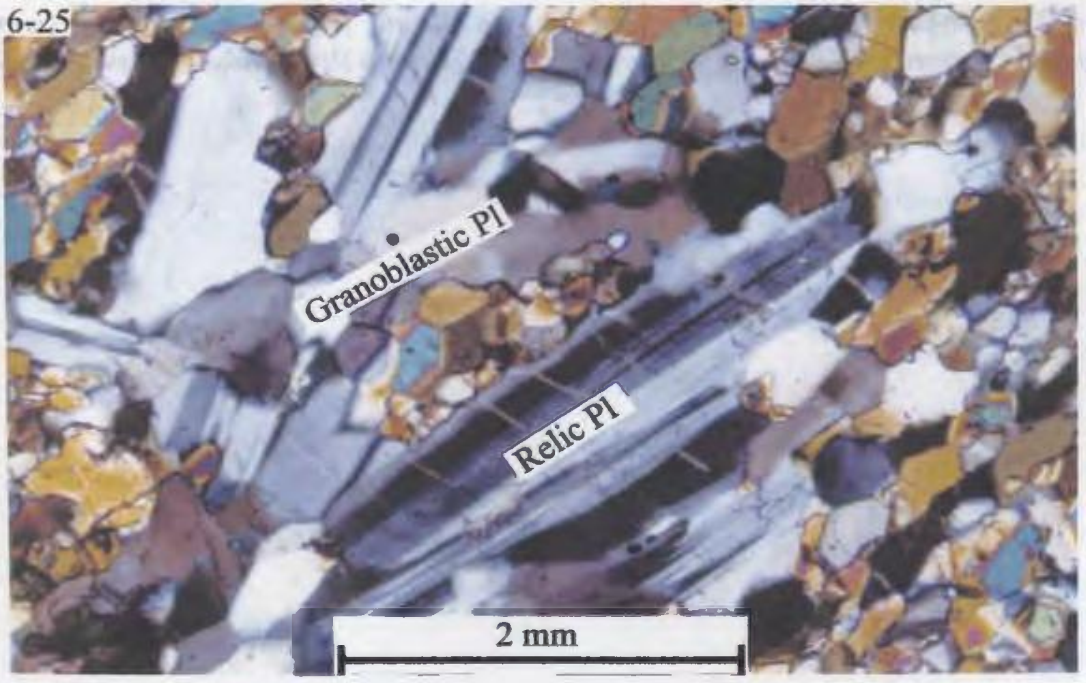
6-25
Granoblastic Pl
Relic Pl
2 mm

***Figure 6-26**: Garnet and clinopyroxene ± amphibole vein in a amphibole, plagioclase, orthopyroxene and clinopyroxene matrix. PPL Northwest River dyke Sample JK-99-122-1*

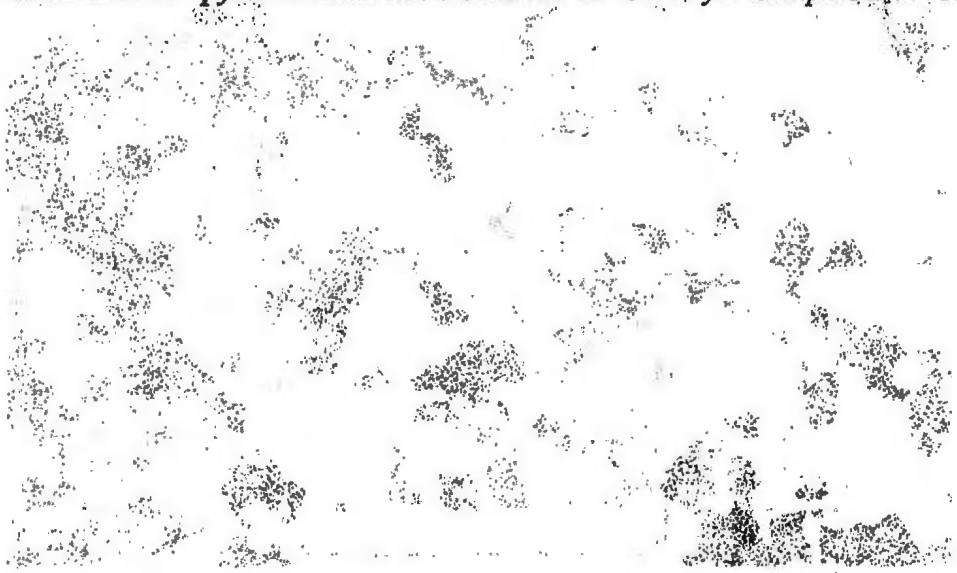

***Figure 6-27**: Kelyphytic corona involving igneous olivine, with orthopyroxene, amphibole with spinel inclusions and igneous feldspar. PPL. Northwest River dyke. Sample JK-99-186*

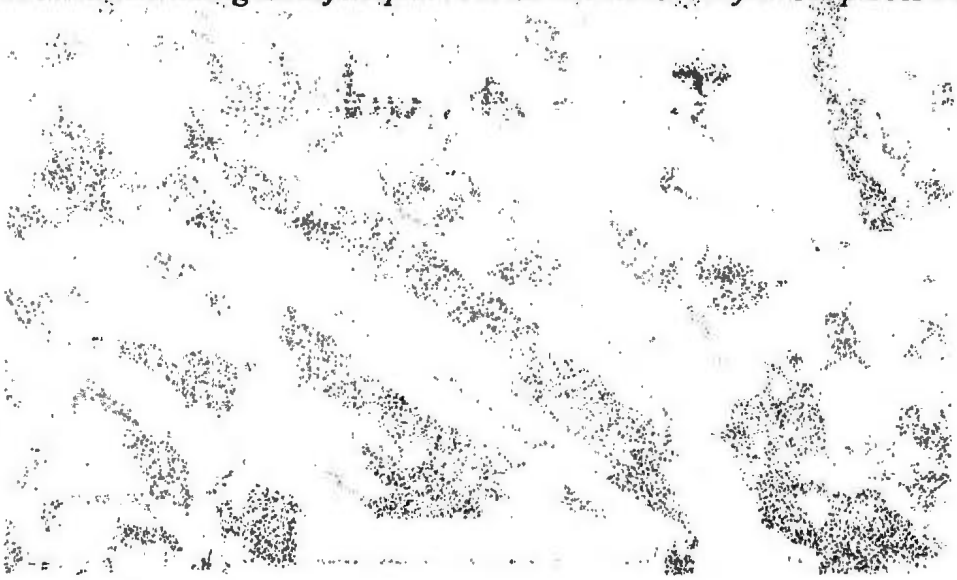

6-26

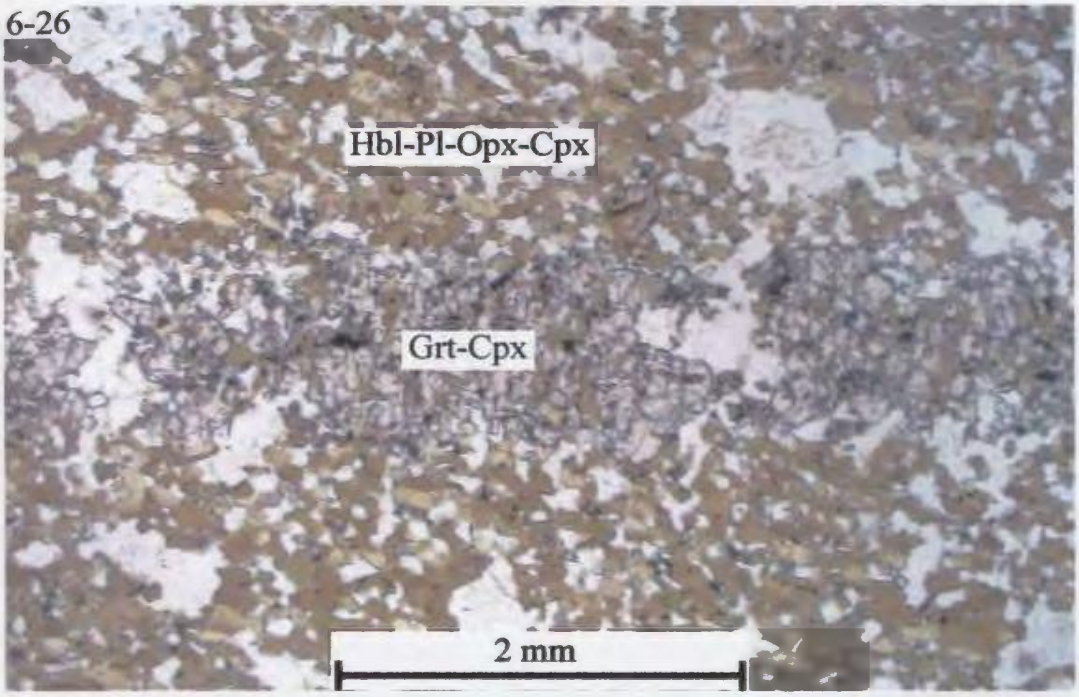

6-27

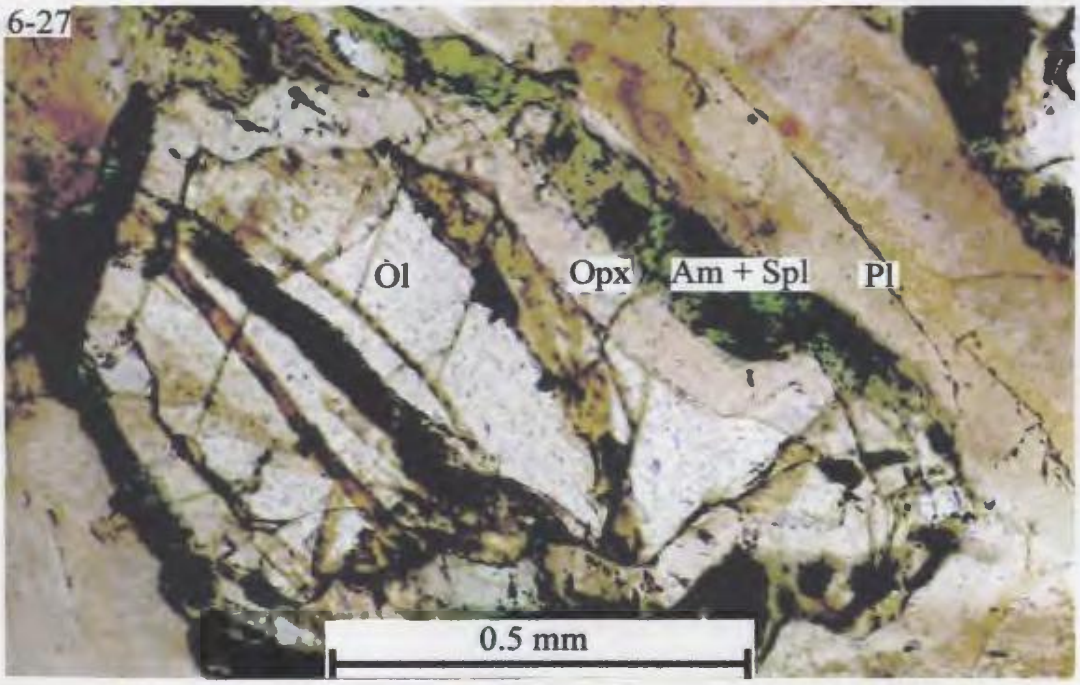

***Figure 6-28**: Kelyphytic coronas involving pseudomorphed olivine (Opx + Mag) in a Northwest River dyke. PPL. Sample JK-99-176*

***Figure 6-29**: Radial pyroxene in an opaque, biotite and spinel charged plagioclase matrix. Note also biotite and amphibole coronas around Fe-Ti oxides. PPL. Northwest River dyke sample JK-99-184a*

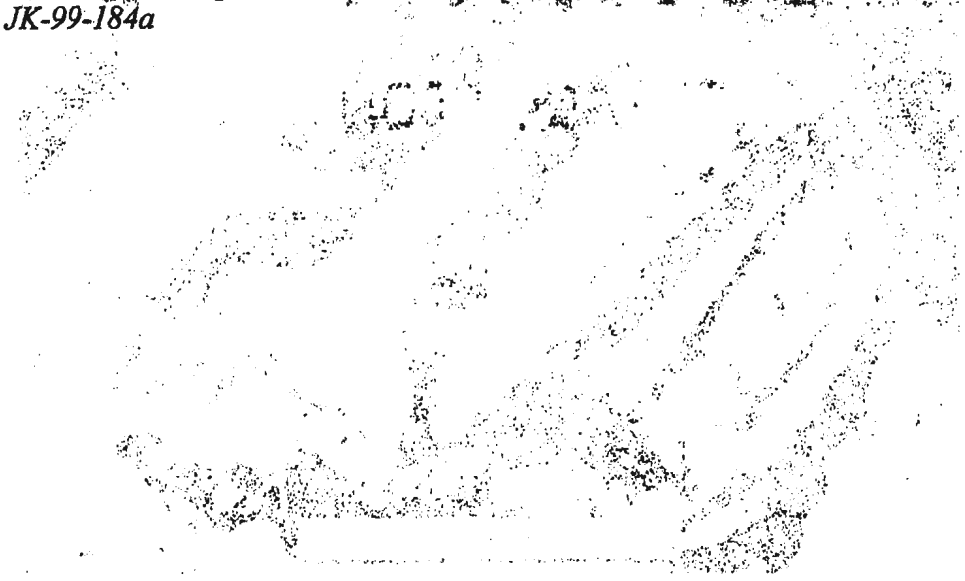

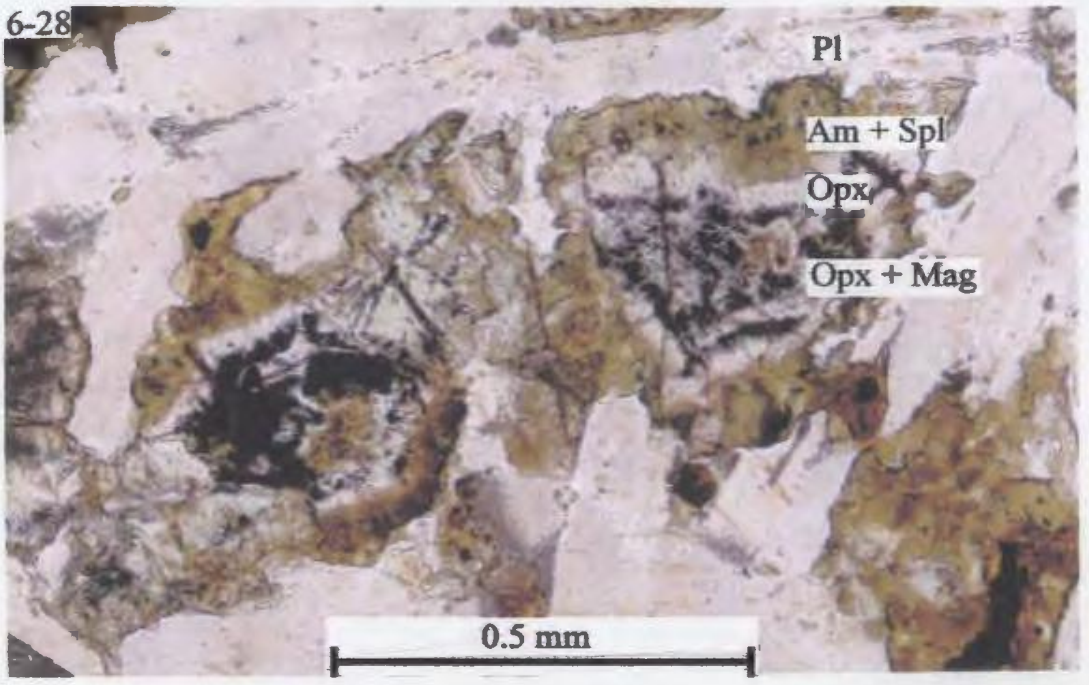
6-28
Pl
Am + Spl
Opx
Opx + Mag
0.5 mm

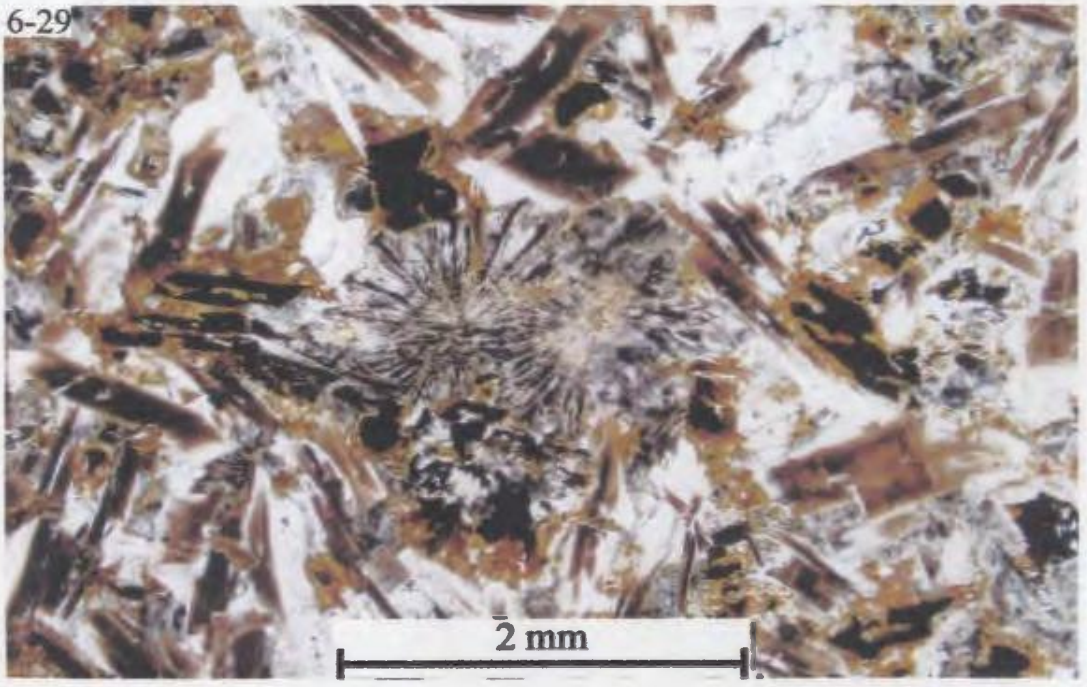
6-29
2 mm

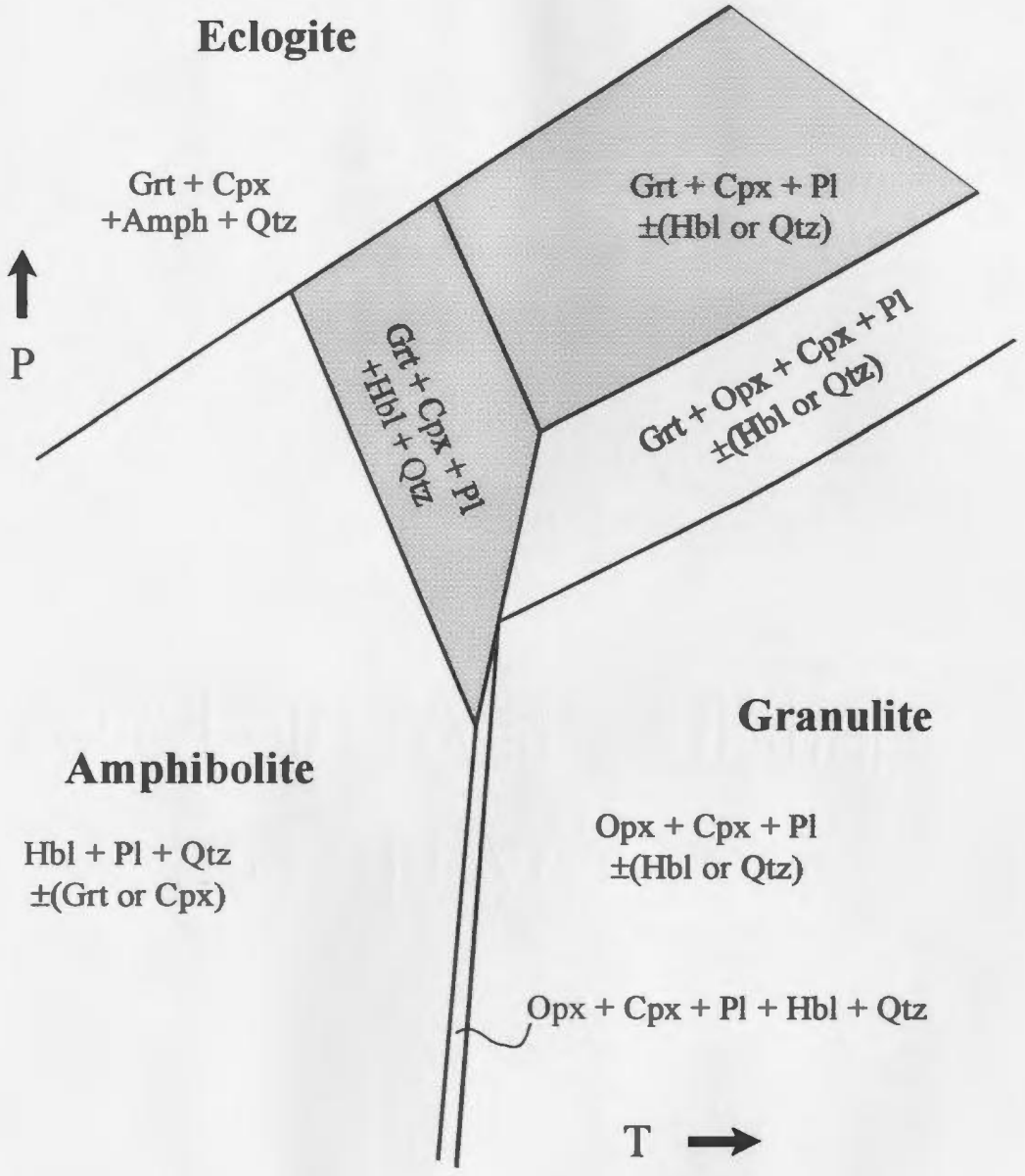

***Figure 6-30** : Schematic P-T diagram showing the generally accepted metamorphic facies with P-T domains (shaded domains) for Opx free assemblages (after Pattison in press).*

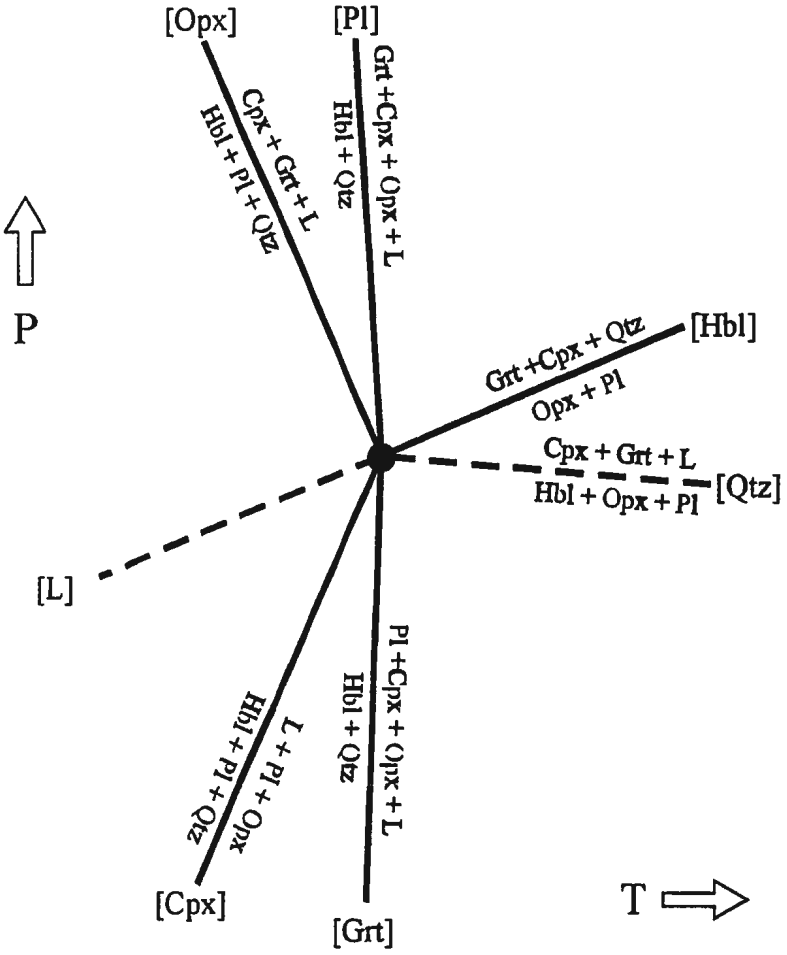

***Figure 6-31**: Phase equilibria in the CaO-MgO-(FeO)-Al_2O_3-SiO_2 (CMASH or CFASH) system after Pattison (in press) assuming the presence of quartz.*

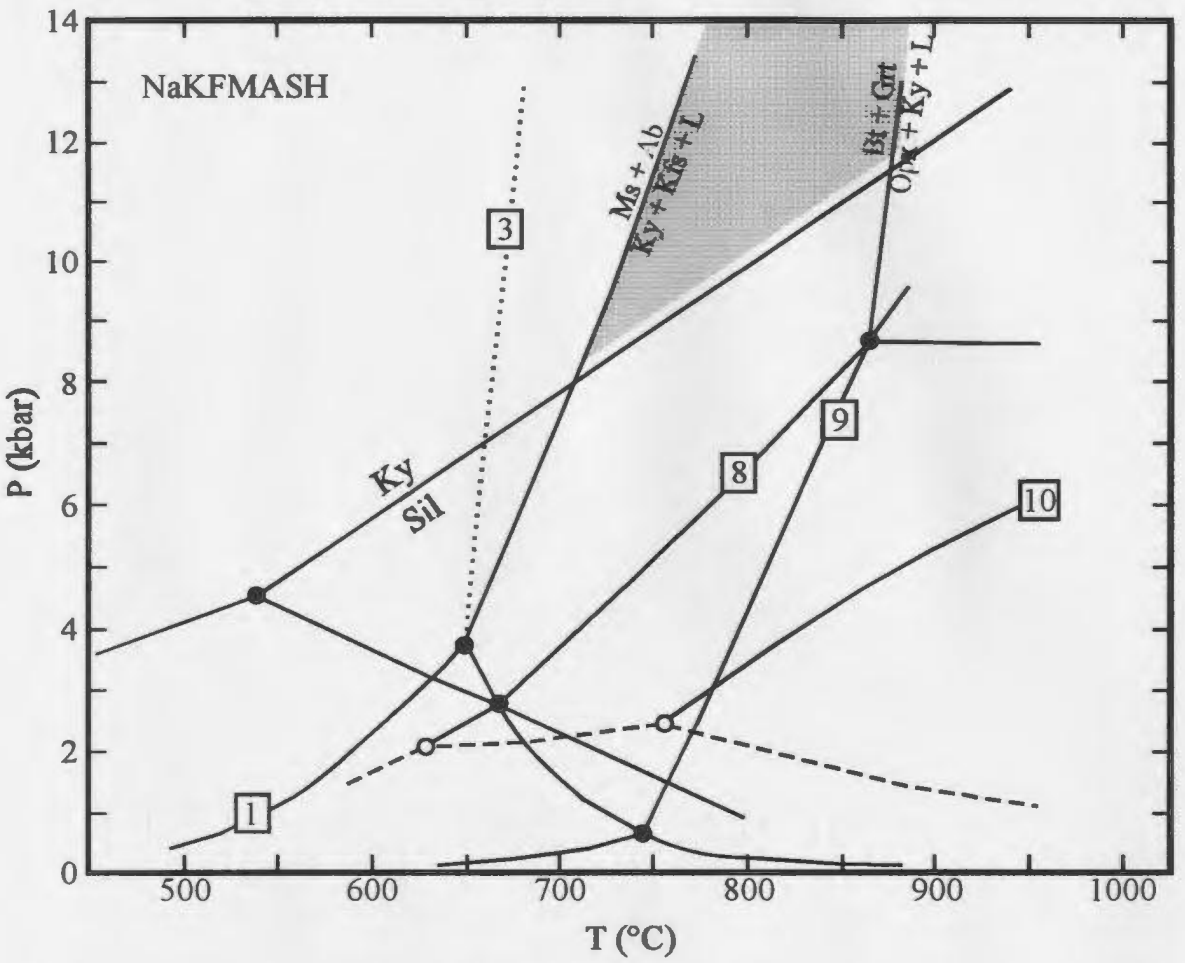

Reactions

1: Ms + Ab = Als + Kfs + V
3: Ms + Ab + V = Als + L
8: Bt + Als = Grt + Crd + L
9: Bt + Grt = Opx + Crd + L
10: Grt + Sil = Spl + Crd

***Figure 6-32**: Petrogenetic grid for the NaKFMASH system (after Spear et al. 1999) showing the P-T field in which the paragneiss rocks achieved peak metamorphic conditions based on reactions and textures discussed in the text. The Bt melting reaction Bt + Als = Grt + Kfs + L cannot be plotted on this grid without compositional data for Bt and Grt (basically Fe/(Fe+Mg)) See Spear et al. 1999 Figure 5.*

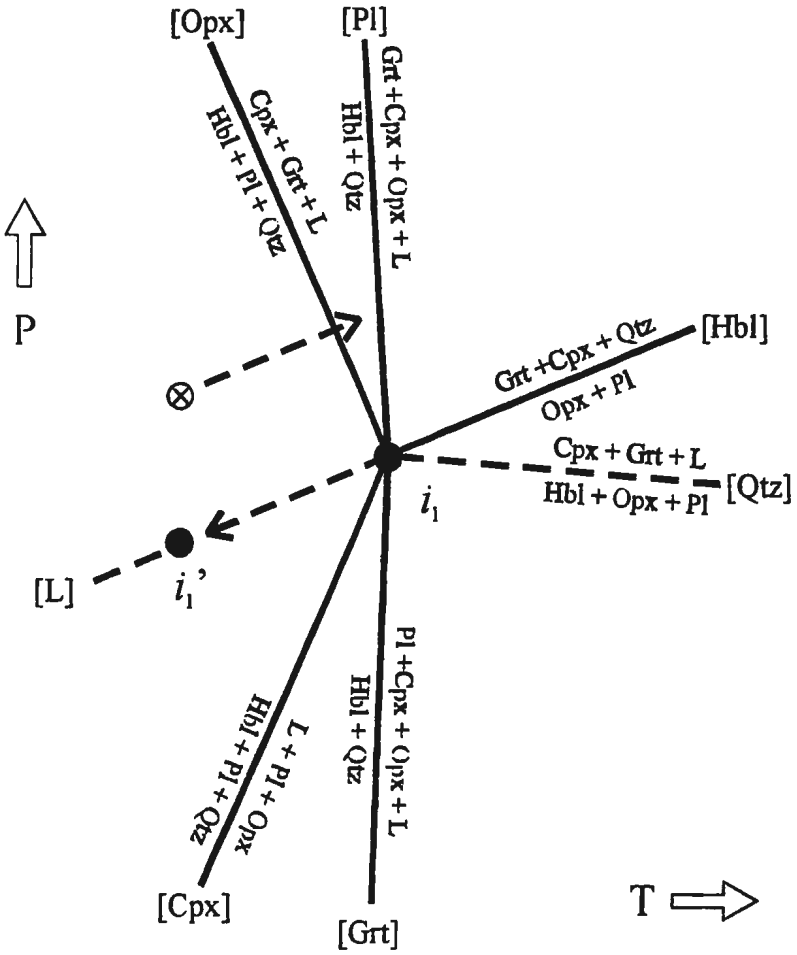

***Figure 6-33**: Phase equilibria in the CaO-MgO-Al_2O_3-SiO_2 (CMASH or CFASH) system after Pattison (in press) assuming the presence of quartz. The point marked i_1 is where the invariant point lies when the activity of H_2O is unity. With the presence of CO_2, the activity of H_2O is reduced and thus the invariant point is shifted accordingly based on the ratio of H_2O:CO_2 to the new location of the invariant point marked i_1' along the projection of the [Hbl] curve. If the assemblage were to lie above the [Hbl] curve(marked by the circled X), as is inferred for the rocks in the field area, the [Opx] reaction would occur. This shift is what is inferred to be responsible for the presence of Grt-Cpx veins in the Northwest River dykes and the HP granulite facies assemblage (Grt-Cpx-Pl) preserved locally in other samples from the field area. See text for discussion.*

Chapter 7

Metamorphism II: Geothermobarometry

7.1 Geothermobarometry of Granulite-facies Rocks

Quantitative metamorphic pressure (P) and temperature (T) estimates from granulite-facies assemblages in metamorphosed mafic rocks typically involve net transfer reactions among garnet, pyroxene (ortho and/or clino) and/or amphibole, plagioclase and quartz (barometers) and the Fe-Mg exchange between ferromagnesian mineral pairs such as garnet-orthopyroxene, garnet-clinopyroxene and garnet-calcic amphibole (thermometer). The availability of thermodynamic mixing models in solid solutions of granulite-facies assemblages should in principle enable fairly accurate metamorphic conditions to be obtained if the assemblage is in equilibrium. However, granulite-facies rocks form at temperatures above the closure temperatures for most thermometers (Fe-Mg cation exchange) and are therefore susceptible to retrograde cation exchange, especially in mylonitic rocks where grain size reduction increases the grain boundary area thereby facilitating retrograde cation diffusion and disequilibrium. A result of retrograde diffusion is that apparent peak metamorphic conditions are determined that underestimate the true peak conditions. Samples that underwent retrogression during post-peak metamorphism along the retrograde path will yield P-T estimates that are geologically meaningless with respect to peak metamorphic conditions. The following sections further discuss this and other pitfalls to

geothermobarometry in granulite-facies rocks and the approaches employed in this study. In the following, "peak *P-T*" refers to the pressure at peak temperature in a clockwise *P-T* path.

7.1.1 Pitfalls of Granulite Geothermobarometry

Three problems with respect to granulite-facies thermobarometry were previously introduced in Chapter 1. These are: i) resetting of the thermometer but not the barometer during retrograde cation diffusion due to the relatively higher closure temperatures of barometers than thermometers, ii) resetting of both the thermometer and barometer together during retrograde cation diffusion, and iii) complete overprinting of the granulite-facies assemblage by a lower grade event. The first of these would result in non-equilibrium mineral compositions, and therefore meaningless estimates of the peak metamorphic conditions. The other two would result in *P-T* estimates lower than the true peak achieved by the rock. The effect of retrograde cation diffusion (i, above) in high temperature rocks that exceeded the closure temperature for cation diffusion in ferromagnesian minerals has been studied by many researchers (e.g., Spear 1991, Spear and Florence 1992). As discussed in Chapter 1, the grain size, along with temperature and the rate of diffusion, control the effects of retrograde diffusion, with smaller grains being more susceptible to retrograde cation diffusion at high temperatures than larger grains. Spear (1991) and Spear and Florence (1992) used cation diffusion models to enable characterization of the effects of diffusion versus radius of garnet and cooling rates. Their studies showed that at high temperatures, Fe-Mg diffusion continues after peak metamorphism, and depending on grain size and rate, diffusion may even affect the cores of the larger grains. This effect is shown in Figure 7-1

where the apparent temperatures recorded by garnet are dependent on both crystal radius and cooling rates. Readily visible on this diagram is the observation that regardless of the crystal radius, the cores record the maximum temperatures whereas the rims record temperatures up to 200 °C lower. The apparent temperatures recorded by the cores of the larger crystals change with cooling rates, with the apparent temperature for a garnet core that has undergone a cooling rate of 100 °C/Ma being just less than 900 °C where the starting temperature was in excess of 900 °C. Where the cooling rate is very slow, the apparent temperature in the core of the largest crystal is reset to 725 °C. In all cases, regardless of the garnet radius, the rim temperatures are in the range of 450-600 °C. Thus in slowly cooled granulite-facies terranes, *P-T* estimates obtained from various crystal sizes of garnet may yield erroneous *T* estimates, thus the inferred peak metamorphic conditions will not lie on the *P-T* path, but rather at the closure temperature for Fe-Mg diffusion. This effect, called the *granulite uncertainty principle* by Frost and Chacko (1989), implies that temperatures greater than 800 °C cannot be readily obtained by geothermometry in slowly cooled granulite-facies rocks due to the closure temperature of ion-exchange thermometers commonly being less than the maximum temperatures actually achieved.

7.1.2 Approach to Avoid Pitfalls

Certain measures can be taken to maximize the likelihood of recovery of true peak metamorphic conditions for granulite-facies rocks the peak conditions. Frost and Chacko (1989) suggested the use of "fossil thermometers"; grains that exhibit evidence of their former high temperature compositions, such as exsolution lamellae in pyroxene. They argued

that reintegration of exsolution lamellae with the host crystal will yield the high temperature composition of the phase, and therefore the maximum temperatures of equilibration can be obtained from such a phase. An obvious stipulation to this method is that the relict textural features must be present. In the case of the GLTS, it is inferred from the presence of synthrusting orthopyroxene that the rocks of the shear zone reached temperatures greater than 800°C. However, the rocks are strongly mylonitized, and as discussed in Chapter 6, pyroxenes do not display any relics of their high temperature compositions due to grain size reduction, thus the Frost and Chacko (1989) method cannot be applied to the rocks of the GLTS.

Fitzsimons and Harley (1994) and Bégin and Pattison (1994) have suggested possible ways in which peak temperatures may be recovered using the garnet-orthopyroxene thermometer. Pattison and Bégin (1994) have shown from zoning patterns for Fe, Mg, Ca, Si and Al in garnet, orthopyroxene and plagioclase, that Fe-Mg exchange continues after Ca and Al have been frozen in. Relatively slow diffusion of certain elements, specifically Ca in garnet and Si and Al in orthopyroxene and plagioclase, compared to Fe and Mg leads to cross-cutting zoning patterns between Fe/(Fe+Mg) and Ca in garnet and Fe/(Fe+Mg) cross-cutting Al in orthopyroxene. This implies that thermometers using Fe-Mg exchange must record retrograde conditions rather than the peak temperature. Furthermore, it has been shown that Fe-Mg feedback during retrogression can affect both the geothermometer and geobarometer, as two of the phases involved in the barometer are ferromagnesian phases and solution models for the slow-diffusing elements are also dependent on the mole fractions of the Fe-Mg components (Fitzsimons and Harley 1994). Both Fitzsimons and Harley (1994)

and Bégin and Pattison (1994) recalculated the composition of garnet and orthopyroxene to the composition at peak temperatures for the GOPQ (garnet-orthopyroxene-plagioclase-quartz) geothermobarometer. The result of this recalculation commonly results in higher temperatures by up to 140 °C (Fitzsimons and Harley 1994) that are inferred to represent peak metamorphic conditions. However, there is not a similar recalculation scheme for the garnet-clinopyroxene equilibria, which is problematic because this thermometer also seems to suffer retrogression (Pattison and Newton 1989).

Fe-Mg retrograde cation diffusion is more likely between ferromagnesian phases that are touching than phases that are separated by an indifferent phase or phases such as quartz and plagioclase. However, in the latter case it is possible that the two Fe-Mg phases were not in equilibrium under peak conditions and would therefore yield incorrect *T* estimates. In this study, generally Fe-Mg bearing minerals that are in contact with one another were sought out to limit the possibility of disequilibrium between the two phases. To circumvent any problems that may be associated with this, all phases used for geothermobarometry were characterized for zoning patterns to allow an informed choice for spot analyses in minerals that are inferred to be part of the peak assemblage with the general knowledge that the cores of minerals typically record higher *P-T* conditions than the rims (see Figure 7-1). However, despite these precautions, it is acknowledged that the estimated *P-T* conditions may be less than the peak conditions attained for the reasons described above. The magnitude of this effect is evaluated after the presentation of the results.

7.2 Application of Geothermobarometry

Two useful ways to estimate metamorphic conditions are *P-T* grids and quantitative geothermobarometry. *P-T* grids are discussed in Chapter 6 where the Spear et al. (1999) NaKFMASH grid applied to the metapelites yields a *P-T* field for the peak assemblage at ~ >8-11 kbar and 700-825 °C. For the rocks of metabasite composition, the grid of Pattison (in press) suggests that, the rocks of the GLTS for example, achieved granulite-facies conditions with pressures exceeding the lower boundary of the orthopyroxene-free HP-granulite facies field. For those samples with an assemblage for which quantitative results may be obtained, the TWEEQU software of Berman (1991) is utilized to quantify the peak conditions achieved by the footwall, hangingwall and GLTS rocks in the Goose Bay area. The resulting data will be used in conjunction with the reaction textures to determine both the conditions and the *P-T* direction of metamorphic reactions.

7.2.1 Sampling Strategy

Syntectonic shear zone assemblages involving garnet-clinopyroxene-orthopyroxene-calcic amphibole-plagioclase-quartz, as discussed in Chapter 6, were sought to provide *P-T* conditions for thrusting in the GLTS shear zone rocks. Syntectonic assemblages, like that shown in Figure 6-19, were scrutinized under the petrographic microscope for the presence of appropriate mineralogy and for suitability of the application of geothermobarometry. The main petrographic criterion that was applied to enhance the possibility of obtaining accurate *P-T* estimates was evidence for textural equilibrium. Eighteen samples from the shear zone

and adjacent footwall and hangingwall rocks samples satisfied equilibrium criteria and were chosen for *P-T* estimates and are listed in Table 7-1 below. The selected mineral data obtained from the electron microprobe used in construction of the *P-T* plots (see below) are found in Appendix C.

Sample	***Rock Type***	***Peak Assemblage***
JK-99-049	LMT mafic gneiss	Grt-Cpx-Opx-Pl-Qtz
JK-99-056	Northwest River dyke (LMT)	Grt-Cam-Pl-Qtz
JK-99-074	GBT diorite orthogneiss	Grt-Cpx-Opx-Pl-Qtz
JK-99-084	GBT orthogneiss	Grt-Cpx-Pl-Qtz
JK-99-122-3	Recrystallized gabbro-diorite (CCRA)	Grt-Cpx-Opx-Pl-Qtz
JK-99-142	Northwest River dyke (CCRA)	Grt-Cpx-Cam-Pl-Qtz
JK-99-196a	Northwest River dyke (CCRA)	Grt-Cpx-Cam-Pl-Qtz
JK-99-008	Straight Gneiss-Mylonite zone	Grt-Cpx-Pl-Qtz
JK-99-012	Straight Gneiss-Mylonite zone	Grt-Cpx-Opx-Cam-Pl-Qtz
JK-99-017	Straight Gneiss-Mylonite zone	Grt-Cpx-Cam-Pl-Qtz
JK-99-028-1	Straight Gneiss-Mylonite zone	Grt-Cpx-Opx-Cam-Pl-Qtz
JK-99-029-1	Straight Gneiss-Mylonite zone	Grt-Cpx-Pl-Qtz
JK-99-059a	Mafic gneiss-Basal mylonite	Grt-Cpx-Opx-Cam-Pl-Qtz
JK-99-065a	Mafic gneiss-Basal mylonite	Grt-Cpx-Opx-Cam-Pl-Qtz
JK-99-071	Granodiorite gneiss-Mylonite zone	Grt-Cpx-Cam-Pl-Qtz
JK-99-072	Granodiorite gneiss-Mylonite zone	Grt-Cpx-Opx-Pl-Qtz
JK-99-086-1	Straight Gneiss-Mylonite zone	Grt-Cpx-Cam-Pl-Qtz
JK-99-090	Straight Gneiss-Mylonite zone	Grt-Cpx-Cam-Pl-Qtz

***Table 7-1**: List of the chosen samples for geothermobarometry with rock types and peak metamorphic assemblages.*

7.2.2 Analysis Strategy

For each of the 18 samples chosen for geothermobarometry, more than one microtextural domain was analysed in order to evaluate possible disequilibrium domains in the sample and to assess reproducibility of *P-T* estimates within the sample. For example, in a sample that contained many examples of equilibrium domains involving garnet-clinopyroxene-plagioclase-quartz, as many as four textural domains were analysed. All phases were analysed at a number of points along core to rim traverses in order to evaluate zoning patterns. Only one sample was chosen for qualitative zoning to express the common zoning trends observed in most samples from the GLTS utilizing the ED mapping capability of the EMP. Different plagioclase crystals were analysed to evaluate the uniformity of composition in different domains, which enabled the assemblage to be analysed for local disequilibrium affects. The core to rim traverse data from the EMP were then analysed for zoning patterns and utilizing the Polaroid images taken at the time of analysis displaying the textures and locations of the analysis points, individual spot analyses were paired up for core and rim geothermobarometry estimates. This procedure was repeated for all the analysis domains in the sample and most samples yield two or more *P-T* estimates, obtained from the mineral cores, that were then averaged (if the sample contained more than one fabric type then those *P-T* estimates from each zone were averaged and so on) and the same was done for rim *P-T* estimates. The resultant *P-T* estimates reported below are the averages obtained by this procedure and in most cases the individual *P-T* estimates do not greatly differ from others established from a similar fabric setting and mineralogy.

7.2.3 Thermometers and Barometers in Metabasites

The calibrations used for geothermobarometry are from the internally consistent databases of Berman (1991; TWEEQU versions 1.01 and 2.02b). As briefly introduced in Chapter 1, two independent reactions or equilibria are needed to establish the *P-T* conditions. These equilibria include cation exchange reactions which have a steep slope in *P-T* space (thermometer) and net transfer reactions that have a shallow slope in *P-T* space (barometer). Examples of the thermometers and barometers used in obtaining *P-T* conditions are listed below.

Fe-Mg exchange thermometers applicable to the chosen samples include the garnet-orthopyroxene thermometer (after Harley 1984):

almandine + enstatite = pyrope + ferrosilite,

the garnet-clinopyroxene thermometer (after Pattison and Newton 1989):

almandine + diopside = pyrope + hedenbergite,

and two versions of the garnet-calcic amphibole thermometer (after Graham and Powell 1984):

almandine + pargasite = pyrope + ferropargasite

and

almandine + tschermakite = pyrope + ferrotschermakite

Net transfer barometers that were used are the GOPQ reaction (after Perkins and Chipera 1985):

6enstatite + 3anorthite = grossular + 2pyrope + 3β-quartz,

the GADS (or GCPQ) barometer (after Moecher et al. 1988):

2grossular + pyrope + 3β-quartz = 3diopside + 3anorthite,

and the GHPQ barometer (after Kohn and Spear 1989):

2grossular + pyrope + 18 β-quartz + 3 pargasite = 3tremolite + 6 anorthite + 3 albite.

Only the Mg end-member reactions are listed above, however similar Fe end-member reactions were also used for geothermobarometry.

7.3 Mineralogy

Mineral analyses from the electron microprobe (EMP) were used to calculate the compositions of the analysed phases and to provide a test for zoning present in the phases. From preliminary analyses, further investigations of zoning patterns were pursued where appropriate. The results of zoning and mineral compositions are presented below. Garnet, clinopyroxene and plagioclase are easily found in all samples, however the presence of free quartz was not always clear optically. Therefore samples that contained the appropriate textures but appeared from petrographic inspection to lack quartz were analysed using the BSE (Back Scattered Electron) imaging available on the EMP to discern between plagioclase and quartz grains that were too small to distinguish with the petrographic microscope. The results of this examination are discussed 7.4.5.

7.3.1 Mineral Zoning

Zoning of minerals used in thermobarometry was determined using spot analyses in

core to rim traverses to approximate zoning profiles. Minor retrograde Fe-Mg exchange (increase in Fe and decrease of Mg towards the rim of garnet) is present in most Fe-Mg bearing minerals such as that shown in Figure 7-2. This retrograde zoning pattern is common for the shear zone and adjacent footwall and hangingwall rocks. Generally, the retrograde Fe-Mg exchange is only present at the grain boundaries where the effects can be observed to occur within the outer 10-50 μm of garnet for example. In samples in which retrogression is more prevalent, garnet porphyroblasts for example, may contain retrograde MnO zoning (relative increase in Mn from core to rim) where the rim of garnet contains up to 3 wt % MnO versus ~1 wt % in the core, which is inferred to be evidence of garnet resorption. In these cases retrogression is readily visible in thin section as resorption of the phase through retrograde reactions (for example see Figure 6-18).

In order to describe chemical changes during retrogression, chemical substitutions or exchange vectors may be used. Exchange vectors are composition vectors that point to an exact position in composition space. Composition space and exchange vectors can be directly correlated with Cartesian axes (x,y,z) and vectors with magnitudes and directions. An example of an exchange vector is the Fe = Mg vector which is prominent in composition space for Fe-Mg bearing phases. For example, the Fe = Mg exchange vector for pyroxene links diopside with hedenbergite or enstatite with ferrosilite. Spear (1993) provides an excellent review of exchange vectors and composition space. Table 7-2 lists the more common exchange vectors applicable to the phases used in geothermobarometry of the Goose Bay area.

Exchange vector	Mineral group	Example	Notes
Fe ⇆ Mg	pyroxene, amphibole, garnet	$Fe_2Si_2O_6$ ⇆ $Mg_2Si_2O_6$ ferrosilite-enstatite	Extremely common. Occurs in all major Fe-Mg silicates.
Ca ⇆ Mg	pyroxene, amphibole, garnet	$Ca_3Al_2Si_3O_{12}$ ⇆ $Mg_3Al_2Si_3O_{12}$ grossularite-pyrope	Common in most mineral groups.
Ca ⇆ Fe	pyroxene, amphibole, garnet	$CaFeSi_2O_6$ ⇆ $Fe_2Si_2O_6$ hedenbergite⇆ferrosilite	Common in most mineral groups.
$MgSi \leftrightarrows Al^{VI}Al^{IV}$ (Tschermak exchange)	amphibole, pyroxene	$CaMgSi_2O_6$ ⇆ $CaAlAlSiO_6$ diopside⇆"Cats"	The dominant Al substitution in most silicates
$NaAl^{IV} \leftrightarrows \square Si$ (edenite exchange)	amphibole	$NaCa_2Mg_5AlSi_7O_{22}(OH)$ ⇆ $\square Ca_2Mg_5Si_8O_{22}(OH)$ edenite⇆tremolite	Vacancy substitution mechanism involving A-site in amphiboles
$NaSi \leftrightarrows CaAl^{IV}$ (plagioclase exchange)	plagioclase, pyroxene, amphibole	$NaAlSi_3O_8$ ⇆ $CaSi_4O_8$ plagioclase	NaSi is favoured at high *P* over CaAl
$NaAl^{VI} \leftrightarrows CaMg$ (jadeite exchange)	pyroxene, amphibole	$NaAlSi_2O_6$ ⇆ $CaMgSi_2O_6$ jadeite⇆diopside	NaAl favoured at high *P*

***Table 7-2**: Table of common exchange vectors especially applicable to the rock forming minerals of the Goose Bay area. □ = vacancy. After Spear (1993).*

When Fe-Mg bearing phases undergo retrogression there are three possible outcomes. The most common outcome is where, for example, garnet, pyroxene and amphibole can exchange Fe and Mg with an adjacent Fe-Mg phase to produce retrograde Fe-Mg zoning via the Fe ⇆ Mg exchange vector. A second outcome is where the Fe-Mg silicate undergoes net transfer reactions in order to re-equilibrate to the new and changing *P-T* conditions. For example, the jadeite content in clinopyroxene could be reduced by a reversal of the jadeite exchange, thereby increasing the diopside content thus eliminating evidence of high pressure. A similar change in plagioclase may also occur, where the plagioclase composition changes from a high-pressure albite-rich composition to more anorthite-rich composition on the

retrograde path by the plagioclase exchange. A third outcome is where the high *P-T* phase is altered to another phase to produce secondary mineralogy including other Fe-Mg phases, plagioclase and quartz. This type of reaction is prominent in many rocks from the shear zone where garnet and clinopyroxene react with water to produce amphibole, plagioclase and quartz (see Figure 6-18).

7.3.2 Mineral Chemistry

Chemical data from single spot analyses from the EMP were used to calculate the end-member compositions for garnet, pyroxene, amphibole and feldspar. Figures 7-3 to 7-6 display the compositional variability of these phases. Due to the fact that the microprobe does not distinguish Fe^{2+} from Fe^{3+}, pyroxene, garnet and amphibole compositions were recalculated to estimate Fe^{3+} to more accurately establish end-member compositions. Without independent analyses for Fe^{3+}, the calculated Fe^{3+} values may not be accurate, since they are dependent on the quality of the mineral analysis (especially SiO_2). However, they should nonetheless give some qualitative indication of the presence and magnitude of Fe^{3+} in the phases, and the consistency of the results may provide an independent estimate of the quality of the analyses. The method of Droop (1987) was used to estimate Fe^{3+} in garnet and pyroxene, whereas for amphibole the method of Leake et al. (1997) was employed. Due to the differences between the mineral groups different approaches to the calculation are necessary.

Pyroxene and garnet, for example, do not contain significant vacancies in the crystal structures nor do they contain any hydroxyl sites for which site occupancy is commonly

poorly known. Thus a stoichiometric scheme for estimation of ferric iron may be employed (Droop 1987). The simple general equation: $F = 2X(1-T/S)$ is based on the difference between the observed cation sum (S) and the correct cation total (T) which can be used to estimate the ferric iron content (F) for a given oxygen total (X). For pyroxene, for example, $T = 4$ and $X = 6$ and S would equal the cation total from the microprobe software. There are two stipulations to the use of this recalculation scheme: i) the mineral in question must not contain significant vacancies and ii) S must be greater than T otherwise a negative ferric content will be obtained in which case all iron is assumed to be ferrous (Fe^{2+}).

Amphiboles may contain both vacancies (in the A-site) and have hydroxyl sites and thus a similar stoichiometric calculation for Fe^{3+} cannot be employed. Leake et al. (1997) proposed a scheme of ideal site assignments where if one of the three criteria, $Si \leq 8$, $\Sigma Ca \leq 15$ and $\Sigma K \leq 16$, is exceeded then Fe^{3+} may be present (the values of ΣCa, for example, is calculated by summing up the total cations from Si to Ca :Σ Si + Al + Fe^{3+} + Cr + Ti + Fe^{2+} + Mg + Mn + Ca). Maximum and minimum amounts of ferric iron may be estimated if one or more of the criteria are exceeded. If the criteria are not exceeded, then all iron is assumed to be Fe^{2+} ($Fe^{3+} = 0$). The minimum ferric estimate is based on cation subtotals (above) where the condition above that is exceeded by the greatest amount determines the equation for the minimum ferric content. For example, if Si = 8.005 apfu (atoms per formula unit), $\Sigma Ca = 15.030$ apfu and $\Sigma K = 15.065$ apfu, the total Si is exceeded by 0.005 apfu and ΣCa by 0.030 apfu. Because ΣCa is exceeded by the greater amount, the amphibole formula is recalculated to $\Sigma Ca = 15.000$ apfu and the minimum ferric content may be estimated.

The maximum ferric content uses three different stoichiometric limits, $\Sigma Al \geq 8$, $\Sigma Mn \geq 13$ and $\Sigma Na \geq 15$, where the minimum difference between the condition and the calculated total gives the maximum ferric content. For example, if $\Sigma Al = 9.105$ apfu, $\Sigma Mn = 13.099$ apfu, and $\Sigma Na = 15.088$ apfu, the ΣAl is exceeded by 1.105 apfu, ΣMn by 0.099 apfu and ΣNa by 0.088 apfu. The ΣNa is closest to its minimum value and thus the amphibole formula is recalculated to $\Sigma Na = 15.000$ to give the maximum ferric content. Leake et al. (1997) tested this empirical calculation against a known amphibole with measured Fe^{3+} and obtained a minimum ferric estimate that closely matched that of the known value. Leake et al. (1997) do not recommend one specific recalculation of either minimum or maximum but rather the average of the two.

Garnet compositions for the footwall, hangingwall and shear zone typically overlap in the almandine rich part of Figure 7-3. Garnet composition is typically in the range of $X_{grs} = 0.15 - 0.28$ $X_{prp} = 0.10 - 0.34$ $X_{alm} = 0.47 - 0.62$. Spessartine contents are typically low ($X_{sps} \sim 0.02$) in all units and are thus included along with almandine on the plots. The variations in the pyrope and almandine contents are likely due to the variation bulk rock composition and retrograde Fe-Mg cation diffusion. Generally all the analysed garnet have a constant X_{grs} implying minimal retrograde effects from net transfer reactions. Retrograde Fe-Mg diffusion (increase in X_{alm} and decrease in X_{prp} towards the rims) is common for all analysed garnets however the intensity of the effect varies between the samples. For instance in sample JK99-072 core composition is $X_{prp} = 0.29$, $X_{alm} = 0.53$, $X_{grs} = 0.17$, $X_{sps} = 0.01$ whereas the rim composition is $X_{prp} = 0.27$, $X_{alm} = 0.55$, $X_{grs} = 0.17$, $X_{sps} = 0.01$. The zoning present in this

sample is mild (see Figure 7-3) compared to that in JK99-084 where garnet is visibly resorbed and yields a core composition of $X_{prp} = 0.18$, $X_{alm} = 0.58$, $X_{grs} = 0.21$, $X_{sps} = 0.03$ and a rim composition of $X_{prp} = 0.14$, $X_{alm} = 0.55$, $X_{grs} = 0.25$, $X_{sps} = 0.08$. This sample has a noticeable increase in X_{sps} (0.05 difference) and an above average X_{grs} implying that this sample has experienced more retrogression than other samples as documented in Chapter 6.

Fe^{3+} recalculation of garnet analyses yielded moderate levels of Fe_2O_3 with an average of 2.43 wt% Fe_2O_3 for garnet in the shear zone, footwall and hangingwall rocks. Several estimates from a single sample however, commonly yield inconsistent Fe_2O_3 weight percent suggesting that the ferric estimates may not be accurate.

To correctly categorize the composition of the ***pyroxenes***, the Fe^{3+} content was first calculated and these data were used to calculate pyroxene end-members after the method of Morimoto (1988). Na end-member components in clinopyroxene such as aegirine ($NaFe^{3+}Si_2O_6$) and jadeite ($NaAlSi_2O_6$) are low ($X_{ae} \sim 0.01$ and $X_{ae} > X_{jd}$). Therefore, pyroxenes can be plotted on the Ca-Fe-Mg ternary diagram (Figure 7-4), where it is readily visible that clinopyroxene is diopside rich ($X_{di} = 0.57 - 0.81$) and orthopyroxene is enstatite rich ($X_{en} = 0.65 - 0.69$) with minor variation in Fe-Mg. From Figure 7-4 it is readily seen that the compositions of clinopyroxene from the shear zone, footwall and hangingwall overlap where the shear zone clinopyroxene has the greatest variability in X_{di} to X_{hd}.

The results of the Fe^{3+} calculation following the method of Droop (1987) yielded Fe_2O_3 wt% estimates that ranged from 0.0 to 6.43 wt% and an average of 3.13 wt% for all analysed pyroxenes. There are no discernible patterns between the shear zone, footwall and

hangingwall with respect to Fe^{3+} estimates in pyroxene. There are only minor differences between individual samples from the shear zone footwall and hangingwall. The highest Fe_2O_3 estimate comes from a sample that yields inconsistent ferric estimates and therefore ferric estimates for this sample, and several others that are also inconsistent, are assumed to be inaccurate.

Amphibole compositions were also recalculated for Fe^{3+} to enable the estimation of end-members following the recommendations of Leake et al. (1997). Figure 7-5 shows that the compositions of calcic amphiboles from the footwall, hangingwall and shear zone are relatively Al-rich and generally lie within the pargasite and ferro-pargasite fields. There is no discernible pattern to amphiboles from the shear zone, footwall and hangingwall as the compositions all plot in a small area of composition space.

However, the results of estimation of Fe^{3+} by the method of Leake et al. (1997) for the amphiboles of the field area differed for the shear zone and the footwall and hangingwall. The amphiboles from the shear zone generally are estimated to not contain any Fe_2O_3, excepting for 3 samples (max = 1.49 wt% Fe_2O_3, average of 18 samples = 0.11wt% Fe_2O_3), whereas both the footwall and hangingwall samples proved to contain an estimated maximum Fe_2O_3 of 1.23 wt% averaging 0.75 wt% Fe_2O_3. This difference is consistent with higher metamorphic pressure in the shear zone, as Ti^{3+} ions are apparently preferentially partitioned compared to Fe^{3+} ions at higher pressures, (avg 2.31wt % TiO_2 in the shear zone v.s.1.85 wt% TiO_2 in the footwall and hangingwall). Fe_2O_3 wt% is inconsistent within

samples from the hangingwall and footwall, suggesting that the estimated values are incorrect and an independent measure of Fe^{3+} is necessary to determine the accurate values.

Plagioclase compositions (Figure 7-6) vary slightly between the footwall and hangingwall and shear zone, with footwall plagioclase typically in the range of An_{20}-An_{35}, the hangingwall plagioclase in the range An_{25} to An_{45}. In contrast, plagioclase from the shear zone has a mich wider compositional range from An_{12} to An_{40}. Analyses from the Northwest River dykes yielded plagioclase compositions from An_{27} to An_{42}. The few more anorthite-rich feldspars in the hangingwall (An_{61} and An_{55}) and shear zone (An_{65}) are analyses from matrix plagioclase in samples JK99-122-3 and JK99-028-1 respectively. These anorthite-rich feldspars are inferred to be relics from either an earlier metamorphic assemblage or an igneous precursor. The albite-rich feldspars in some of the shear zone samples (e.g., An_{12}) suggest that there is a range of bulk compositions within the shear zone but the lack of bulk composition information for the shear zone rocks does not allow this to be quantified.

Based on the above discussion, the compositions of the phases imply that the metamorphic conditions attained are at minimum upper amphibolite to granulite facies (almandine-rich garnet; diopside-rich clinopyroxene; pargasitic amphibole) at moderate to high pressures (low jadeite content in clinopyroxene; low anorthite content in plagioclase). In the following section, the chemistry of the analysed phases is used in thermodynamic models of equilibrium for the various assemblages to calculate the *P-T* conditions of recrystallization.

7.4 Geothermobarometric Results

Results of quantitative thermobarometry utilizing the TWEEQU software are presented in Figure 7-7 a-c. A total of 18 samples were chosen for geothermobarometry, four from the footwall, three from the hangingwall and eleven from the shear zone. The petrography of these samples is discussed briefly below, and more detailed petrographic descriptions can be found in the appendix. Figure 7-8 shows the locations and average apparent peak *P-T* results for all analysed samples. The error on *P-T* estimates reported below is assumed to be ± 1 kbar and ± 50 °C. *P-T* estimates were obtained assuming all Fe as FeO. This assumption was made because of the inconsistencies resulting from the ferric recalculations schemes and the likelihood that it would introduce additional errors into the *P-T* estimates. Results of a test involving the assumption of all Fe as Fe^{2+} versus recalculated Fe^{3+} on selected *P-T* determinations test may be found in Appendix E.

7.4.1 P-T Estimates for the Footwall Rocks

Sample 049 comes from the LMT on the south shore of Grand Lake. The sample was taken from a mafic gneiss outcrop which contains abundant garnet, clinopyroxene and plagioclase. Garnet grain size is in the range of 2000-3000 μm (1mm = 1000 μm) in diameter and clinopyroxene grains are typically less than 1000 μm in diameter. Quartz is distributed sporadically in the sample and is generally restricted to the garnet-clinopyroxene domain. It is inferred from this texture that garnet, clinopyroxene, plagioclase and quartz were in equilibrium. This sample preserves petrographic evidence for the reaction of amphibole and

plagioclase and quartz reacting to produce garnet and clinopyroxene. This is a prograde (increasing temperature) reaction, and Figure 6-11 shows an example of this texture. This sample yields apparent metamorphic peak *P-T* conditions of about 12 kbar and 825 °C. Retrograde effects are minimal, with metamorphic conditions of 11.7 kbar and 800 °C being obtained from rim analyses.

Sample 056 was taken from one of the Northwest River dykes which outcrop on the southern shore of Grand Lake in the LMT. This dyke is primarily composed of garnet, amphibole, plagioclase and minor quartz. Garnet, with grain sizes around 1000 μm in diameter, has an ameoboid texture with inclusions of quartz, plagioclase and biotite. This texture implies rapid growth in response to amphibolitization (see Figure 6-23). This sample yields apparent peak metamorphic conditions of 8.9 kbar and 740 °C. Retrograde *P-T* conditions are determined at 7 kbar and 660 °C.

Sample 074 was taken from a dioritic gneiss in the GBT in the northern part of the map area. This sample contains garnet, clinopyroxene, orthopyroxene, plagioclase and quartz. Grain sizes for the assemblage are typically around 500 μm in diameter or smaller. Orthopyroxene is stable in the assemblage and is occurs locally in the sample, although no association with garnet could be found and thus garnet-clinopyroxene thermometer and the GADS barometer were employed. Orthopyroxene occurs sporadically in the sample and is generally absent from garnet-clinopyroxene domains. There is little evidence for disequilibrium or retrogression in the sample, except for the lack of garnet-orthopyroxene associations implying that orthopyroxene may not be stable in the garnet-clinopyroxene-plagioclase-quartz assemblage. Apparent peak metamorphic conditions for this sample are

established at 12.9 kbar and 725 °C. Retrograde conditions are established at 11.3 kbar and 630 °C. The presence of orthopyroxene in this sample is not compatible with the temperature obtained from garnet-clinopyroxene thermometry, suggesting that the thermometer may not be recording the peak temperature in this sample and has been reset.

Sample 084 comes from the northern part of the map area from directly beneath the shear zone. The rock is a dioritic gneiss that contains garnet, clinopyroxene, amphibole, plagioclase and quartz. Porphyroblasts of garnet are typically 1000-1500 μm in diameter with a few larger grains (5000-9000 μm in diameter) and clinopyroxene grains are smaller, usually ≤ 100 μm in diameter. The presence of clinopyroxene inclusions in garnet implies that the two minerals grew simultaneously (see Figure 6-18 for an example of this texture) and thus garnet-clinopyroxene thermometry and the GCPQ barometer were used for peak metamorphism determination. There is evidence for minor retrogression through resorption of garnet and clinopyroxene to produce secondary amphibole and plagioclase. Apparent peak metamorphic conditions determined for this sample are 13.3 kbar and 890 °C. Retrograde conditions are very similar to the peak conditions of 12.9 kbar and 840 °C. This implies that the disequilibrium textures present in the sample formed at or near estimated peak conditions.

7.4.2 P-T Estimates for the Hangingwall Rocks

Sample 122-3 was obtained from a dioritic gneiss containing the inferred peak assemblage garnet, clinopyroxene, orthopyroxene, calcic amphibole, plagioclase and quartz, where many examples of garnet-orthopyroxene, garnet-clinopyroxene and garnet-calcic

amphibole pairs occur. Grain sizes for garnet lie in the range 500-1000 μm and pyroxene and amphibole grains range from 100-500 μm in diameter. GCPQ geothermobarometry yields a range of pressures from 10.7 kbar and 800 °C to 14.1kbar and 850 °C, with the majority of estimates lying around 11.4 kbar and 800 °C. Metamorphic conditions constrained by garnet-orthopyroxene and garnet-calcic amphibole thermobarometry yield slightly lower peak *P-T* conditions of 9.4 kbar and 775 °C. Retrograde *P-T* conditions, calculated by GCPQ geothermobarometry, are estimated at 11.2 kbar and 775 °C. The reason for the range in the peak pressure determined by the GCPQ calibration is principally due to the differences in clinopyroxene compositions. Clinopyroxene used in this *P-T* determination plots in the augite field of Figure 7-4 (see cpx2-6 of 122-232 in Appendix C). This clinopyroxene may be an igneous relic that did not equilibrate during Grenvillian metamorphism.

Sample 142 was taken from a Northwest River dyke that outcrops along the Cape Caribou River forestry service road at the location for the U-Pb sample C-050D. The dyke contains garnet-clinopyroxene veins in an amphibole plagioclase matrix (see Figure 6-26 for an example of this texture). Grain size is typically small in the recrystallized Northwest River dykes, with garnet crystals being the largest (100-200 μm) and pyroxene and amphibole grains commonly ≤75 μm in diameter. The veins contain both plagioclase and quartz which made geothermobarometry possible for this sample. As discussed in Chapter 6, the presence of calcite in these veins is interpreted to be associated with an influx of CO_2-rich fluids enabling the growth of garnet and clinopyroxene at the expense of amphibole and plagioclase. Apparent peak metamorphic conditions determined for the garnet-clinopyroxene veins is 12.6 kbar and 840 °C. Garnet-amphibole thermobarometry was also used and

yielded peak *P-T* conditions of 11.8 kbar and 840 °C suggesting that amphibole was a stable phase in the peak assemblage. The pressures are within error of each other yielding an inferred average peak *P-T* estimate at 12.2 kbar and 840 °C. Retrograde metamorphic conditions for this sample are estimated at 11.5 kbar and 775 °C.

Sample 196a, also taken from a Northwest River dyke, is located on the eastern flank of the allochthon along the Grand Lake forestry access road. This dyke also contains the garnet-clinopyroxene-calcite vein assemblage in a matrix composed of amphibole, plagioclase and orthopyroxene. Grain sizes in this sample are similar to that observed in sample 142. Orthopyroxene appears to be growing at the expense of amphibole (Figure 7-9) implying that amphibole may have become unstable during the ingress of CO_2-bearing fluids associated with the production of the garnet-clinopyroxene-calcite veins. Estimated apparent peak metamorphic conditions are determined to be 11.2 kbar and 800 °C via GCPQ geothermobarometry. Retrograde conditions are almost identical at 11 kbar and 790 °C. GHPQ thermobarometry yields lower peak *P-T* conditions of 8.9 kbar and 750 °C and retrograde conditions are even lower at 7.7 kbar and 690 °C. Domainal equilibrium in this sample is inferred to be responsible for the differences in peak conditions determined by both thermobarometric systems. Garnet is stable in the vein assemblage and not in the matrix, so the use of the GHPQ calibration may not be warranted.

7.4.3 P-T Estimates for the Shear Zone Rocks

Of the eleven samples, eight were taken from the mylonite zone unit proper (008, 012, 017, 028-1, 029-1, 071, 072 and 086-1) and three were taken from the structurally

higher levels of the shear zone in the granitoid gneiss unit and in the mafic gneiss unit overlying the mylonite zone (059a, 065a, and 090).

Sample 008 was taken from Big Point in the lower structural levels of the shear zone. Similar to the other mylonitic gneisses in the shear zone, this sample contained layers primarily composed of mafic minerals whereas the remainder of the sample contains mafic minerals plus plagioclase and quartz (Figure 7-10). Garnet, clinopyroxene, amphibole, plagioclase and minor quartz are present in mafic layers. Garnet commonly occurs as the largest grains in thin section ranging from 700-2000 μm in diameter, with calcic amphibole and clinopyroxene being generally much smaller (100-500 μm) in diameter. From these layers GCPQ geothermobarometry yields an apparent peak metamorphic *P-T* conditions of 13.9 kbar and 875 °C. Retrograde conditions are estimated at 11.8 kbar and 725 °C, compatible with estimates from the GHPQ calibration, implying that some calcic amphibole is retrograde, in accord with textural interpretations.

Sample 012 was taken from the mylonite zone and contains three types of textural domain shown on Figure 7-14, each of which displays equilibrium textures between garnet and clinopyroxene. All three zones were investigated to determine if they represented different *P-T* conditions. One domain composed of garnet-clinopyroxene-plagioclase-quartz is characterized by the presence of a large garnet porphyroblast 1.2cm in diameter together with inclusions of clinopyroxene, plagioclase and quartz. The second domain composed of garnet-clinopyroxene-calcic amphibole-plagioclase-quartz, where garnet is generally much smaller (average 700 μm in diameter) and the fabric is defined by clinopyroxene calcic amphibole and quartz stringers. The third domain contains mineralogy garnet-clinopyroxene-

calcic amphibole-plagioclase-quartz, but also includes orthopyroxene. The grain size of garnet is similar (~800 μm in diameter) to the second textural variety, but the mafic mineralogy is less abundant. The three domains comprise different parts of a layered mylonite in which the fabric wraps around the large garnet porphyroblasts. The first zone yields apparent peak metamorphic conditions of 14.2 kbar and 840 °C, the second at 13.6 kbar and 850 °C and the third at 14.7 kbar and 850 °C using the GCPQ calibration. These estimates do not greatly differ and are within error of one another and is concluded that all developed under the same metamorphic conditions. The average *P-T* condition for this sample thus is inferred to be 14.2 kbar and 850 °C. Retrograde *P-T* estimates also do not vary greatly and yield average retrograde metamorphic conditions of 11.8 kbar and 775 °C.

Sample 017 was taken from a mafic layer in the mylonite zone. It contains garnet, clinopyroxene, amphibole, plagioclase and minor quartz. The sample displays syntectonic fabrics discussed in Chapter 6 (see Figure 6-19 for an example) and also displays equilibrium textures among garnet-clinopyroxene-plagioclase-quartz grains. The grain size of garnet ranges from 1000-3000μm in diameter, and that of clinopyroxene from 200-2500 μm, whereas plagioclase grain size is consistent around 200μm. The apparent peak metamorphic conditions obtained from this sample yield a *P-T* point at 14.0 kbar and 855 °C. Garnet-calcic amphibole-plagioclase-quartz geothermobarometry yields apparent peak metamorphic conditions of 13.4 kbar and 837 °C. No retrograde conditions were established for this sample due to apparent disequilibrium of the rim compositions.

Sample 028-1 was taken from the mylonite zone near the contact with the overlying mafic gneiss unit. This sample contains garnet, orthopyroxene, clinopyroxene, amphibole,

plagioclase and quartz. The grain size of garnet in this sample ranges from 1000-3000 μm in diameter with much smaller grain sizes from clinopyroxene and plagioclase (<<1000 μm). There is evidence for minor retrogression present as amphibole overgrowths on pyroxene and partially resorbed garnet. Both pyroxenes, amphibole and quartz define the mylonitic foliation in this sample. Garnet-orthopyroxene-plagioclase-quartz geothermobarometry yields apparent peak metamorphic conditions of 11.8 kbar and 845 °C. Retrograde conditions determined with the GOPQ thermobarometer yield a *P-T* point at 9.0 kbar and 740 °C. GCPQ thermobarometry yields apparent peak metamorphic conditions of 11.1 kbar and 905 °C and retrograde conditions of 10.6 kbar and 872 °C. Retrograde conditions estimated through the GHPQ thermobarometer yield *P-T* conditions of 8.1 kbar and 785 °C. The difference in *P-T* estimates for the GOPQ and the GCPQ thermobarometers are within error of each other, therefore the inferred average apparent peak metamorphic conditions for this sample is 11.5 kbar and 875 °C.

Sample 029-1 was taken from a mafic layer at the contact with the overlying mafic gneiss unit and contains the assemblage garnet-clinopyroxene-calcic amphibole-plagioclase-quartz. This sample displays excellent examples of syntectonic growth of garnet (for example see Figure 6-19), typically 1000-2000 μm in diameter and a single grain 3600 μm in diameter, and clinopyroxene is flattened out into lenses wrapped by the mylonitic foliation. Grains of clinopyroxene and plagioclase are granoblastic and are typically <100 μm in diameter. Quartz is not found in the plagioclase layers, but occurs in the garnet, clinopyroxene lenses implying that garnet, clinopyroxene and quartz were in equilibrium during formation of the mylonitic fabric. Based on this texture it is inferred that

geothermobarometry performed on such a sample would yield the *P-T* conditions for thrusting. GCPQ geothermobarometry applied to this sample yields apparent peak metamorphic conditions of 14.4 kbar and 870 °C and retrograde conditions of 13.7 kbar and 820 °C. GHPQ thermobarometry yields conditions of 12.2 kbar and 765 °C suggesting that Cam is a retrograde phase.

Sample 059a was taken from the mafic (dioritic) gneiss component of an outcrop largely composed of granitoid gneiss. The mafic gneiss is composed of amphibole, clinopyroxene, orthopyroxene, garnet, plagioclase and minor quartz. Garnet and clinopyroxene occur in specific domains in the sample (see Figure 7-12 for example of this texture). The grain size of garnet in these domains ranges from 400 to 800 μm in diameter with clinopyroxene grains occurring as smaller grains, typically 200-400 μm in diameter. Orthopyroxene is partially retrogressed and occurs with amphibole and plagioclase in the matrix. The garnet-clinopyroxene domains in this sample are inferred to be the result of an increase in pressure through the *T*-sensitive reaction: Pl + Cam = Grt + Cpx +Qtz + H_2O. GCPQ geothermobarometry applied to this sample yielded apparent peak metamorphic conditions of 13.3 kbar and 885 °C and retrograde conditions of 11.9 kbar and 810 °C. GHPQ thermobarometry yields apparent peak metamorphic conditions of 12.6 kbar and 875 °C and retrograde conditions of 11.5 kbar and 775 °C. Both thermobarometers yield similar *P-T* conditions so the apparent peak conditions are inferred to be 13 kbar and 880 °C for this sample.

Sample 065a was taken from an outcrop of mafic gneiss along the shore at Cape Caribou that contains large, up to 8cm in diameter, garnet porphyroblasts. This sample is

primarily composed of clinopyroxene, orthopyroxene, amphibole and plagioclase with garnet being confined to certain domains in the sample (e.g., Figure 7-12). In thin section, garnet is observed to form coronas around Fe-Ti oxides and also to occur together with clinopyroxene, with garnet in this texture containing abundant inclusions of plagioclase and quartz. Aside from the ~8cm garnet porphyroblasts observed in outcrop, the typical grain size of garnet in thin section ranges from 300 to 750 μm in diameter together with clinopyroxene with grain sizes in the range 200-600 μm in diameter. Garnet-clinopyroxene domains in this sample are inferred to reflect the transition from a two-pyroxene granulite to a garnet granulite. GCPQ geothermobarometry applied to the garnet-clinopyroxene domains yields apparent peak metamorphic conditions of 13.7 kbar and 850 °C and retrograde conditions of 12.1 kbar and 750 °C. A second retrograde *P-T* point of 9.3 kbar and 614 °C for this sample is inferred to reflect the *P-T* conditions associated with amphibolitization that is evident in the sample and present in many parts of the Goose Bay area.

Sample 071 was taken from the granitoid gneiss unit at an outcrop near the northern tip of the CCRA on the south shore of Grand Lake. The sample contains garnet, clinopyroxene, amphibole, plagioclase, quartz and scapolite with the foliation being defined by flattened grains of clinopyroxene and amphibole that exhibit subgrain formation and patchy extinction. Garnet occurs as euhedral grains, with a range of grain sizes from 400-1000 μm, and may contain inclusions of clinopyroxene-plagioclase-quartz. Grains of clinopyroxene and amphibole, with grain sizes around 450 μm, also occur in the pressure shadows of garnet, implying syntectonic growth of garnet, clinopyroxene and amphibole (see Figure 6-19). Amphibole, however, also occurs as a partial replacement of clinopyroxene and

is inferred also to be a retrograde phase. GCPQ geothermobarometry yields apparent peak metamorphic conditions of 14.3 kbar and 880 °C and retrograde conditions of 14 kbar and 860 °C. The similarity of the apparent peak and retrograde *P-T* conditions implies that this rock did not undergo extensive late thermal re-equilibration.

Sample 072 comes from close by sample 071 and contains similar mineralogy plus orthopyroxene, although the grain size is slightly smaller than in 071, with garnet grain size being the range of 500-800 μm, and clinopyroxene in the range of 150-500 μm. Orthopyroxene in this sample is retrogressed, generally lacking a fresh appearance. Similar to 071, clinopyroxene occurs in the pressure shadows of garnet together with granoblastic plagioclase, with quartz occurring as inclusions in subhedral garnet grains (Figure 6-19). This texture, also inferred to be syntectonic, was analysed using GCPQ geothermobarometry, which yielded apparent peak metamorphic conditions for thrusting of 14 kbar and 875 °C and retrograde conditions of 13.4 kbar and 840 °C. Again in this sample, apparent peak and retrograde conditions are close and the rock is inferred to have cooled quickly thus locking in the high *P-T* compositions.

Sample 086-1 was taken at the contact with the footwall in the shear zone at the northern end of the allochthon on Grand Lake. This rock contains the assemblage garnet-clinopyroxene-calcic amphibole-plagioclase-quartz and does not exhibit the "classic" mylonitic textures found elsewhere in the shear zone. The texture exhibited is inferred to be the product of retrogression where resorbed garnet porphyroblasts that are 500-100 μm in diameter, are mantled by plagioclase and amphibole (see Figure 6-18). Clinopyroxene is present in the assemblage along with quartz although clinopyroxene in many parts of the

sample is partially replaced by amphibole. The cooling-hydration reaction: Grt + Cpx + H_2O = Cam + Pl+ Qtz, is inferred to have taken place in this rock along with many rocks from the Goose Bay area. GCPQ thermobarometry yielded apparent peak metamorphic conditions of 13.6 kbar and 925 °C and retrograde conditions of 11.6 kbar and 770 °C. GHPQ thermobarometry yielded slightly lower pressure apparent peak metamorphic conditions of 12.7 kbar and 965 °C and retrograde conditions of 10.7 kbar and 780 °C. Both peak and retrograde conditions are within error of each other and average apparent peak conditions of 13.2 kbar and 940 °C and 11.2 kbar and 775 °C for retrograde conditions are inferred.

Sample 090 was taken from an outcrop in the mafic gneiss unit on the northern shore of Grand Lake. This sample contains garnet, clinopyroxene, amphibole, plagioclase and quartz where both pyroxene and amphibole together with quartz stringers define the mylonitic foliation. Garnet porphyroblasts, with grain sizes in the range of 1500-2000 μm, are observed to contain clinopyroxene and quartz inclusions implying simultaneous growth. GCPQ geothermobarometry yields apparent peak metamorphic conditions of 13.9 kbar and 850 °C and retrograde conditions of 12.7 kbar and 800 °C. GHPQ thermobarometry yields retrograde metamorphic conditions of 9.7 kbar and 785 °C which are inferred to reflect the *P-T* conditions for amphibolitization present in parts of the Goose Bay area.

7.4.4 Summary of P-T Estimates

The following table (Table7-3) summarizes the calculated apparent peak and retrograde conditions for the rocks of the Goose Bay area discussed above. All samples from the shear zone, except for 028-1, yield consistent apparent peak metamorphic conditions of

around 13.9 ± 0.5 kbar and 873 ± 40 °C (028-1 yields 11.5 kbar and 875 °C). This suggests that pervasive recrystallization during shearing and thrust emplacement of the allochthon took place in the shear zone and that the mineral assemblages in the shear zone were chemically reset at this time. Estimated retrograde conditions in the shear zone samples are much more variable, ranging from 14 to 8.1 kbar and 860 to 614 °C, suggesting that domainal equilibrium was important during the retrograde path. This may have also contributed to the relatively lower metamorphic apparent peak conditions obtained from sample 028-1, suggesting that the conditions recorded by this sample reflect retrograde conditions rather than peak. Furthermore, several samples exhibiting evidence for the retrograde reaction: Grt + Cpx + H_2O = Cam + Pl + Qtz, yield *P-T* estimates in the range of 11-12 kbar and 750-800 °C, suggesting that hydrous retrogression was initiated shortly after apparent peak *P-T* conditions.

Sample	Apparent Peak	Retrograde	Sample	Apparent Peak	Retrograde
FW	P (kbar) T (°C)	P (kbar) T (°C)	SZ	P (kbar) T (°C)	P (kbar) T (°C)
049	12.0, 825	11.7, 800	008	13.9, 875	11.8, 725
056	8.9, 740	7.0, 660	012	14.2, 850	11.8, 775
074	12.9, 725	11.3, 630	017	14.0, 855	-
084	13.3, 890	12.9, 840	028-1	11.5, 875	8.1, 785
HW			029-1	14.4, 870	13.7, 820
122-3	11.4, 800	9.2, 780	086-1	13.2, 940	11.2, 775
142	12.2, 840	11.5, 775	059a	13.0, 880	11.7, 790
196a	11.2, 800	7.7, 690	065a	13.7, 850	9.3, 614
			071	14.3, 880	14.0, 860
			072	14.0, 875	13.4, 840
			090	13.9, 850	9.7, 785

Table 7-3: *Geothermobarometric results for samples from the footwall, hangingwall and shear zone rocks in the Goose Bay area. Errors on P-T estimates are ± 1 kbar and ± 50 °C.*

The samples from the footwall yield a more varied range of apparent peak conditions from 13.3 to 8.9 kbar and 890 to 725 °C. This variability is also inferred to be the result of domainal equilibrium on the retrograde *P-T* path. An alternative possibility, incomplete resetting of Labradorian fabrics during Grenvillian thrusting, is not favoured on the basis of the development of penetrative fabrics of inferred Grenvillian age. The estimated retrograde conditions overlap those from the shear zone, from 12.9 to7.0 kbar and 840 to 630°C, suggesting that retrogression in the footwall was also driven by domainal equilibrium.

P-T estimates for hangingwall samples do not vary as greatly as those for the footwall samples and yield apparent peak metamorphic conditions of around 11.6 ± 0.6 kbar and 810 ± 25 °C, suggesting that the CCRA was not as affected by domainal equilibrium as the

footwall. However, retrograde conditions obtained from the hangingwall range from 11.5 to 7.7 kbar and 780 to 690 °C, overlapping with those from the footwall, implying that domainal equilibrium was also important during retrogression in the hangingwall.

The estimated range of the apparent peak conditions in the shear zone is consistent with the mineralogy and fabrics in the shear zone. There is no evidence for partial melting in any of the dioritic gneisses, however the presence of syntectonic migmatitic patches and veins does confirm that the shear zone reached temperatures great enough for partial melting of the pelitic compositions. The lack of eclogite facies mineralogy in the shear zone is consistent with the apparent peak pressures. Therefore the estimated apparent peak *P-T* conditions straddles the general reaction Opx + Pl = Grt + Cpx + Qtz and Hbl + Pl + Qtz = Grt + Cpx (see Figure 6-16), or the garnet-clinopyroxene-orthopyroxene-plagioclase ± (calcic amphibole or quartz) field to orthopyroxene-free garnet clinopyroxene-plagioclase ± (calcic amphibole or quartz) field shown on Figure 6-30. Thus it is inferred that there is no discrepancy between the estimated peak metamorphic conditions and the lithologies of the shear zone.

However, given the granulite uncertainty principle, the important question arises: Are the apparent peak *P-T* estimates accurate? It could be argued on *a priori* grounds that the consistency of the apparent peak *P-T* estimates (determined from grain cores) in the shear zone would appear to imply that all garnet porphyroblasts were of similar in diameter and experienced similar degrees of diffusional resetting at peak temperatures (e.g., Figure 7-1).

However, as noted above, this inference would not be correct as the diameters of analysed garnet grains vary from sample to sample. Alternatively the rate of intergranular diffusion at peak temperature could have varied within the shear zone, possibly as a result of different defect densities in the analysed grains, thereby allowing garnets of different diameter to record similar temperatures in their cores. However this also seems unlikely, so the conclusion is forced that the apparent peak conditions may not reflect the true peak *P-T* conditions, but rather part of the retrograde path, or they may be a meaningless artifact if there was non-synchronous closure of the thermometer and barometer.

It therefore becomes important to try to determine the magnitude of the absolute difference between the true and apparent peak *P-T*'s. There are several lines of qualitative petrological evidence that suggest that the difference between the two may not be large. i) There is no evidence for ultra-high temperature (>900 °C) mineralogy in the shear zone, suggesting that the upper apparent *T* estimates may not significantly underestimate the true *T*; ii) The absence of melting in the mafic (dioritic) gneisses is compatible with maximum *T* in the range 800-850 °C; iii) The widespread presence of prograde biotite in the pelitic gneisses suggests that temperatures did not exceed ~ 850 °C. For overthrust terranes, which typically evolve along a clockwise *P-T* path, the maximum pressure achieved is greater than the pressure attained at maximum temperature (referred to as peak *P-T* in this text), thus the apparent peak *P-T* estimates are inferred to be similar to, but a small undetermined amount less than, the true peak metamorphic conditions.

7.4.5 a_{SiO_2} and P-T Results

For most of the samples, several *P-T* determinations from the same sample yielded very similar estimates providing confidence in the results. However, for 4 of the 18 samples (samples 008, 012, 017 and 084), one or more of the *P-T* estimates was significantly different from the majority, indicating a local source of error in the calculations. Examination of the data (see Table 7-4 and Appendix F) indicates that the temperature estimates are within error of the modal results for the sample, but the pressure results are systematically higher. These samples yielded peak pressures from ≥14.1 (minimum) up to 16.1 kbar but estimated pressures either from within the same sample or from a nearby sample yielded peak pressures that were significantly lower (by 0.2 kbar to 2.2 kbar). This suggests that there is a non-systematic error in some of the pressure estimates. One way that this could occur (assuming that equilibrium was achieved between the analysed minerals), is if the samples with anomalously high pressures crystallized under a reduced activity of SiO_2. To test this hypothesis, the samples that yielded anomalously high pressure estimates were examined using BSE imaging to search for quartz. Results of this examination led to the observation that quartz is principally confined to certain layers or domains in these samples, leading to the conclusion that the a_{SiO_2} may have varied domainally within these samples. Where quartz is abundant (>5% by area), the *P-T* estimate obtained from the analysis area appears to be geologically reasonable. However, in domains in which quartz is absent, shielded in another mineral or generally in low abundance (<5% by area) the resultant *P-T* estimate obtained yielded anomalously high pressure estimates. These observations imply that the cause of the

error is a function of the reduced activity of SiO_2 in parts of the analysed sample; e.g., a_{SiO_2} varies on a domainal scale that is smaller than the thin section. If this interpretation is correct, and assuming that the average apparent peak *P-T* estimate derived from the majority of the determinations in theses samples is also correct, it is possible to quantify the reduced a_{SiO_2} that caused the anomalous pressure estimates. To establish the actual a_{SiO_2}, the a_{SiO_2} of the silica-poor assemblage can be adjusted to reflect the average estimated pressure from the quartz-bearing (a_{SiO_2}=1) domains. Figure 7-13 displays the variation of pressure with Log (a_{SiO_2}) for the range -1 < Log a_{SiO_2} > 0 (or 0.1 < a_{SiO_2} >1) for the GCPQ barometer. The activity of silica for individual sets of analyses can be estimated from these diagrams and when these silica activities are re-entered into the geothermobarometric equation, the previously determined average pressure and a slightly modified temperature are calculated. Note that an a_{SiO_2} = 1 yields a maximum pressure, labelled P_{max} on Figure 7-13. Once the a_{SiO_2} was established for a peak *P-T* domain in the sample, the same silica activity was also applied to the retrograde *P-T* calculations to obtain the corrected retrograde *P-T* point.

Table 7-4 displays the calculated silica activities with recalculated peak and retrograde *P-T* results for samples which yielded maximum pressures that are not consistent with the mineralogy, such as the low jadeite content in clinopyroxene. These results have already been incorporated into the results discussed above.

Sample	P_{max}	T_{max}	$P_{determined}$	True $aSiO_2$ =	Resultant P	Resultant T
008-1*	16.1	915	13.9	0.62	13.8	908
008-11	12.8	798	13.9	0.62	10.7	792
012-11*	15.8	902	14.2	0.71	14.2	896
012-12	14.2	843	14.2	0.71	12.6	839
012-13*	14.1	815	14.2	0.71	8.9	788
012-14	13.3	809	14.2	0.71	11.8	805
017-1*	14.3	863	14	0.96	14.1	864
017-1*	14.2	842	14	0.96	13.4	837
017-2*	15.1	887	14	0.96	14.8	885
017-3*	13.4	818	14	0.96	13.2	818
084-1*	15.8	907	13.6	0.63	13.5	900
084-12	14.5	851	13.6	0.63	12.4	843
084-3*	15.1	948	13.6	0.63	12.7	940
084-31	14.6	865	13.6	0.63	12.5	857

***Table 7-4**: Recalculated P-T estimates for samples which yield unreasonable maximum pressures at $aSiO_2$ = 1 based on the mineralogy of the samples. P_{max} and T_{max} are estimates assuming $aSiO_2$ = 1. $P_{determined}$ is from domains of the samples where $aSiO_2$ is reliably considered to be unity. True $aSiO_2$ is reduced activity of SiO_2 to conform with $P_{determined}$ (see Figure 7-13). Resultant P and T are P-T estimates calculated with the estimated reduced $aSiO_2$. Samples with an * indicate peak P-T estimates. Samples 008, 012 and 017 are from the shear zone and 084 is from the footwall. Pressures are in kbars and temperatures are in °C. All P-T estimates, including those in this table, can be found in Appendix F.*

7.5 Discussion

Now that *P-T* estimates for the footwall, hangingwall and shear zone have been determined, interpretations concerning the *P-T* paths, followed by these rocks may be considered. Although it is generally assumed that a *P-T* point lies on the *P-T* path

experienced by the rock, there is a very real possibility in high grade rocks that the geothermometer and geobarometer could have closed at different times as discussed above, thereby yielding incorrect *P-T* points and hence a geologically meaningless *P-T* path. For example if the thermometer were to continue to reset after the barometer was frozen in, the resultant *P-T* path from core and rim analyses (apparent peak and retrograde) would give an apparent isobaric cooling path with a slope that would coincide with the slope of the geobarometer in *P-T* space (Frost and Chacko 1989, Selverstone and Chamberlain 1990). Figure 7-14 displays the core and rim (apparent peak and retrograde) conditions for the 18 analysed samples. The apparent *P-T* path followed by some of the samples suggests that non-synchronous closure of the geobarometer and geothermometer has occurred, as some of the *P-T* paths are parallel to or nearly parallel to the slopes of the geobarometers. This is discussed in more detail for the footwall, hangingwall and shear zone in the following sections.

7.5.1 Footwall P-T Path

For the four samples from the footwall, all the apparent *P-T* paths can be interpreted in terms of non-synchronous closure of the geobarometer and geothermometer to some degree. For samples 084 and 049 in particular, the *P-T* path closely parallels that of the GADS calibration (Figure 7-14a). The effects of non-synchronous closure are minimal in these two samples however, due to the relatively short *P-T* vectors. Sample 074 involves the same barometer, but the *P-T* vector is much steeper and considerably longer than in 084 and 049. These results suggest that non-synchronous closure, especially in sample 084, may have

been a factor here as well, but there is also the possibility that the barometer also reset during retrogression, yielding an apparent *P-T* vector that is steeper than isopleths for the GADS barometer. Sample 056 involves the GHPQ calibration which has steeper isopleths in *P-T* space and so non-synchronous closure of the thermometer and barometer would result in a steeper *P-T* vector, but the calculated vector is even steeper than isopleths for the GHPQ reaction, suggesting that this sample also may record a real change in *P* as well as *T* during retrogression. However, it is difficult to estimate the magnitude of any such change as the resultant vector may incorporate the effects of both non-synchronous closure and retrograde resetting.

Based on the observed mineralogy in the metasediments, the *P-T* path of the footwall rocks must have crossed from the Ky to the Sil field. Therefore, it is likely that the true *P-T* path was steeper than those shown in Figure 7-14a, assuming that the apparent peak *P-T* estimates are close to the true *P-T* conditions, as argued above. Thus the slope of the apparent *P-T* path obtained for the footwall rocks is underestimated and must be significantly greater than that estimated from core and rim analyses.

7.5.2 Hangingwall P-T path

Samples from the hangingwall, especially 142 and 122-3, yield apparent *P-T* vectors that also suggest non-synchronous closure in the GCPQ calibration occurred post-peak metamorphism (Figure 7-14b). These two samples yield relatively short *P-T* vectors indicating that the thermometer must have closed shortly after apparent peak conditions were locked in. The same is true of sample 196a, although in this case, the *P-T* vector is much

steeper, suggesting that decompression occurred during cooling. Apparent *P-T* vectors obtained from the GHPQ calibration for sample 196a also indicate decompression during cooling. As with the footwall samples, it is concluded that the resultant *P-T* vector has a minimum possible slope for the hangingwall rocks. However in this case, there is little independent evidence to support a steeper *P-T* path than that shown on Figure 7-14b.

7.5.3 Shear Zone P-T path

As discussed above, the apparent peak *P-T* estimates are consistent across the shear zone, but the apparent retrograde paths followed by the samples differ considerably in length and display a range of slopes (Figure 7-14c). Some of the retrograde paths follow a slope that is parallel or subparallel to isopleths of the barometer used for the *P-T* calibration (samples 029-1, 059a, 071, 086-1). As before, this implies that these samples have also experienced non-synchronous closure of the barometer and thermometer. However, all the remaining samples yield *P-T* vectors that are steeper than the slope of the geobarometer, suggesting that cooling was accompanied by decompression. The magnitudes of the *P-T* vectors vary from sample to sample implying that retrogression was driven by domainal equilibrium in the shear zone rocks. Thus, it cannot be assumed that all the samples recorded their *P-T* conditions at the same time; it is more likely that shearing and hence recrystallization occurred over a protracted period, but at different times in samples from different parts of the shear zone. This assumption is consistent with the different lengths of the *P-T* vectors obtained from different samples. The small size of some domains in which this has occurred is indicated by the different lengths of vectors derived from a single sample, e.g., sample

028-1 (Figure 7-14c). Thus the samples record different parts of the *P-T* path of the shear zone rocks as a whole, and by putting them all together, a larger part of the *P-T* path can be recovered. However, once again, independent evidence must be sought to establish whether the *P-T* path is real or in part an artifact of non-synchronous closure of the thermometer and barometer. Unfortunately, in this case no independent evidence was found in the shear zone rocks to either support or refute this point.

The apparent differences in the maximum *P-T* estimates between the shear zone, footwall and hangingwall are consistent and may thus be real. They are inferred to be a result of recrystallization of the footwall and hangingwall assemblages after early displacement on the shear zone had taken place. As discussed above, the rocks of the shear zone have been completely recrystallized, although heterogeneously, both during and following peak Grenvillian metamorphism. The adjacent footwall and hangingwall rocks, however, are inferred to have undergone less penetrative recrystallization during Grenvillian orogenesis, the later time (inferred from the lower pressure estimate) being compatible with growth (broadening) of the shear zone during its early evolution. Those samples from the footwall that were taken from closest to the shear zone are inferred to have undergone penetrative recrystallization at an early stage during the Grenvillian orogeny, whereas those further away were recrystallized at a later stage during uplift. Even farther away from the shear zone, partial retention of Labradorian signatures is likely. However, these rocks were not sampled in this study. In contrast to their peak *P-T* conditions, the estimated *P-T* conditions for the retrograde paths in the footwall, hangingwall and shear zone overlap, indicating that they all

underwent similar, although heterogeneous, retrograde conditions during uplift. In contrast, the footwall and hangingwall rocks are inferred to have undergone only partial or incomplete recrystallization during the Grenvillian orogenesis and likely also underwent less pervasive retrogression during uplift. The Northwest River dykes are monocyclic with respect to the Grenvillian orogenesis, and thus are assumed to only record Grenvillian metamorphism and deformation. *P-T* estimates from the dykes especially samples 142 and 196a record apparent peak metamorphic conditions at ~11.5 kbar and 820 °C suggesting that they recrystallized under those conditions, but the strain may not have been sufficient to cause a similar level of recrystallization in the host rock as recorded by the dykes. Thus, the Labradorian assemblages must have been partially recrystallized, depending on the location of the rock with respect to the site of to deformation.

Figure 7-14d shows the extrapolated *P-T* paths from the shear zone, footwall and hangingwall. As discussed above, these paths represent minimal slopes if the thermometer continued to reset after the barometer was frozen in. Thus the true slopes of the *P-T* paths however are inferred to be steeper than the calculated slopes, although by how much is not known. On the basis of arguments given above, and the consistency of the estimated apparent peak metamorphic conditions in the shear zone, it is assumed that a *P-T* point at the apparent peak *P-T* conditions lies on or close to part of the *P-T* path followed by rocks from the shear zone and adjacent footwall and hangingwall. A second *P-T* point on the path can be deduced from mineralogical observations, i.e., the coexistence of sillimanite with kyanite in the paragneiss unit adjacent to the shear zone. The true *P-T* path must therefore have crossed the

kyanite to sillimanite transition so the inferred *P-T* path shown on Figure 7-14d, passes through the apparent peak *P-T* point and crosses the kyanite-sillimanite boundary with a steeper slope than was extrapolated from the *P-T* data. This inferred path suggests that the shear zone and footwall (and hangingwall?) rocks initially experienced a steep decompression path with minor cooling in the kyanite field, with the lower pressure *P-T* evolution possibly being approximately subparallel to the kyanite-sillimanite boundary. This inferred *P-T* path (Figure 7-14d) suggests that the thermometers continued to reset at temperatures up to 100 °C or so lower than the barometers, compatible with diffusion theory, and thereby resulting in apparent *P-T* paths that are less steep than the true paths.

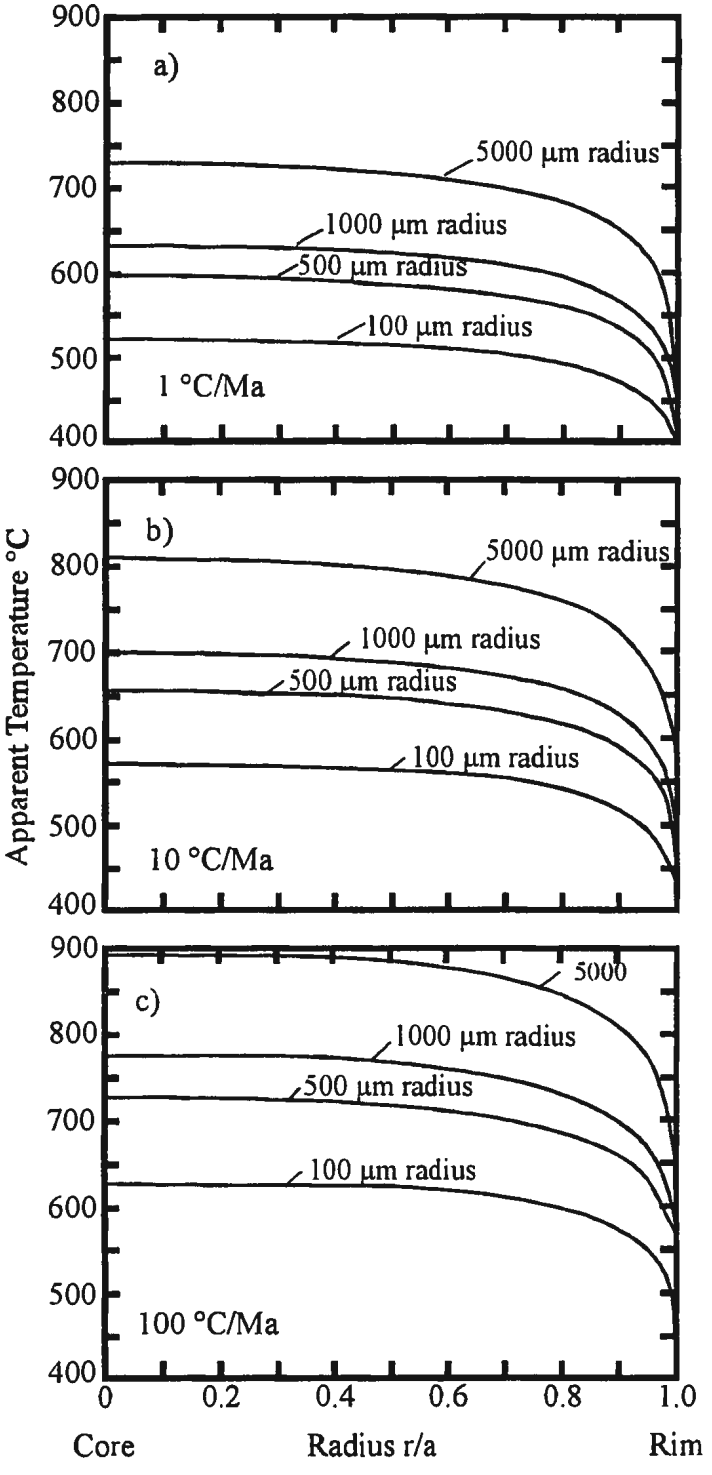

***Figure 7-1**: Plot of apparent temperature against a normalized garnet radius (so that the rims all plot at 1.0) for varying cooling rates for Fe-Mg diffusion only for garnet in the presence of biotite. The starting temperature for the computer model is in excess of 900°C. Diagram is after Spear 1991.*

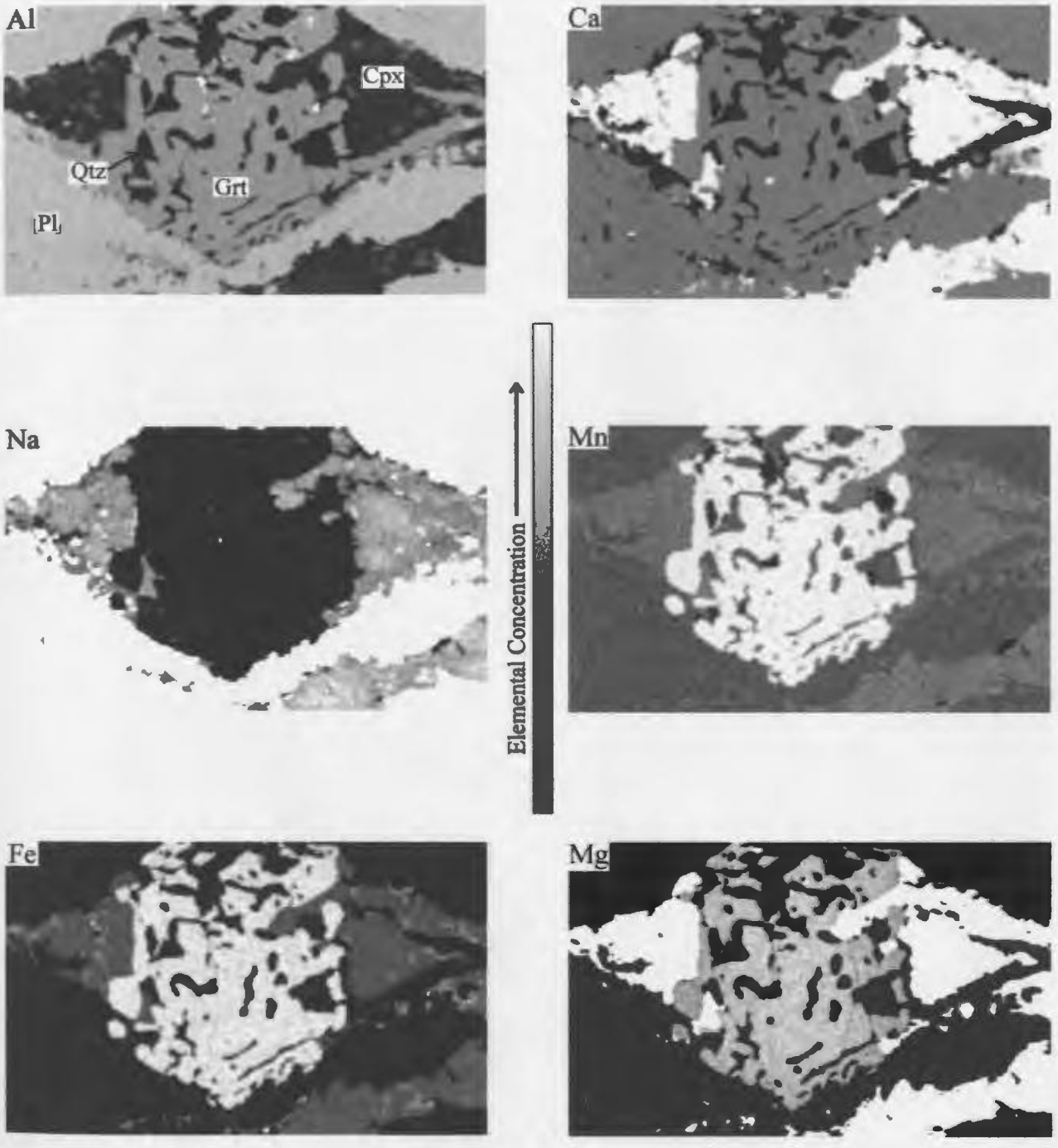

***Figure 7-2**: Electron microprobe energy diffraction (ED) maps for the elements Al, Ca, Na, Mn, Fe, Mg for a syntectonic metabasite assemblage. Note the weak zoning present for garnet in the Mg map and the Na zoning present in clinopyroxene. The zoning present in both clinopyroxene and garnet suggest minor retrogression. Sample JK-99-072.*

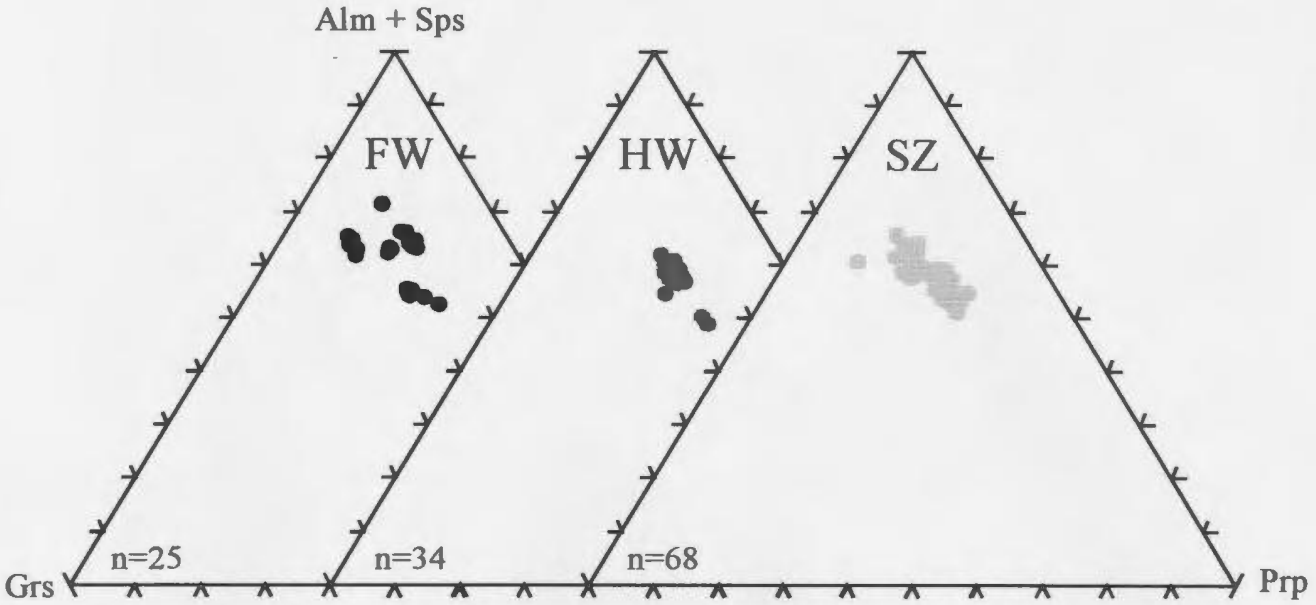

***Figure 7-3**: Compositional diagrams for garnet from the footwall (FW), hangingwall (HW) and the shear zone (SZ).*

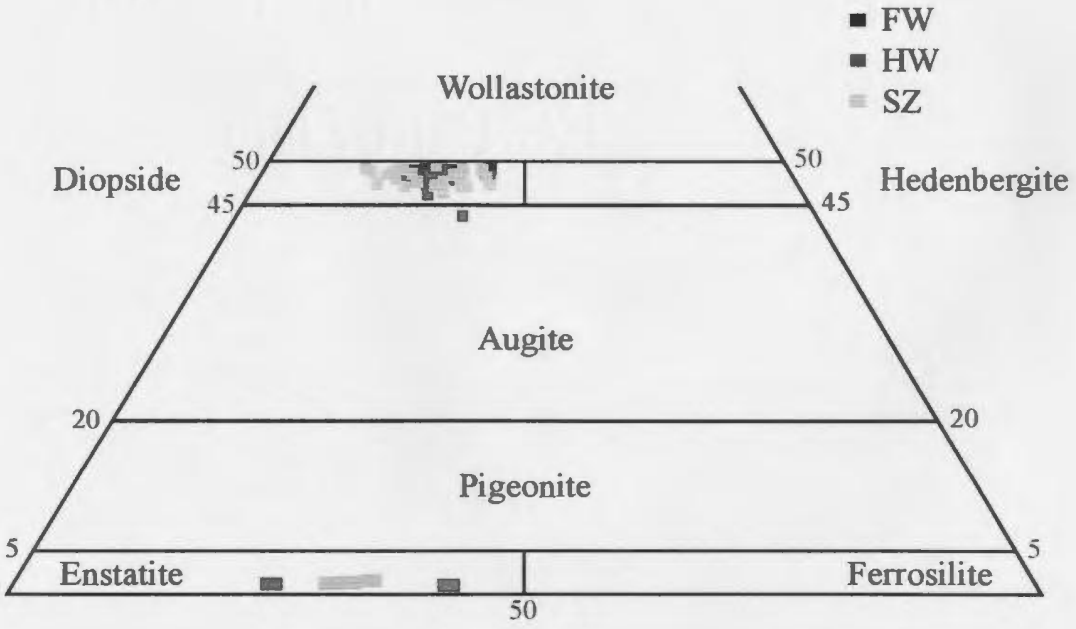

***Figure 7-4**: Composition ranges for Ca-Mg-Fe pyroxenes from the Goose Bay area (ranges and nomenclature after Morimoto 1988).*

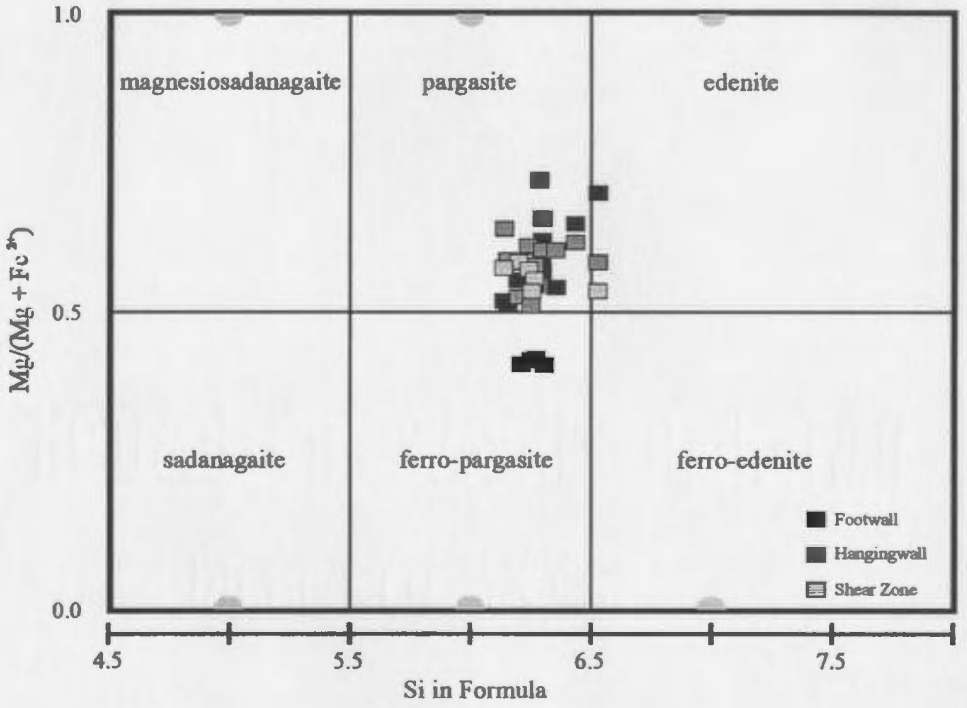

Figure 7-6: *Classification of calcic amphiboles from the shear zone, footwall and hangingwall rocks (after Leake et al. 1997). The semicircle symbols indicate the locations of the end-members. Diagram parameters:* $Ca_B \geq 1.50$; $(Na + K)_A \geq 0.50$; $Ti < 0.50$

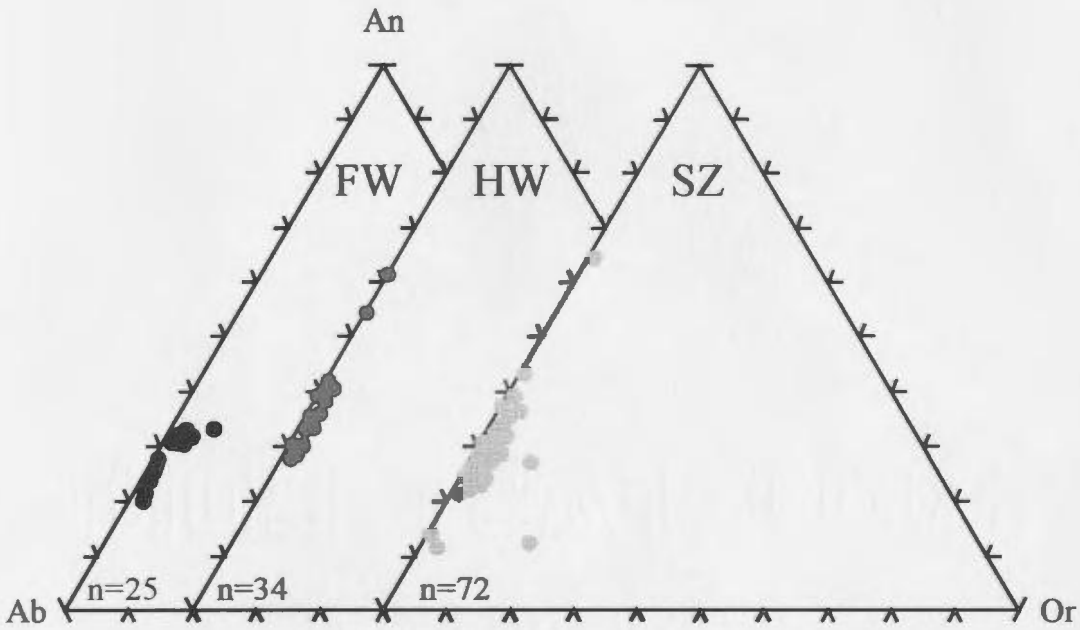

***Figure 7-6**: Compositional diagrams for plagioclase from the footwall (FW), hangingwall (HW) and the shear zone (SZ). Higher anorthite content feldspars are samples 122-3 (HW) and 028-1 (SZ). The lowest anorthite values in the shear zone come from samples 017 and 086.*

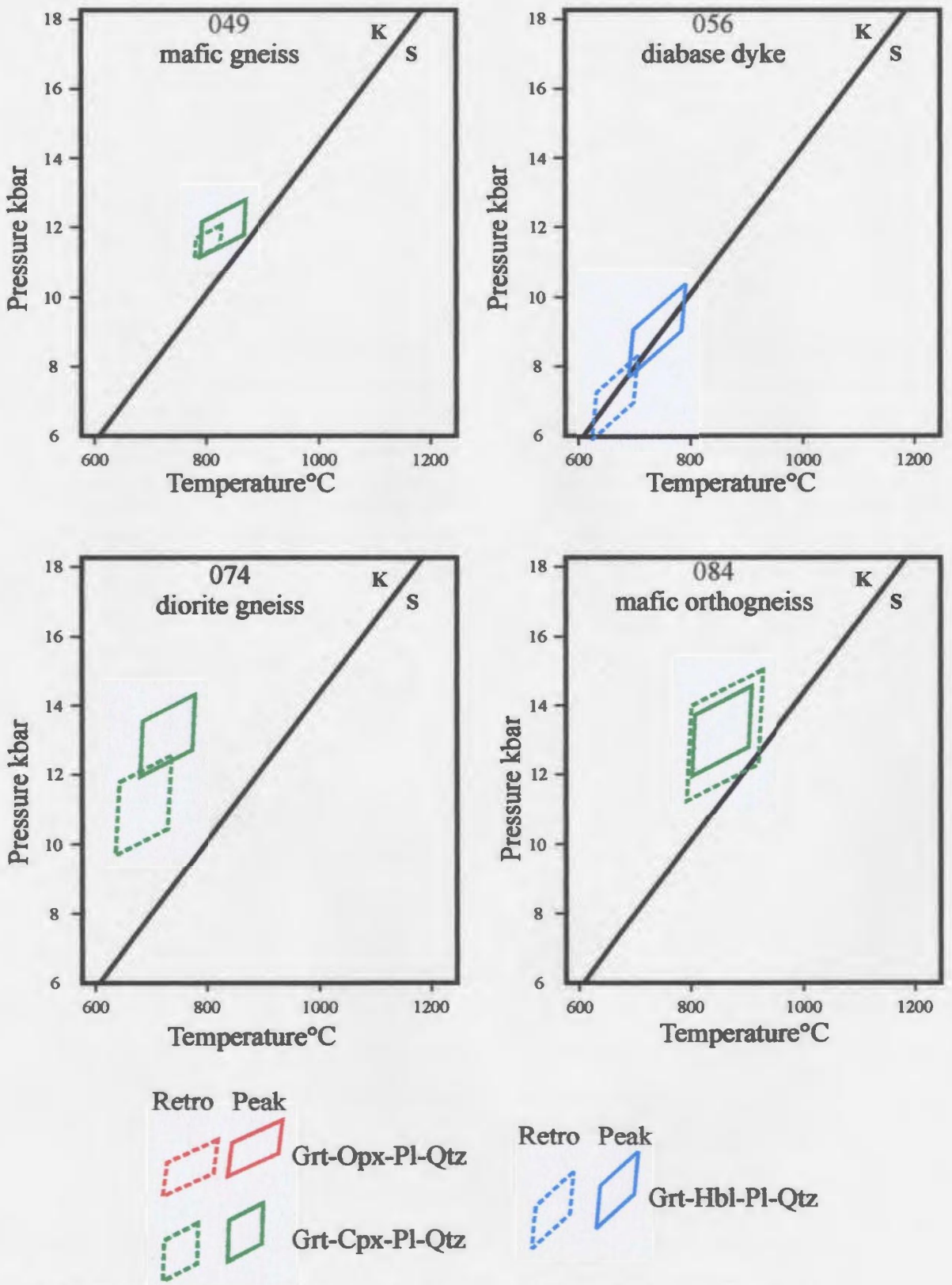

***Figure 7-7a**: Geothermobarometric results for samples from the footwall rocks.*

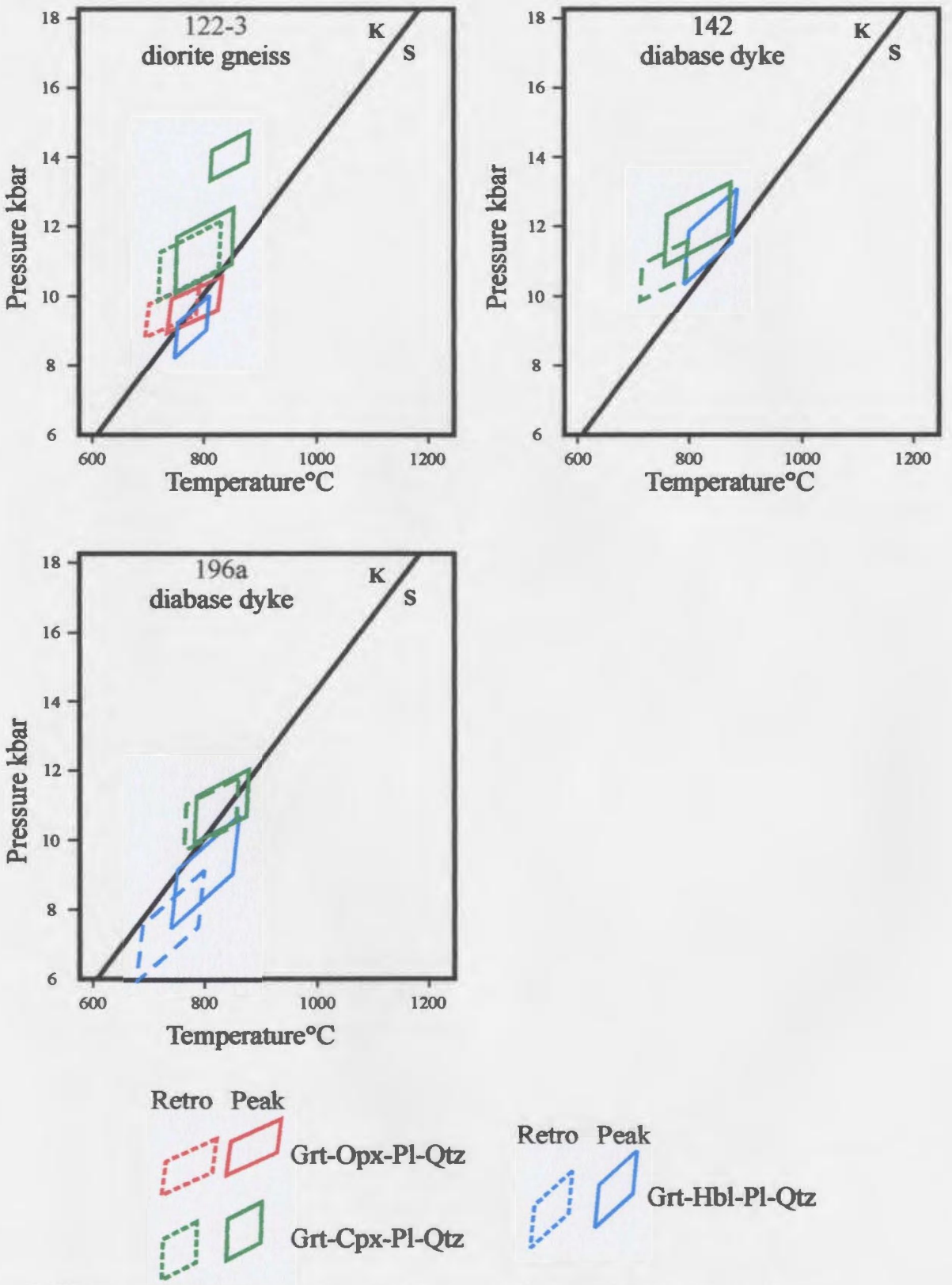

***Figure 7-7b**: Geothermobarometric results for samples from the hangingwall rocks.*

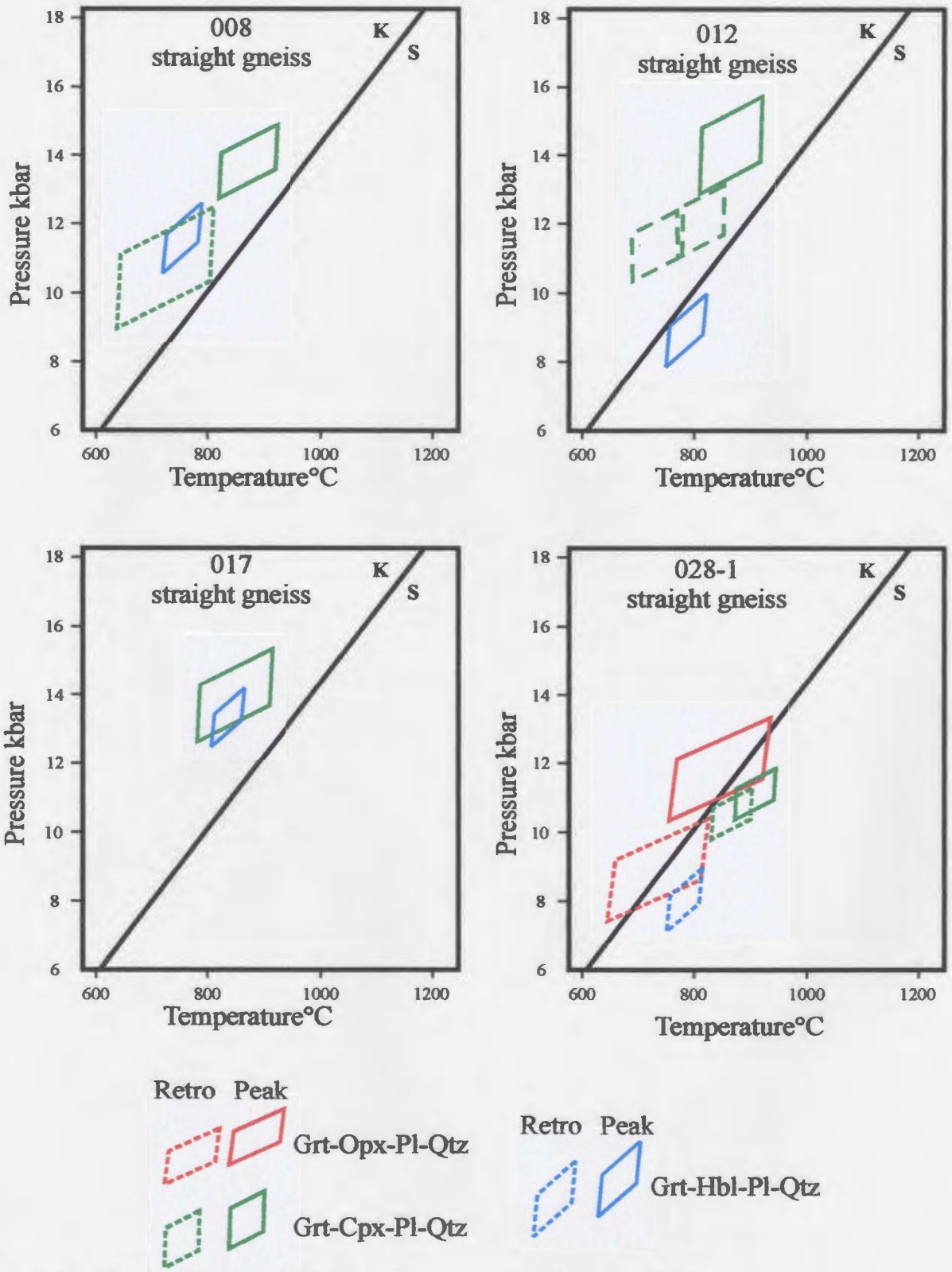

Figure 7-7c: *Geothermobarometric results for samples from the shear zone.*

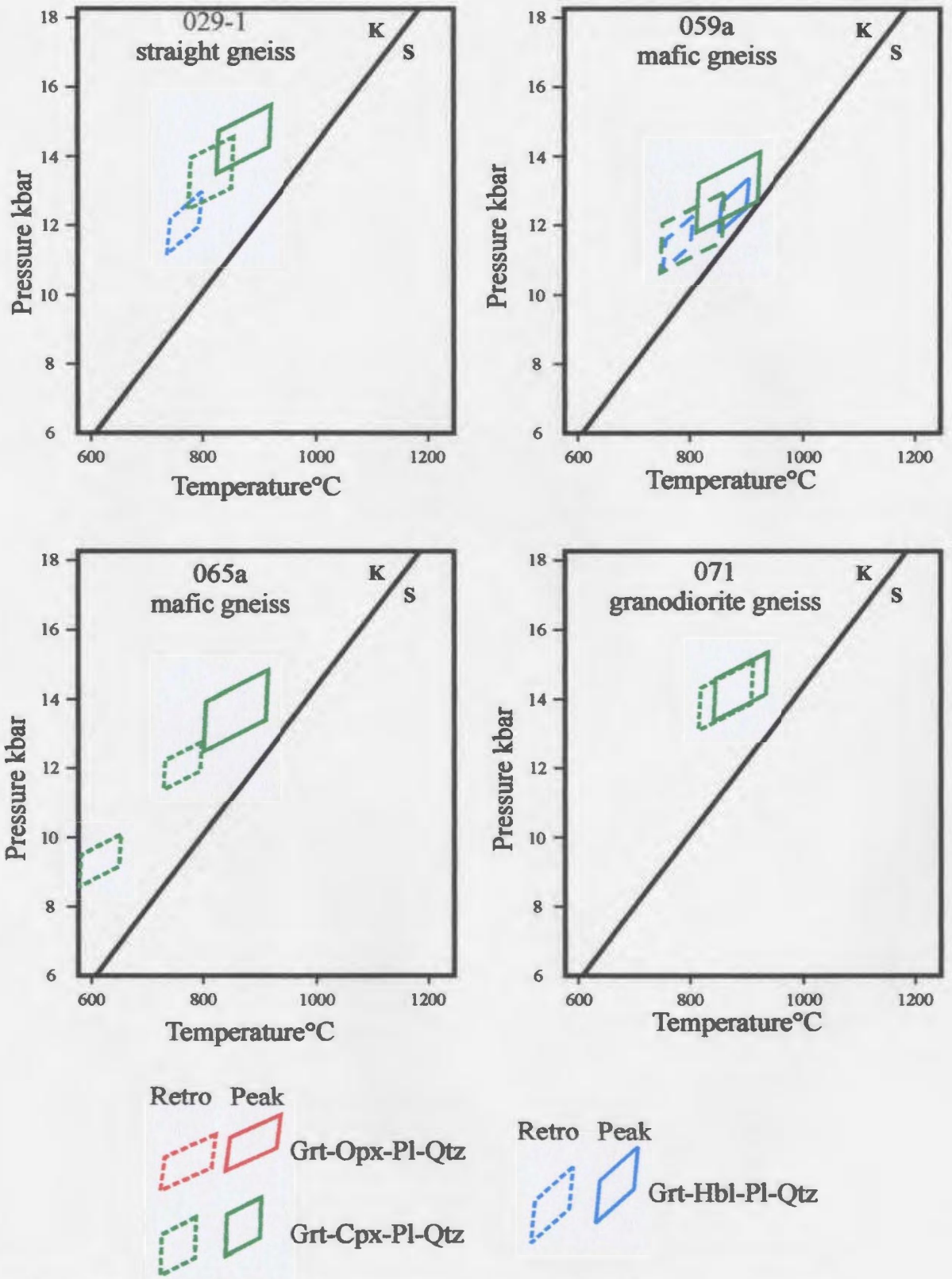

***Figure 7-7c cont'd**: Geothermobarometric results for samples from the shear zone.*

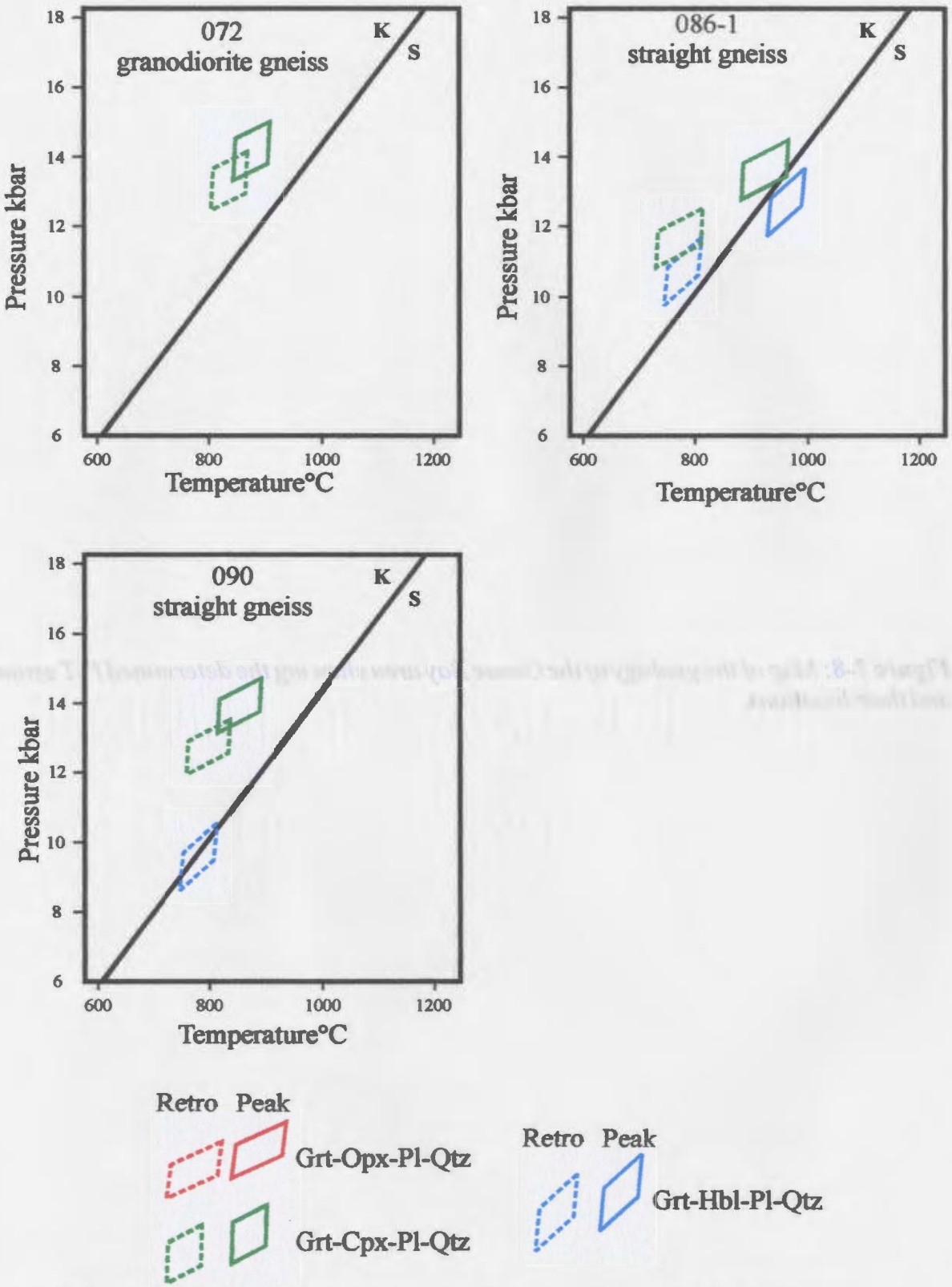

***Figure 7-10c cont'd**: Geothermobarometric results for samples from the shear zone.*

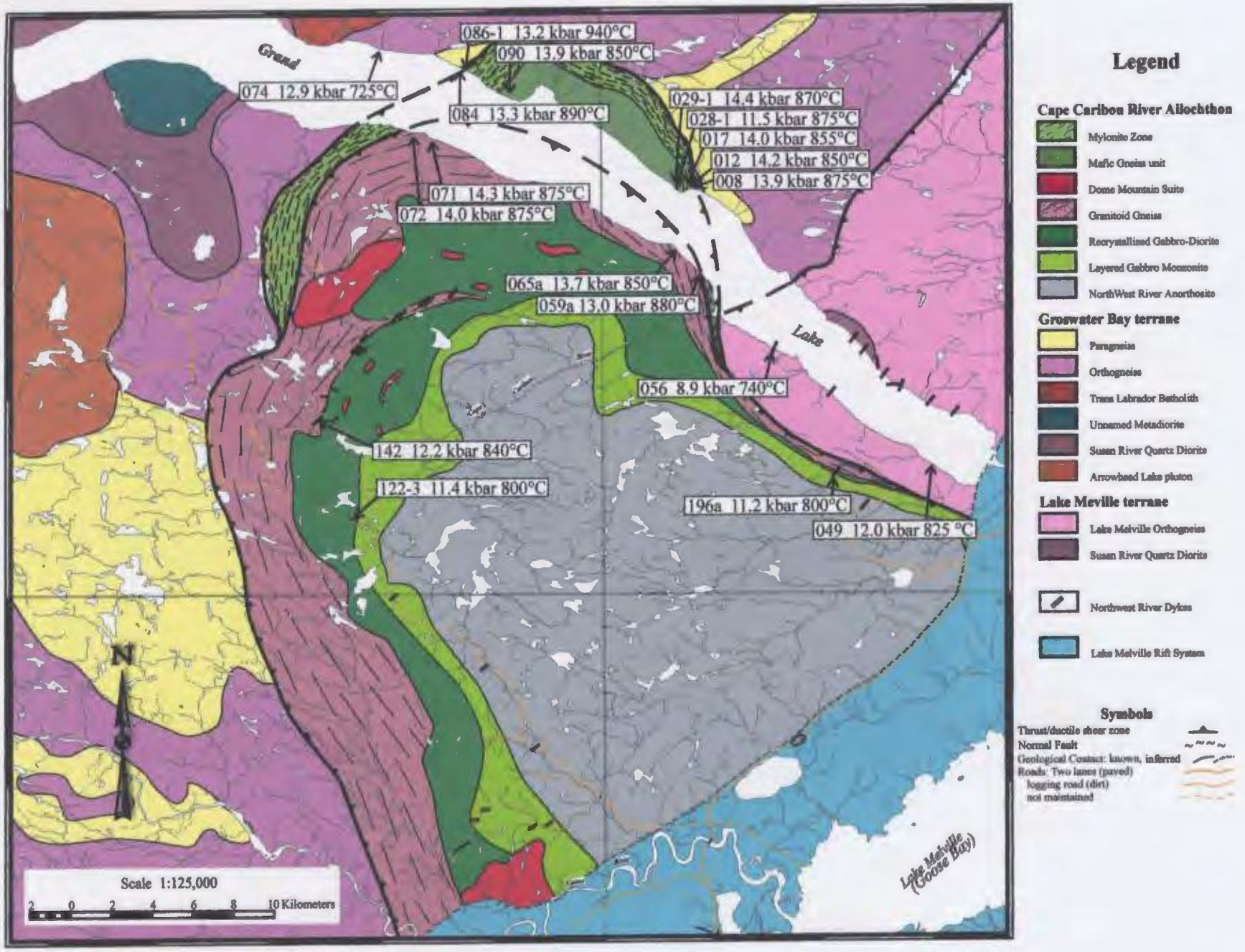
086-1 13.2 kbar 940°C
090 13.9 kbar 850°C
Grand
074 12.9 kbar 725°C
084 13.3 kbar 890°C
029-1 14.4 kbar 870°C
028-1 11.5 kbar 875°C
017 14.0 kbar 855°C
012 14.2 kbar 850°C
008 13.9 kbar 875°C
071 14.3 kbar 875°C
072 14.0 kbar 875°C
065a 13.7 kbar 850°C
059a 13.0 kbar 880°C
Lake
056 8.9 kbar 740°C
142 12.2 kbar 840°C
122-3 11.4 kbar 800°C
196a 11.2 kbar 800°C
049 12.0 kbar 825 °C
N
Scale 1:125,000
2 0 2 4 6 8 10 Kilometers
Lake Melville (Goose Bay)
Legend
Cape Caribou River Allochthon
Mylonite Zone
Mafic Gneiss unit
Dome Mountain Suite
Granitoid Gneiss
Recrystallized Gabbro-Diorite
Layered Gabbro Monzonite
NorthWest River Anorthosite
Groswater Bay terrane
Paragneiss
Orthogneiss
Trans Labrador Batholith
Unnamed Metadiorite
Susan River Quartz Diorite
Arrowhead Lake pluton
Lake Melville terrane
Lake Melville Orthogneiss
Susan River Quartz Diorite
Northwest River Dykes
Lake Melville Rift System
Symbols
Thrust/ductile shear zone
Normal Fault
Geological Contact: known, inferred
Roads: Two lanes (paved)
logging road (dirt)
not maintained

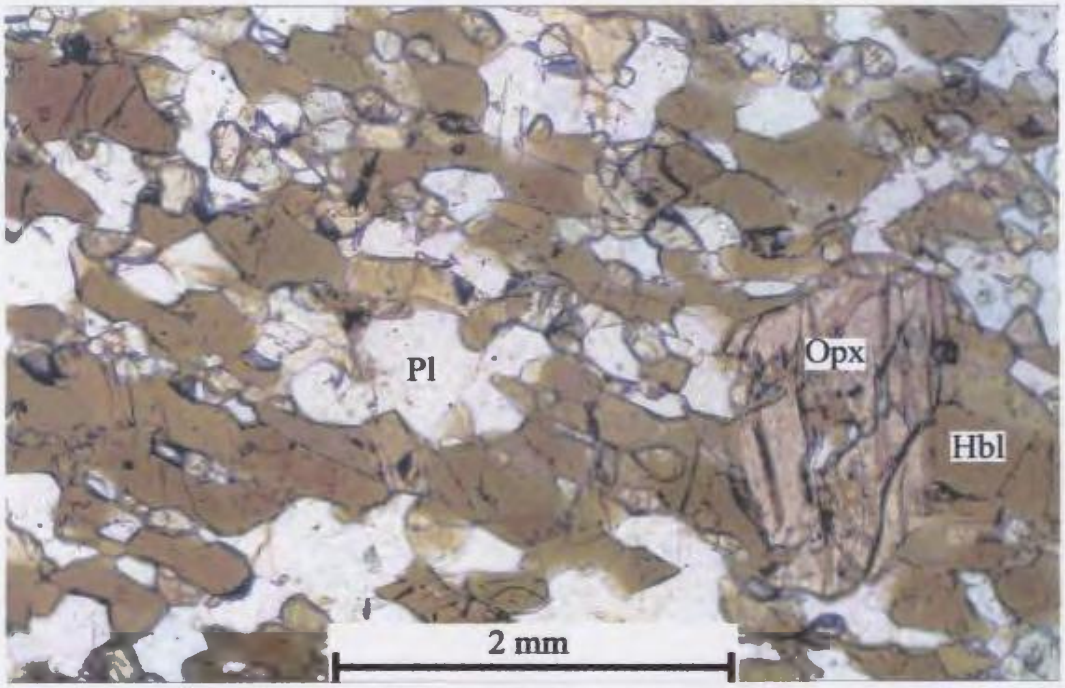

***Figure 7-9**: Photomicrograph displaying orthopyroxene growth at the expense of amphibole in a Northwest River Dyke sample JK-99-122-1. PPL*

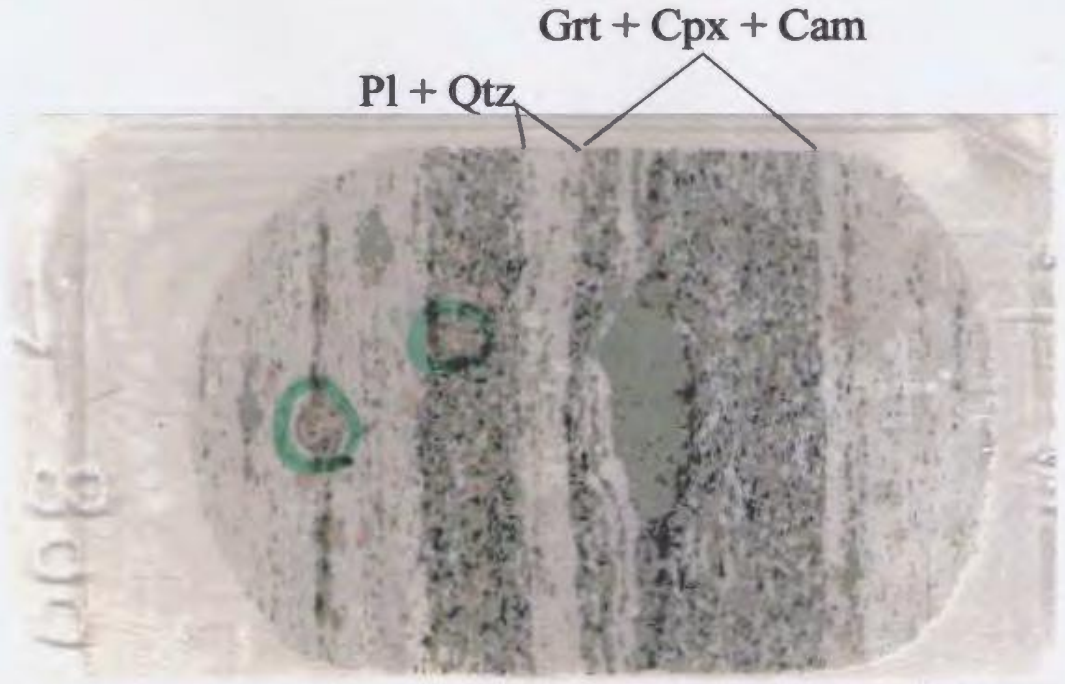

***Figure 7-10**: Photograph of the thin section cut from sample JK99-008. Note the layering of felsic and mafic layers. The green circles indicate the analysis areas chosen for geothermobarometry. GLTS straight gneiss.*

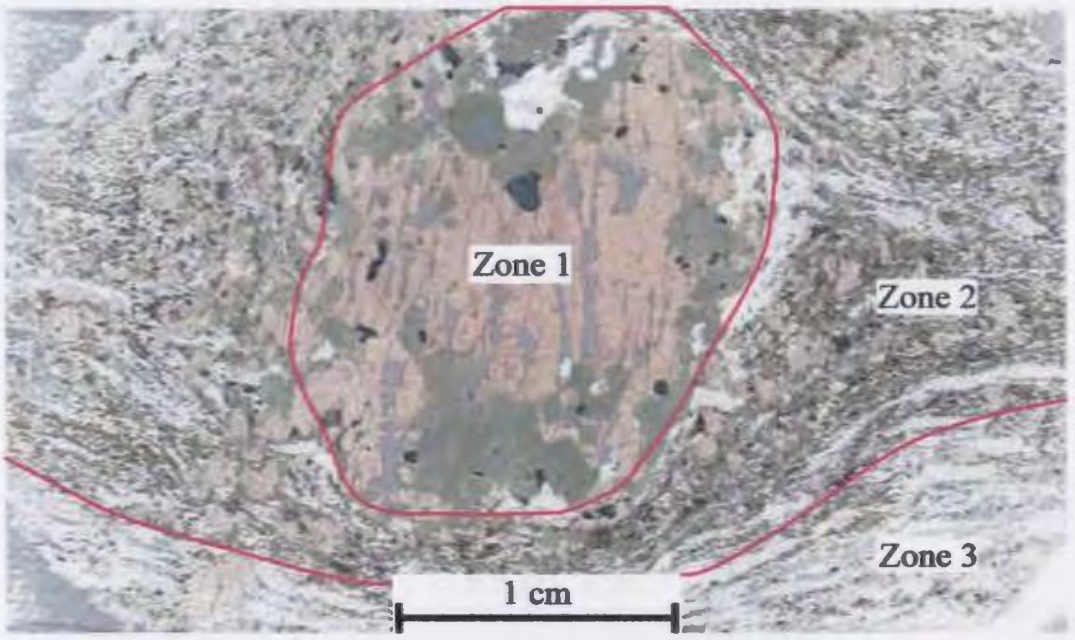

***Figure 7-11**: Photograph of a thin section cut from sample JK99-012 from the straight gneiss, GLTS. This sample displays three textural zones. Zone 1 is comprised of the large Grt and Cpx, Pl, Qtz inclusions in that garnet. Zone 2 is composed of matrix Grt with Cpx, Cam, Pl and Qtz. Zone three contains Grt-Cpx-Opx-Cam-Pl-Qtz.*

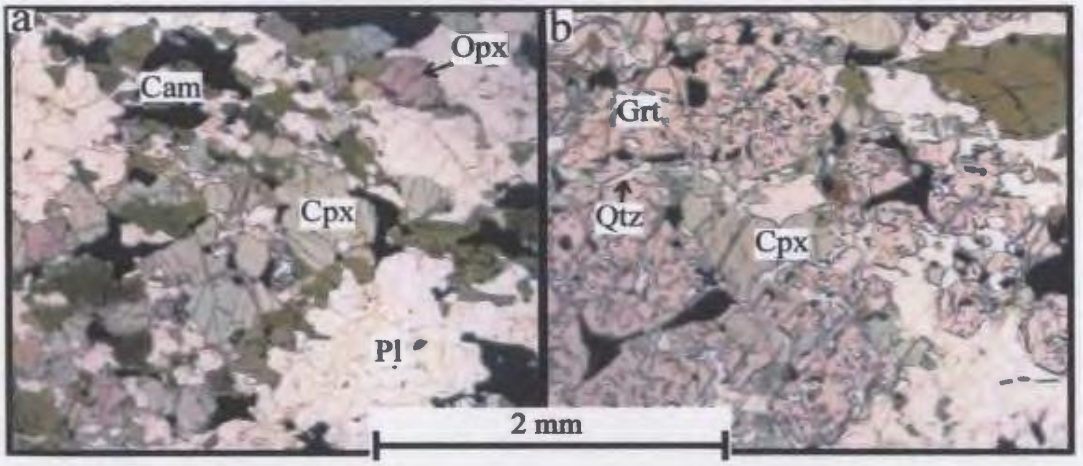

***Figure 7-12**: Photomicrographs of a) two pyroxene plus amphibole granulite and b) garnet granulite from within the same thin section (sample JK99-065a). Domainal equilibrium has driven the prograde reaction in this sample to produce the higher pressure assemblage shown in b). Sample was taken from Cape Caribou.*

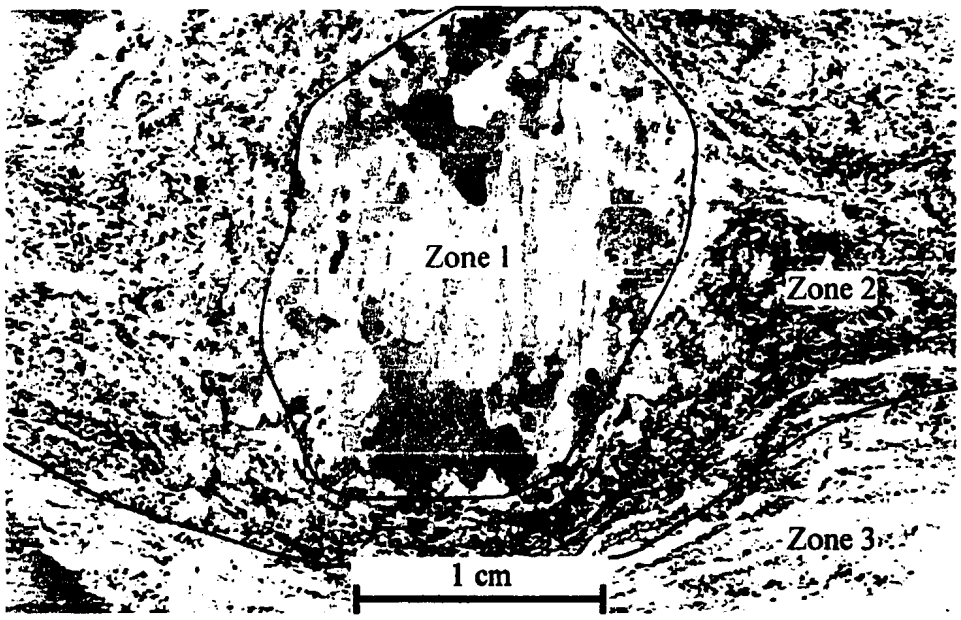

***Figure 7-11**: Photograph of a thin section cut from sample JK99-012 from the straight gneiss, GLTS. This sample displays three textural zones. Zone 1 is comprised of the large Grt and Cpx, Pl, Qtz inclusions in that garnet. Zone 2 is composed of matrix Grt with Cpx, Cam, Pl and Qtz. Zone three contains Grt-Cpx-Opx-Cam-Pl-Qtz.*

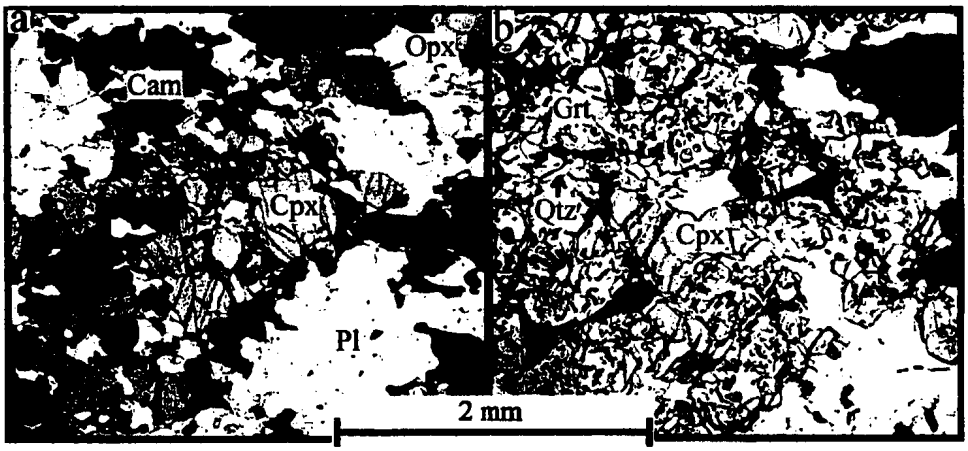

***Figure 7-12**: Photomicrographs of a) two pyroxene plus amphibole granulite and b) garnet granulite from within the same thin section (sample JK99-065a). Domainal equilibrium has driven the prograde reaction in this sample to produce the higher pressure assemblage shown in b). Sample was taken from Cape Caribou.*

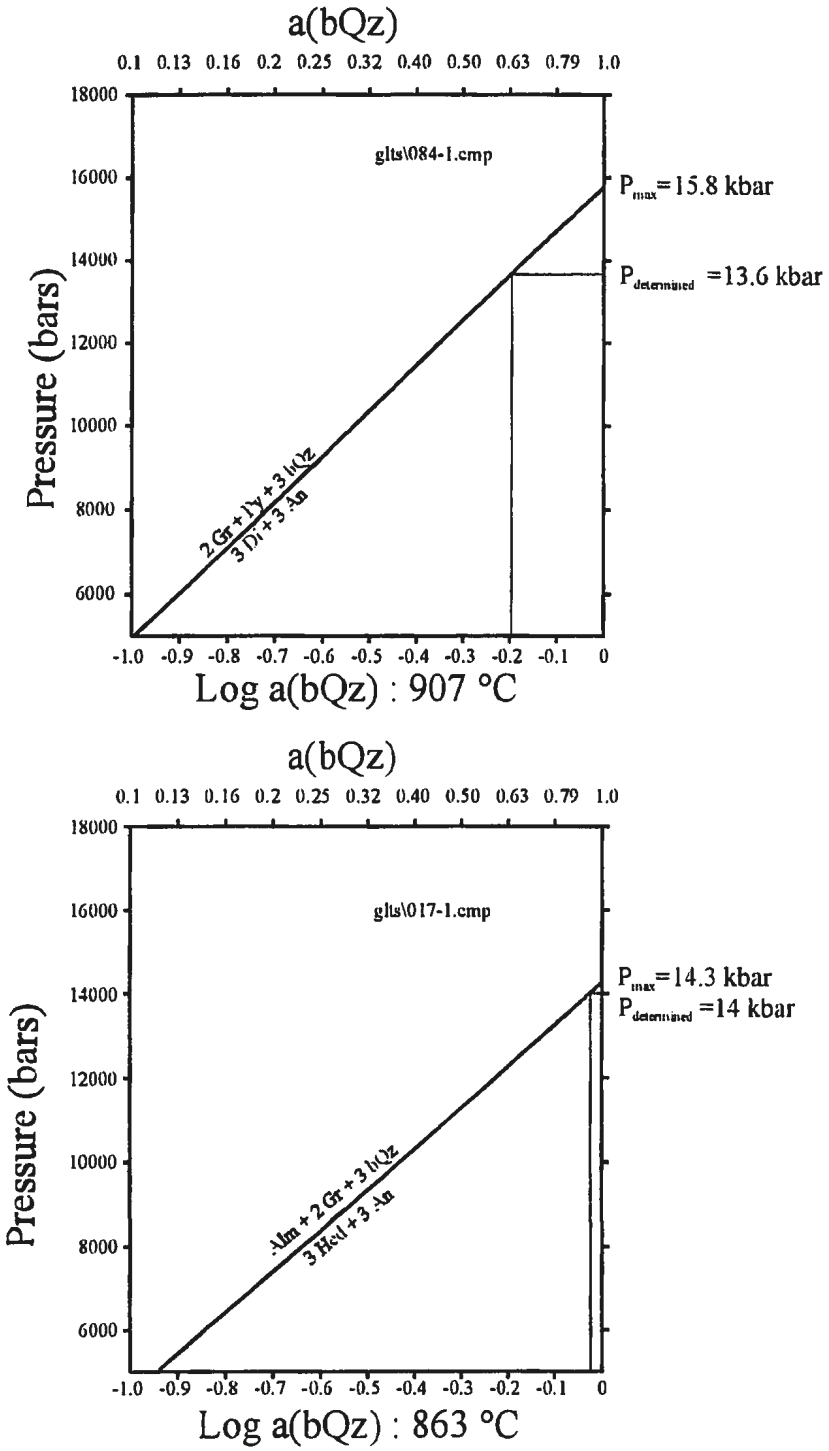

***Figure 7-13**: Plot of the variation of silica activity versus pressure for the Grt-Cpx-Pl-Qtz barometer for two samples. Both samples yield maximum pressures estimates (P_{max}) greater (and outside the range of error) than the pressure determined from elsewhere in the same thin section ($P_{determined}$). Estimated silica activity for the two samples is a_{SiO2} 0.63 (084-1) and 0.96 (017-1).*

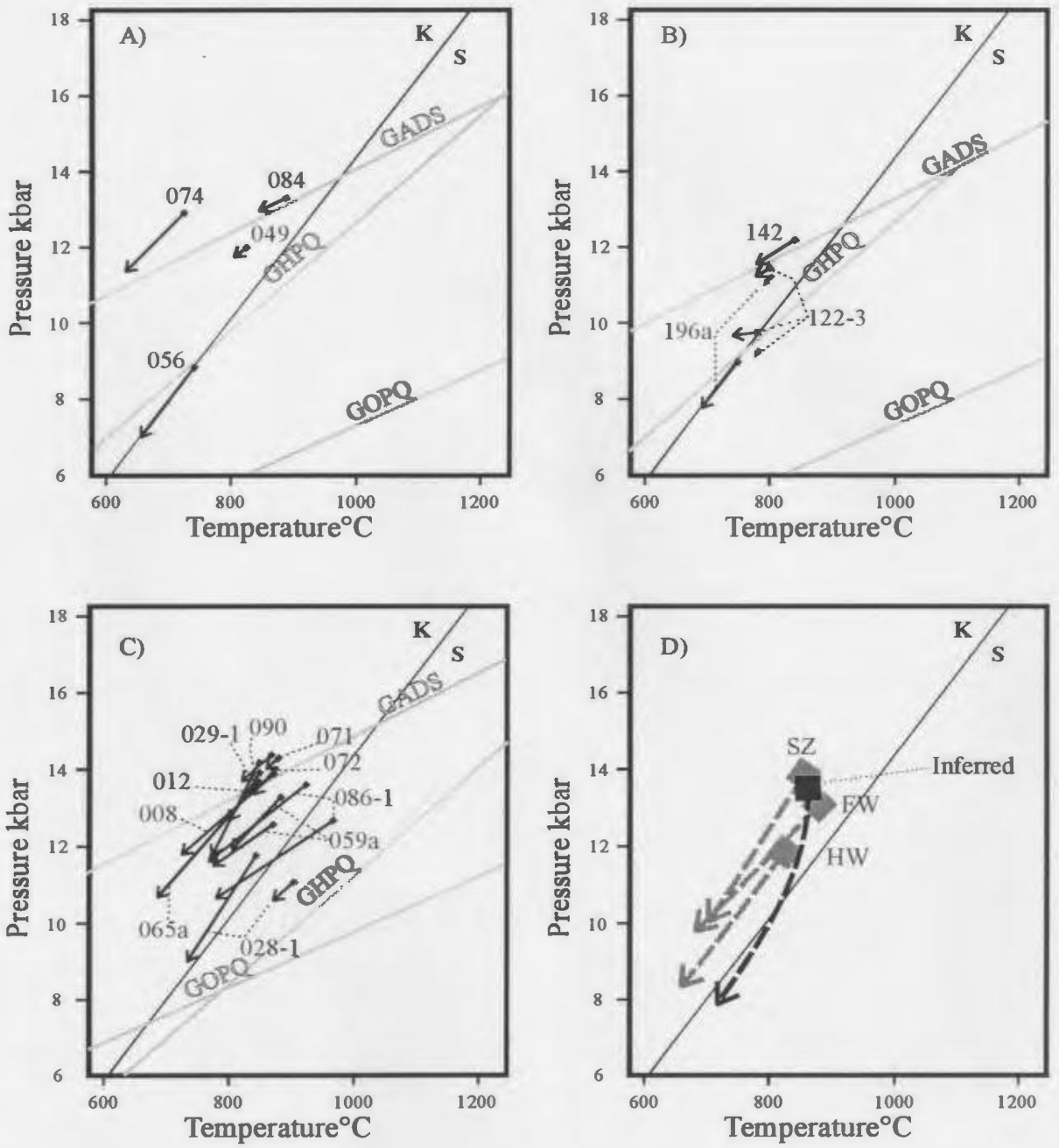

***Figure 7-14**: Apparent P-T paths for the a) footwall, b) hangingwall and c) shear zone rocks of the Goose bay area. The lightly shaded lines in a, b and c indicate the slopes of the three geobarometers used in P-T determinations. These represent the slopes for apparent isobaric cooling paths that would result if the thermometer were to continue to reset after the barometer closed. d) shows the extrapolated path from the results in a), b) and c) and the inferred P-T path. See text for discussion.*

Chapter 8

P-T-t path of the GLTS

In the previous chapter, the *P-T* conditions for thrusting were established and together with the petrographic information discussed in Chapter 6, these data will be integrated with the available U-Pb ages to develop a Grenvillian *P-T-t* path for the rocks in the Goose Bay area. It was also established that many samples from the GLTS possess two distinct fabrics, with local evidence for pretectonic growth of garnet and pyroxene porphyroblasts. It was established that there is a range of fabric development (i.e., strain) in the GLTS, with some samples or parts of samples preserving evidence of pretectonic porphyroblasts. Given the heterogeneous and progressive nature of strain in shear zones, it is not possible without *in-situ* dating to determine the age of any particular fabric element, or in this case to assign it to either Ottawan or Rigolet stages of the Grenvillian orogenesis. This problem is assessed in the next section, in which the response of the U-Pb system in accessory minerals to high temperature deformation and recrystallization is discussed in order to evaluate the linkage between the U-Pb ages, fabrics and estimated *P-T* conditions. The final outcome of the chapter is the presentation of a tectonic history for the Goose Bay area during the Grenvillian orogenesis and a *P-T-t* path for the evolution of the Grand Lake thrust system.

8.1 Response of the U-Pb system to Deformation

8.1.1 Geochronological Response

Chapter 1 introduced the concepts of re-equilibration of U-Pb systematics in accessory phases in response to ductile deformation. There are two end-member possibilities: i) Individual crystals breakdown completely and the liberated material recrystallizes as overgrowths on existing crystals or as individual new crystals. This will only occur if the *P-T*-X conditions of deformation are within the field of stability of the accessory phase and reactions for the growth of the accessory phase progress in a forward direction (e.g., Fraser et al. 1997). ii) The second possibility occurs if the crystal lattice of the accessory mineral is subjected to mechanical, thermal or chemical strain thereby causing Pb loss and changing the U-Pb systematics. Included under this heading are intra-crystallization deformation (lattice strain), prolonged or episodic thermal disturbance, hydrothermal alteration and chemical leaching (Ashwal et al. 1999). There are thus several mechanisms by which the U-Pb systematics of accessory minerals can be altered and therefore the appropriate choice of phases and grains for analysis must be made with care.

In recent years, geochronologists have employed several tools to aid with grain selection. For instance, cathodoluminescence (CL), and back-scattered electron (BSE) images have been widely used for characterization of zircon for evidence of growth zoning, overgrowths, *in-situ* recrystallization and metamictization. Typically zircons with a prismatic morphology and concentric zoning are interpreted to be the result of growth in a melt and these grains are inferred to yield the age of crystallization. A variation of this type includes

a prismatic crystal shape surrounding an inherited core of either igneous or metamorphic zircon. Round "soccer ball" shaped zircons are interpreted to have formed in a metamorphic environment and may also contain an inherited core of igneous zircon. The cores and overgrowths in this type are assumed to have formed at different times. Other round zircon shapes may exhibit a high degree of cracking and partial annealing as a result of intracrystalline deformation. Of the four examples discussed above, grains undergoing the latter three processes may be both chemically zoned and age zoned.

If a sample has experienced two thermal episodes, and assuming that the zircons had no inherited core and were significantly reset during the second episode, data obtained from the analysed zircons would lie on a cord on the concordia diagram that joins the two ages. It is possible to distinguish the two events more accurately by abrading off the overgrowths and analysing the remaining bulk sample to yield the older or upper intercept age (Krogh 1982). Most discordant zircons analyses are the result of age mixing when zircon with inherited cores or zircon with incomplete abrasion are analysed. Zircon from polymetamorphosed rock must be characterized with care to distinguish cores, overgrowths and zones to enable proper interpretation of the resultant analyses.

Recognition of the importance of appropriate grain selection has led some authors to question the significance of older analyses that employed multi-grain fractions without imaging of the grains. For instance, several recent articles concerning geochronology of polydeformed and/or polymetamorphosed rocks (e.g., Hanchar and Miller 1993, Mezger and Krogstad 1997, Ashwal et al. 1999; Connelly 2000) suggest that ages derived from multi-grain fractions may yield inaccurate and/or inconclusive results.

8.1.2 The Available U-Pb Data Set for the Goose Bay Area

The U-Pb ages established for the field area were determined by Krogh (1986), Krogh and Heaman (1988), Philippe et al. (1993), Bussy et al. (1995), Corrigan et al. (1997). The available data are given in Table 8-1. The locations of the samples are shown in Figure 2-4.

Sample #	age (Ma)		method	Interpretation	Reference
C-050	1622 ± 6	zrn	b	late Labradorian metamorphism	1
	1008 ± 2	zrn	c	Grenvillian reworking	1
C-050P	1016 +7/-3	zrn	c + a	Rigolet orogeny	2
C-050A	1012 ± 3	zrn	c + a	Rigolet orogeny	2
C-050D	1011 ± 3	zrn	b	Rigolet orogeny	2
C-050AM	1660 ± 3	zrn	b	Labradorian orogeny	2
W-266A	1631 ± 2	zrn	b	MMIS intrusive age	2
	1636 ± 3	zrn	b	MMIS intrusive age	2
W-266B	1626 ± 3	zrn	a	MMIS intrusive age	2
	1702 ± 3	zrn	a	island arc, pre-Labradorian crust	2
W-251	1625 ± 6	zrn	a	MMIS intrusive age	2
US-09	1586 ± 167	zrn	c	Labradorian orogeny	3
	1013 +5/-8	zrn	c	Rigolet orogeny	3
US-10	1656 +74/-69	zrn	c	Labradorian orogeny	3
	1005 ± 2	mnz	c	Rigolet orogeny	3
US-11	1038 ± 2	mnz	c	Ottawan with Mixed ages (see text)	3
US-12	1775 ± 16	zrn	c	island arc, pre-Labradorian crust	3
	1015 ± 2	zrn	c	Rigolet orogeny	3
US-16	1659 ± 8	zrn	c	Labradorian orogeny	3
	994 ± 2	ttn	c	late Rigolet orogeny	3
DC-97	1007 +3/-2	zrn	c	Rigolet orogeny	4
W83-001-1	1613 ± 40	zrn	b	late-Labradorian orogeny	5
	1044 ± 4	zrn	b	Ottawan orogeny	5

***Table 8-1**: Available U-Pb ages for the Goose Bay area with geochronological interpretations based on zircon, monazite and titanite fractions. Method of analysis: a= single crystals or fragments, b= fragments and small populations of crystals or fragments, c= multi-grain populations. References: 1 = Krogh and Heaman 1988, 2= Bussy et al. 1995, 3= Philippe et al. 1993, 4= Corrigan et al. 1997 and 5= Krogh 1986.*

Philippe et al. (1993) collected samples from the gneissic rocks of the Goose Bay area and zircon and monazite were analysed using the multi-grain fraction technique. CL and/or BSE imaging methods described above were not undertaken during the selection and analysis of those grains. Instead, the grains were characterized based on clarity, gem quality, colour and size. Thus, although the resultant U-Pb data are analytically precise and accurate, their interpretation is difficult given the problems listed above and the knowledge that the rocks adjacent to and in the GLTS have seen more than two metamorphic and deformation episodes. For the remaining geochronological data, however, this problem is less acute. For instance, some samples were taken from synthrusting pegmatites and may thus be reasonably assumed to yield the age of thrusting (e.g., Corrigan et al. 1997), whereas other fractions analysed consisted of single grains or tips of crystals and are assumed to yield accurate ages (e.g., C-050; 1008 ± 2 Ma and 1622 ± 6 Ma, Krogh and Heaman 1988 and Bussy et al. 1995). Samples from the polydeformed gneisses are more difficult to interpret and require some discussion. Below, two samples, US-11 (Philippe et al. 1993) from the shear zone and C-050 (Krogh and Heaman 1988) from the hangingwall are discussed in detail to illustrate the nature of the problem and possible interpretations. The original data for these analyses are reproduced as Table 8-2, and the two concordia diagrams are reproduced as Figure 8-1a, 8-1b.

US-11							
		Atomic	Ratios		Apparent	Age (Ma)	
fraction	mineral	Pb^{207}/U^{235}	Pb^{206}/U^{238}	Pb^{207}/Pb^{206}	Pb^{207}/U^{235}	Pb^{206}/U^{238}	Pb^{207}/Pb^{206}
35	zircon	1.963	0.1840	0.07739	1089	1103	1131
36	zircon	1.794	0.1750	0.07437	1040	1043	1051
37	zircon	1.732	0.1710	0.07347	1017	1020	1027
38	monazite	1.780	0.1748	0.07386	1038	1038	1038
39	monazite	1.731	0.1709	0.07343	1017	1020	1026
40	titanite	1.704	0.1691	0.07307	1007	1010	1016
41	titanite	1.669	0.1663	0.07280	991	996	1008
C-050							
		Atomic	Ratios		Apparent	Age (Ma)	
fraction	mineral	Pb^{207}/U^{235}	Pb^{206}/U^{238}	Pb^{207}/Pb^{206}	Pb^{207}/U^{235}	Pb^{206}/U^{238}	Pb^{207}/Pb^{206}
18	zircon	1.683	0.1680	0.07266	1001	1002	1005
19	zircon	1.687	0.1683	0.07270	1003	1004	1006
20	zircon	1.623	0.1625	0.07244	971	979	998
21	zircon	1.345	0.1384	0.07051	835	865	943
22	zircon	3.831	0.2804	0.09907	1594	1599	1607

***Table 8-2**: U-Pb data for samples US-11 (Philippe et al 1993) and C-050 (Krogh and Heaman 1988; data from Bussy et al. 1995).*

Sample ***US-11*** was taken from the "ultramylonite" (referred to in this text as the basal mylonite unit) and yielded a concordant monazite age of 1038 ± 2 Ma. This age was interpreted by Philippe et al. (1993) to represent the timing of thrusting and metamorphism. This result is not questioned, although inspection of the published data and the concordia diagram, reproduced here as Figure 8-1a, shows the presence of another monazite fraction, three zircon fractions and two titanite fractions that should not be ignored. The second monazite (fraction 39) is slightly discordant and yields a Pb^{207}/Pb^{206} age of 1026 Ma, Pb^{206}/U^{238} age of 1017 Ma and Pb^{207}/U^{235} age of 1020 Ma. Three zircon fractions yield a range of ages. One is strongly discordant and clearly displays inheritance, whereas the other two are only marginally discordant and appear to be slightly reset. Pb\Pb ages for these two

fractions are1051 Ma and 1027 Ma. Finally the titanite fractions and the last zircon fraction (37) are slightly discordant between 990 and 1004 Ma. The sample DC-97, collected by Corrigan et al. (1997) from a synthrusting pegmatite near the same sample site as Philippe et al. (1993), yielded a U-Pb zircon age of 1007 +3/-2 Ma. This age implies that the shear zone, or at least parts of it were active ~ 1007 Ma. Thus, considering the results of both Philippe et al. (1993) and Corrigan et al. (1997), there is evidence that the GLTS was active during both Ottawan and Rigolet times. In detail, the results suggest that monazite and zircon both recrystallized at about 1038 Ma, slightly discordant grains with ages between ~1020 and 1010 Ma are interpreted to have been partially reset as a result of Rigolet metamorphism which took place about 1007 Ma. Because of the use of multi-grain fractions and the lack of imaging, however, it is not known if the U-Pb systematics of the analysed grains were all partially reset, or if the fractions composed both concordant and discordant grains. The slight discordance of titanite analyses suggests that this mineral continued to undergo minor Pb loss after 990 Ma.

In the hangingwall, sample ***C-050*** from a deformed pegmatite yielded an upper intercept of 1622 ± 6 Ma and a lower intercept of 1008 Ma (Figure 8-1b; Krogh and Heaman 1988). Both ages are concordant and there are no discordant zircons present that lie on a cord between the two concordant analyses. Bussy et al. (1995) interpreted these results to reflect Grenvillian reworking of a Labradorian pegmatite. However, the absence of fractions plotting along the cord suggests that a second period of zircon growth at 1008 Ma is more likely than resetting of Labradorian zircons, implying the existence of zircon-forming reactions during

regional metamorphism at 1008 Ma. This explanation is also compatible with the difference in morphologies between the two fractions (Bussy et al. 1995), with the older brown blocky Labradorian zircon grains being unaffected during the Grenvillian high temperature metamorphism that produced the new, round and colourless zircons. Thus, this sample from the hangingwall retains evidence of its Labradorian crystallization age and also shows evidence of zircon-forming reactions during Grenvillian metamorphism.

In conclusion, based on the published U-Pb ages, the footwall and hangingwall rocks may retain evidence of their Labradorian crystallization ages as well as evidence for their Grenvillian overprint, whereas shear zone rocks from the GLTS show evidence for two Grenvillian orogenic events, namely the Ottawan and Rigolet orogenies at about 1040-1030 Ma and 1016-990 Ma respectively, and appear to have completely lost all evidence of their Labradorian crystallization ages. The presence of zircon and monazite with ages of ~1040-1030 and ~1016-990 Ma in the GLTS implies that the fabrics, discussed in Chapter 6, developed during the Ottawan and Rigolet orogenies, and a tectonic history and *P-T-t* path for the Goose Bay area may be extrapolated on this basis.

8.2 Tectonic Evolution of the Goose Bay Area

Based on the available U-Pb ages and the *P-T* estimates from this study, a tentative Grenvillian tectonic history for the Goose Bay area can be proposed. Chapter 2 described the general evolution of central-eastern Labrador and the Goose Bay area over the entire time

span from the Paleoproterozoic to the Neoproterozoic. The following discussion focuses primarily on the Grenvillian evolution in the Goose Bay area. However, before beginning, it is important to recall that during the late Labradorian orogeny, the LMT was thrust over the GBT along the Rigolet thrust during the late Labradorian at ca. ~1610 Ma (Corrigan et al. 2000), and that this shear zone was subsequently reactivated during the Ottawan orogeny. Figure 8-2 schematically illustrates the proposed tectonic evolution during the Grenvillian orogenic cycle based on the data presented in this thesis.

8.2.1 Ottawan Orogeny

Figure 8-2a shows the inferred pre-Grenvillian situation, with crustal stacking and inactive thrust faults inherited from the Paleoproterozoic Labradorian orogeny and negligible topographic relief. Initiation of crustal thickening during the Ottawan orogeny at ~1040 Ma (Figure 8-2 b) resulted in reactivation of the Rigolet thrust and the formation of an orogenic thrust wedge comprising LMT and MMT as the latter were thrust onto the foreland to the northwest over GBT. Peak pressure estimates of ~14 kbars (this study) determined from the high pressure granulites in the shear zone and adjacent hangingwall of the Rigolet thrust, imply that the orogenic wedge was at least 40 km thick and thus that the SE-dipping Rigolet thrust was a crustal-scale structure during the Ottawan orogeny. Based on the massive appearance of many units in the MMT (e.g., Mealy Mountains anorthosite), the preservation of pre-Grenvillian Ar/Ar and K/Ar ages in the Mealy dykes (Reynolds 1989; Emslie et al. 1984), and the apparent lack of penetrative Grenvillian fabrics and metamorphic overprint

in the MMT (e.g., Gower 1996), it is inferred that the MMT comprised the upper crustal, relatively cold and little deformed part of the crustal-scale thrust wedge.

At a later stage of the Ottawan orogeny (Figure 8-2c), the basal thrust of the orogenic wedge cut up structural section from the Rigolet thrust (at the base of LMT) to the GLTS (at the base of MMT), thereby truncating the Rigolet thrust. Thrusting thus stepped back into the thrust wedge (out-of-sequence thrusting or overstacking), and the Rigolet thrust became inactive. The part of the GLTS that is exposed around Grand Lake represents a flat, which is inferred to give way to a crustal-scale ramp towards the hinterland in the southeast. Uplift of the CCRA and the high pressure granulites in its basal shear zone up the ramp, and associated exhumation and cooling, is inferred to have been initiated during the Ottawan orogeny, as indicated in Figure 8-2c. Cooling to below the closure temperatures of the geothermometers (~500-725 °C, Frost & Chacko 1989) must have been rapid in order to preserve the mineral compositions and assemblages of the high temperature granulites (875 ± 50 °C, this study). Rapid uplift is inferred to be a result of the ramp geometry, and it is also inferred that rapid exhumation and cooling were accomplished by SE-directed normal faulting (tectonic erosion) in the upper part of the wedge above the ramp (Figure 8-2c). This would have occurred as a response to overthickening of the wedge and have been driven by the need to maintain critical taper. Based on the available geochronological data, the effects of Ottawan thrusting were largely confined to the shear zones of the Rigolet and Grand Lake thrust systems, suggesting that recrystallization in U-Pb-bearing accessory minerals was dynamically controlled by strain energy. Similarly, as noted in Chapter 6 and from the *P-T* data in Chapter 7, the effects of recrystallization on structures and mineral assemblages were

penetrative in the Grand Lake shear zone, but were heterogeneous away from the shear zone. However, the formation of the garnet-clinopyroxene±calcite assemblages in the Northwest River dykes in the hangingwall to the GLTS do not fit this pattern, since they occur in rocks lacking penetrative strain, and the reactions are inferred to have been driven by CO_2-rich fluids, as discussed in Chapter 6. The carbonate lenses in the GLTS may provide a possible source for the CO_2 for these reactions.

Formation of the high-pressure granulite-facies assemblages is related to a classical clockwise *P-T* path as a result of thrust loading, as shown in Figure 8-3. 'Peak' *P-T* conditions (i.e., the *P* associated with the apparent peak *T* conditions) are inferred to have been achieved during the Ottawan orogeny at about 1040 Ma, with initiation of decompression and cooling following shortly after the 'peak'. Decompression and ingress of H_2O resulted in the sub-assemblage garnet-clinopyroxene reacting to calcic amphibole-plagioclase-quartz, as discussed in Chapters 6 and 7. However, ingress of H_2O was domainal on outcrop and thin section scales, resulting in both assemblages being present in many individual samples.

8.2.2 Rigolet Orogeny

The onset of the Rigolet orogeny in the Goose Bay area (Figure 8-2d) is interpreted to have begun when the thrust wedge with the CCRA at its base was thrust farther north-northwest along the flat at ca. ~1016 Ma (Bussy et al 1995), probably resulting in widening the GLTS shear zone. The Rigolet thrust in the footwall remained inactive at this time. Thrusting is inferred to have continued sporadically for a few million years, on the basis of

groups of U-Pb ages of ~1012 Ma and ~1007 Ma. Both monazite and zircon formed at these times, and it is inferred that their growth was again induced by dynamic recrystallization of existing grains in the shear zone as a result of prograde reactions (e.g., breakdown of amphibole and epidote group minerals, Fraser et al. 1997; Ferry 2000) In either case, the implication is that the ages are linked to growth of these minerals in the active shear zone. Mylonitic fabrics that wrap around porphyroblasts of garnet and clinopyroxene may have been formed at this time, but they cannot be unequivocally distinguished from Ottawan fabrics.

On the basis of the observation that Rigolet ages are restricted to the GLTS and the immediately adjacent footwall and hangingwall rocks, it is interpreted that the thrust wedge maintained a critical taper at this time, deforming principally by basal shear with recrystallization largely restricted to the shear zone. The high-pressure granulite-facies rocks formed during the Ottawan orogeny, were carried up the ramp and onto the flat during the Rigolet orogeny. It is inferred that the mineral assemblages in syntectonically recrystallized ductile mylonites that yield retrograde *P-T* conditions probably formed during the Rigolet orogeny. However, as noted above, in the absence of *in-situ* dating there are no unequivocal microstructural criteria available to distinguish Ottawan and Rigolet assemblages.

Recrystallization and concomitant resetting of the geothermobarometers continued until conditions of ~7 kbar and 650 °C were achieved. This implies that exhumation was ongoing during the Rigolet orogeny, with recrystallization and retrogression in the cooled

shear zone taking place below the closure temperature of the geothermobarometers and being driven by the input of strain energy and hydrous fluids.

On the basis of independent data, it is also known that the orogenic wedge cut down into its footwall and advanced into its foreland by basal accretion during the Rigolet orogeny, leading to the formation of the Grenville Front about 100 km north of the GLTS, and the GBT as part of the Parautochthonous belt (Figure 8-2e). Formation of the Grenville Front has been dated at ~1005 Ma (Krogh 1994), slightly post-dating early Rigolet displacements on the GLTS and probably synchronous with later displacements. On the basis of Lithoprobe crustal-scale seismic sections in the western and central Grenville Province (Ludden & Hynes 2000), the Grenville Front is the lowest thrust in the Grenville orogen, and so it is inferred to underlie the GLTS at depth (Figure 8-2e). Thus thrust displacement on the Grenville Front would have resulted in the strain being focussed at the base of the enlarged orogenic wedge, with the GLTS and MMT being essentially passively transported as orogenic float at this time. This resultant uplift of the wedge may have promoted a second stage of normal faulting in the hanging wall, as indicated in Figure 8-2e. Thus the Rigolet orogeny resulted in the thrust wedge undergoing rapid uplift and exhumation, and the inferred retrograde *P-T* path is shown in Figure 8-3. It shows a steep decompression path from the kyanite field through the sillimanite field in accordance with petrographic observations.

Titanite growth at ~994 Ma in the GBT and cooling ages recorded by the K/Ar ages of the Mealy dykes in the MMT at ~ 960 Ma (Emslie et al. 1984) are interpreted as cooling ages recording the time that the wedge cooled through the respective closure temperatures.

These are associated with the waning stages of the Grenvillian orogeny, and are essentially post-tectonic

The final stage in the tectonic evolution of the Goose Bay region illustrated in Figure 8-2f was the formation of the Lake Melville rift in the late Neoproterozoic. The graben structure was a failed rift associated with the opening of the Iapetus Ocean and the initiation of the Appalachian 'Wilson cycle' (Gower 1986). One important result of the formation of the Lake Melville rift is that the relationship between the CCRA and the MMT is obscured. In the model presented in Figure 8-2f, the two terranes are inferred to be separated by a major Grenvillian extensional fault. However, this has not been observed in the field and hence it is a putative structure. Its existence is supported by the absence of Grenvillian metamorphism in the MMT, in contrast to the high-pressure granulite-facies metamorphism in the CCRA.

8.2.3 Summary

The overall *P-T-t* path for the Goose Bay area, summarized in Figure 8-3, includes both the Ottawan and Rigolet orogenies. Based on the textures and directions of reactions discussed in Chapter 6, it is inferred that the Ottawan orogeny involved high pressure-temperature metamorphism together with north-northwest directed thrusting that was followed by post-peak upper-amphibolite facies retrogression. Uplift and retrogression under upper amphibolite facies conditions continued during the Rigolet orogeny, as a result of displacement on the GLTS and approximately coeval displacements on the underlying thrust fault marking the Grenville Front. Uplift was associated with rapid unroofing of the high-pressure rocks by both tectonic and geomorphic erosion as the orogen migrated towards the

northwest into its foreland. The rocks of the shear zone partially re-equilibrated at this time, and new monazite and zircon grew during renewed incomplete conversion of the granulites to amphibolite-facies assemblages. Taken together, the Ottawan and Rigolet orogenies thus form a single *P-T-t* loop for this part of the Grenville orogeny with the end of the Ottawan orogeny (at ~1030 Ma) being followed after a short break by the beginning of the Rigolet orogeny at ~1016 Ma.

8.3 Discussion

The GLTS occurs at the base of a thick-skinned Grenvillian thrust system composed of the CCRA and the MMT, and defines the boundary between the thrust wedge and the underlying footwall rocks of the Parautochthonous belt (Figure 2-1). It acted as the site of localization for shearing during both the Ottawan and Rigolet orogenies of the Grenvillian orogenesis in the Goose Bay area. High-pressure Grenvillian granulite-facies conditions (~14 kbar and 875 °C) experienced by the rocks of the shear zone have not been proven elsewhere in the eastern Grenville Province and remain a locally anomalous feature. However, high-pressure rocks (eclogites and retrogressed eclogites) are known in both the western and central Grenville Province, and in both locations also lie tectonically on top of the Parautochthonous belt in the northwestern Grenville orogen, in a similar structural setting to the CCRA. They have recently been interpreted to comprise a distinct tectonic belt, known as the HP belt, which overlies the Parautochthonous belt and is overlain by the LP belt (Rivers et al. in press). Thus, it is possible that the transitional HP granulites in the GLTS and CCRA form the northeastern continuation of the HP belt in the eastern Grenville Province,

and the overlying MMT forms the continuation of the LP belt. However, the 'peak' pressures in the Goose Bay area are significantly lower than those determined farther west (~14 kbar versus ~18 kbar, Rivers et al. in press).

There appear to be several possible reasons why the peak pressures recorded by the metamorphic rocks in the HP belt could vary along the length of the belt. These include the following: i) The basal fault of the orogenic wedge may have cut down to different depths along strike, thus the pressure difference recorded by the exhumed rocks from the base of the wedge could reflect a real difference as a result of the changing architecture of the wedge along the strike of the orogen. ii) The peak pressure estimates calculated for the Goose Bay area may be apparent peak pressures and significantly underestimate the true peak pressure at the base of the active wedge. This possibility is discussed in Chapter 7 and although it cannot be ruled out or quantified precisely, it has been argued on petrological grounds that the calculated maximum apparent peak pressures probably do not underestimate the actual peak pressures significantly. iii) It is possible that the lithological makeup of the footwall may exert a significant influence on the rate of exhumation of HP rocks. The cross-sections of Ludden and Hynes (2000) and Rivers et al. (in press) show that the footwall in the western and central Grenville Province consists of a wedge of Archaean rocks (and their Paleoproterozoic cover) under the Allochthon Boundary Thrust (ABT). The Archaean rocks are inferred to have been a cold, relatively rigid unit that acted as a ramp up which the HP granulite and eclogite facies rocks were thrust during the Grenvillian orogenesis. However, Archaean rocks are not known at the surface in the Goose Bay area, their absence in central and eastern Labrador possibly being due to strike-slip tectonism associated with the

Paleoproterozoic Labradorian orogeny (Wardle et al. 1990a,b; Rivers 1997). As a result, it is inferred that the ramp beneath the CCRA is composed of Paleoproterozoic granitoid gneisses and the Trans-Labrador batholith (see Figure 2-2). It has already been noted that some Grenvillian thrust faults utilized existing Labradorian shear zones (e.g., the Rigolet shear zone), and it is feasible that the GLTS also utilized existing heterogeneities within the Labradorian crust, possibly creating a less steep ramp and flat geometry. Alternatively, the ramp and flat geometry may have been less well developed here than where the Archaean crust is present, possibly because of more ductile lithologies, which could correlate with the absence of eclogite facies rocks.

8.4 Further Research

Considerations for further research following from this study include:

- *In-situ* dating of U-Pb phases (LAM-ICP-MS, SHRIMP, SIMS) on samples used for geothermobarometry, to better establish the *P-T-t* from a single rock sample.
- Establishment of the *P-T* gradient in the footwall and hangingwall for modelling thrust characteristics in thick-skinned thrust systems.
- Dating of the Northwest River dykes
- Numerical modelling of thrust emplacement
- Search for normal faults in the hangingwall in the CCRA and MMT
- Search for continuation of the HP belt in eastern Labrador

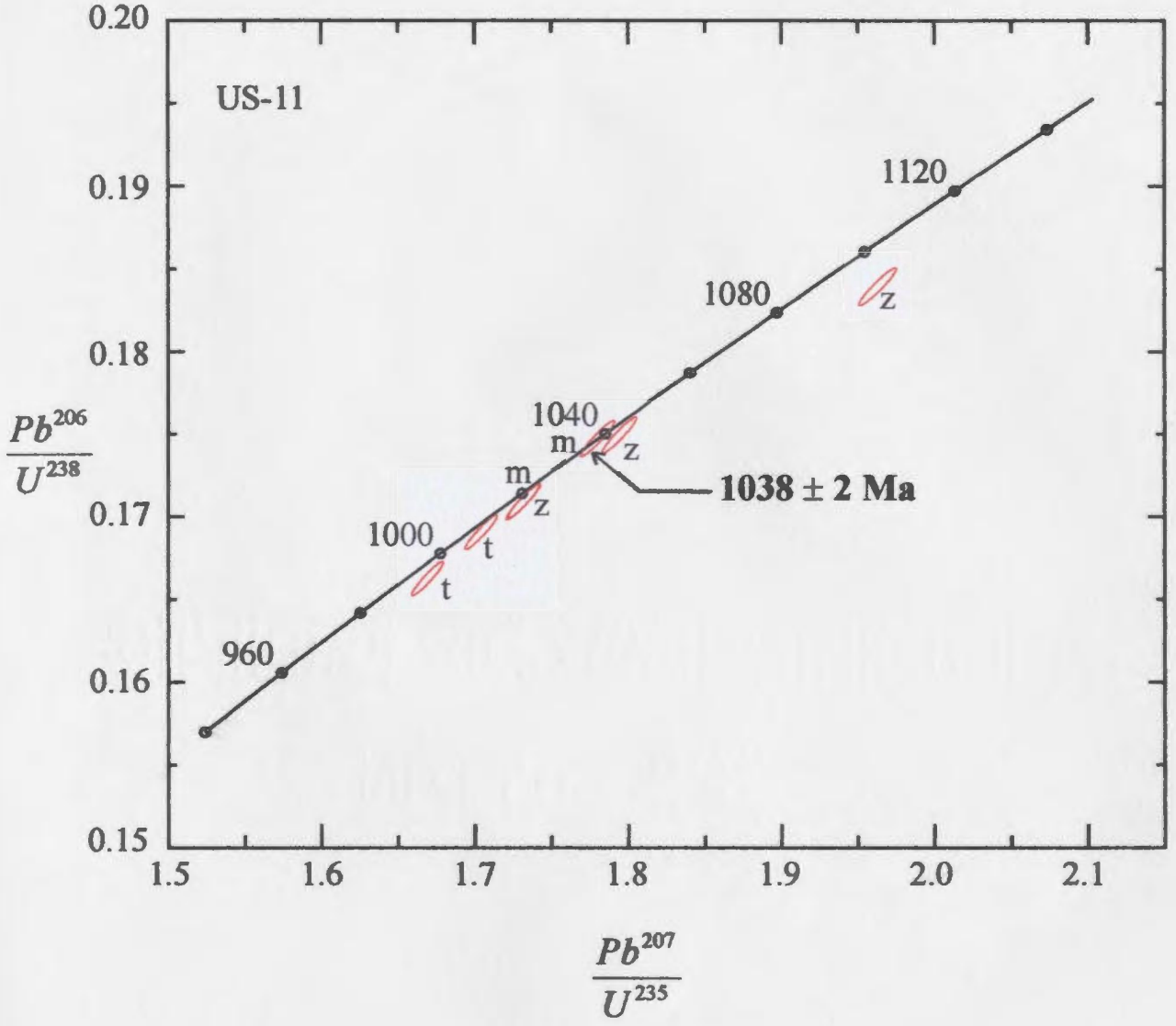

***Figure 8-1a**: Concordia diagram for the sample US-11 of Philippe et al. (1993). The age determined for this sample (1038 ± 2 Ma) reflects Ottawan aged thrusting, however the other monazite fraction and two zircon and two titanite fractions yield Rigolet ages, see text for discussion.*

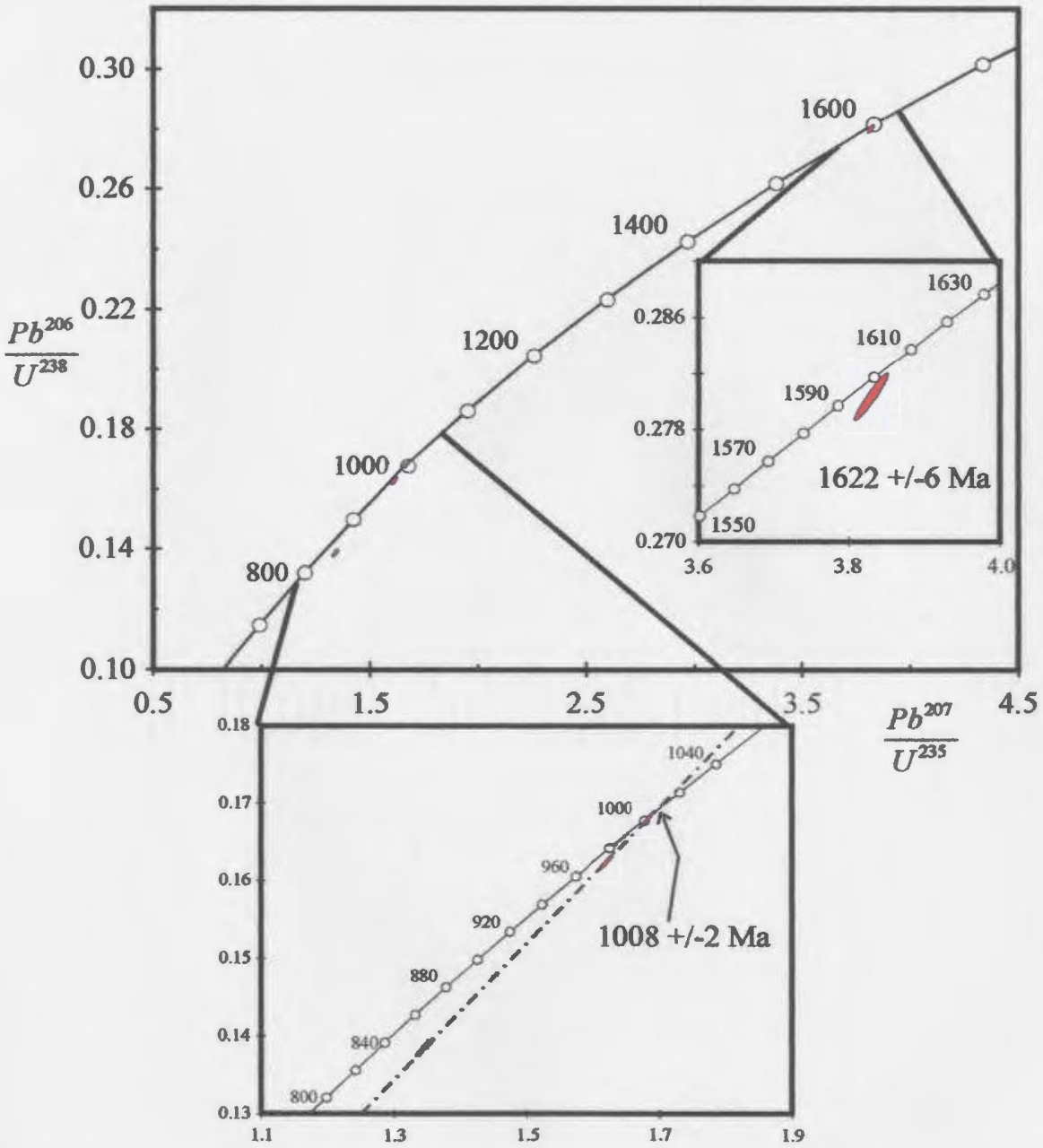

***Figure 8-1b**: Concordia diagram for the sample C-050 of Krogh and Heaman (1988). The analyses are slightly discordant and yield two populations at ~1620 Ma and 1008 Ma. This sample is interpreted to record both the age of crystallization of the pegmatite and the age of the zircon forming reaction induced in the pegmatite during the Rigolet orogeny.*

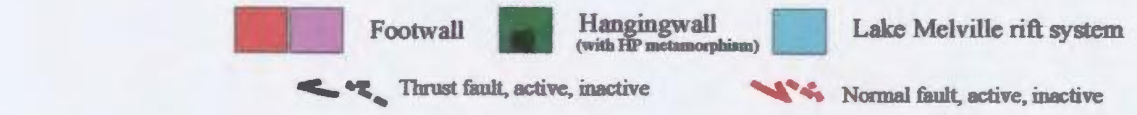

A

Pre-Grenvillian situation: eroded Labradorian terranes separated by inactive faults.

B

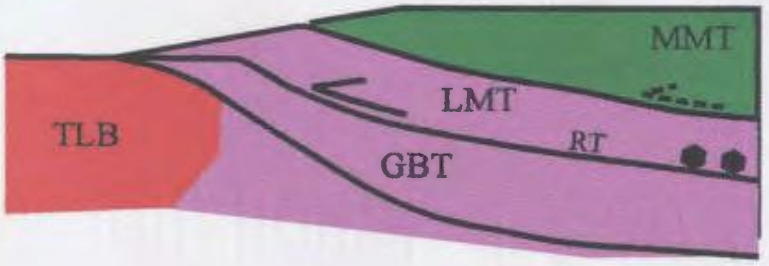

Ottawan orogeny i) Rigolet thrust is reactivated and LMT and MMT together form a crustal-scale orogenic wedge and are thrust northwest over the GBT.

C

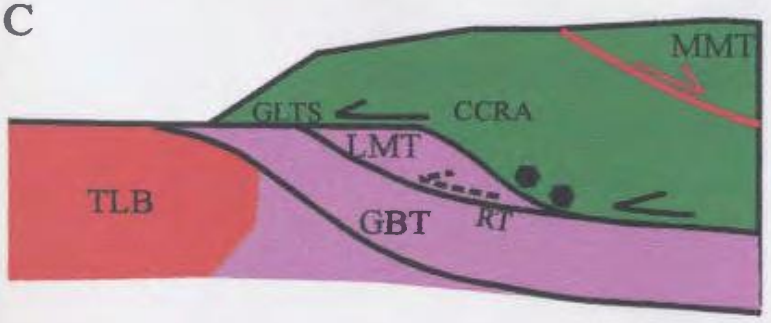

Ottawan orogeny ii) Out of sequence thrusting. The CCRA is thrust northward over LMT and the Rigolet thrust is cut off becoming inactive. The GLTS is developed and is inferred to have a ramp-flat geometry. Formation of the GLTS comprises the first stage of uplift of HP granulites up ramp. Inferred normal displacement of MMT with respect to the CCRA due to collapse of upper part of orogenic wedge, as the wedge exceeds critical taper.

***Figure 8-2**: Schematic tectonic evolution for the Goose Bay area during the Grenvillian orogenesis..*

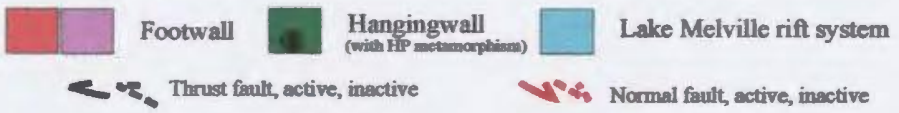

D

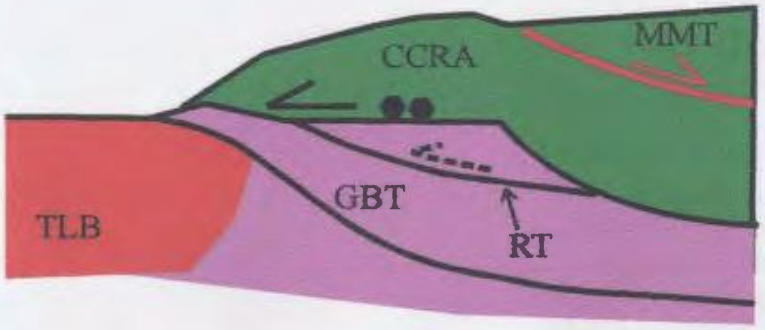

Rigolet orogeny (1016-1000 Ma)
i) Emplacement of HP granulites onto the flat as MMT and LMT are thrust further NNW. Continued normal faulting beneath the MMT at the top of the wedge.

Rigolet orogeny i + ii may have been contemporaneous based on the available geochronology from the field area and Grenville Front.

E

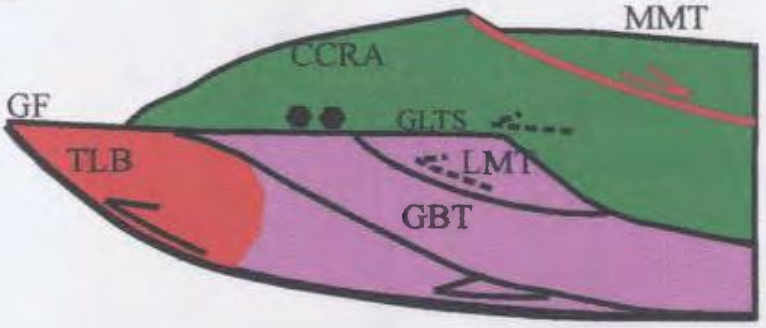

Rigolet orogeny (~ 1000 Ma) ii)
Continued normal faulting in the upper parts of the thrust wedge and formation of the Grenville Front (GF), the lowest most thrust in the system.

F

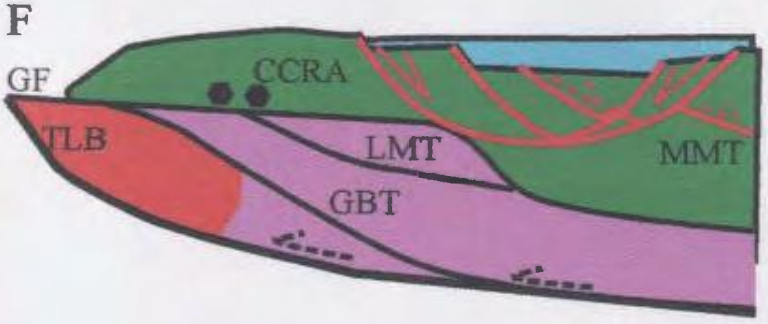

Latest Precambrian (~ 600 ma)
Formation of the Lake Melville rift system normal faults separating the CCRA from the MMT obscuring any evidence of inferred extension.

***Figure 8-2**: Schematic tectonic evolution for the Goose Bay area during the Grenvillian orogenesis continued. See text for discussion.*

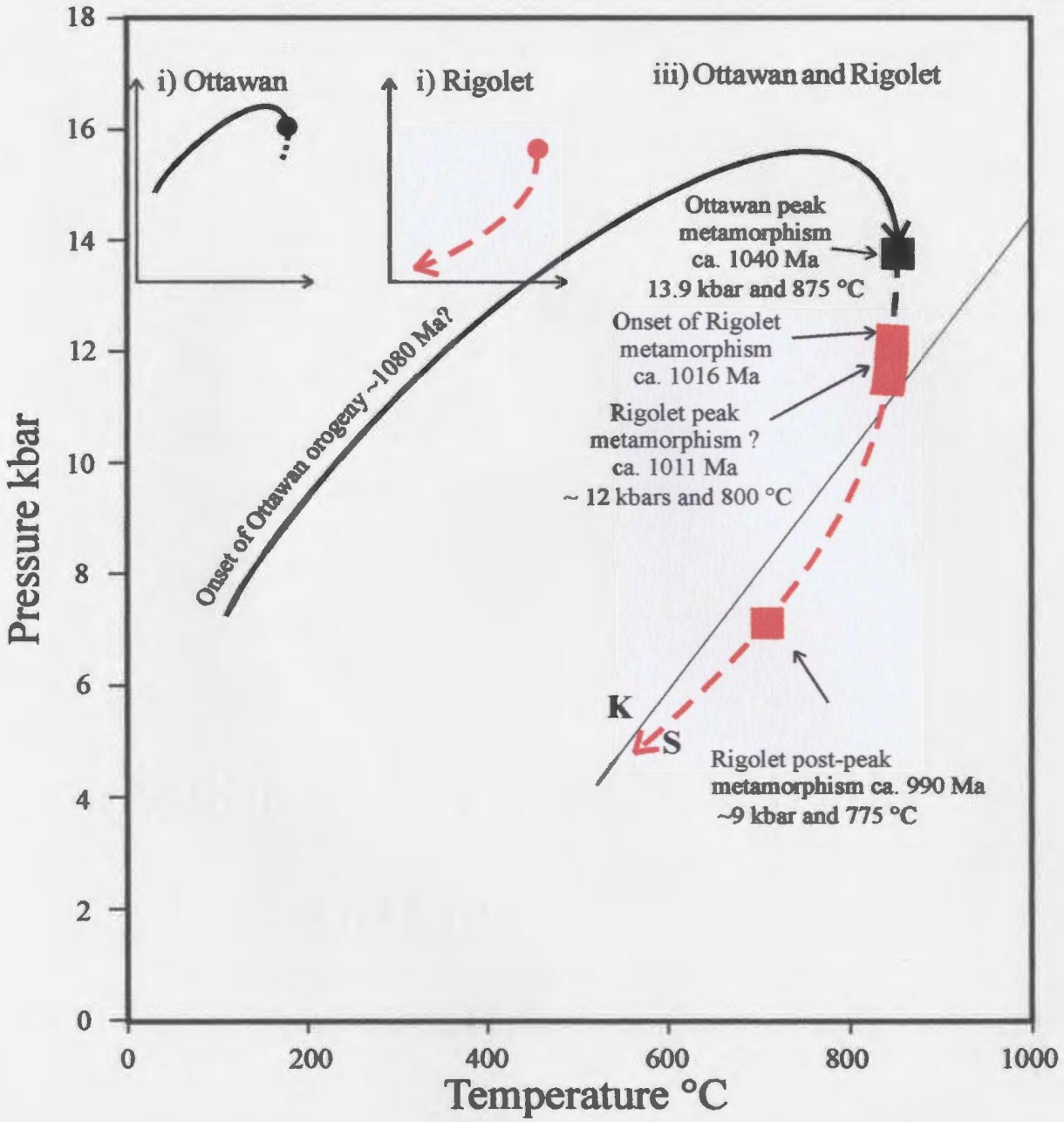

***Figure 8-3**: P-T-t path for the Goose Bay area. i) is the P-T path taken during the Ottawan orogeny. ii) is the P-T path taken during the Rigolet orogeny. iii) is the overall P-T-t path during the Grenvillian orogenesis. The peak metamorphic conditions for Rigolet metamorphism (red area) is not well constrained, but may be inferred from sample 142 (a Northwest River dyke) which yields peak metamorphic conditions of ~12 kbar and 800 °C and was dated by Bussy et al. (1995) at 1011 ± 3 Ma from metamorphic zircon in sample C-050D.*

References

Ash, C.H., 1985. Structural evolution and regional significance of the Cape Caribou River Allochthon. Unpublished Honours Thesis, 98 p., Memorial University of Newfoundland, St. John's.

Ashwal, L.D., Wooden, J.L. and Emslie, R.F., 1986. Sr, Nd and Pb isotopes in Proterozoic intrusives astride the Grenville Front in Labrador: Implications for crustal contamination and basement mapping. *Geochimica et Cosmochimica Acta*, **50**, p. 2571-2585.

Ashwal, L.D., Tucker, R.D. and Zinner E.K., 1999. Slow cooling of deep crustal granulites and Pb-loss in zircon. *Geochimica et Cosmochimica Acta*, **63**, p. 2839-2851.

Baker, J. and Newton, R.C., 1995. Experimentally determined activity-composition relations for Ca-rich scapolite in the system $CaAl_2Si_2O_8$-$NaAlSi_3O_8$-$CaCO_3$, at 7 kbar. *American Mineralogist*, **80**, p. 744-751.

Bégin, N.J., and Pattison, D.R.M. 1994. Metamorphic evolution of granulites in the Minto Block, northern Québec: extraction of peak *P-T* conditions taking account of late Fe-Mg exchange. *Journal of Metamorphic Geology*, **12**, p. 411-428.

Berman, R.G., 1991. Thermobarometry using multi-equilibrium calculations: a new technique, with petrological applications. *Canadian Mineralogist*, **29**, p. 833-855.

Best, K.A.D., 1997. The Grand Lake thrust zone: a petrographic study and pressure-temperature path analysis. Unpublished Honours Thesis, 70 p., Memorial University of Newfoundland, St. John's.

Bussy, F., Krogh, T.E. and Wardle, R.J., 1995. Late Labradorian metamorphism and anorthosite-granitoid intrusion, Cape Caribou River Allochthon, Grenville Province, Labrador: evidence from U-Pb geochronology. *Canadian Journal of Earth Sciences*, **32**, p. 1411-1425.

Butt, J. M., 2000. Mineral chemistry and mineral reactions in a meta-anorthosite complex, Cape Caribou River Allochthon, Grenville Province, Labrador. Unpublished Hons. Diss. (B.Sc.), Memorial University of Newfoundland. 111 p.

Cherniak, D.J., 1993. Lead diffusion in titanite and preliminary results on the effects of radiation damage. *Chemical Geology*, **110**, p. 177-194.

Cherniak, D.J., 2000. Pb diffusion in rutile. *Contributions to Mineralogy and Petrology*, **139**, p.198-207.

Clark, T. and Machado, N., 1994. New U-Pb dates form the Wakeham terrane and its basement. *In:* Lithoprobe ESCOOT and Abitibi-Grenville Workshop. *An overview of the Grenville Province from the Great Lakes to the Labrador sea*, Abstract. Lithoprobe unpublished.

Connelly, J.N., 2000. Degree of preservation of igneous zonation in zircon as a signpost for concordancy in U-Pb geochronology. *Chemical Geology*, **172**, p. 25-39.

Connelly, J.N., Rivers, T. and James. D.T., 1995. Thermotectonic evolution of the Grenville Province, western Labrador. *Tectonics*, **14**, p. 202-217.

Corrigan, D. and Hamner, S., 1995. Arc accretion, thickening, post collisional extension and plutonism in the Grenville orogen; constraints from the Mauricie region, south-central Quebec. In: *Precambrian '95, International Conference on Tectonics and Metallogeny of Early/Mid Precambrian orogenic Belts*, Program and Abstracts, Montreal, p. 106.

Corrigan, D., Rivers, T. and Dunning, G.R., 1997. Preliminary report on the evolution of the Allochthon Boundary Thrust in eastern Labrador; Mechin River to Goose Bay. *In: ESCOOT Transect Meeting* (April, 14-15, 1997) Lithoprobe Report No. 61, p. 45-56.

Corrigan, D., Rivers, T. and Dunning, G.R., 2000. U-Pb constraints for the plutonic and tectonometamorphic evolution of the Lake Melville terrane, Labrador and implications for basement reworking in the northeastern Grenville Province. *Precambrian Research*, **99**, p. 65-90.

Culshaw, N., Ketchum, J. and Barr, S., 2000. Structural evolution of the Makkovik Province, Labrador, Canada: Tectonic processes during 200Myr at a Paleoproterozoic active margin. *Tectonics*, **19**, p. 961-977.

Deer, W.A., Howie, R.A. and Zussman, J., 1992. *An introduction to the rock-forming minerals,* 2nd ed. Longman Scientific and Technical, London. 696p.

Droop, G.T.R., 1987. A general equation for estimating Fe^{3+} concentrations in ferromagnesian silicates and oxides fro microprobe analyses, using stoichiometric criteria. *Mineralogical Magazine*, **51**, p. 431-435.

Emslie, R.F., 1976. Mealy Mountains Complex, Grenville Province, southern Labrador. *In:* Report of Activities, Part A. Geological Survey of Canada, Paper 76-1A, p. 165-170.

Emslie, R.F., Loveridge, W.D. and Stevens, R.D., 1984. The Mealy dykes, Labrador: petrology, age and tectonic significance. *Canadian Journal of Earth Sciences*, **21**, p. 437-446.

Emslie, R.F. and Hunt, P.A., 1990. Ages and petrogenetic significance of igneous mangerite-charnockite suites associated with massif anorthosites, Grenville Province. *Journal of Geology*, **98**, p. 213-231.

Fahrig, W.F. and Loveridge, W.D., 1981. Rb-Sr study of the Michael Gabbro, Labrador. *In:* Current Research, part C, Geological Survey of Canada, Paper 81-1C, p. 99-103.

Ferry, J.M., 2000. Patterns of mineral occurrences in metamorphic rocks. Presidential Address, *American Mineralogist*, **85**, p. 1573-1588.

Fitzsimons, I.C.W. and Harley, S.L., 1994. The influence of retrograde cation exchange on granulite P-T estimates and a convergence technique for the recovery of peak metamorphic conditions. *Journal of Petrology*, **35**, p. 543-576.

Fraser, G., Ellis, D. and Eggins, S., 1997. Zirconium abundance in granulite-facies minerals, with implications for zircon geochronology in high-grade rocks. *Geology*, **25**, p. 607-610.

Fritz, H., Dallmeyer, R.D. and Neubauer, F., 1996. Thick-skinned versus thin-skinned thrusting: rheology controlled thrust propagation in the Variscan collisional belt (The southeastern Bohemian Massif, Czech Republic-Austria). *Tectonics*, **15**, p. 1389-1413.

Frost, B.R. and Chacko, T., 1989. The granulite uncertainty principle: limitations on thermobarometry in granulites. *Journal of Geology*, **97**, p. 435-450.

Fryer, B.J., 1983. Report of geochronology-Labrador mapping. Unpublished report to the Newfoundland Department of Mines and Energy. Open File Lab-617.

Foster, G., Kinny, P., Vance, D., Prince, C. and Harris, N., 2000. The significance of monazite U-Th-Pb age data in metamorphic assemblages; a combined study of monazite and garnet chronometry. *Earth and Planetary Science Letters*, **181**, p. 327-340.

Gittins, J., 1972. A note on the age of basalt dykes in the Mealy Mountains, Labrador, Canada. *Canadian Journal of Earth Sciences*, **9**, p. 133-1338.

Gower, C.F., 1986. Geology of the Double Mer White Hills and surrounding region, Grenville Province, eastern Labrador. *Geological Survey of Canada*, Paper **86-15**.

Gower, C.F., 1996. The evolution of the Grenville Province in eastern Labrador, Canada. *In:* Brewer, T.S. (ed) *Precambrian Crustal Evolution in the North Atlantic Region.* Geological Society Special Publication No. **112**, p. 197-218.

Gower, C.F. and Owen, V., 1984. Pre-Grenvillian and Grenvillian lithotectonic terranes in eastern Labrador - correlations with the Sveconorwegian Orogenic Belt in Sweden. *Canadian Journal of Earth Sciences*, **21**, p. 678-693.

Gower, C.F. and Tucker, R.D. 1994. Distribution of pre-1400 Ma crust in the Grenville Province: Implications for rifting in Laurentia-Baltica during geon 14. *Geology*, **22**, p. 827-830.

Gower, C.F., Rivers, T. and Brewer, T.S., 1990. Middle Proterozoic mafic magmatism in Labrador, eastern Canada. *In:* Gower, C.F., Rivers, T. and Ryan, A.B. (eds) *Mid-Proterozoic Laurentica-Baltica*: Geological Association of Canada, Special Paper No. **38**, p. 485-506.

Gower, C.F., Scharer, U. and Heaman, L.M, 1992. The Labradorian orogeny in the Grenville Province, eastern Labrador, Canada. *Canadian Journal of Earth Sciences*, **29**, p. 1944-1957.

Graham, C.M. and Powell, R., 1984. A garnet-hornblende geothermometer: calibration testing and application to the Pelona Schist, southern California. *Journal of Metamorphic Geology*, **2**, p. 13-31.

Hamilton, M.A., and Emslie, R.F., 1997. Mealy dykes, Labrador, revisited: U-Pb baddeleyite age and implications for the eastern Grenville Province (abs). GAC-MAC Annual Meeting, May 19-21, Ottawa, **22**, p. A-62.

Hanchar, J.M. and Miller, C.F., 1993. Zircon zonation patterns as revealed by cathodoluminescence and backscattered electron images: implications for interpretation of complex crustal histories. *Chemical Geology*, **110**, p. 1-13.

Harley, S.L., 1984. An experimental study of the partitioning of Fe and Mg between garnet and orthopyroxene. *Contributions to Mineralogy and Petrology*, **86**, p. 359-373.

Hobbs, B.E., Means, W.D. and Williams, P.F., 1976. *An Outline of Structural Geology*. John Wiley and Sons, 571 p.

Indares, A., Dunning, G., 1997. Coronitic metagabbro and eclogite from the Grenville Province of western Quebec: interpretation of U-Pb geochronology and metamorphism. *Canadian Journal of Earth Sciences*, **34**, p. 891-901.

James, D.T. and Connelly, J.N, 1995. Geology of the Paleoproterozoic Blueberry Lake Group, Grenville Province, western Labrador. *In: Current Research.* Newfoundland Department of Natural Resources, Report **95-1**. Newfoundland Department of Natural Resources, Newfoundland, Canada. p. 25-36.

Jensen, L.S., 1976. *A new cation plot for classifying subalkalic volcanic rocks*. Ontario Division of Mines, Miscellaneous Paper **66**.

Ji, S., Zhao, P. and Saruwatari, K., 1997. Fracturing of garnet crystals in anisotropic metamorphic rocks during uplift. *Journal of Structural Geology*, **19**, p. 603-620.

Kamo, S., Gower, C.F. and Krogh, T.E., 1989. A birthdate for the Iapetus ocean? A precise U-Pb zircon and baddeleyite age for the Long Range dykes, SE Labrador. *Geology*, **17**, p. 602-605.

Karabinos, P. and Ketcham, R., 1988. Thermal structure of active thrust belts. *Journal of Metamorphic Geology*, **6**, p. 559-570.

Kohn, M.J., and Spear, F.S., 1989. Empirical calibration of geobarometers for the assemblage garnet + hornblende + plagioclase + quartz. *American Mineralogist*, **74**, p. 77-84.

Kretz, R., 1983. Symbols for rock-forming minerals. *American Mineralogist*, **68**, p. 277-279.

Krogh, T.E., 1982. Improved accuracy of U-Pb zircon ages by the creation of more concordant systems using an air-abrasion technique. *Geochimica et Cosmochimica Acta*, **46**, p. 637-649.

Krogh, T.E., 1986. Report to Newfoundland Department of Mines and Energy on U-Pb isotopic dating results from the 1985-86 contract: Unpublished Report: Geological Survey Branch, Newfoundland Department of Mines and Energy, Open File LAB (707), 106 p.

Krogh, T.E., 1994. Precise U-Pb ages for Grenvillian and Pre-Grenvillian thrusting of Proterozoic and Archean metamorphic assemblages in the Grenville Front tectonic zone, Canada. *Tectonics*, **13**, p. 963-982.

Krogh, T.E. and Heaman, L., 1988. Report on 1987-1988 contract geochronology, Labrador: Unpublished report to Mineral Development Division, Newfoundland Department of Mines, Open File, LAB (765), 102 p.

Krogh, T.E, Gower, C.F. and Wardle R.J., 1996. Pre-Labradorian crust and later Labradorian, Pinwarian and Grenvillian metamorphism in the Mealy Mountains Terrane, Grenville Province, eastern Labrador. *In*: Gower, C.F. (compiler), Program and Abstracts, *Proterozoic Evolution in the North Atlantic Realm, COPENA-ESCOOT-IBTA Conference*, Goose Bay, Labrador, July 29-August 2 1996, Newfoundland Department of Mines and Energy, St. John's, NF, Canada, pp. 106-107.

Leake, B.R., Wooley, A.R., Arps, C.E.S., Birch, W.D., Gilbert, M.C., Grice, J.D., Hawthorne, F.C., Kato, A., Kisch, H.J., Krivovichev, V.G., Linthout, K., Laird, J., Mandarino, J.A., Maresch, W.V., Nickel, E.H., Rock, N.M.S., Schumacher, J.C., Smith, D.C., Stephenson, N.C.N., Ungaretti, L., Whittaker, E.J.W., and Youzhi, G., 1997. Nomenclature of amphiboles: Report of the Subcommittee on amphiboles of the International Mineralogical Association. Commission on new minerals and mineral names. *American Mineralogist*, **82**, p. 1019-1037.

Ludden, J. and Hynes A., 2000. The Lithoprobe Abitibi-Grenville transect: two billion years of crust formation and recycling in the Precambrian Shield of Canada. *Canadian Journal of Earth Sciences*, **37**, p. 459-476.

Martignole, J., Machado, N. and Indares, A., 1994. The Wakeham terrane: a Mesoproterozoic terrestrial rift in the eastern part of the Grenville Province. *Precambrian Research*, **68**, p. 291-306.

Mengel, F. and Rivers, T., 1991. Decompression reactions and P-T conditions in high-grade rocks, northern Labrador: P-T-*t* paths from individual samples and implications for early Proterozoic tectonic evolution. *Journal of Petrology*, **32**, p. 139-167.

Meschede, M., 1986. A method of discriminating between different types of mid-ocean ridge basalts and continental tholeiites with the Nb-Zr-Y diagram. *Chemical Geology*, **56**, p. 207-218.

Mezger, K. and Krogstad, E.J., 1997. Interpretation of discordant U-Pb zircon ages: an evaluation. *Journal of Metamorphic Geology*, **15**, p. 127-140.

Milnes, A.G. and Koestler A.G., 1985.Geological structure of Jotunheimen, southern Norway. *In:* Gee, D.G. and Sturt, B.A. (eds) *The Caledonide Orogen- Scandinavia and Related Areas*, p. 457-474

Miyashiro, A.. 1974. Volcanic rock series in island arcs and active continental margins. *American Journal of Science*, **274**, p. 321-355.

Moecher, D.P., Essene E.J. and Annovitz, L.M., 1988. Calculation and application of clinopyroxene - garnet - plagioclase - quartz geobarometers. *Contributions to Mineralogy and Petrology*, **100**, p. 92-106.

Morimoto, N., 1988. Nomenclature of pyroxenes. Subcommittee on Pyroxenes, IMA. *Mineralogical Magazine*, **52**, p. 535-550.

Pan, Y. and Fleet, M.E., 1996. Rare earth element mobility during prograde granulite facies metamorphism: significance of fluorine. *Contributions to Mineralogy and Petrology*, **123**, p. 251-262.

Parrish, R.R., 1990. U-Pb dating of monazite and its applications to geological problems. *Canadian Journal of Earth Sciences*, **27**, p. 1431-1450.

Passchier, C.W. and Trouw, R.A.J., 1998. *Micro-tectonics*. Springer-Verlag, 289 p.

Pattison, D.R.M. and Newton, R.C., 1989. Reversed experimental calibration of the garnet-clinopyroxene Fe-Mg exchange thermometer. *Contributions to Mineralogy and Petrology*, **101**, p. 87-103.

Pattison, D.R.M. and Bégin, N.J., 1994. Zoning patterns in orthopyroxene and garnet in granulites: implications for geothermometry. *Journal of Metamorphic Geology*, **12**, p. 387-410.

Pattison, D.R.M., in press. Petrogenetic significance of orthopyroxene-free garnet + clinopyroxene + plagioclase-bearing metabasites with respect to the amphibolite and granulite facies. *Journal of Metamorphic Geology*, **21**

Pavlis, T.L., 1986. The role of strain heating in the evolution of megathrusts. *Journal of Geophysical Research*, **91**, No. B12, p. 12407-12422.

Pearce, J.A. and Cann, J.R., 1973. Tectonic setting of basic volcanic rocks determined using trace element analyses. *Earth and Planetary Science Letters*, **19**, p. 290-300.

Perkins, D. and Chipera, S.J., 1985. Garnet-orthopyroxene-plagioclase-quartz barometry: refinement and application to the English River subprovince and the Minnesota River valley. *Contributions to Mineralogy and Petrology*, **89**, p. 69-80.

Philippe, S., Wardle, R.J. and Schärer, U., 1993. Labradorian and Grenvillian crustal evolution of the Goose Bay region, Labrador: new U-Pb geochronological constraints. *Canadian Journal of Earth Sciences*, **30**, p. 2315-2327.

Reynolds, P.H., 1989. $^{40}Ar/^{39}Ar$ dating of the Mealy Dykes of Labrador: paleomagnetic implications. *Canadian Journal of Earth Sciences*, **26**, p. 1567-1573.

Rivers, T., 1997. Lithotectonic elements of the Grenville Province: review and tectonic implications. *Precambrian Research*, **86**, p. 117-154.

Rivers, T. and Chown, E.H., 1986. The Grenville Orogen in eastern Quebec and western Labrador-definition, identification and tectonometamorphic relationships of autochthonous, parautochthonous and allochthonous terranes. *In:* Moore, J.M., Davidson A. and Baer, A. (eds) *The Grenville Province*. Geological Association of Canada, Special Paper No. **31**, p. 31-50.

Rivers, T., Martignole, J., Gower C.F. and Davidson, A., 1989. New tectonic divisions of the Grenville Province, southeast Canadian Shield. *Tectonics*, **8**, p. 63-84.

Rivers, T. and Corrigan, D., 2000. Convergent Margin on southeastern Laurentia during the Mesoproterozoic: tectonic implications. *Canadian Journal of Earth Sciences*, **37**, p. 359-383.

Rivers, T., Ketchum, J., Indares, A., and Hynes, A., in press. The High Pressure belt in the Grenville Province: Architecture, timing and exhumation models. *Canadian Journal of Earth Sciences*.

Royden, L.H. 1993. The steady state thermal structure of eroding orogenic belts and accretionary prisms. *Journal of Geophysical Research*, **98**, No. B3, p. 4478-4507.

Ryan, A.B., Neale ,T. and McGuire, J., 1982. Descriptive notes to accompany geological maps of the Grand Lake area, Labrador 13F/10, 11, 14, 15. Newfoundland and Labrador Department of Mines and Energy, Mineral Development Division, Maps 82-64 to 82-67.

Schärer, U., Krogh, T.E. and Gower, C.F., 1986. Age and evolution of the Grenville Province in eastern Labrador from U-Pb systematics in accessory minerals. *Contributions to Mineralogy and Petrology*, **94**, p. 438-451.

Schärer, U., Krogh, T.E., Wardle, R.J., Ryan, B. and Gandhi, S.S., 1988. U-Pb ages of early and middle Proterozoic volcanism and metamorphism in the Makkovik Orogen, Labrador. *Canadian Journal of Earth Sciences*, **25**, p. 1098-1107.

Schmid, S.M., 1983. Microfabric studies as indicators of deformation mechanisms and flow laws operative in mountain building. *In:* Hsü, K.J. (ed) *Mountain Building Processes*, Academic Press, p. 95-110.

Scott, D.J., Machado, N., Hanmer, S. and Gariepy, C., 1993. Dating ductile deformation using U-Pb geochronology; examples from the Gilbert River Belt, Grenville Province, Labrador, Canada. *Canadian Journal of Earth Sciences*, **30**, p. 1458-1469.

Scott, D.J. and Hynes, A., 1994. U-Pb geochronology along the Manicouagan corridor, preliminary results: evidence for ca. 1.47 Ga metamorphism. *In:* Lithoprobe ESCOOT and Abitibi-Grenville Workshop. *An overview of the Grenville Province from the Great Lakes to the Labrador sea*, Abstract.

Selverstone, J. and Chamberlain, C.P., 1990. Apparent isobaric cooling paths from granulites: Two counter examples from British Columbia and New Hampshire. *Geology*, **18**, p. 307-310.

Spear, F.S., 1991. On the interpretation of peak metamorphic temperatures in light of garnet diffusion during cooling. *Journal of Metamorphic Geology*, **9**, p. 379-388.

Spear, F.S., 1993. *Metamorphic phase equilibria and Pressure-Temperature-time paths.* Mineralogical Society of America Monograph, Washington, D.C. 799 p.

Spear, F.S. and Florence, F.P., 1992. Thermobarometry in granulites: pitfalls and new approaches. *Precambrian Research*, **55**, p. 209-241.

Spear F.S., Kohn, M.J. and Cheney, J.T. 1999. P-T paths from anatectic pelites. *Contributions to Mineralogy and Petrology*, **134**, p. 17-32.

Stevenson, I.M., 1967. Goose Bay map-area, Labrador. *Geological Survey of Canada*, Paper **67-33**, 12 p.

Tucker, R.D. and Gower C.F., 1994. A U-Pb geochronological framework for the Pinware terrane Grenville Province, southern Labrador. *Journal of Geology*, **102**, p. 67-78.

Wardle, R.J. and Ash, C., 1984. Geology of the Northwest River area. *In:* Current Research, Mineral Development Division, Department of Mines and Energy, Newfoundland and Labrador, Report **84-1**, p. 53-67.

Wardle, R.J. and Ash, C., 1986. Geology of the Goose Bay - Goose River area. *In:* Current Research, Mineral Development Division, Department of Mines and Energy, Newfoundland and Labrador, Report **86-1**, p. 113-123.

Wardle, R.J., Rivers, T., Gower, C.F., Nunn, G.A.G. and Thomas, A., 1986. The northeastern Grenville Province: new insights. *In:* Moore, J.M., Davidson, A. and Baer, A.J. (eds) *The Grenville Province:* Geological Association of Canada, Special Paper No. **31**, p. 13-29.

Wardle R.J., Ryan, A.B., Philippe, S. and Schärer, U., 1990a. Proterozoic crustal development, Goose Bay region, Grenville Province, Labrador, Canada. *In:* Gower, C.F., Rivers, T. and Ryan, A.B. (eds) *Mid-Proterozoic Laurentica-Baltica*: Geological Association of Canada, Special Paper No. **38**, p. 197-214.

Wardle R.J., Gower, C.F. and Kerr, A., 1990b. The southeastern margin of Laurentia ca. 1.7 Ga: the case of the missing crust (abs). GAC/MAC General Meeting Vancouver B.C. May 16-18, **15**, p. A-137.

Wardle, R.J. and Ryan, A.B., 1996. Field Excursion: The Grenville Province in the Goose Bay area. Mid-conference field excursion; Proterozoic Evolution in the North Atlantic Realm. COPENA-ESCOOT-IBTA conference, Goose Bay, Labrador, July 29-August 2, 1996, Field Excursion Guide No. **3**, 40 p.

Williams, P.F., Goodwin, L.B. and Rasler, S., 1994. Ductile deformation processes. *In*: Hancock, P.L. (ed) *Continental Deformation*, Pergamon Press, p. 1-27.

Winchester, J.A. and Floyd, P.A., 1977. Geochemical discrimination of different magma series and their differentiation products using immobile elements. *Chemical Geology*, **20**, p. 325-343.

Yoshino, T, and Satish-Kumar, M., 2001. Origin of scapolite in deep-seated metagabbros of the Kohistan Arc, NW Himalayas. *Contributions to Mineralogy and Petrology*, **140**, p. 511-531.

Zhu, X.K. and O'Nions, R.K., 1999. Zonation of monazite in metamorphic rocks and its implications for high temperature thermochronology: a case study from the Lewisian terrain. *Earth and Planetary Science Letters*, **171**, p. 209-220.

Appendix A

Geochemistry of the Northwest River dykes and the compiled geochemical data for the Mealy dykes from Emslie et al. (1984), Ashwal et al. (1988) and Gower et al. (1990). Samples of the Northwest River dykes were analysed using the XRF facilities at Memorial University.

Geochemistry of the Northwest River dykes

Sample	SiO2	Al2O3	TiO2	FeO*	MgO	MnO	CaO	Na2O	K2O	P2O5	total
	wt%	wt%	wt%	wt%	wt%	wt%	wt%	wt%	wt%	wt%	
JK-99-037A	43.23	13.80	1.97	12.67	8.32	0.17	9.00	2.53	1.15	0.32	93.16
JK-99-038A	42.82	11.13	1.50	13.65	12.04	0.22	9.60	2.26	1.36	0.10	94.69
JK-99-039A	44.44	13.45	1.37	11.49	9.69	0.19	10.25	2.97	0.83	0.14	94.82
JK-99-040A	44.31	13.57	2.57	13.50	7.73	0.20	8.53	3.33	1.39	0.36	95.48
JK-99-041A	44.01	13.56	2.76	13.25	6.90	0.18	7.99	3.11	1.57	0.79	94.12
JK-99-043A	43.96	13.78	2.59	12.66	7.41	0.23	8.31	3.16	1.47	0.69	94.28
JK-99-056	46.09	13.48	3.61	14.37	6.32	0.22	8.11	3.09	1.73	1.01	98.03
JK-99-122	43.03	14.89	0.93	9.11	9.44	0.14	10.55	2.39	0.23	0.11	90.81
JK-99-123A	43.76	13.08	3.27	14.60	6.14	0.19	7.60	3.15	1.49	0.97	94.24
JK-99-124A	43.72	12.65	2.23	13.47	7.04	0.17	8.44	2.76	1.20	0.51	92.19
JK-99-130A	44.74	12.31	1.87	14.90	8.10	0.23	8.16	3.19	0.99	0.22	94.71
JK-99-134	43.52	13.11	2.26	13.14	7.41	0.18	7.79	2.55	1.39	0.51	91.86
JK-99-137A	49.03	11.90	2.94	13.62	4.86	0.22	8.36	2.60	1.48	0.60	95.61
JK-99-141A	44.25	12.85	1.86	12.90	8.04	0.18	9.51	2.51	0.98	0.31	93.40
JK-99-141C	41.99	11.87	2.35	13.77	6.86	0.21	8.37	2.03	1.70	0.42	89.57
JK-99-142	43.74	12.19	2.62	15.15	7.28	0.21	9.27	2.47	0.89	0.49	94.30
JK-99-143	43.00	12.49	3.27	13.99	6.31	0.18	8.31	2.89	1.52	1.00	92.97
JK-99-149	43.99	12.49	2.04	13.60	7.29	0.21	8.43	2.44	1.19	0.37	92.04
JK-99-148A	45.74	12.32	1.90	14.19	7.34	0.21	8.91	2.38	0.69	0.28	93.96
JK-99-168	43.34	15.15	2.87	13.66	6.63	0.18	8.95	2.89	1.02	0.65	95.34
JK-99-172	44.10	15.07	2.35	13.68	5.67	0.21	9.10	2.90	0.74	0.34	94.15
JK-99-174A	41.40	13.03	2.49	13.68	7.68	0.19	8.59	2.49	1.62	0.63	91.78
JK-99-176	44.02	16.55	2.20	12.79	5.64	0.18	9.24	2.98	0.77	0.43	94.81
JK-99-177A	42.67	15.45	2.02	13.07	4.86	0.19	8.38	2.76	0.92	0.38	90.70
JK-99-178	44.18	15.42	2.54	14.67	6.34	0.21	8.40	2.66	1.21	0.43	96.07
JK-99-184A	41.61	13.25	3.63	15.73	5.38	0.21	7.37	2.74	1.64	1.01	92.57
JK-99-186	41.81	15.65	2.37	13.29	6.12	0.18	8.56	2.66	1.06	0.49	92.20
JK-99-193	42.47	12.70	1.49	12.29	9.34	0.16	9.87	2.17	0.51	0.17	91.18
JK-99-196	44.00	14.03	1.61	12.31	8.12	0.18	9.67	2.73	0.62	0.27	93.53

All Fe calculated as FeO

Sample	S	Cl	Sc	V	Cr	Ni	Cu	Zn	Ga	As	Rb	Sr	Y
	ppm	ppm	ppm	ppm	ppm	ppm	ppm	ppm	ppm	ppm	ppm	ppm	ppm
JK-99-037A	837	263	30	216	125	113.21	91.75	61.74	20.76	0.00	37.22	280.83	28.42
JK-99-038A	1129	298	24	277	686	319.30	58.71	60.75	18.12	0.75	23.72	265.10	15.34
JK-99-039A	1033	215	32	221	224	140.75	21.33	49.03	16.55	0.00	16.91	211.35	21.78
JK-99-040A	1093	939	28	237	94	87.04	43.43	88.49	24.04	2.03	21.09	518.14	35.78
JK-99-041A	1277	377	28	177	68	45.96	44.87	91.81	21.15	0.00	38.81	320.48	39.59
JK-99-043A	1073	371	32	186	58	51.80	59.55	92.57	21.63	2.75	26.69	308.90	39.44
JK-99-056	1600	511	28	237	35	21.69	56.98	116.19	21.96	0.00	48.92	299.95	49.62
JK-99-122	364	70	28	213	228	140.53	28.19	29.13	16.02	0.00	3.08	320.42	14.27
JK-99-123A	837	567	19	222	72	83.92	86.11	105.26	26.68	8.27	36.60	256.24	52.39
JK-99-124A	491	195	25	224	135	106.99	71.75	93.16	23.17	0.00	27.06	280.31	32.57
JK-99-130A	1127	285	40	332	81	64.16	91.89	81.87	21.42	1.52	25.72	407.57	31.09
JK-99-134	776	203	29	197	82	135.96	122.33	101.19	28.33	0.00	31.80	288.21	34.82
JK-99-137A	190	458	46	423	52	11.34	67.38	69.61	23.23	0.00	37.31	242.42	53.55
JK-99-141A	641	303	41	251	333	98.44	88.78	85.73	20.87	2.33	17.02	264.76	29.19
JK-99-141C	1359	693	46	289	129	61.07	199.17	98.96	21.95	0.00	38.94	299.60	34.84
JK-99-142	1465	288	30	319	77	62.16	74.51	105.01	24.09	0.00	21.50	237.23	43.13
JK-99-143	1617	708	24	233	78	62.80	126.10	111.52	28.96	8.04	36.55	254.61	53.01
JK-99-149	955	273	36	239	140	74.28	90.64	81.60	21.93	0.70	21.20	309.75	32.37
JK-99-148A	568	146	37	311	115	65.12	98.62	74.32	24.19	0.00	17.27	207.56	33.47
JK-99-168	1369	253	30	265	102	96.33	67.33	80.65	23.23	1.12	22.34	327.28	35.56
JK-99-172	855	170	35	247	155	47.83	129.81	63.04	23.00	0.00	13.75	266.70	32.55
JK-99-174A	409	696	29	271	135	81.65	63.10	79.52	23.37	0.91	46.31	319.92	32.05
JK-99-176	294	322	32	238	95	96.69	84.78	60.92	23.43	0.00	15.11	281.98	34.33
JK-99-177A	1132	174	31	218	81	67.81	143.69	78.56	24.88	0.10	18.67	247.39	34.49
JK-99-178	1225	176	26	218	108	117.27	133.13	87.08	24.76	8.09	27.90	265.53	39.14
JK-99-184A	1640	622	27	223	88	75.21	111.43	116.18	28.24	0.00	35.76	241.33	55.84
JK-99-186	1599	348	25	197	94	118.53	94.03	67.44	23.79	17.30	19.16	308.67	31.00
JK-99-193	578	249	35	234	196	154.87	60.15	57.81	21.21	0.00	9.81	242.79	18.97
JK-99-196	531	204	32	241	221	134.33	38.37	61.94	21.69	4.35	14.86	290.67	27.10

Sample	Zr	Nb	Ba	Ce	Pb	Th	U
	ppm	ppm	ppm	ppm	ppm	ppm	ppm
JK-99-037A	147.94	15.98	399.65	23.69	4.26	2.11	3.46
JK-99-038A	62.98	8.14	263.44	0.00	5.55	0.79	0.00
JK-99-039A	66.55	8.83	134.73	0.00	2.30	3.34	3.04
JK-99-040A	167.84	19.48	607.40	96.14	9.30	2.70	0.57
JK-99-041A	227.55	18.66	668.73	32.36	6.88	3.24	0.77
JK-99-043A	230.59	19.95	543.20	44.53	7.91	4.01	0.00
JK-99-056	233.88	26.46	575.22	113.71	9.81	1.88	0.00
JK-99-122	42.45	3.73	99.35	0.00	0.00	0.00	0.00
JK-99-123A	354.79	29.17	568.13	77.05	5.06	1.94	0.00
JK-99-124A	171.42	12.94	538.70	28.25	6.08	2.28	2.56
JK-99-130A	125.18	14.10	511.38	39.14	3.19	3.35	1.80
JK-99-134	199.15	13.17	605.62	51.01	6.96	5.43	1.64
JK-99-137A	307.09	23.98	488.60	70.92	4.73	4.05	0.58
JK-99-141A	124.91	10.43	314.04	9.13	11.14	2.51	1.61
JK-99-141C	158.50	14.38	451.47	29.46	10.65	1.22	3.73
JK-99-142	218.49	17.39	323.98	32.69	8.65	3.99	1.90
JK-99-143	363.68	28.36	561.49	112.99	10.92	5.15	0.00
JK-99-149	146.64	11.37	491.67	3.97	7.09	0.11	0.00
JK-99-148A	125.48	10.76	257.41	0.00	4.91	0.18	0.00
JK-99-168	230.18	19.78	431.94	21.31	6.93	2.11	0.70
JK-99-172	150.67	10.38	252.36	12.38	3.74	2.43	0.92
JK-99-174A	210.60	16.58	513.10	53.41	19.16	2.49	2.40
JK-99-176	199.11	12.47	442.90	12.60	2.19	1.91	0.71
JK-99-177A	139.49	9.70	366.65	10.00	6.11	4.23	0.10
JK-99-178	197.40	14.65	437.55	35.30	6.91	3.54	0.61
JK-99-184A	396.59	31.04	572.90	111.63	12.98	5.24	1.64
JK-99-186	155.67	13.14	481.39	21.13	3.37	2.38	0.00
JK-99-193	84.37	6.52	187.44	0.00	2.90	2.89	0.00
JK-99-196	118.69	10.05	268.76	5.31	4.88	2.76	0.00

Geochemistry of the Mealy dykes

Sample	SiO2	Al2O3	TiO2	FeO*	MgO	MnO	CaO	Na2O	K2O	P2O5	CO2	H2O	S	total
	wt%	wt%	wt%	wt%	wt%	wt%	wt%	wt%	wt%	wt%	wt%	wt%	wt%	
EC75-44	40.00	13.70	4.30	14.34	4.70	0.18	10.33	3.40	1.70	4.76	0.10	0.70	0.14	98.35
EC75-185A	45.70	15.00	4.31	15.50	5.05	0.22	7.90	2.60	1.48	0.87	0.10	0.60	0.24	99.57
EC75-185B	45.40	16.40	3.25	12.91	6.34	0.18	9.66	3.20	0.68	1.18	0.00	0.40	0.08	99.68
EC75-166B	45.70	16.90	3.02	12.86	5.52	0.18	8.34	3.10	1.23	0.83	0.10	1.10	0.16	99.04
EC75-238A	46.00	16.40	3.28	13.20	5.45	0.19	8.60	2.80	1.12	0.58	0.30	0.50	0.14	98.56
EC75-163A	47.00	16.60	2.51	13.32	7.32	0.20	9.48	2.00	0.62	0.38	0.00	0.10	0.06	99.59
EC75-83A	47.20	18.00	1.92	10.93	7.25	0.16	9.56	2.70	0.60	0.42	0.10	0.40	0.10	99.34
EC75-176	47.20	15.10	2.56	14.88	5.44	0.21	8.19	2.40	1.38	0.58	0.00	1.10	0.14	99.18
EC75-176A	47.80	16.80	2.66	12.98	4.63	0.17	7.90	3.00	1.63	0.61	0.00	0.60	0.06	98.84
EC75-180E	47.20	14.60	2.62	14.34	5.74	0.22	9.06	2.60	0.93	0.34	0.00	0.60	0.14	98.39
EC75-138A	47.40	17.40	2.12	11.99	5.52	0.17	8.86	3.30	1.04	0.52	0.20	1.00	0.17	99.69
EC75-40	47.60	15.00	2.65	13.99	5.78	0.22	8.89	2.70	1.00	0.34	0.00	0.80	0.08	99.05
EC75-201B	48.00	17.50	1.36	10.34	8.12	0.17	10.67	1.80	0.44	0.16	0.10	0.20	0.14	99.00
EC75-89B	48.90	18.60	1.35	9.79	6.86	0.14	9.84	2.60	0.63	0.15	0.00	0.30	0.14	99.30
EC75-35	52.30	18.20	0.86	9.03	6.18	0.17	8.10	3.10	0.88	0.46	0.00	0.20	0.02	99.50
Mealy Avg	47.63	16.60	2.62	13.38	6.05	0.20	9.01	2.85	1.05	0.60	0.00	0.00	N/A	99.99

Mealy dyke data is from Emslie et al. (1984). All Fe calculated as FeO
Mealy Avg data from Gower et al. (1990)
Extended trace element data for samples EC75-40, EC75201B and EC74-44 are from Ahwal et al. (1986)

Sample	S	Cl	Cr	Ni	Sc	V	Cu	Zn	Ga	As	Rb	Sr	Y	Zr	Nb
	ppm	ppm	ppm	ppm	ppm	ppm	ppm	ppm	ppm	ppm	ppm	ppm	ppm	ppm	ppm
EC75-44			33	80	17.07		77	69.5			59	310		290	
EC75-185A			71	100			90				42	300		440	
EC75-185B			72	120			69				8	290		440	
EC75-166B			76	160			200				32	250		200	
EC75-238A			73	140			140				23	280		300	
EC75-163A			62	110			62				7	240		110	
EC75-83A			70	200			120				14	280		79	
EC75-176			80	120			170				57	200		300	
EC75-176A			55	110			250				81	230		420	
EC75-180E			110	90			160				29	200		280	
EC75-138A			80	110			100				18	520		170	
EC75-40			100	100	36.14		120	124			25	320		240	
EC75-201B			200	160	29.98		98	63.3			3	300		110	
EC75-89B			180	160			110				10	280		140	
EC75-35			260	73			49				10	530		46	
Mealy Avg			95	122		261	120	121	33		27	265	70	220	28.00

Sample	Ba	Pb	Th	U	La	Ce	Pr	Nd	Sm	Eu	Gd	Tb	Yb	Lu	Cs
	ppm	ppm	ppm	ppm	ppm	ppm	ppm	ppm	ppm	ppm	ppm	ppm	ppm	ppm	ppm
EC75-44	680		8.13	1.9	86.37	211.5		125.9	25.01	5.48		3.925	7.71	1.143	0.428
EC75-185A	580														
EC75-185B	290														
EC75-166B	370														
EC75-238A	510														
EC75-163A	210														
EC75-83A	210														
EC75-176	420														
EC75-176A	550														
EC75-180E	370														
EC75-138A	740														
EC75-40	410		1.305	1.2	18.45	42.65		26.68	6.58	1.972		1.185	3.27	0.513	0.288
EC75-201B	210		0.499	0	6.794	16.33		11.22	3.09	1.155		0.629	1.91	0.298	0.252
EC75-89B	240														
EC75-35	790														
Mealy Avg	432	1	3	2	23.9	57.8	7.3	33.5	7.3	2.2	8		3.2	0.5	

Sample	Hf	Ta	Sb
	ppm	ppm	ppm
EC75-44	8.13	1.898	0.246
EC75-185A			
EC75-185B			
EC75-166B			
EC75-238A			
EC75-163A			
EC75-83A			
EC75-176			
EC75-176A			
EC75-180E			
EC75-138A			
EC75-40	4.68	1.305	0.269
EC75-201B	2.13	0.499	0.19
EC75-89B			
EC75-35			
Mealy Avg			

Appendix B

This appendix displays the list of samples and the mineralogy in each of those samples collected during the field season. All thin sections were made in the Lapidary facilities at Memorial University.

		Primary Mineralogy												Accessory Mineralogy						Secondary Mineralogy				
Sample	**Rock**	**opx**	**cpx**	**amph**	**grt**	**bt**	**pl**	**kfs**	**qtz**	**als**	**ep**	**scp**	**other**	**opq**	**apa**	**zrn**	**aln**	**ttn**		**cal**	**ms**	**ep**	**chl**	**amph**
001	1				x	x	x	x	x	x				x	x	x	x							
001a	2			x	x				x		x							x						
002	1				x	x	x	x	x	x	x			x	x	x								
002a	2			x	x				x		x		cal	x		x		x						
002um	5	x		x										x										
002	5			x	x	x	x		x			x		x		x								
003	1				x	x	x	x	x	x	x			x		x								
004	3			x	x	x	x	x	x					x	x	x								
004a	3		x	x	x	x	x	x	x			x		x	x	x								
005	3			x	x	x	x		x					x	x	x								
006	3		x	x	x	x	x		x			x		x	x	x								
007	3			x	x	x	x	x	x			x		x	x	x								
008	6		x	x	x	x	x	x	x		?			x	x	x		?						
009	6		x	x	x	x	x	x	x					x	x	x								
010	3			x	x	x	x	x	x					x	x	x	x							
011-1	6		x	x	x	x	x	x	x					x		x			spl					
011-2	6				x	x	x	x	x					x		x				x	x		x	
012-1	6	x	x	x	x	x	x	?	x					x	x	x								
012-2	6	x	x	x	x	x	x	?	x					x						x				
013	6	x	x	x	x	x	x	?	x					x	x	x								
013-1	6	x	x	x	x	x	x	?	x			x		x	x	x								
014-1	6				x	x	x	?	x		x			x	x	x			rt, spl					
014-2	6	x	x	x	x	x	x	?	x			x		x	x	x								
015	6			x	x	x	x	?	x					x	x	x							x	
016	6			x	x	x	x	?	x					x	x	x								
016a	6	x	x	x			x	x				x		x	x	x		x	rt					
017	6		x	x	x	x	x	x	x					x	x	x								
018	6		x	x	x		x	x						x	x	x			rt					
019	1					x	x	x	x	x*				x	x	x					x			
020	3			x	x	x	x	x	x					x	x	x							x	
021	3			x	x	x	x	x	x					x	x	x	x				x		x	
022	3			x	x	x	x	x	x			x		x	x	x								
023	3			x	x	x	x	x	x			x		x	x	x	x	x						
024	1					x	x	x	x	x*				x	x	x					x			

		Primary Mineralogy												Accessory Mineralogy						Secondary Mineralogy				
Sample	**Rock**	**opx**	**cpx**	**amph**	**grt**	**bt**	**pl**	**kfs**	**qtz**	**als**	**ep**	**scp**	**other**	**opq**	**apa**	**zrn**	**aln**	**ttn**		**cal**	**ms**	**ep**	**chl**	**amph**
024a	2			x	x				x		x		cal		x			x					x	
025	3			x	x	x	x	x	x			x		x	x	x	x							
026	3				x	x	x	x	x					x	x	x	x							
027	1				x	x	x	x	x	x*				x	x	x					x			
028	6	x	x	x	x	x	x	?	x			x		x	x	x								
029-1	6		x	x	x	x	x	?	?					x	x	x								
029-2	6		x	x	x	x	x		x					x	x	x				x				
030	7	x	x	x		x	x		?			x		x	x	x				x				
031-1	7	x		x	x		x					x			x						x			
031-2	7	x	x	x	x		x					x							rt					
032	11			x		x	x	x	x					x	x	x	x						x	
032a	4	x	x	x		x	x							x										x
034	4		x	x		x	x	x	x					x	x	x	x			x				x
037	4	x	x	x			x		x					x	x	x				x	x			
037b	5	x		x		x							ol, sr	x										
038	4	x		x		x	x	x	x					x	x	x								
039	4	x		x		x	x	x	x					x	x	x				x				
040	4	x	x	x		x	x	x	x					x	x	x								
041	4			x		x	x	x	x			x		x	x	x				x	x			x
042	4					x	x	x	x					x	x	x	x				x		x	
042a	4			x	x	x	x	x	x					x		x							x	x
043	4	x		x		x	x	x	x					x		x					x		x	
044	7	x	x	x	x	x	x		x					x	x	x								
045	7	x	x	x	x	x	x		x			x		x	x	x								
046	7		x	x	x		x		x			x		x										
046	7			x	x		x					x		x		x			rt	x				
047	7	x	x	x	x	x	x	x	x			x		x	x	x								
048	4			x		x	x							x	x					x	x	x		
049	4		x	x	x		x		x					x	x	x			rt					
050	4	?	x	x		x	x	x	x					x	x	x								
051	4			x			x							x	x	x		x						
052	4			x	x	x	x	x	x					x	x	x	x							
054-1	4	x	x	x	x		x		x					x	x	x								
054-2	4	x	x	x	x	x	x		x					x	x	x								

		Primary Mineralogy												Accessory Mineralogy						Secondary Mineralogy				
Sample	**Rock**	**opx**	**cpx**	**amph**	**grt**	**bt**	**pl**	**kfs**	**qtz**	**als**	**ep**	**scp**	**other**	**opq**	**apa**	**zrn**	**aln**	**ttn**		**cal**	**ms**	**ep**	**chl**	**amph**
055	4			x		x	x	x	x					x	x	x	x				x	x		x
058	4				x	x	x	x	x					x	x	x								
059	6	x			x	x	x	?	x		?			x	x	x							?	
059a	6	x	x	x	x		x		x					x	x	x					x			
061	6				x	x	x		x					x	x	x				x	x	x	x	
062	6	x	x	x		x	x		x					x	x	x								
063	6	x				x	x					x		x	x	x			spl					
064	6		x	x		x	x	x	?					x	x	x								
065a	6	x	x	x	x	x	x	x	x					x	x	x								
067	6	x	x	x		x	x	x	x					x	x	x								
068-1	6	x	x	x	x	x	x	x	x					x	x	x								
068-2	6	x	x	x			x		x					x	x	x								
070	6			x	x	x	x		?					x	x	x				x	x			
070a	6		x	x	x		x		x					x	x	x								
071	6		x	x	x	x	x	x	x			x		x	x	x								
072	6	x	x		x	x	x	x	x			x		x	x	x								
074	3	x	x		x	x	x	x	x					x	x	x				x				x
075	3			x	x	x	x		x			x		x	x		x						x	
076	3																							
076a	5			x		x								x						x				
079	1				x	x	x	x	x	x				x	x	x								
079a	5		x	x	x		x		x					x	x				rt					
079b	5	x	x	x			x							x		x			spl					
079c	5		x	x	x		x		x			x		x				x	rt					
079d	5		x	x	x		x								x				rt		x			x
080	1				x	x	x	x	x	x	x			x	x	x								
081	1				x	x	x	x	x	x				x	x	x					x		x	
082-1	1				x	x	x	x	x	x*				x	x	x								
082-2	1				x	x	x	x	x	x	x			x	x	x								
083	3				x	x	x	x	x					x	x	x					x		x	
084	3		x	x	x		x		x					x	x	x								
085	3		x	x	x	x	x		x					x	x	x								
085a	6		x	x	x	x	x		?					x	x	x		x	rt					
086-1	6		x	x	x	x	x							x	x	x		x					x	

		Primary Mineralogy												Accessory Mineralogy						Secondary Mineralogy				
Sample	**Rock**	**opx**	**cpx**	**amph**	**grt**	**bt**	**pl**	**kfs**	**qtz**	**als**	**ep**	**scp**	**other**	**opq**	**apa**	**zrn**	**aln**	**ttn**		**cal**	**ms**	**ep**	**chl**	**amph**
086-2	6		x	x	x	x	x	x	x					x	x	x		x	rt	x				
087	6		x	x	x		x	?	x					x	x	x					x			
088	6		x	x	x		x		x					x	x	x					x			
089	7	x	x	x	x	x	x		?			x		x	x	x								
090	7		x	x	x	x	x	?	x					x	x	x								
091	7		x	x	x	x	x	x	x					x	x	x								
092	8		x	x	x		x							x	x	x								
093	8			x	x	x	x	x	x			x		x	x	x	x	x						
094	8	x	x	x	x	x	x	?	x					x	x	x								
095	3			x	x	x	x	x	x			x		x	x	x	x				x		x	
097	3			x		x	x	x	x					x	x	x	x							
099	3					x	x	x	x						x	x								
100	3			x		x	x	x	x			x		x	x	x	x							
101	3			x		x	x	x	x					x	x	x	x						x	
102	3			x	x		x							x	x	x	x	x	rt		x		x	
106	3			x		x	x	x	x						x	x	x	x			x			
107	3			x	x	x	x	x	x					x	x	x	x	x			x		x	
109	3			x	x	x	x	x	x					x	x	x	x				x		x	
110	3			x		x	x	x	x					x	x	x	x				x	x	x	
113	10	x	x		x	x	x							x	x	x		x	rt					
114	10	x	x	x	x	x	x	x	x					x	x	x								
117	8			x	x	x	x	x	x			x		x	x	x	x				x		x	
122-2	9	x	x	x	x	x	x	?	x					x	x	x								
123	8				x	x	x	x	x					x	x	x	x	x			x		x	
125	8			x	x	x	x	?	x					x	x	x	x							
127	9			x	x	x	x	?	x					x	x	x	x	x					x	
128	9	x	x	x		x	x		x					x	x	x								
131a	8		x	x			x								x	x								
136	8			x	x	x	x	?	x					x	x	x	x			x				
137	8				x	x	x	x	x					x	x	x		x			x		x	
138	8				x	x	x	x	x					x	x	x				x	x			
141	9			x	x	x	x		x					x	x	x								
141b	11			x	x	x	x	x	x					x	x	x					x		x	
141d	11						x	x	x					x	x	x					x		x	

		Primary Mineralogy											Accessory Mineralogy					Secondary Mineralogy				
Sample	**Rock**	**opx**	**cpx**	**amph**	**grt**	**bt**	**pl**	**kfs**	**qtz**	**als**	**ep**	**scp other**	**opq**	**apa**	**zrn**	**aln**	**ttn**	**cal**	**ms**	**ep**	**chl**	**amph**
148	9				x	x	x	x	x		x		x	x	x				x			
150	9	x	x	x			x						x	x	x							
151	10	x	x	x	x	x							x	x	x							
153	12		x	x		x	x	x	x				x	x	x				x			
154	12	x	x	x		x	x	x	?				x	x	x							
157	10	x	x	x	x	x	x						x									
191	10	x	x	x		x	x						x									
195	9	x		x			x						x	x	x							
196	9	x	x	x		x	x		x				x	x	x							

x* indicates the presence of retrograde sil with ky in the PGN

x* indicates that the [illegible] was both igneous and metamorphic [illegible]

Samples with a letter following a three digit number indicate different samples taken at the station.

Samples with a dash then a number indicate the thin section number from the sample e.g., 012-1 indicates that ample 1 cut for the sample 012

These samples have multiple thin sections to enable better chatacterization of textural domains present in the samples.

Rock Type Legend

1 paragneiss
2 calc-silicate
3 GBT orthogneiess
4 LMT orthogneiss
5 mafic boudin
6 straight gneiss
7 mafic gneiss
8 basal granitoid gneiss
9 recrystallized gabbro-diorite
10 gabbro/anorthosite
11 pegmatite
12 Dome Mountain suite

Mineralogy of the Northwest River dykes

		Primary Mineralogy									Accessory Phases				Secondary Mineralogy				
Sample	**texture**	**opx**	**cpx**	**amph**	**grt**	**bt**	**pl**	**kfs**	**qtz**	**other**	**opaque**	**apa**	**zrn**	**other**	**chl**	**ms**	**amph**	**cal**	**other**
037a	recrystallized			x		x	x		x		x	x	x						
038a	recrystallized	x		x	x	x	x		x		x	x	x	aln			x	x	
039a	recrystallized			x		x	x		x		x	x	x	aln			x	x	
040a	recrystallized		x	x		x	x		x		x	x	x						
041a	recrystallized	x	x	x		x	x	x	x		x	x							
043a	recrystallized			x		x	x		x		x	x	x						
056	recrystallized			x	x	x	x		x		x	x	x						
122-1	recrystallized	x	x	x	x		x*				x	x	x						
122-3	recrystallized	x	x	x	x		x*				x	x	x						
123a	recrystallized	x	x	x	x	x	x		?		x	x	x						
124a	recrystallized	?	x	x	x	x	x		x		x	x	x						
130a	recrystallized		x	x	x	x	x		?		x	x	x					x	
134	recrystallized		x	x	x	x	x		?		x	x	x						
137a	recrystallized		x	x	x	x	x		x		x	x	x						
141a	recrystallized			x	x	x	x		x		x	x	x					x	scp
141c	recrystallized		x	x	x	x	x		?		x	x	x						
142	recrystallized		x	x	x		x		x		x	x	x					x	
143	recrystallized	x	x	x	x	x	x		?		x	x	x						
148a	recrystallized		x	x	x	x	x		x		x	x	x						
149	recrystallized			x	x	x	x		x		x	x	x					x	
156b	coronitic		x	x	x	x	x*				x	x	x						
161	coronitic	x	x		x		x*				x	x							
168	coronitic	x	x	x	x	x	x*				x	x							
172	coronitic	x	x	x	x	x	x*				x	x		spl					
174a	coronitic	x	?	x		x	x*				x	x							
176	coronitic	x	x	x		x	x*				x	x							
177a	coronitic	x	x	x		x	x*				x	x							
178	coronitic	x	x	x	x	x	x*				x	x							
184a	coronitic	x	x	x	x	x	x*				x	x							
186	coronitic	x*	x*	x	?	x	x*			ol	x	x		spl					
193	recrystallized			x	x		x*		x		x	x	x						
196	recrystallized	x	x	x	x	x	x*		x		x	x	x	rt					

x* indicates that the phase is present as both igneous and metamorphic crystals

Appendix C

Chemical data sets of analysed phases used for geothermobarometry from 18 samples from the shear zone, footwall and hangingwall rocks in the Goose Bay area. All mineral chemistries determined for geothermobarometry were made using a Cameca SX-50 electron microprobe equipped with an LINK electron dispersive (EDS) spectrometer X-Ray analyser located in the Department of Earth Sciences at Memorial University of Newfoundland. The conditions for analysis were set at 15 kV accelerating voltage and 20 nA beam current for all silicates excepting feldspar, which was analysed at the same voltage but at 10 nA to minimize the effects of Na volatilization during analysis. All minerals were analysed for 100s. The results were corrected using the ZAF software.

Sample	**008**									
twq filename	**008-1**			**008-11**			**008-2**			
mineral	grt1-1	cpx1-4	pl1-1	grt1-8	cpx1-1	pl1-3	grt2-1	cpx2-1	amp2-3	pl2-4
point	core	core	core	rim	rim	rim	core	core	core	core
SiO_2	39.29	51.72	62.21	39.80	52.63	62.53	39.24	51.14	42.00	62.64
Al_2O_3	21.91	4.22	23.73	21.38	3.16	24.74	21.64	3.59	12.46	24.59
TiO_2	0.15	0.30	0.00	0.07	0.25	0.10	0.03	0.30	2.40	0.13
Cr_2O_3	0.01	0.06	0.15	0.07	0.00	0.05	0.06	0.10	0.05	0.31
FeO	26.60	12.65	0.26	27.04	10.34	0.72	28.00	11.79	16.00	0.02
MgO	5.62	11.15	0.00	5.51	11.74	0.00	5.17	10.67	10.69	0.06
MnO	1.64	0.31	0.00	2.14	0.37	0.00	1.93	0.37	0.00	0.00
CaO	8.18	19.82	5.54	7.51	21.61	5.73	7.44	20.59	11.22	5.04
Na_2O	0.06	1.27	8.44	0.06	1.25	7.99	0.18	1.44	1.89	8.44
K_2O	0.00	0.01	0.18	0.09	0.06	0.32	0.03	0.06	1.92	0.21
Total	103.46	101.51	100.52	103.66	101.39	102.16	103.71	100.06	98.64	101.45

Sample	**008**				**012**					
twq filename	**008-21**				**012-11**			**012-12**		
mineral	grt2-10	cpx2-4	amp2-4	pl2-1	grt1-2	cpx1-7	pl1-5	grt1-9	cpx1-1	pl1-9
point	rim	rim	rim	rim	core	core	core	rim	rim	rim
SiO_2	38.51	54.28	42.02	63.30	39.39	51.58	62.00	39.10	52.62	61.99
Al_2O_3	21.46	3.02	12.57	23.75	21.54	4.27	23.91	21.66	2.91	24.08
TiO_2	0.12	0.30	2.35	0.14	0.09	0.55	0.11	0.17	0.27	0.12
Cr_2O_3	0.07	0.10	0.20	0.06	0.06	0.07	0.01	0.06	0.08	0.00
FeO	29.28	10.60	16.27	0.28	25.17	9.18	0.06	25.61	8.84	0.13
MgO	3.99	13.20	11.04	0.00	8.12	11.80	0.11	8.07	13.12	0.12
MnO	1.86	0.24	0.13	0.14	0.55	0.05	0.00	0.71	0.04	0.07
CaO	7.29	21.40	11.45	5.06	6.34	21.00	5.46	6.09	21.54	5.51
Na_2O	0.06	1.44	2.17	8.49	0.22	1.81	8.60	0.26	1.28	8.69
K_2O	0.03	0.00	1.89	0.08	0.00	0.02	0.68	0.00	0.02	0.57
Total	102.67	104.57	100.08	101.30	101.48	100.34	100.95	101.73	100.72	101.27

***Appendix C**: Mineral data from the EMP used in P-T determination for the shear zone rocks.*

Sample	**012**								
twq filename	**012-13**			**012-14**			**012-21**		
mineral	grt1-10	cpx(am)1	pl1-10	grt1-13	cpx1-11	pl1-2	grt2-1	cpx2-4	pl2-4
point	core	core	core	rim	rim	rim	core	core	core
SiO_2	39.06	42.40	61.84	38.90	52.27	61.53	39.18	51.47	60.53
Al_2O_3	21.44	11.98	24.01	21.65	3.21	23.96	21.25	3.66	24.76
TiO_2	0.00	2.39	0.04	0.02	0.33	0.00	0.10	0.44	0.00
Cr_2O_3	0.10	0.10	0.06	0.05	0.05	0.00	0.01	0.08	0.00
FeO	25.40	13.32	0.07	26.25	8.66	0.17	25.92	9.30	0.26
MgO	7.76	12.48	0.05	7.81	13.04	0.12	7.42	12.35	0.14
MnO	0.71	0.01	0.04	0.65	0.10	0.00	0.67	0.18	0.00
CaO	6.18	11.48	5.37	6.07	21.84	5.67	6.49	21.54	6.48
Na_2O	0.05	2.04	9.23	0.30	1.47	8.35	0.21	1.35	8.06
K_2O	0.00	1.88	0.51	0.04	0.00	0.50	0.00	0.01	0.24
Total	100.71	98.08	101.23	101.74	100.98	100.31	101.23	100.38	100.47

Sample	**012**								
twq filename	**012-22**			**012-31**			**012-32**		
mineral	grt2-6	cpx2-5	pl2-1	grt3-1	cpx3-4	pl3-1	grt3-6	cpx3-1	pl3-3
point	rim	rim	rim	core	core	core	rim	rim	rim
SiO_2	38.76	52.57	60.21	39.14	52.09	61.17	38.97	52.48	56.94
Al_2O_3	21.40	2.34	24.74	21.64	4.24	24.26	21.49	3.88	27.40
TiO_2	0.08	0.19	0.00	0.01	0.43	0.00	0.03	0.40	0.00
Cr_2O_3	0.00	0.11	0.04	0.01	0.12	0.08	0.03	0.17	0.00
FeO	27.24	8.57	0.06	25.42	8.61	0.04	25.35	6.37	0.42
MgO	6.62	13.35	0.01	8.30	12.23	0.13	7.58	13.63	0.00
MnO	1.00	0.05	0.00	0.56	0.00	0.00	0.60	0.04	0.00
CaO	6.37	22.34	6.41	6.22	21.34	5.68	7.08	23.16	9.51
Na_2O	0.26	0.91	7.85	0.17	1.95	8.57	0.20	1.11	6.71
K_2O	0.00	0.02	0.27	0.02	0.00	0.32	0.03	0.00	0.16
Total	101.73	100.46	99.58	101.49	101.01	100.23	101.37	101.25	101.13

***Appendix C**: Mineral data from the EMP used in P-T determination for the shear zone rocks continued.*

Sample	**012**							**017**			
twq filename	**012-41**			**012-42**				**017-1**			
mineral	grt4-1	amp4-3	pl4-4	grt4-6	amp4-1	pl4-1		grt1-1	cpx1-5	amp1-3	pl1-3
point	core	core	core	rim	rim	rim		core	core	core	core
SiO_2	38.29	42.24	61.39	38.66	42.33	61.03		39.35	52.74	45.53	60.74
Al_2O_3	21.08	12.03	24.16	21.09	12.19	25.04		22.39	3.53	11.79	24.80
TiO_2	0.02	2.81	0.00	0.00	2.75	0.00		0.07	0.38	1.65	0.07
Cr_2O_3	0.11	0.11	0.00	0.10	0.09	0.00		0.00	0.10	0.15	0.06
FeO	25.13	14.48	0.25	26.09	13.49	0.19		23.76	7.29	11.74	0.02
MgO	7.75	11.40	0.02	7.59	11.99	0.10		8.56	14.04	13.70	0.04
MnO	0.59	0.00	0.00	0.79	0.10	0.11		0.96	0.08	0.15	0.12
CaO	6.23	11.45	5.83	6.23	11.47	6.70		6.70	22.61	11.82	5.99
Na_2O	0.27	2.07	8.70	0.29	2.11	8.37		0.16	0.76	2.02	8.14
K_2O	0.04	1.94	0.35	0.00	1.94	0.38		0.00	0.00	0.46	0.22
Total	99.52	98.53	100.71	100.84	98.45	101.91		101.94	101.52	99.01	100.19

Sample	**017**								
twq filename	**017-11**			**017-2**			**017-3**		
mineral	grt1-5	amp1-1	pl1-2	grt2-4	cpx2-3	pl2-2	grt3-5	cpx3-4	pl3-5
point	rim	rim	rim	core	core	core	core	core	core
SiO_2	39.63	41.07	65.12	38.30	50.97	62.79	37.93	52.13	62.73
Al_2O_3	22.05	12.75	21.57	20.96	3.26	22.99	21.43	3.11	23.46
TiO_2	0.00	3.00	0.00	0.12	0.30	0.02	0.16	0.40	0.03
Cr_2O_3	0.00	0.00	0.13	0.00	0.13	0.00	0.00	0.05	0.00
FeO	28.74	15.41	0.15	28.54	12.87	0.14	28.79	11.79	0.00
MgO	5.16	10.32	0.00	5.11	10.46	0.00	5.17	11.14	0.20
MnO	1.10	0.07	0.07	0.89	0.16	0.07	1.03	0.02	0.00
CaO	6.93	11.13	2.77	7.02	20.91	4.38	6.68	21.45	4.71
Na_2O	0.27	1.88	9.35	0.00	0.96	8.59	0.15	1.26	8.65
K_2O	0.00	2.15	0.13	0.00	0.00	0.25	0.03	0.00	0.39
Total	103.88	97.78	99.31	100.94	100.02	99.22	101.37	101.36	100.18

Appendix C: Mineral data from the EMP used in P-T determination for the shear zone rocks continued.

Sample	**017**				**028-1**					
twq filename	**017-31**				**028-1-1**			**028-1-2**		
mineral	grt3-9	cpx3-3	pl3-3		grt1-1	opx1-2	pl1-1	grt2-3	opx2-6	pl2-2
point	rim	rim	rim		core	core	core	core	core	core
SiO_2	38.80	52.23	60.21		40.67	52.46	61.03	39.96	52.08	62.16
Al_2O_3	21.52	2.39	28.60		21.84	1.85	22.95	21.99	1.60	24.06
TiO_2	0.11	0.23	0.07		0.03	0.11	0.02	0.04	0.14	0.04
Cr_2O_3	0.08	0.06	0.26		0.23	0.00	0.00	0.00	0.00	0.10
FeO	29.55	11.24	0.22		26.78	24.48	0.12	28.02	24.82	0.16
MgO	4.57	11.66	0.23		8.74	20.65	0.00	7.73	20.29	0.00
MnO	1.08	0.09	0.15		0.67	0.31	0.00	1.02	0.26	0.00
CaO	7.31	21.99	2.15		5.52	0.54	5.96	5.99	0.57	5.50
Na_2O	0.10	0.91	8.68		0.30	0.24	7.83	0.28	0.24	7.39
K_2O	0.00	0.00	0.44		0.00	0.00	0.47	0.01	0.00	0.31
Total	103.12	100.81	100.99		104.78	100.64	98.39	105.05	100.00	99.72

Sample	**028-1**						**028-1**		
twq filename	**028-1-2rim**			**028-1-3**			**028-1-32**		
mineral	grt2-4	opx2-8	pl2-3	grt3-8	cpx3-4	pl3-2	grt3-10	opx2-8	pl3-2
point	rim	rim	rim	core	core	core	rim	rim	rim
SiO_2	36.21	53.78	59.94	40.24	52.31	47.81	39.64	52.81	47.81
Al_2O_3	19.77	1.83	26.56	21.84	3.87	24.40	21.88	1.31	24.40
TiO_2	0.10	0.12	0.03	0.15	0.42	0.21	0.03	0.07	0.21
Cr_2O_3	0.05	0.02	0.01	0.08	0.05	0.00	0.12	0.03	0.00
FeO	26.32	23.58	0.11	26.76	10.98	0.00	26.79	24.25	0.00
MgO	6.59	21.49	0.05	7.58	12.19	0.17	7.40	21.15	0.17
MnO	1.03	0.40	0.10	0.88	0.23	0.17	0.76	0.30	0.17
CaO	5.61	0.44	7.74	6.44	20.99	15.43	6.37	0.36	15.43
Na_2O	0.05	0.23	7.13	0.12	0.87	4.47	0.17	0.22	4.47
K_2O	0.06	0.00	0.05	0.00	0.00	0.25	0.00	0.00	0.25
Total	95.80	101.89	101.72	104.10	101.91	92.92	103.16	100.50	92.91

***Appendix C**: Mineral data from the EMP used in P-T determination for the shear zone rocks continued.*

Sample	**028-1**							**029-1**		
twq filename	**028-1-32**			**028-1-32**				**029-1-1**		
mineral	grt3-10	cpx3-4	pl3-2	grt3-10	amp3-1	pl3-2		grt1-4	cpx1-3	pl1-3
point	rim	rim	rim	rim	rim	rim		core	core	core
SiO_2	39.64	51.66	47.81	39.64	43.77	47.81		38.78	50.86	60.90
Al_2O_3	21.88	4.44	24.40	21.88	11.72	24.40		21.04	3.89	24.84
TiO_2	0.03	0.43	0.21	0.03	1.71	0.21		0.05	0.37	0.00
Cr_2O_3	0.12	0.00	0.00	0.12	0.00	0.00		0.06	0.16	0.00
FeO	26.79	9.92	0.00	26.79	12.61	0.00		27.11	11.73	0.09
MgO	7.40	11.39	0.17	7.40	13.09	0.17		5.72	11.02	0.09
MnO	0.76	0.21	0.17	0.76	0.00	0.17		0.74	0.15	0.00
CaO	6.37	22.11	15.43	6.37	12.20	15.43		7.60	21.64	6.44
Na_2O	0.17	1.13	4.47	0.17	1.59	4.47		0.09	1.07	7.94
K_2O	0.00	0.00	0.25	0.00	1.45	0.25		0.00	0.01	0.37
Total	103.16	101.29	92.91	103.16	98.13	92.91		101.18	100.90	100.67

Sample	**029-1**									
twq filename	**029-1-12**			**029-1-2**				**029-1-22**		
mineral	grt1-8	cpx1-2	pl1-1	grt2-9	cpx2-3	amp2-7	pl2-2	grt2-7	cpx2-5	pl2-1
point	rim	rim	rim	core	core	core	core	rim	rim	rim
SiO_2	38.69	50.94	60.49	39.23	51.71	41.67	61.31	39.09	52.08	60.94
Al_2O_3	21.13	3.63	24.14	21.80	4.63	12.59	24.77	21.66	4.44	24.64
TiO_2	0.12	0.34	0.19	0.12	0.39	2.52	0.07	0.12	0.49	0.03
Cr_2O_3	0.05	0.16	0.00	0.09	0.12	0.12	0.00	0.00	0.08	0.00
FeO	27.46	10.91	0.00	25.38	9.03	14.09	0.04	25.44	8.92	0.04
MgO	5.37	11.23	0.00	7.52	12.30	11.36	0.02	7.34	12.51	0.00
MnO	0.77	0.05	0.00	0.71	0.11	-0.03	0.01	0.83	0.07	0.06
CaO	7.89	22.34	6.43	6.70	21.64	11.38	6.14	6.85	21.70	6.44
Na_2O	0.25	1.16	7.93	0.00	1.29	1.98	7.93	0.00	1.31	7.95
K_2O	0.00	0.00	0.36	0.02	0.00	2.01	0.37	0.00	0.00	0.41
Total	101.73	100.76	99.54	101.56	101.21	97.69	100.68	101.32	101.60	100.50

***Appendix C**: Mineral data from the EMP used in P-T determination for the shear zone rocks continued.*

Sample	**029-1**								
twq filename	**029-1-23**			**029-1-3**			**029-1-32**		
mineral	grt2-11	amp2-6	pl2-3	grt3-2	amp3-3	pl3-2	grt3-4	amp3-1	pl3-4
point	rim	rim	rim	core	core	core	rim	rim	rim
SiO_2	39.20	42.34	60.59	38.80	40.72	61.50	38.59	40.63	61.21
Al_2O_3	21.61	12.74	24.66	21.15	13.38	24.68	21.25	13.22	24.79
TiO_2	0.10	2.36	0.00	0.17	3.26	0.00	0.09	3.35	0.03
Cr_2O_3	0.05	0.11	0.00	0.04	0.02	0.00	0.00	0.00	0.02
FeO	26.31	13.41	0.17	27.55	15.15	0.32	27.85	15.02	0.33
MgO	6.97	12.20	0.00	5.81	10.00	0.00	5.64	9.99	0.03
MnO	0.66	0.12	0.05	0.82	0.12	0.08	0.79	0.08	0.00
CaO	7.01	11.81	6.41	7.55	11.13	6.04	7.18	11.14	6.30
Na_2O	0.01	2.09	7.98	0.16	2.16	7.87	0.09	2.12	7.77
K_2O	0.00	1.80	0.33	0.00	2.27	0.65	0.00	2.26	0.56
Total	101.93	98.98	100.19	102.05	98.21	101.14	101.47	97.81	101.04

Sample	**029-1**								
twq filename	**029-1-4**			**029-1-41**			**029-1-42**		
mineral	grt4-2	cpx4-3	pl4-5	grt4-1	cpx4-6	pl4-5	grt4-1	cpx4-1	pl4-2
point	core	core	core	core	core	core	rim	rim	rim
SiO_2	38.86	50.74	60.71	38.95	51.40	60.71	38.95	51.75	61.19
Al_2O_3	21.11	4.54	24.51	21.12	3.44	24.51	21.12	3.10	24.29
TiO_2	0.09	0.45	0.00	0.06	0.31	0.00	0.06	0.31	0.03
Cr_2O_3	0.12	0.18	0.05	0.03	0.15	0.05	0.03	0.18	0.00
FeO	27.16	11.29	0.27	27.11	11.16	0.27	27.11	10.72	0.11
MgO	5.54	11.30	0.02	5.19	11.54	0.02	5.19	11.81	0.00
MnO	0.74	0.14	0.00	0.77	0.07	0.00	0.77	0.13	0.00
CaO	8.12	21.23	6.12	8.39	21.69	6.12	8.39	21.47	6.07
Na_2O	0.11	1.31	8.03	0.14	1.11	8.03	0.14	1.21	8.16
K_2O	0.00	0.00	0.49	0.00	0.00	0.49	0.00	0.00	0.28
Total	101.86	101.18	100.20	101.77	100.87	100.20	101.77	100.67	100.14

***Appendix C**: Mineral data from the EMP used in P-T determination for the shear zone rocks continued.*

Sample	**029-1**				**059a**					
twq filename	**029-1-43**				**059a-1**			**059a-12**		
mineral	grt4-7	cpx4-5	pl4-6		grt1-1	amp1-4	pl1-5	grt1-4	amp1-1	pl1-1
point	rim	rim	rim		core	core	core	rim	rim	rim
SiO_2	38.77	51.90	61.44		38.94	42.43	59.10	38.39	41.89	58.40
Al_2O_3	21.43	2.74	24.39		21.31	12.41	25.44	21.22	12.96	24.71
TiO_2	0.07	0.18	0.06		0.06	2.52	0.00	0.11	2.13	0.00
Cr_2O_3	0.00	0.29	0.08		0.01	0.07	0.06	0.06	0.07	0.00
FeO	27.19	9.80	0.14		24.39	13.72	0.05	25.92	13.00	0.29
MgO	5.61	12.29	0.00		8.17	11.81	0.04	7.28	12.16	0.01
MnO	0.85	0.00	0.00		0.72	0.02	0.00	0.90	0.09	0.06
CaO	7.92	22.47	6.11		6.52	11.76	7.43	6.36	11.78	7.03
Na_2O	0.22	1.06	7.80		0.31	2.06	7.55	0.32	2.11	7.55
K_2O	0.00	0.00	0.44		0.00	1.59	0.34	0.00	1.59	0.39
Total	102.06	100.72	100.46		100.41	98.38	100.00	100.55	97.78	98.44

Sample	**059a**								
twq filename	**059a-13**			**059a-14**			**059a-2**		
mineral	grt1-8	cpx1-6	pl1-9	grt1-11	cpx1-3	pl1-6	grt2-1	cpx2-5	pl2-2
point	core	core	core	rim	rim	rim	core	core	core
SiO_2	38.79	50.60	58.49	38.81	51.50	59.16	38.52	50.98	58.43
Al_2O_3	21.08	4.55	25.32	21.42	3.51	25.79	21.44	3.64	25.04
TiO_2	0.06	0.54	0.00	0.10	0.34	0.00	0.01	0.51	0.00
Cr_2O_3	0.00	0.01	0.06	0.03	0.07	0.08	0.09	0.18	0.08
FeO	24.73	9.08	0.06	25.09	7.89	0.13	25.05	8.28	0.13
MgO	8.15	11.99	0.02	7.68	13.02	0.00	7.85	12.52	0.00
MnO	0.77	0.11	0.01	0.66	0.09	0.00	0.80	0.03	0.01
CaO	6.57	21.08	7.46	6.48	22.16	7.83	6.60	22.24	7.53
Na_2O	0.15	1.44	7.40	0.17	1.37	7.44	0.23	1.15	7.48
K_2O	0.00	0.01	0.40	0.01	0.00	0.45	0.02	0.00	0.30
Total	100.30	99.43	99.23	100.45	99.98	100.87	100.62	99.54	98.98

***Appendix C**: Mineral data from the EMP used in P-T determination for the shear zone rocks continued.*

Sample	**059a**								
twq filename	**059a-21**			**059a-22**			**059a-23**		
mineral	grt2-5	cpx2-6	pl2-1	grt2-6	cpx2-11	pl2-8	grt2-9	cpx2-14	pl2-4
point	rim	rim	rim	core	core	core	rim	rim	rim
SiO_2	38.57	51.82	58.35	39.12	50.80	58.47	38.83	52.18	59.54
Al_2O_3	21.26	3.27	25.42	21.41	4.45	26.21	21.27	2.96	24.81
TiO_2	0.11	0.36	0.09	0.00	0.54	0.00	0.02	0.30	0.20
Cr_2O_3	0.04	0.08	0.04	0.15	0.08	0.00	0.04	0.16	0.02
FeO	24.87	8.89	0.03	24.55	8.94	0.11	25.58	8.11	0.10
MgO	7.97	13.30	0.06	8.26	12.13	0.01	7.46	13.03	0.02
MnO	0.81	0.06	0.00	0.83	0.11	0.02	0.79	0.09	0.01
CaO	6.40	21.79	7.56	6.44	21.49	8.40	6.39	22.27	6.77
Na_2O	0.22	1.16	7.44	0.20	1.48	7.03	0.16	1.21	7.88
K_2O	0.02	0.02	0.24	0.00	0.00	0.29	0.00	0.00	0.29
Total	100.27	100.75	99.22	100.96	100.03	100.54	100.53	100.31	99.65

Sample	**059a**								
twq filename	**059a-3**			**059a-31**			**059a-4**		
mineral	grt3-2	cpx3-4	pl3-2	grt3-5	cpx3-1	pl3-1	grt4-9	cpx4-4	pl4-4
point	core	core	core	rim	rim	rim	core	core	core
SiO_2	39.17	50.81	58.67	38.82	52.21	57.46	39.20	51.40	59.21
Al_2O_3	21.64	4.31	24.75	21.20	3.07	25.58	21.67	3.95	25.07
TiO_2	0.00	0.53	0.06	0.00	0.28	0.00	0.16	0.45	0.00
Cr_2O_3	0.00	0.00	0.00	0.06	0.11	0.07	0.00	0.00	0.00
FeO	24.99	10.66	0.25	25.06	8.61	0.34	25.25	9.37	0.08
MgO	8.20	12.67	0.00	7.45	12.91	0.10	8.16	12.71	0.09
MnO	0.82	0.06	0.11	0.73	0.13	0.00	0.78	0.06	0.00
CaO	6.77	19.98	7.15	6.68	21.99	7.76	6.51	21.13	7.17
Na_2O	0.14	1.32	7.49	0.22	1.08	6.97	0.29	1.31	7.77
K_2O	0.00	0.00	0.32	0.00	0.00	0.40	0.07	0.00	0.35
Total	101.74	100.34	98.81	100.23	100.40	98.68	102.07	100.38	99.73

***Appendix C**: Mineral data from the EMP used in P-T determination for the shear zone rocks continued.*

Sample	**059a**				**065a**					
twq filename	**059a-41**				**065a-1**			**065a-12**		
mineral	grt4-7	cpx4-6	pl4-1		grt1-1	cpx1-5	pl1-5	grt1-8	cpx1-1	pl1-1
point	rim	rim	rim		core	core	core	rim	rim	rim
SiO_2	37.30	52.10	58.50		38.06	50.30	60.39	37.29	52.48	59.26
Al_2O_3	20.45	3.09	25.48		21.06	4.13	25.08	20.65	1.52	24.45
TiO_2	0.07	0.27	0.00		0.00	0.44	0.00	0.05	0.16	0.00
Cr_2O_3	0.00	0.11	0.00		0.05	0.06	0.14	0.03	0.06	0.03
FeO	25.57	8.37	0.18		26.63	9.98	0.13	28.12	7.62	0.27
MgO	7.07	13.07	0.04		6.37	11.38	0.09	4.79	14.41	0.00
MnO	0.86	0.12	0.00		1.03	0.09	0.02	1.12	0.09	0.00
CaO	6.28	21.99	7.36		6.34	20.59	6.23	6.18	21.63	6.22
Na_2O	0.17	1.14	7.48		0.12	1.64	8.45	0.08	0.97	8.39
K_2O	0.06	0.01	0.37		0.01	0.00	0.24	0.00	0.10	0.19
Total	97.83	100.28	99.40		99.67	98.61	100.76	98.30	99.03	98.80

Sample	**065a**						**071**		
twq filename	**065a-2**			**065a-21**			**071-1**		
mineral	grt2-1	cpx2-5	pl2-4	grt2-6	cpx2-1	pl2-2	grt1-1	cpx1-4	pl1-4
point	core	core	core	rim	rim	rim	core	core	core
SiO_2	38.30	49.91	59.50	37.83	52.12	59.41	38.71	51.46	60.16
Al_2O_3	21.20	4.20	24.70	21.09	1.91	24.56	21.16	4.44	24.73
TiO_2	0.11	0.37	0.03	0.15	0.16	0.05	0.15	0.44	0.00
Cr_2O_3	0.00	0.10	0.01	0.06	0.08	0.00	0.02	0.09	0.08
FeO	26.14	10.67	0.06	26.46	9.26	0.17	25.35	10.64	0.28
MgO	6.57	11.55	0.05	5.86	13.65	0.00	7.53	11.89	0.04
MnO	0.87	0.15	0.06	1.04	0.05	0.14	0.79	0.11	0.02
CaO	6.61	20.30	6.22	6.79	21.15	6.29	6.26	20.15	6.49
Na_2O	0.17	1.35	8.21	0.28	1.03	8.22	0.00	1.39	7.76
K_2O	0.00	0.00	0.29	0.00	0.01	0.29	0.00	0.04	0.37
Total	99.97	98.59	99.12	99.54	99.40	99.13	99.97	100.66	99.93

***Appendix C**: Mineral data from the EMP used in P-T determination for the shear zone rocks continued.*

Sample	071								
twq filename	071-12			071-2			071-21		
mineral	grt1-5	cpx1-1	pl1-5	grt2-1	cpx2-4	pl2-4	grt2-5	cpx2-1	pl2-2
point	rim	rim	rim	core	core	core	rim	rim	rim
SiO_2	38.70	51.21	59.30	38.97	51.18	60.28	38.73	51.11	60.52
Al_2O_3	21.17	4.24	25.12	21.58	4.34	23.93	21.52	4.00	23.98
TiO_2	0.09	0.29	0.00	0.11	0.50	0.05	0.01	0.44	0.00
Cr_2O_3	0.03	0.03	0.00	0.04	0.01	0.00	0.06	0.17	0.11
FeO	25.80	9.49	0.34	26.14	10.32	0.00	25.91	9.87	0.25
MgO	7.58	11.74	0.00	7.30	12.16	0.00	7.00	11.84	0.00
MnO	0.87	0.08	0.08	0.81	0.16	0.04	0.86	0.09	0.00
CaO	6.59	20.66	6.76	6.72	20.65	5.62	6.76	20.79	5.80
Na_2O	0.25	1.51	7.40	0.02	1.56	7.17	0.13	1.60	7.94
K_2O	0.00	0.00	0.66	0.04	0.02	1.68	0.00	0.00	0.47
Total	101.09	99.24	99.66	101.73	100.90	98.76	100.99	99.90	99.07

Sample	071								
twq filename	071-3			071-31			071-32		
mineral	grt3-1	cpx3-3	pl3-3	grt3-6	cpx3-1	pl3-2	grt3-5	cpx3-5	pl3-5
point	core	core	core	core	core	core	rim	rim	rim
SiO_2	39.06	51.83	60.32	38.91	51.52	60.84	38.93	51.51	60.95
Al_2O_3	21.54	4.33	24.45	21.42	4.02	24.60	21.44	4.18	24.64
TiO_2	0.10	0.42	0.01	0.17	0.37	0.00	0.15	0.46	0.00
Cr_2O_3	0.06	0.00	0.10	0.02	0.00	0.20	0.07	0.00	0.00
FeO	25.92	9.88	0.13	25.79	9.60	0.30	26.51	9.77	0.14
MgO	7.76	12.28	0.03	7.57	12.30	0.00	6.99	12.36	0.00
MnO	0.74	0.12	0.08	0.71	0.08	0.10	0.81	0.11	0.04
CaO	6.26	21.19	6.38	6.31	20.94	6.24	6.74	21.14	6.04
Na_2O	0.13	1.72	8.06	0.01	1.61	7.81	0.08	1.38	7.82
K_2O	0.01	0.02	0.64	0.00	0.00	0.72	0.03	0.00	0.76
Total	101.59	101.79	100.19	100.91	100.43	100.81	101.74	100.91	100.39

***Appendix C**: Mineral data from the EMP used in P-T determination for the shear zone rocks continued.*

Sample	**072**								
twq filename	**072-1**			**072-12**			**072-2**		
mineral	grt1-1	cpx1-5	pl1-2	grt1-4	cpx1-1	pl1-5	grt2-5	cpx2-5	pl2-3
point	core	core	core	rim	rim	rim	core	core	core
SiO_2	38.99	51.49	60.95	39.17	51.70	60.40	39.24	51.86	60.78
Al_2O_3	21.32	3.62	24.45	21.38	3.79	24.62	21.44	3.59	24.30
TiO_2	0.01	0.30	0.00	0.08	0.40	0.03	0.00	0.26	0.00
Cr_2O_3	0.00	0.12	0.08	0.00	0.04	0.10	0.00	0.09	0.00
FeO	25.81	9.25	0.16	26.36	9.35	0.00	25.90	9.63	0.11
MgO	7.95	12.37	0.00	7.67	12.26	0.00	7.54	12.68	0.00
MnO	0.72	0.15	0.00	0.75	0.11	0.00	0.73	0.16	0.14
CaO	6.26	21.55	6.31	6.16	21.22	6.20	6.28	21.86	5.89
Na_2O	0.08	1.27	8.03	0.18	1.39	8.26	0.14	1.05	8.22
K_2O	0.01	0.00	0.28	0.03	0.01	0.27	0.00	0.01	0.27
Total	101.14	100.12	100.27	101.77	100.27	99.88	101.27	101.18	99.71

Sample	**072**								
twq filename	**072-21**			**072-3**			**072-31**		
mineral	grt2-4	cpx2-1	pl2-1	grt3-1	cpx3-4	pl3-3	grt3-4	cpx3-1	pl3-2
point	rim	rim	rim	core	core	core	rim	rim	rim
SiO_2	39.01	52.18	61.48	38.99	51.47	60.95	38.90	52.08	60.07
Al_2O_3	21.49	3.68	23.97	21.23	3.77	24.61	21.42	3.66	24.72
TiO_2	0.08	0.39	0.00	0.03	0.24	0.00	0.16	0.43	0.01
Cr_2O_3	0.00	0.06	0.03	0.00	0.10	0.11	0.06	0.15	0.15
FeO	26.68	9.96	0.10	25.93	9.42	0.02	26.47	9.44	0.22
MgO	7.21	12.77	0.00	7.85	12.15	0.02	7.54	12.59	0.00
MnO	0.79	0.13	0.00	0.70	0.14	0.07	0.71	0.07	0.00
CaO	6.20	20.88	5.65	6.37	21.54	6.07	6.24	21.23	6.69
Na_2O	0.07	1.26	8.30	0.14	1.21	7.82	0.15	1.42	7.86
K_2O	0.01	0.00	0.27	0.00	0.02	0.41	0.00	0.00	0.41
Total	101.53	101.30	99.81	101.25	100.07	100.07	101.65	101.07	100.13

***Appendix C**: Mineral data from the EMP used in P-T determination for the shear zone rocks continued.*

Sample	**072**							**086-1**			
twq filename	**072-4**			**072-41**				**086-1-1**			
mineral	grt4-4	cpx4-4	pl4-2	grt4-6	cpx4-1	pl4-5		grt2-4	cpx1-5	amp1-3	pl4-2
point	core	core	core	rim	rim	rim		core	core	core	core
SiO_2	39.24	51.76	61.42	38.81	51.75	61.55		38.58	49.94	41.46	60.93
Al_2O_3	21.58	3.46	24.50	21.49	3.53	24.36		20.92	4.60	12.34	24.48
TiO_2	0.08	0.27	0.12	0.10	0.28	0.02		0.23	0.18	1.72	0.02
Cr_2O_3	0.00	0.04	0.00	0.00	0.03	0.00		0.00	0.13	0.00	0.04
FeO	25.77	9.48	0.00	26.80	9.61	0.09		27.94	13.11	19.88	0.07
MgO	8.01	11.99	0.05	6.98	12.30	0.07		5.21	9.67	8.04	0.00
MnO	0.71	0.08	0.03	0.72	0.04	0.00		1.45	0.47	0.16	0.00
CaO	6.28	21.33	6.15	6.36	21.79	5.88		7.55	21.79	11.81	6.93
Na_2O	0.09	1.46	8.15	0.01	1.23	8.35		0.12	0.97	1.47	7.71
K_2O	0.05	0.00	0.40	0.03	0.01	0.36		0.07	0.02	1.97	0.24
Total	101.80	99.87	100.83	101.30	100.56	100.67		102.07	100.88	98.86	100.41

Sample	**086-1**							
twq filename	**086-1-12**				**086-1-2**			
mineral	grt1-4	cpx1-1	amp2-1	pl1-2	grt3-1	cpx3-1	amp3-3	pl3-2
point	rim	rim	rim	rim	core	core	core	core
SiO_2	38.64	52.13	41.16	60.62	38.91	50.44	41.74	59.57
Al_2O_3	21.09	3.57	12.94	25.69	20.63	3.82	12.67	25.85
TiO_2	0.06	0.19	1.91	0.15	0.07	0.06	1.83	0.00
Cr_2O_3	0.15	0.08	0.15	0.13	0.04	0.00	0.00	0.05
FeO	25.74	12.53	19.91	0.22	27.98	13.35	19.84	0.63
MgO	3.05	10.27	8.01	0.00	4.52	10.02	8.33	0.00
MnO	3.91	0.24	0.22	0.00	1.62	0.43	0.04	0.00
CaO	10.73	22.71	11.80	7.06	8.23	22.62	11.81	7.33
Na_2O	0.01	1.14	1.66	6.95	0.00	1.02	1.82	6.64
K_2O	0.06	0.08	1.99	0.51	0.00	0.08	1.90	0.50
Total	103.44	102.93	99.76	101.34	102.00	101.85	99.99	100.58

***Appendix C**: Mineral data from the EMP used in P-T determination for the shear zone rocks continued.*

Sample	**086-1**			
twq filename	**086-1-21**			
mineral	grt3-1	cpx2-1	amp3-1	pl3-1
point	rim	rim	rim	rim
SiO_2	38.91	51.10	41.19	61.21
Al_2O_3	20.63	3.85	12.54	24.69
TiO_2	0.07	0.19	1.55	0.19
Cr_2O_3	0.04	0.12	0.00	0.10
FeO	27.98	13.04	19.81	0.66
MgO	4.52	10.25	8.32	0.00
MnO	1.62	0.33	0.22	0.02
CaO	8.23	22.62	11.95	2.36
Na_2O	0.00	1.39	1.68	7.24
K_2O	0.00	0.11	2.09	2.60
Total	102.00	103.00	99.35	99.07

Sample	**090**						
twq filename	**090-1**			**090-2**			
mineral	grt1-3	cpx1-2	pl1-2	grt2-3	cpx2-3	amp2-2	pl2-1
point	core	core	core	core	core	core	core
SiO_2	38.72	51.67	62.27	38.74	51.70	42.01	61.69
Al_2O_3	20.73	3.97	23.64	20.61	3.61	11.03	23.69
TiO_2	0.05	0.35	0.00	0.14	0.28	2.31	0.00
Cr_2O_3	0.00	0.02	0.08	0.00	0.12	0.00	0.00
FeO	27.08	11.13	0.08	27.37	9.81	15.66	0.27
MgO	6.06	11.38	0.00	6.45	11.82	11.01	0.00
MnO	1.09	0.04	0.00	1.20	0.21	0.19	0.03
CaO	6.62	21.13	5.35	6.25	21.71	12.13	5.63
Na_2O	0.00	1.65	8.06	0.03	1.66	1.57	8.54
K_2O	0.03	0.02	0.43	0.00	0.00	1.98	0.40
Total	100.38	101.38	99.91	100.79	100.92	97.89	100.24

***Appendix C**: Mineral data from the EMP used in P-T determination for the shear zone rocks continued.*

Sample	**049**											
twq filename	**049-1**			**049-12**			**049-2**			**049-21**		
mineral	grt1-1	cpx1-2	pl1-3	grt1-3	cpx1-1	pl1-1	grt2-3	cpx2-2	pl2-1	grt2-4	cpx2-1	pl2-3
point	core	core	core	rim	rim	rim	core	core	core	rim	rim	rim
SiO_2	37.71	50.68	59.18	37.93	50.72	58.93	37.73	50.55	58.77	37.73	51.20	59.55
Al_2O_3	20.71	3.21	24.72	20.60	3.00	24.32	20.44	3.23	24.75	20.83	3.02	24.87
TiO_2	0.00	0.28	0.02	0.06	0.26	0.09	0.16	0.26	0.12	0.02	0.20	0.09
Cr_2O_3	0.00	0.18	0.04	0.11	0.08	0.06	0.00	0.15	0.09	0.00	0.15	0.08
FeO	28.20	12.97	0.14	28.00	11.83	0.05	27.65	12.06	0.05	27.92	11.85	0.23
MgO	4.84	10.67	0.00	4.67	10.89	0.00	4.74	10.59	0.05	4.79	11.11	0.01
MnO	1.72	0.26	0.01	1.72	0.21	0.00	1.61	0.16	0.00	1.69	0.26	0.06
CaO	7.12	20.77	6.76	7.13	21.77	6.66	7.36	21.31	6.93	7.20	21.26	6.71
Na_2O	0.11	0.81	7.58	0.07	0.94	7.94	0.00	1.05	7.68	0.03	1.03	8.12
K_2O	0.00	0.00	0.37	0.00	0.00	0.34	0.00	0.01	0.24	0.03	0.00	0.21
Total	100.40	99.82	98.81	100.30	99.71	98.39	99.68	99.38	98.66	100.26	100.07	99.94

Sample	**056**											
twq filename	**056-1**			**056-11**			**056-2**			**056-21**		
mineral	grt1-1	amp1-1	pl1-3	grt1-6	amp1-1	pl1-1	grt2-8	amp2-7	pl2-7	grt2-1	amp2-6	pl2-4
point	core	core	core	rim	rim	rim	core	core	core	rim	rim	rim
SiO_2	38.70	42.29	62.62	38.68	42.29	61.45	39.08	43.05	62.03	39.36	43.79	62.12
Al_2O_3	21.28	12.25	24.97	21.27	12.25	25.48	21.74	12.01	25.06	21.88	12.39	24.65
TiO_2	0.09	1.88	0.00	0.09	1.88	0.04	0.00	1.78	0.00	0.00	1.46	0.00
Cr_2O_3	0.00	0.00	0.02	0.00	0.00	0.09	0.08	0.00	0.00	0.09	0.10	0.10
FeO	28.03	16.65	0.21	27.87	16.65	0.36	28.30	16.32	0.10	28.33	15.66	0.42
MgO	5.56	10.25	0.19	4.71	10.25	0.00	5.46	10.72	0.20	4.91	11.23	0.00
MnO	2.52	0.21	0.03	4.01	0.21	0.00	2.14	0.26	0.00	3.22	0.21	0.05
CaO	5.60	11.55	5.51	5.66	11.55	6.56	5.89	11.42	5.84	5.90	12.14	5.77
Na_2O	0.02	1.77	8.59	0.21	1.77	8.00	0.00	1.73	8.42	0.02	1.58	8.56
K_2O	0.00	1.31	0.17	0.00	1.31	0.24	0.05	1.31	0.20	0.00	1.11	0.10
Total	101.80	98.16	102.32	102.49	98.16	102.22	102.76	98.60	101.84	103.71	99.67	101.78

***Appendix C**: Mineral data from the EMP used in P-T determination for the footwall rocks.*

Sample	**056**							**074**		
twq filename	**056-3**			**056-31**				**074-11**		
mineral	grt3-5	amp3-3	pl3-1	grt3-1	amp3-6	pl3-3		grt1-1	cpx1-4	pl1-4
point	core	core	core	rim	rim	rim		core	core	core
SiO_2	39.13	43.05	62.00	38.56	43.20	62.51		37.77	51.62	61.65
Al_2O_3	21.58	13.14	24.70	21.30	12.57	24.75		21.36	1.32	23.93
TiO_2	0.07	1.74	0.01	0.00	1.93	0.01		0.02	0.12	0.00
Cr_2O_3	0.00	0.20	0.00	0.04	0.03	0.16		0.02	0.04	0.07
FeO	28.98	15.12	0.14	28.40	14.88	0.23		26.86	10.63	0.17
MgO	5.91	11.26	0.00	5.04	10.90	0.00		3.25	11.23	0.05
MnO	1.78	0.01	0.13	3.11	0.35	0.00		1.44	0.10	0.12
CaO	5.93	11.57	5.79	5.73	11.69	5.76		8.87	22.41	4.93
Na_2O	0.18	1.90	8.19	0.09	1.81	8.36		0.15	0.80	9.39
K_2O	0.00	1.30	0.12	0.00	1.11	0.10		0.00	0.00	0.23
Total	103.54	99.28	101.08	102.28	98.46	101.88		99.74	98.27	100.54

Sample	**074**											
twq filename	**074-12**			**074-13**			**074-14**			**074-2**		
mineral	grt1-5	cpx1-8	pl1-9	grt1-4	cpx1-1	pl1-1	grt1-9	cpx1-5	pl1-5	grt2-1	cpx2-4	pl2-4
point	core	core	core	rim	rim	rim	rim	rim	rim	core	core	core
SiO_2	37.41	51.32	61.87	37.41	52.07	60.60	37.41	51.95	60.34	37.77	51.90	61.38
Al_2O_3	21.21	2.07	23.57	21.02	1.34	23.84	20.77	1.21	24.40	21.02	1.98	23.54
TiO_2	0.00	0.19	0.10	0.00	0.18	0.06	0.04	0.02	0.00	0.06	0.15	0.00
Cr_2O_3	0.08	0.13	0.00	0.09	0.03	0.02	0.00	0.05	0.03	0.06	0.01	0.06
FeO	27.22	11.44	0.12	27.73	10.89	0.23	27.94	11.27	0.17	27.15	11.20	0.02
MgO	3.27	10.95	0.07	2.96	11.41	0.04	2.63	11.50	0.14	3.08	10.95	0.00
MnO	1.59	0.11	0.07	1.53	0.19	0.07	1.86	0.16	0.00	1.47	0.14	0.00
CaO	8.67	21.34	4.70	8.73	22.50	5.12	8.74	22.22	5.71	8.82	21.59	4.83
Na_2O	0.08	1.11	9.34	0.37	1.03	8.71	0.20	0.87	8.88	0.14	1.08	9.20
K_2O	0.00	0.00	0.26	0.00	0.00	0.35	0.04	0.00	0.19	0.03	0.00	0.30
Total	99.54	98.66	100.09	99.83	99.65	99.03	99.63	99.26	99.86	99.60	99.01	99.32

***Appendix C**: Mineral data from the EMP used in P-T determination for the footwall rocks continued.*

Sample	**074**											
twq filename	**074-21**			**074-31**			**074-32**			**074-33**		
mineral	grt2-5	cpx2-1	pl2-1	grt3-1	cpx3-5	pl3-4	grt3-9	cpx3-5	pl3-8	grt3-4	cpx3-1	pl3-1
point	rim	rim	rim	core	core	core	core	core	core	rim	rim	rim
SiO_2	37.50	51.92	60.86	37.50	52.04	61.78	37.48	52.04	61.59	37.53	51.95	60.70
Al_2O_3	20.96	1.93	23.79	21.04	1.65	22.93	21.13	1.65	23.47	21.20	2.18	23.76
TiO_2	0.00	0.17	0.00	0.00	0.16	0.00	0.09	0.16	0.00	0.00	0.12	0.00
Cr_2O_3	0.02	0.01	0.00	0.00	0.03	0.00	0.10	0.03	0.00	0.00	0.16	0.02
FeO	27.78	11.35	0.21	26.71	10.77	0.04	27.26	10.77	0.00	28.07	11.54	0.44
MgO	2.92	11.11	0.01	3.33	11.33	0.00	3.03	11.33	0.00	2.92	11.35	0.00
MnO	1.41	0.17	0.06	1.29	0.13	0.01	1.49	0.13	0.03	1.43	0.09	0.00
CaO	8.99	21.74	4.97	8.89	21.92	4.41	8.92	21.92	4.90	8.80	21.51	5.46
Na_2O	0.22	0.87	8.78	0.19	1.09	9.27	0.16	1.09	9.25	0.02	0.86	8.83
K_2O	0.05	0.02	0.31	0.04	0.00	0.35	0.03	0.00	0.24	0.06	0.00	0.27
Total	99.84	99.28	99.00	98.99	99.13	98.79	99.69	99.13	99.47	100.04	99.76	99.49

Sample	**084**								
twq filename	**084-1**			**084-12**			**084-2**		
mineral	grt1-3	cpx1-2	pl1-2	grt1-4	cpx1-1	pl1-2	grt2-3	cpx2-2	pl2-2
point	core	core	core	rim	rim	rim	core	core	core
SiO_2	39.92	51.76	60.68	39.81	51.74	60.68	40.13	51.96	59.63
Al_2O_3	21.42	4.62	24.88	21.60	4.40	24.88	21.57	4.57	24.88
TiO_2	0.03	0.61	0.07	0.03	0.51	0.07	0.00	0.46	0.07
Cr_2O_3	0.00	0.09	0.00	0.00	0.17	0.00	0.00	0.17	0.00
FeO	24.94	10.30	0.02	25.88	9.21	0.02	26.41	9.21	0.14
MgO	6.83	11.37	0.09	6.83	11.64	0.09	6.99	11.78	0.00
MnO	1.09	0.25	0.00	0.86	0.14	0.00	0.97	0.07	0.19
CaO	7.95	20.87	6.80	8.09	22.28	6.80	7.67	22.18	6.75
Na_2O	0.14	2.10	7.56	0.22	1.31	7.56	0.02	1.49	6.67
K_2O	0.03	0.02	0.69	0.00	0.04	0.69	0.00	0.00	1.05
Total	102.35	102.00	100.78	103.33	101.46	100.78	103.76	101.88	99.39

***Appendix C**: Mineral data from the EMP used in P-T determination for the footwall rocks continued.*

Sample	**084**								
twq filename	**084-21**			**084-3**			**084-31**		
mineral	grt2-5	cpx2-3	pl2-1	grt3-10	cpx3-4	pl3-3	grt3-6	cpx3-5	pl3-4
point	rim	rim	rim	core	core	core	rim	rim	rim
SiO_2	40.13	52.07	61.02	39.98	51.97	61.53	39.86	51.87	63.08
Al_2O_3	21.60	4.04	24.63	21.53	4.92	24.24	21.19	4.97	24.51
TiO_2	0.12	0.54	0.00	0.14	0.49	0.00	0.00	0.53	0.00
Cr_2O_3	0.05	0.00	0.00	0.13	0.21	0.00	0.00	0.10	0.02
FeO	26.22	8.90	0.12	24.98	9.81	0.02	25.51	9.06	0.00
MgO	6.68	12.29	0.00	8.44	11.57	0.00	7.67	11.74	0.03
MnO	0.82	0.19	0.20	0.62	0.00	0.00	0.87	0.00	0.00
CaO	7.93	22.30	6.50	6.50	21.51	6.49	7.18	21.92	6.39
Na_2O	0.20	1.04	7.33	0.03	1.47	7.05	0.08	1.73	7.59
K_2O	0.07	0.03	0.54	0.07	0.12	0.40	0.03	0.07	0.54
Total	103.83	101.40	100.33	102.42	102.05	99.72	102.40	101.99	102.15

***Appendix C**: Mineral data from the EMP used in P-T determination for the footwall rocks continued.*

Sample	**122-3**									
twq filename	**122-31**				**122-312**			**122-313**		
mineral	grt1-2	opx1-1	cpx-1	pl1-2	grt1-5	amp1-2	pl1-7	grt1-1	opx1-4	pl1-4
point	core	core	core	core	core	core	core	rim	rim	rim
SiO_2	39.19	52.14	51.87	58.66	38.93	42.90	59.53	39.27	52.42	59.66
Al_2O_3	21.68	1.52	3.45	26.15	21.09	12.10	25.83	21.72	1.28	25.49
TiO_2	0.00	0.08	0.33	0.00	0.08	1.72	0.05	0.03	0.10	0.07
Cr_2O_3	0.02	0.00	0.12	0.06	0.00	0.05	0.00	0.06	0.00	0.00
FeO	27.23	25.83	9.74	0.06	27.49	15.23	0.17	27.57	25.66	0.11
MgO	6.59	20.02	12.51	0.03	6.61	11.27	0.00	6.19	20.03	0.03
MnO	1.30	0.37	0.22	0.03	1.01	0.14	0.00	1.24	0.43	0.00
CaO	6.31	0.45	22.05	8.16	6.52	11.63	7.49	6.16	0.36	7.18
Na_2O	0.14	0.41	0.85	6.90	0.11	1.77	7.14	0.14	0.34	7.66
K_2O	0.02	0.02	0.00	0.30	0.00	1.20	0.39	0.00	0.00	0.40
Total	102.48	100.83	101.15	100.36	101.85	98.01	100.60	102.36	100.61	100.58

Sample	**122-3**								
twq filename	**122-314**			**122-321**			**122-322**		
mineral	grt1-6	amp1-1	pl1-8	grt2-3	cpx2-2	pl2-1	grt2-4	cpx2-1	pl2-2
point	rim	rim	rim	core	core	core	rim	rim	rim
SiO_2	39.06	42.60	58.13	38.68	51.98	57.34	38.82	52.14	58.65
Al_2O_3	21.30	12.56	26.83	21.10	3.26	25.60	21.57	2.65	25.80
TiO_2	0.12	1.85	0.05	0.04	0.30	0.09	0.13	0.28	0.05
Cr_2O_3	0.00	0.15	0.08	0.06	0.17	0.00	0.01	0.12	0.05
FeO	27.03	14.51	0.51	26.52	9.70	0.31	27.58	9.21	0.18
MgO	6.39	11.04	0.05	6.20	12.55	0.05	5.74	13.01	0.02
MnO	1.06	0.02	0.05	0.89	0.16	0.00	1.07	0.17	0.05
CaO	6.53	11.56	8.57	7.07	21.81	7.87	6.84	22.43	7.55
Na_2O	0.19	1.88	6.75	0.14	1.02	6.99	0.03	0.94	7.54
K_2O	0.00	1.18	0.26	0.00	0.00	0.29	0.01	0.07	0.18
Total	101.67	97.35	101.27	100.70	100.93	98.52	101.80	101.03	100.07

***Appendix C**: Mineral data from the EMP used in P-T determination for the hangingwall rocks.*

Sample									
twq filename	**122-323**			**122-324**			**122-325**		
mineral	grt2-6	cpx2-6	pl2-4	grt2-6	cpx2-5	pl2-4	grt2-5	cpx2-7	pl2-8
point	core	core	core	core	core	core	rim	rim	rim
SiO_2	39.09	48.75	58.88	39.09	52.56	58.88	38.57	51.74	59.51
Al_2O_3	21.50	6.82	24.99	21.50	2.38	24.99	21.49	2.63	25.99
TiO_2	0.00	0.91	0.00	0.00	0.18	0.00	0.01	0.22	0.07
Cr_2O_3	0.00	0.00	0.00	0.00	0.15	0.00	0.04	0.10	0.00
FeO	27.23	12.61	1.19	27.23	9.27	1.19	27.82	10.04	0.33
MgO	6.06	12.31	0.00	6.06	13.13	0.00	5.95	12.79	0.09
MnO	0.80	0.06	0.05	0.80	0.14	0.05	0.92	0.10	0.00
CaO	6.74	16.55	6.85	6.74	22.41	6.85	6.60	21.94	7.30
Na_2O	0.13	1.29	7.36	0.13	0.90	7.36	0.05	0.74	7.38
K_2O	0.01	0.33	0.27	0.01	0.02	0.27	0.00	0.00	0.27
Total	101.54	99.63	99.58	101.54	101.13	99.58	101.44	100.29	100.95

Sample	**122-3**						**142**		
twq filename	**122-331**			**122-332**			**142-1**		
mineral	grt3-2	cpx3-2	pl3-6	grt3-4	cpx3-1	pl3-4	grt1-1	cpx1-4	pl1-3
point	core	core	core	rim	rim	rim	core	core	core
SiO_2	39.80	53.25	52.49	39.68	53.05	54.50	38.48	50.89	60.52
Al_2O_3	21.90	2.99	30.28	21.88	3.00	29.16	20.96	3.33	23.99
TiO_2	0.03	0.20	0.00	0.04	0.38	0.00	0.06	0.26	0.01
Cr_2O_3	0.07	0.21	0.06	0.10	0.22	0.04	0.02	0.08	0.05
FeO	22.89	7.21	0.00	23.18	7.23	0.15	27.75	10.90	0.12
MgO	9.19	14.15	0.00	8.81	14.20	0.05	6.26	11.85	0.00
MnO	0.94	0.08	0.03	1.01	0.16	0.00	1.11	0.20	0.00
CaO	6.56	22.48	12.73	6.53	22.18	11.57	6.56	20.97	5.82
Na_2O	0.19	0.91	4.40	0.20	0.85	5.32	0.18	1.54	8.26
K_2O	0.00	0.00	0.03	0.00	0.00	0.03	0.00	0.03	0.29
Total	101.56	101.48	100.01	101.42	101.27	100.83	101.37	100.04	99.08

***Appendix C**: Mineral data from the EMP used in P-T determination for the hangingwall rocks continued.*

Sample	**142**								
twq filename	**142-12**			**142-13**			**142-14**		
mineral	grt1-6	cpx1-1	pl1-2	grt1-8	amp1-3	pl1-4	grt1-7	m(cpx)1-4	pl1-5
point	rim	rim	rim	core	core	core	rim	rim	rim
SiO_2	38.58	51.50	60.27	38.31	41.84	60.60	39.68	51.24	58.93
Al_2O_3	21.05	3.00	24.50	21.09	11.86	24.08	18.16	3.31	25.57
TiO_2	0.06	0.28	0.06	0.05	2.05	0.07	0.01	0.33	0.05
Cr_2O_3	0.04	0.06	0.00	0.00	0.02	0.05	0.00	0.16	0.04
FeO	27.34	11.03	0.27	27.83	16.34	0.09	26.16	11.14	0.03
MgO	5.89	12.18	0.03	5.93	10.19	0.00	6.75	11.75	0.00
MnO	1.10	0.15	0.00	0.97	0.21	0.05	0.87	0.18	0.00
CaO	6.89	21.03	6.22	6.77	11.50	5.94	8.15	21.37	7.52
Na_2O	0.20	1.35	8.47	0.19	1.80	8.30	0.34	1.32	7.44
K_2O	0.00	0.00	0.31	0.01	1.62	0.22	0.00	0.01	0.15
Total	101.15	100.59	100.14	101.14	97.42	99.41	100.14	100.81	99.73

Sample	**142**								
twq filename	**142-2**			**142-21**			**142-22**		
mineral	grt2-1	cpx2-2	pl2-2	grt2-5	cpx2-1	pl2-1	grt2-1	amp2-2	pl2-2
point	core	core	core	rim	rim	rim	core	core	core
SiO_2	38.41	53.17	60.47	38.24	52.75	59.88	38.41	41.26	60.47
Al_2O_3	20.89	1.61	24.04	20.95	2.02	24.48	20.89	11.79	24.04
TiO_2	0.03	0.07	0.04	0.03	0.16	0.01	0.03	2.17	0.04
Cr_2O_3	0.00	0.06	0.00	0.04	0.16	0.09	0.00	0.00	0.00
FeO	27.71	9.87	0.43	27.70	9.49	0.52	27.71	16.91	0.43
MgO	5.94	12.50	0.07	5.59	13.48	0.00	5.94	9.88	0.07
MnO	0.99	0.15	0.01	1.08	0.08	0.00	0.99	0.16	0.01
CaO	6.58	23.17	5.87	6.73	22.13	6.33	6.58	11.38	5.87
Na_2O	0.12	0.92	8.37	0.10	0.93	7.83	0.12	1.97	8.37
K_2O	0.01	0.01	0.32	0.00	0.01	0.36	0.01	1.57	0.32
Total	100.68	101.53	99.63	100.46	101.20	99.51	100.68	97.09	99.63

***Appendix C**: Mineral data from the EMP used in P-T determination for the hangingwall rocks continued.*

Sample	**142**					
twq filename	**142-3**			**142-31**		
mineral	grt3-3	cpx3-4	pl3-3	grt3-6	cpx3-1	pl3-1
point	core	core	core	rim	rim	rim
SiO_2	38.46	51.21	60.40	37.90	51.14	60.61
Al_2O_3	21.11	3.44	24.26	20.84	3.33	24.47
TiO_2	0.06	0.28	0.07	0.09	0.31	0.00
Cr_2O_3	0.09	0.07	0.00	0.09	0.07	0.05
FeO	27.57	12.55	0.23	28.45	10.69	0.23
MgO	6.36	12.09	0.00	5.41	11.87	0.14
MnO	0.99	0.10	0.05	1.03	0.09	0.00
CaO	6.61	19.51	5.87	6.58	21.59	6.30
Na_2O	0.28	1.06	8.27	0.20	1.23	8.04
K_2O	0.00	0.03	0.28	0.00	0.00	0.18
Total	101.53	100.35	99.43	100.58	100.32	100.02

Sample	**196a**									
twq filename	**196a-11**				**196a-12**			**196a-13**		
mineral	grt1-2	cpx1-5	x(am)1-2	pl1-4	grt1-7	cpx1-3	pl1-2	grt1-3	x(am)1-1	pl1-2
point	core	core	core	core	rim	rim	rim	rim	rim	rim
SiO_2	39.12	52.21	43.64	57.54	38.82	52.12	57.83	38.36	44.10	57.83
Al_2O_3	21.33	2.83	11.65	27.24	21.33	2.36	26.63	21.20	11.54	26.63
TiO_2	0.02	0.29	2.32	0.00	0.02	0.23	0.02	0.07	2.25	0.02
Cr_2O_3	0.00	0.00	0.00	0.10	0.07	0.16	0.00	0.03	0.05	0.00
FeO	26.57	9.61	13.04	0.04	26.67	9.37	0.22	26.65	12.26	0.22
MgO	6.42	12.78	12.65	0.09	6.30	13.08	0.03	6.25	12.85	0.03
MnO	1.75	0.26	0.12	0.05	1.79	0.22	0.09	1.66	0.10	0.09
CaO	6.62	21.85	11.46	8.96	6.80	22.13	8.79	6.52	11.40	8.79
Na_2O	0.13	1.02	2.35	6.99	0.15	0.88	7.13	0.16	2.07	7.13
K_2O	0.00	0.02	1.01	0.19	0.00	0.00	0.17	0.00	0.95	0.17
Total	101.96	100.87	98.26	101.18	101.95	100.55	100.90	100.88	97.58	100.90

***Appendix C**: Mineral data from the EMP used in P-T determination for the hangingwall rocks continued.*

Sample	**196a**								
twq filename	**196a-14**			**196a-15**			**196a-21**		
mineral	grt1-8	amp1-4	pl1-8	grt1-12	amp1-1	pl1-5	grt2-2	cpx2-2	pl2-2
point	core	core	core	rim	rim	rim	core	core	core
SiO_2	38.43	43.52	57.59	38.36	42.82	57.99	38.59	52.44	58.01
Al_2O_3	21.39	12.03	26.34	21.06	11.75	26.43	21.21	1.98	26.52
TiO_2	0.07	1.98	0.00	0.06	2.42	0.03	0.07	0.22	0.06
Cr_2O_3	0.02	0.05	0.02	0.06	0.00	0.10	0.00	0.13	0.12
FeO	26.89	14.57	0.18	27.55	14.25	0.10	26.89	8.01	0.59
MgO	5.89	11.98	0.00	5.56	11.61	0.06	6.45	13.61	0.14
MnO	1.81	0.07	0.02	1.78	0.19	0.00	1.37	0.07	0.00
CaO	6.79	11.68	8.55	6.79	11.32	8.57	6.64	23.23	8.37
Na_2O	0.13	2.04	7.03	0.23	2.05	7.15	0.17	0.68	7.25
K_2O	0.00	0.93	0.19	0.00	1.02	0.16	0.02	0.00	0.08
Total	101.42	98.83	99.92	101.47	97.44	100.59	101.42	100.36	101.13

Sample	**196a**								
twq filename	**196a-22**			**196a-23**			**196a-24**		
mineral	grt2-1	x(am)2-3	pl2-1	grt2-4	cpx2-6	pl2-6	grt2-7	cpx2-4	pl2-4
point	rim	rim	rim	core	core	core	rim	rim	rim
SiO_2	38.28	48.23	57.50	38.86	51.43	57.08	38.58	52.38	56.87
Al_2O_3	21.12	9.03	26.59	21.44	2.97	26.68	21.49	2.49	26.19
TiO_2	0.10	0.67	0.08	0.06	0.34	0.03	0.00	0.25	0.00
Cr_2O_3	0.03	0.00	0.01	0.01	0.00	0.00	0.05	0.05	0.02
FeO	26.88	11.38	0.37	26.08	9.84	0.01	26.80	9.90	0.41
MgO	6.10	15.08	0.03	6.72	12.55	0.09	6.52	13.08	0.08
MnO	1.42	0.00	0.02	1.36	0.15	0.07	1.28	0.20	0.04
CaO	6.85	12.38	8.46	6.72	21.80	9.12	6.82	21.65	8.62
Na_2O	0.26	1.56	7.45	0.27	1.03	7.00	0.14	0.98	6.71
K_2O	0.02	0.41	0.08	0.00	0.00	0.15	0.06	0.03	0.13
Total	101.06	98.74	100.60	101.51	100.11	100.24	101.72	101.00	99.08

***Appendix C**: Mineral data from the EMP used in P-T determination for the hangingwall rocks continued.*

Sample	**196a**								
twq filename	**196a-25**			**196a-26**			**196a-31**		
mineral	grt2-10	amp2-3	pl2-6	grt2-9	amp2-4	pl2-3	grt3-1	cpx3-4	pl3-2
point	core	core	core	rim	rim	rim	core	core	core
SiO_2	38.45	43.09	57.08	38.34	44.03	57.42	38.67	52.01	57.65
Al_2O_3	21.34	12.00	26.68	21.33	11.18	26.62	21.44	2.82	26.63
TiO_2	0.08	1.96	0.03	0.01	1.61	0.02	0.01	0.31	0.01
Cr_2O_3	0.00	0.09	0.00	0.10	0.10	0.07	0.03	0.13	0.00
FeO	26.88	14.51	0.01	26.71	14.37	0.29	25.85	9.49	0.21
MgO	6.32	11.42	0.09	5.96	12.20	0.00	6.82	12.95	0.01
MnO	1.37	0.04	0.07	1.28	0.03	0.12	1.45	0.12	0.03
CaO	6.96	11.65	9.12	7.07	11.67	8.78	6.59	22.03	8.55
Na_2O	0.19	1.92	7.00	0.29	2.03	6.81	0.21	1.02	7.25
K_2O	0.00	1.09	0.15	0.01	0.89	0.06	0.00	0.00	0.11
Total	101.59	97.76	100.24	101.12	98.12	100.19	101.07	100.88	100.45

Sample	**196a**								
twq filename	**196a-32**			**196a-33**			**196a-34**		
mineral	grt3-5	cpx3-1	pl3-1	grt3-7	cpx3-4	pl3-6	grt3-10	amp3-1	pl3-4
point	rim	rim	rim	core	core	core	rim	rim	rim
SiO_2	38.56	52.00	57.22	38.67	52.01	57.44	38.31	43.57	57.80
Al_2O_3	21.17	2.36	26.36	21.56	2.82	26.68	21.37	11.84	26.58
TiO_2	0.00	0.19	0.01	0.06	0.31	0.00	0.08	1.90	0.00
Cr_2O_3	0.04	0.09	0.01	0.04	0.13	0.00	0.06	0.02	0.00
FeO	26.04	8.97	0.17	26.50	9.49	0.13	27.70	13.97	0.19
MgO	6.61	13.33	0.08	6.71	12.95	0.23	5.68	11.82	0.00
MnO	1.31	0.16	0.00	1.28	0.12	0.00	1.43	0.01	0.00
CaO	6.78	21.96	8.54	6.58	22.03	8.78	6.83	11.75	8.67
Na_2O	0.14	1.06	7.07	0.06	1.02	7.24	0.30	2.01	7.12
K_2O	0.04	0.02	0.07	0.05	0.00	0.17	0.00	0.98	0.12
Total	100.68	100.15	99.54	101.49	100.88	100.68	101.75	97.86	100.47

***Appendix C**: Mineral data from the EMP used in P-T determination for the hangingwall rocks continued.*

Appendix D

In this appendix, a detailed description of the petrography of the 18 samples that were analysed for *P-T* determinations is provided. Those samples include those from the footwall (JK99-049, JK99-056, JK99-074 and JK99-084), hangingwall (JK99-122-3, JK99-142 and JK99-196a) and the shear zone (JK99-008, JK99-012, JK99-017, JK99-028, JK99-029, JK99-059a, JK99-065a, JK99-071, JK99-072, JK99-086 and JK99-090).

Footwall Samples

JK99-049: Collected from the southern shore of Grand Lake in the southeast part of the field area in the Lake Melville terrane, this sample was obtained from a layered mafic gneiss. The alternating layers of felsic to mafic gneiss are composed of felsic gneiss comprising the mineralogy Pl, Grt, Cam (Cpx?) and Qtz and the mafic gneiss component is composed of Cam, Bt, Grt with discrete pods of Cpx-OPx, Grt and Pl.

In thin section the sample contains the mineralogy Grt-Cpx-Cam-Pl- Fe-Ti oxides with minor Qtz and accessory Rt. This sample contains distinct domains, where the assemblage Grt-Cpx-Cam-Pl-Qtz form one domain and Cpx-Cam-Pl constitutes the second zone. Two textural varieties of Grt are present; 1) anhedral, inclusion rich with Pl-Qtz-opaque-Cpx-Cam and 2) anhedral as well, however the inclusions are much larger. Both varieties are skeletal in texture, implying fast growth of Grt. Cpx grains are pale green in plane polarized light and display mild micro-deformation characteristics. Grains of Cpx are partially replaced by Cam in the Cpx-Cam-Pl domain, whereas there is evidence for partial Cpx replacement of Cam in the Grt-Cpx domain. SPO grains of Cam define the mild fabric present in the sample and is principally restricted to Cpx-Cam-Pl domain. Pl shows patchy extinction, annealing and lamellar twinning. Qtz is restricted to the Grt-Cpx zone, implying synchronous crystallization of Grt and Cpx. This texture is inferred to reflect an increase in

temperature following the reaction:

$$Cam + Pl + Qtz \rightarrow Grt + Cpx + H_2O$$

or possibly the result of a change in fluid activity/composition as discussed in Chapter 6.

JK99-056: This sample was collected from the southern shore of Grand Lake, in the Lake Melville terrane, from a Northwest River dyke hosted by layered mafic/felsic rocks located near to the presumed location of the shear zone. The dyke was observed to contain melt pockets containing Opx-Cpx-Pl in a Grt-Cam-Pl matrix.

In thin section, the dyke is composed of the assemblage: Cam-Grt-Pl-Bt-Qtz with accessory Ap and Fe-Ti oxide. Grt occurs as anhedral grains displaying skeletal type growth with inclusions of Qtz-Bt±Pl. Cam grains display tan to green pleochroism and contain inclusions of Qtz-Bt-Pl. Bt grains principally define the foliation in the sample forming apparent *C-S* fabrics. Cam and Grt crystals appear to be stable with Pl and thus this sample was chosen for geothermobarometry to constrain the *P-T* conditions for amphibolitization that is present in many rocks in the field area.

JK99-074: This sample was collected from an outcrop north of the shear zone in the Groswater Bay terrane. The foliated dioritic outcrop is composed of the assemblage Pl-Cam-Bt-Grt. The outcrop was observed to change composition over its extent, implying that previous to Grenvillian deformation and metamorphism, the rock was part of a large diorite-granodiorite pluton possibly related to the Trans-Labrador Batholith.

In thin section, the sample is composed of Opx-Cpx-Grt-Bt-Pl-Qtz with accessory Ap-Zrn and Fe-Ti oxides. The rock is fine to medium grained where the grains are equigranular and anhedral. Opx grains are partially replaced by Bt. All grains of Opx exhibit pale-pink pleochroism and when in contact with Bt, Opx may be zoned. Cpx is difficult to distinguish from Opx in plane polarized light but reveals its higher birefringence in cross polarized light. Grains of Cpx are also stable in the assemblage and are found in contact with garnet in many areas. Grt grains, partially replaced by Bt, are slightly larger that the pyroxene crystals and contain inclusions of Qtz-Bt. Pl grains exhibit normal zoning, lamellar twinning

and contain inclusions of Kfs. This texture is interpreted to be the result feldspar annealing during a metamorphic episode (Grenvillian or Labradorian orogeny?) where Kfs inclusions are inferred to have been Ser grains previous to Grenvillian metamorphism.

JK99-084: This sample was taken from an outcrop composed of a mafic component of the Groswater Bay orthogneiss, adjacent to the shear zone on the north shore of Grand Lake. The rock contains Grt-Cam-Cpx-Bt-Pl and is strongly deformed.

In thin section the mineralogy is the same as reported above with accessory Ap, Zrn Fe-Ti oxides and Rt. Large (up to ~1cm) anhedral Grt porphyroblasts contain inclusions of Cpx- Fe-Ti oxide-Pl-Rt±Qtz and are wrapped by the mylonitic fabric. SPO grains of Cam and Cpx grains define the foliation. Grt and Cpx are inferred to be in equilibrium due to inclusions of Cpx in Grt and the lack of discernable evidence of reaction between the two phases. The presence of secondary Cam and Pl suggests the general reaction:

$$Cpx + Grt + H_2O \rightarrow Cam + Pl + Qtz$$

occurred, inferred to be the result of cooling and hydration along the retrograde *P-T* path. Based on the textures present in this sample and the available U-Pb data set, it is inferred that this sample may have experienced both the Ottawan and the Rigolet orogeny, although this rock has not been directly dated.

Hangingwall Samples

JK99-122-3: This sample was collected along the Cape Caribou River forestry access road at the same locality that the U-Pb sample C-050AM was taken. The outcrop is composed of three distinct rocks types, namely the recrystallized gabbro-diorite layer, pegmatites and Northwest River dykes. The host rock is cut by both dyke and pegmatite but the dyke is also cut by the same pegmatites, implying that the host rock is oldest and the pegmatite the youngest. The host rock is composed of Pl-Cam-Cpx-Opx-Grt-Bt, the pegmatites are primarily composed of Pl-Kfs-Qtz-Bt and the dykes are fine grained with a

Pl-Cam matrix with Grt-Cpx veining. Knots of Pl present are inferred to be a relic igneous attribute. From the sample that was taken, three thin sections were cut which include the host rock (122-1), the dyke (122-2) and a thin section (122-3) that encompasses both the host and dyke.

The dyke and the host rock were investigated for suitability of geothermobarometry and the dyke unfortunately lacked free Qtz and was unsuitable. The host rock has no discernable foliation and is composed of the peak assemblage Cpx-Opx-Grt-Cam-Bt-Pl-Qtz with accessory Ap, Fe-Ti oxides and Zrn. Both Cpx and Opx are anhedral in form, vary in crystal size and are found as inclusions in Grt. Grt porphyroblasts are anhedral and form agglomerations with Cpx and Opx near the contact with the dyke. Grt growth at this contact is inferred to be possibly related to the Grt-Cpx veins that continue from within the dyke into the host rock. Qtz is commonly associated with Grt and Cpx and less commonly with Grt-Opx. It is inferred that Grt, Opx, Cpx ± Cam were in equilibrium and thus the sample was chosen for geothermobarometry.

JK99-142: This sample was collected from a Northwest River dyke along the Cape Caribou River forestry access roads at the same location as the U-Pb sample C-050D. The dyke is composed of Cam-Pl with Grt-Cpx veins similar to the veins observed in other dykes in the CCRA.

In thin section there is a very slight foliation observed by the alignment of Cam grains. Pl crystals retain lamellar twins with most grains showing patchy extinction. The veins contain Grt-Cpx-Pl-Qtz and Cal. Grt is subhedral in form and may contain inclusions of Cpx-Pl±Qtz. Cpx is partially retrogressed, although this degradation is interpreted to be the result of hydration by fluids during a late stage of fluid ingression that also deposited Cal. The vein assemblage implies that the growth of Grt and Cpx may have been facilitated by the presence of CO_2-bearing fluids that allowed the production of Grt and Cpx as a result of a change in fluid composition/activity as discussed in Chapter 6. Despite the apparent instability of Cpx, it was assumed that Grt and Cpx grew together and were stable and would yield peak metamorphic conditions upon application of geothermobarometry.

JK99-196a: This sample was taken from outcrop exposures along the Grand Lake forestry access road. At the sample location a Northwest River dyke is present hosted by a host rock composed of Opx-Grt-Cam-Bt-Pl. The dyke is composed of Pl-Cam-Bt with irregular Grt-Cpx veins.

The dyke was chosen to test for suitability for geothermobarometry as it is assumed that the dyke would better record Grenvillian metamorphism. The matrix of the dyke is composed of the mineralogy Cam-Opx-Pl and Fe-Ti oxides. The fabric is defined by the SPO of cam grains that display the typical Hbl pleochroism and contain inclusions of Fe-Ti oxides. Granoblastic Opx grains are smaller relative to Cam and display typical pale-pink pleochroism. Opx appears to be forming at the expense of amphibole implying dehydration as a result of an increase in temperature. Pl crystals are granoblastic, normal zoned and may preserve lamellar twinning. The veins are composed of Grt-Cpx-Pl-Qtz where Grt porphyroblasts are subhedral and contain inclusions of Cpx-Cam-Pl-Qtz. Cpx appears to have been in equilibrium with Grt but is some parts is retrogressed. Similar to other dykes in the field area these veins are inferred to reflect a domainal change in the activity of H_2O as discussed in Chapter 6. These veins were chosen for analysis to yield *P-T* estimates for the formation of the veins and thus the effects of metamorphism related to thrusting on the eastern flank of the CCRA.

Shear Zone Samples

JK99-008: This sample was obtained from the mylonitic gneiss at the lowest level of the shear zone adjacent to the contact with the footwall orthogneisses along the nearly 100% exposed shear zone at Big Point, Grand Lake. The outcrop is composed of alternating layers of amphibolite and felsic rock.

In thin section, the amphibolite layers are composed of the assemblage Grt-Cpx-Cam-Bt-Pl and the felsic layers contain Pl-Qtz±Kfs±Grt. Fe-Ti oxides, Zrn, Ap are present as accessory phases and Ep occurs as a retrograde phase together with secondary Cam. In the

amphibolite layers Grt occurs as ~3mm in diameter subhedral crystals that contain inclusions of Fe-Ti oxides and Cpx. SPO crystals of Cpx, partially replaced by a secondary Cam, define the mylonitic foliation together with Cam, implying that some Cam was in equilibrium with Cpx and Grt during shearing. Pl occurs as sub millimetre granoblastic grains. Qtz principally occurs as stringers in the felsic layers or as inclusions in some Grt porphyroblasts in the amphibolite layer. It is inferred that Grt-Cpx-Cam-Pl±Qtz assemblage was stable during shearing and would yield peak metamorphic conditions for thrusting in the lower structural sections of the shear zone and thus this sample was chosen for geothermobarometry.

JK99-012: This sample was taken from the shear zone at Big Point, approximately 75 metres north along the shore from sample 008. The rock type is similar to that of 008, however at this locality there are large (up to 3cm) porphyroblasts of Grt that occur throughout the outcrop together with much smaller garnet porphyroblasts. Also at this outcrop there is evidence for two ductile shearing events as discussed in Chapter 4 of this study.

In thin section the mineralogy present in the rocks is Grt-Cpx-Opx-Cam-Bt-Pl-Qtz with accessory Fe-Ti oxides, Ap and Zrn. Grt occurs as three textural varieties; the first as large anhedral porphyroblasts (~1 cm diameter) that contain inclusions of Cpx-Pl and Fe-Ti oxides, the second variety occurs as much smaller subhedral porphyroblasts that occur in the mylonitic fabric. The third variety occurs as anhedral skeletal shaped SPO Grt that define the mylonitic foliation. The larger variety of Grt porphyroblasts are wrapped by the mylonitic fabric implying pretectonic growth which is consistent with observations made at the outcrop. Cpx occurs in both the mylonitic fabric as well as inclusions in the large Grt porphyroblast. Those grains in Grt do not show any evidence of deformation and are assumed to have been shielded by the rigid Grt crystal. Cpx in the matrix are shape preferred and define the mylonitic foliation. Those grains occur as large discrete grains with sweeping extinction or as subgrains in the more highly strained portions of the sample. SPO crystals of Opx define the foliation with Cpx and Cam. Opx is principally confined to the less mafic portions of the slide (e.g., where more Pl and Qtz stringers occur). Opx appears to have been

texturally stable during shearing implying that this rock achieved temperatures in excess of 800 °C. This sample was thus chosen for geothermobarometry to obtain the *P-T* conditions the rock experienced during the two ductile shearing events.

JK99-017: This sample was also collected at Big Point at an outcrop with similar alternating layers of mafic and felsic rock with Grt-Cpx-Cam-Pl±Opx in the mafic layers with the felsic layers being composed of Pl-Kfs-Qtz-Grt.

The thin section was cut from a more mafic component of the rock where the layering is not well defined and is only discernable by the lack of or presence of certain minerals. For example in the more mafic parts of the thin section, the mineralogy is Cam-Bt-Pl-Qtz±Grt±Cpx. Otherwise the rock is made up of Grt-Cpx-Pl-Qtz Fe-Ti oxides±Cam±Bt. Grt occurs as subhedral porphyroblasts that may contain inclusions of Fe-Ti oxides. Cpx appears to be stable in the assemblage despite partial replacement by secondary Cam. Cpx occurs as subgrains that occur in the pressure shadows of Grt and Qtz where Pl crystals are granoblastic. Grt-Cpx-Pl±Qtz appear to have been stable during thrusting therefore this sample was chosen for the application of geothermobarometry to obtain peak metamorphic conditions during shearing.

JK99-028: This sample was taken from an outcrop that occurs near the contact with the mafic gneiss unit that lays in the upper structural levels of the shear zone on the northern shore of Grand Lake. The outcrop is composed of alternating layers of mafic and felsic rocks where Cam and Opx were observed to have been stretched out and form the stretching mineral lineation in the outcrop along with Pl-Kfs and Qtz.

In thin section the mineralogy is Grt-Opx-Cpx-Cam-Pl-Qtz with accessory Fe-Ti oxides, Scp, Zrn and Ap. Porphyroblasts of Grt are anhedral, primarily due to resorption, and contain inclusions of Qtz and more rarely Opx. Opx grains also occur in the matrix as SPO crystals that define the foliation with Cpx and Cam where those grains may be partially replaced by secondary Cam. Opx is inferred to occur as a result of the resorption of Grt during decompression via the reaction:

$$Grt + Qtz \rightarrow Opx + Pl$$

Porphyroblastic Grt-Opx and Grt-Cpx together with Pl-Qtz appear to have been stable during thrusting and thus this sample was chosen for application of geothermobarometry to establish the metamorphic conditions experienced by a rock in the upper structural levels of the shear zone.

JK99-029: This sample was taken within close proximity of 028 at the contact with the overlying mafic gneiss unit. This outcrop is composed of the same alternating mafic and felsic layers however there are observed Qtz-rich layers within the mafic layers. The whole outcrop has been folded to produce metre scale open synform-antiform pairs that have their axial planes orientated parallel to the mineral stretching lineation.

The thin section cut from this sample reveals the mineralogy comprising Grt-Cpx-Cam-Bt-Pl±Qtz with accessory Fe-Ti oxides-Ap-Zrn. In the more felsic parts of the sample, Grt occurs as subhedral crystals that may contain inclusions of Cpx-Cam-Pl. Cpx occurs as equigranular granoblastic grains that are found as lense shaped clusters of subgrains in the pressure shadows of Grt where granoblastic Pl grains wrap around those structures. This texture and the SPO of Cam and Bt define the foliation implying that Grt-Cpx-Pl-Cam±Qtz were stable during thrusting. This sample was primarily chosen for geothermobarometry based on this texture which is inferred to have formed during peak metamorphic conditions at the time of thrusting.

JK99-059a: This sample was taken from the outcrop that occurs at Cape Caribou, Grand Lake across from Big Point. The sample was taken at the first possible outcrop that lays to the north of the assumed location of the contact with the footwall and the mylonitic rocks. The outcrop is highly strained and contains alternating mafic and felsic layers similar to the rocks at Big Point. Two samples were taken at this locality and 059a is representative of the mafic rocks.

In thin section the mineralogy that composes the rock is Grt-Cpx-Cam-Opx-Pl-Qtz with accessory Fe-ti oxides-Zrn-Ap. There are two domains present in thin section where one

domain is principally composed of Cam-Opx-Cpx-Pl±Qtz and the second domain is composed of Grt-Cpx-Pl±Qtz±Cam. Opx crystals are hydrated and retrogressed to secondary Cam. Cpx is partially retrogressed to secondary Cam in the Grt-free domain and occurs as larger grains in the second domain. Grt occurs as subhedral grains that contain inclusions of Cpx-Pl±Qtz. Grt and Cpx in this domain are inferred to be the product of an increase in pressure resulting in domainal production of the higher pressure assemblage from the two-pyroxene plus amphibole granulite-facies rock. The general reaction:

$$Pl + Opx \rightarrow Grt + Cpx + Qtz$$

is inferred to have taken place during a later metamorphic event (Rigolet?) that surpassed the pressure achieved during the previous metamorphic episode (Ottawan?) for this rock. However it is acknowledged that the two assemblages (Cam-Opx-Cpx-Pl±Qtz and Grt-Cpx-Pl±Qtz±Cam) coexist for a range of pressures for the continuos reaction above in the CFMASH system (Pattison in press) or due to bulk composition difference in the layering in the rock.

JK99-065a: This sample was also taken at Cape Caribou from an outcrop principally composed of a mafic rock that contains large, 4-5 cm diameter, Grt porphyroblasts. The sample comprises the mineralogy Grt-cam-Cpx-Bt-Pl. This sample is not as highly deformed as those elsewhere along the cape and is inferred to represent a possible low strain zone in the shear zone.

The thin section cut from the sample reveals that the matrix is composed of Opx-Cpx-Cam-Pl and Grt-Cpx-Pl-Qtz occurs in discrete domains interpreted to have been produced by the general reaction:

$$Pl + Opx \rightarrow Grt + Cpx + Qtz$$

inferred to reflect an increase in pressure similar to sample 059a (coexisting due to the continuos reaction and/or bulk composition differences). Opx in the matrix has not undergone retrogression in the two-pyroxene plus amphibole matrix with minor retrogression to secondary Cam. Grt commonly occurs as collars around Fe-Ti oxides and contains inclusions of Qtz-Pl and may also be found in contact with grains of Cpx that were produced

via the reaction given above. Based on this texture this sample was chosen for geothermobarometry to establish the peak metamorphic conditions of a second metamorphic event.

JK99-071: This sample was taken from one of the last outcrops visited along the south shore of Grand Lake in the basal granitoid gneiss unit. The sample contains the mineralogy Cam-Grt-Pl±Kfs±Qtz in a highly strained fabric.

In thin section the mineralogy is Grt-Cpx-Cam-Pl-Qtz-Scp with accessory Fe-Ti oxides-Bt-Ap-Zrn. Grt occurs in three textural varieties where one variety is characterized by euhedral to subhedral grains that may contain inclusions of Cpx-Pl-Ap±Qtz. The second variety are anhedral grains, with resorbed rims, that are interspersed with grains of Cpx. The third variety are grains that contain many inclusions of Pl-Qtz and are rarely subhedral in shape. The second variety is interpreted to be the oldest in the rock possibly related to an earlier metamorphic event (Labradorian? or Ottawan?). The SPO of Cpx grains define the foliation and those grains exhibit microstructures including subgrain formation, tiltwall boundaries and patchy extinction. Cam grains are also SPO and define the foliation with Cpx implying that Cam was stable during shearing. Pl grains have curved to straight grain boundaries and are seriate when in contact with Qtz. Qtz forms discrete grains in the matrix and do not define the foliation, suggesting that the rock was annealed after the previous deformation episode. Scp crystals are sometimes found in association with Cpx however it is interpreted that Scp growth occurred with the production of secondary Cam in the rock. Based on the textures in this rock is it assumed that Grt-Cpx-Pl-Qtz was in equilibrium during shearing and would yield the *P-T* conditions for thrusting near the nose of the CCRA.

JK99-072: This sample was taken from an outcrop in close proximity to 071 at the last outcrop before the assumed location of the contact of the CCRA with the footwall rocks. The outcrop is very similar in appearance to 071 and was observed contain a similar mineralogical assemblage plus Opx, but was finer grained.

In thin section the mineralogy of the sample is Grt-Cpx-Pl-Qtz-Scp-Cam±Opx with

accessory Ap-Zrn and Fe-Ti oxides. Porphyroblasts of grt occur as subhedral to anhedral grains that contain inclusions of Qtz-Pl-Cpx. SPO grains of Cpx define the foliation and are found in the pressure shadows of Grt or wrapping around garnet. Cpx grains have undergone subgrain formation and those individual grains may also show evidence for sweeping extinction and further subgrain formation. Pl grains have also undergone subgrain formation and in parts of the thin section form granoblastic textures. Qtz occurs as SPO crystals defining the foliation with Cpx and in parts of the sample, Qtz grains are LPO. Grains of Scp also define the foliation with a late amphibole and both are inferred to have grown during a late stage fluid ingression. Grains of Opx are retrogressed and show evidence for hydration, likely the product of Scp-Cam growth during the late stages of metamorphism. Opx tends to occur separately from Grt and Cpx but is still inferred to have formed part of the peak metamorphic assemblage in the rock It is inferred that Grt-Cpx-Opx-Pl-Qtz were stable during peak metamorphism and intense shearing, thus this sample was chosen for geothermobarometry principally due to the syntectonic textures.

JK99-086: This sample was taken from an outcrop at the northern exposure of the shear zone on Grand Lake at the lowest structural part of the mylonitic rocks. The outcrop is composed of similar rocks found at Big Point, namely the alternating mafic and felsic layers, however in this outcrop, large (~8 cm) Grt porphyroblasts wrapped by the mylonitic foliation were observed implying that garnet was present previous to the intense mylonite development.

The thin section was cut from the mafic component of the hand specimen and yields the mineralogy: Grt-Cam-Cpx-Pl-Bt±Qtz with accessory Zrn-Ttn-Ap-Fe-Ti oxides. There exists two domains in the section defined principally by the type of Cam and mineralogy. In the first domain, Cam grains define the foliation, characterized by pale green-turquoise-tan pleochroism, and occur with Pl grains and retrogressed grains of Cpx. The second domain is where the Cam is characterized by the more typical Hbl pleochroism, tan to dark-green, and is poikiloblastic with Pl-Qtz. Grt in this zone occurs as heavily resorbed crystals surrounded by a collar of partially sericitized Pl that contains many euhedral Ap crystals. Pl

crystals found away from theses zone typically do not show any evidence for sericitization implying that the Pl collars are a secondary Pl of a more calcic composition from that of the matrix Pl. Cpx grains are partially replaced by Cam and are principally observed to occur in Cam rich zones that form an irregular collar around Pl and Grt. The texture involving resorbed Grt surrounded by Pl then Cam with Cpx is inferred to be the result of the general reaction:

$$Grt + Cpx + H_2O \rightarrow Hbl + Pl + Qtz$$

interpreted to have been the result of cooling and hydeation in the shear zone during retrogression. It is inferred from this sample that Grt-Cpx-Pl±Qtz were stable during peak metamorphic conditions and Grt-Cam-Pl-Qtz would yield the conditions for decompression that would give the *P-T* path for this part of the shear zone.

JK99-090: This sample was taken from an outcrop in the mafic gneiss unit at the contact with the upper levels of the mylonitic rocks at the northern exposure of the shear zone, Grand Lake. The outcrop comprises the alternating mafic and felsic layering typical to this unit where the mafic layers were observed to contain Grt-Cpx-Cam-Bt-Pl and the felsic layers contain Pl-Bt-Qtz.

The thin section was cut from the mafic component of the sample and yields the mineralogy: Grt-Cpx-Cam-Pl-Qtz±Bt where SPO crystals of Cpx and Cam define the mylonitic foliation. Grt occurs as anhedral grains that contain Cpx-Pl-Qtz inclusions and has an overall lenticular shape that also defines the foliation. Cpx grains occur in three textural varieties. The first variety are Cpx grains in the matrix with lenticular shapes defining the foliation that are partially replaced by secondary Cam. The second variety occurs as larger (~5mm) grains that exhibit exsolution lamellae and grain boundary adjustments in the form of subgrain formation. The third variety occurs as grains that have completely undergone subgrain formation and form an undulating layer of Cpx. Pl occurs as granoblastic grains that may retain lamellar twinning and show patchy extinction and twin gliding. Qtz occurs as stringers that define the foliation and show patchy extinction. This sample shows the general reaction:

$$Grt + Cpx + H_2O \rightarrow Hbl + Pl + Qtz$$

interpreted to reflect a stage of cooling and hydration after peak metamorphism similar to other samples investigated from the field area. This sample was chosen for geothermobarometry based on the interpretation that Grt-Cpx-Pl-Qtz was stable during peak metamorphic conditions and to establish the effects of Grenvillian thrusting in the northern part of the mafic gneiss unit of the CCRA.

Appendix E

All Fe as Fe^{2+} vs recalculated Fe^{3+} P-T Determinations

This appendix displays the results of *P-T* estimates for 13 mineral pairs in 4 samples obtained using mineral analyses for which Fe^{3+} was recalculated. Table E1 contains the results of ferric iron recalculation for garnet, pyroxene (after Droop 1987) and amphibole (after Leake et al. 1997) analyses in these samples. These recalculated analyses were then used to obtain *P-T* estimates that are compared the *all ferrous P-T* estimates. This test was carried out to determine the approximate range of *P-T* estimates by the two methods and to assess the two approaches.

The 13 mineral pairs are from samples JK99-029-1, 056, 071and 142. Samples029-1, 071 and 142 were chosen because they employed the GCPQ calibration and yielded consistent apparent peak temperature estimates using the *all ferrous* assumption. In sample 056, the GHPQ calibration is used. In addition to the GCPQ assemblage, sample also 142 contains two GHPQ mineral pairs allowing cross-referencing between the two calibrations. All mineral analyses (Table E-1) represent the compositions of mineral cores that are inferred to have equilibrated during peak metamorphism. The resultant *P-T* estimates are shown in Table E-2.

Sample	twq filename	Mineral	Label	SiO_2	Al_2O_3	Cr_2O_3	TiO_2	Fe_2O_3	FeO	MgO	MnO	CaO	K_2O	Na_2O	Total
029-1	029-1-1c	grt1-4	core	38.78	21.04	0.06	0.05	1.96	25.34	5.72	0.74	7.60	0.00	0.09	101.38
		cpx1-3	core	50.86	3.89	0.16	0.37	3.39	8.68	11.02	0.15	21.64	0.01	1.07	101.24
		pl1-3	core	60.90	24.84	0.00	0.00	0.00	0.09	0.09	0.00	6.44	0.37	7.94	100.67
	029-1-2c	grt2-9	core	39.23	21.80	0.09	0.12	1.18	24.32	7.52	0.71	6.70	0.02	0.00	101.68
		cpx2-3	core	51.71	4.63	0.12	0.39	2.85	6.47	12.30	0.11	21.64	0.00	1.29	101.50
		pl2-2	core	61.31	24.77	0.00	0.07	0.00	0.04	0.02	0.01	6.14	0.37	7.93	100.68
	029-1-41c	grt4-2	core	38.86	21.11	0.12	0.09	2.34	25.06	5.54	0.74	8.12	0.00	0.11	102.09
		cpx4-6	core	51.40	3.44	0.15	0.31	3.32	8.17	11.54	0.07	21.69	0.00	1.11	101.20
		pl4-5	core	60.71	24.51	0.05	0.00	0.00	0.27	0.02	0.00	6.12	0.49	8.03	100.20
056	056-1c	grt1-1	core	38.70	21.28	0.00	0.09	1.54	26.65	5.56	2.52	5.60	0.00	0.02	101.95
		amp1-1	core	42.29	12.25	0.00	1.88	0.82	15.91	10.25	0.21	11.55	2.62	0.34	98.12
		pl1-3	core	62.62	24.97	0.02	0.00	0.00	0.21	0.19	0.03	5.51	0.17	8.59	102.32
	056-2c	grt2-8	core	39.08	21.74	0.08	0.00	1.22	27.21	5.46	2.14	5.89	0.05	0.00	102.88
		amp2-7	core	43.05	12.01	0.00	1.78	1.22	15.21	10.72	0.26	11.42	2.63	0.52	98.83
		pl2-7	core	62.03	25.06	0.00	0.00	0.00	0.10	0.20	0.00	5.84	0.20	8.42	101.84
	056-3c	grt3-5	core	39.13	21.58	0.00	0.07	3.19	26.11	5.91	1.78	5.93	0.00	0.18	103.86
		amp3-3	core	43.05	13.14	0.20	1.74	0.94	14.27	11.26	0.01	11.57	2.60	0.60	99.38
		pl3-1	core	62.00	24.70	0.00	0.01	0.00	0.14	0.00	0.13	5.79	0.12	8.19	101.08
071	071-1c	grt1-1	core	38.71	21.16	0.02	0.15	1.30	24.18	7.53	0.79	6.26	0.00	0.00	100.10
		cpx1-4	core	51.46	4.44	0.09	0.44	2.53	8.36	11.89	0.11	20.15	0.04	1.39	100.92
		pl1-4	core	60.16	24.73	0.08	0.00	0.00	0.28	0.04	0.02	6.49	0.37	7.76	99.93
	071-2c	grt2-1	core	38.97	21.58	0.04	0.11	2.20	24.16	7.30	0.81	6.72	0.04	0.02	101.95
		cpx2-4	core	51.18	4.34	0.01	0.50	4.63	6.15	12.16	0.16	20.65	0.02	1.56	101.37
		pl2-4	core	60.28	23.93	0.00	0.05	0.00	0.00	0.00	0.04	5.62	1.68	7.17	98.76
	071-3c	grt3-1	core	39.06	21.54	0.06	0.10	2.60	23.59	7.76	0.74	6.26	0.01	0.13	101.85
		cpx3-3	core	51.83	4.33	0.00	0.42	5.11	5.27	12.28	0.12	21.19	0.02	1.72	102.31
		pl3-3	core	60.32	24.45	0.10	0.01	0.00	0.13	0.03	0.08	6.38	0.64	8.06	100.19
	071-31c	grt3-6	core	38.91	21.42	0.02	0.17	1.59	24.36	7.57	0.71	6.31	0.00	0.01	101.07
		cpx3-1	core	51.52	4.02	0.00	0.37	4.33	5.70	12.30	0.08	20.94	0.00	1.61	100.86
		pl3-2	core	60.84	24.60	0.20	0.00	0.00	0.30	0.00	0.10	6.24	0.72	7.81	100.81

Sample	twq filename	Mineral	Label	SiO_2	Al_2O_3	Cr_2O_3	TiO_2	Fe_2O_3	FeO	MgO	MnO	CaO	K_2O	Na_2O	Total
142	142-11c	grt1-1	core	38.48	20.96	0.02	0.06	3.50	24.60	6.26	1.11	6.56	0.00	0.18	101.72
		cpx1-4	core	50.89	3.33	0.08	0.26	5.65	5.81	11.85	0.20	20.97	0.03	1.54	100.61
		pl1-3	core	60.52	23.99	0.05	0.01	0.00	0.12	0.00	0.00	5.82	0.29	8.26	99.08
	142-2c	grt2-1	core	38.41	20.89	0.00	0.03	2.59	25.38	5.94	0.99	6.58	0.01	0.12	100.94
		cpx2-2	core	53.17	1.61	0.06	0.07	2.91	7.25	12.50	0.15	23.17	0.01	0.92	101.82
		pl2-2	core	60.47	24.04	0.00	0.04	0.00	0.43	0.07	0.01	5.87	0.32	8.37	99.63
	142-3c	grt3-3	core	38.46	21.11	0.09	0.06	3.98	23.98	6.36	0.99	6.61	0.00	0.28	101.93
		cpx3-4	core	51.21	3.44	0.07	0.28	2.92	9.92	12.09	0.10	19.51	0.03	1.06	100.64
		pl3-3	core	60.40	24.26	0.00	0.07	0.00	0.23	0.00	0.05	5.87	0.28	8.27	99.43

Table E-1: Analyses from 4 samples that are recalculated for Fe^{3+} to establish the effect on *P-T* estimates assuming all Fe as Fe^{2+}.

Readily apparent in Table E-1 is the variation of calculated Fe_2O_3 in garnet, pyroxene and amphibole in an individual sample. For instance in all the samples, Fe_2O_3 in garnet may vary between 1-3 wt% difference between analyses. The variation in pyroxene is much less in only one sample (029-1, 2.85-3.39 wt%) whereas the other clinopyroxene analyses from the other samples yield much more variation in Fe_2O_3 (e.g., 071, 2.53-5.11 wt% Fe_2O_3). Recalculated amphibole analyses yield a minor variation in Fe_2O_3 from 0.82 - 1.22.

To test if the estimated Fe_2O_3 quantities are compatible with crystal chemistry, the sum of Fe^{2+}, Mg, Ca, Mn in garnet should be ≤ 3, and for pyroxene if Fe^{3+} is present in the pyroxene structure, then a monovalent cation such as Na must be present to allow the charges to balance. The relatively large spread of Fe_2O_3 in garnet implies that the recalculation scheme may not yield correct values of Fe_2O_3. The sum of Fe^{2+}, Mg, Ca, Mn in all cases is ≤ 3, and if Fe^{3+} is included in the sum the result is always > 3. This implies that the estimated quantity of Fe^{3+} is incorrect for garnet.

For pyroxene, if Fe^{3+} is present in the pyroxene structure then a monovalent cation such as Na must be present to allow the charges to balance. There must a direct relationship between the quantity of Fe^{3+} and Na in the M2 site of the pyroxene structure. This relationship is not observed in the pyroxene analyses, suggesting that the quantities of ferric iron estimated are incorrect.

If the estimates of the quantity of Fe_2O_3 in garnet, pyroxene and amphibole are incorrect ,then the P-T estimates made using the ferric calibrations should yield inconsistent results. The effect of the ferric calibration on P-T estimates is discussed below.

analysis set	*P* Fe^{3+}	*T* Fe^{3+}	*P* Fe^{2+}	*T* Fe^{2+}	*P* difference	*T* difference
029-1-1c	14.2	825	14.5	900	0.3	75
029-1-2c	13.6	755	14.2	845	0.6	90
029-1-4c	14.3	793	14.7	854	0.4	61
056-1c	5.2	710	9.2	767	4.0	57
056-2c	5.9	709	8.7	740	2.8	31
056-3c	6.3	693	8.9	718	2.6	25
071-1c	14.3	850	13.8	868	-0.5	18
071-2c	13.6	738	14.6	877	1.0	139
071-3c	13	705	14	872	1.0	167
071-31c	12.9	719	13.9	858	1.0	139
142-11c	12.5	690	12.6	832	0.1	142
142-2c	12	737	11.4	791	-0.6	54
142-3c	14.8	864	13.8	896	-1.0	32

***Table E-2**: Pressure-Temperature results for 13 analyses recalculated for Fe^{3+} (**P** Fe^{3+}, **T** Fe^{3+}) compared to the results of assuming all Fe as Fe^{2+} (**P** Fe^{2+}, **T** Fe^{2+}).*

Sample 029-1 yields temperatures 61-90 °C greater for the *all ferrous* calibration and the range of temperature estimates changes from 55 °C for the *all ferrous* calibration to 65 °C for the ferric calibration. The differences in calculated pressures is relatively small (0.3 to 0.6 kbar) however the spread of pressures is slightly greater in the ferric calibration than *all ferrous* (0.6 kbar vs 0.5 kbar).

Sample 056 yields the smallest temperature difference between calibrations 25-57 °C and a decrease in temperature range from 49 °C in the all ferrous calibration versus 17 °C in the ferric calibration. This suggests that the ferric estimates are correct for this sample, however the difference in estimated pressures, vary greatly from 2.6 kbar to 4.0 kbar. Pressures from the all ferrous calibration lie within a 0.5 kbar range whereas the ferric calibration yields pressures that lie in the a 1.1kbar range. This suggests that the ferric estimates are not correct.

Sample 071 yields the greatest difference in estimated temperatures where the results of ferric recalculation shown above show that the effect of assuming all Fe as Fe^{2+} yields

temperatures that are up to 167 °C greater than the ferric recalculation for the same analyses. The range in estimate peak temperatures differ between the analyses with *all ferrous* calibration yielding a 14 °C spread whereas the ferric calibration yields a range of 145 °C. The difference between pressure calibrations yields an anomalous increase in pressure by 0.5 kbar (see 071-1c) whereas the three others yield a decrease in pressure of 1 kbar and the range of estimated pressure increased from 0.8 to 1.2 kbar for the ferric calibration. The large range of temperature differences and the general increase in P-T ranges suggests that the ferric estimates are incorrect.

Sample 142 also yields a large temperature difference between calibrations (32-142 °C) and two of the three analysis sets yields pressures from the ferric calibration to be greater than the all ferrous pressure estimates especially 142-3c with estimated pressures ~14.8 kbar. The range of 105 °C in *all ferrous* temperature estimates increases to 174 °C for the ferric calibration. This implies that the ferric recalculation estimates are incorrect.

Based on the observations above, without an independent measure of Fe^{3+} for the samples the true affect of the ferric recalculation on *P-T* estimates cannot be accurately estimated. Based on the greater scatter in temperature estimates produced using the ferric calibration, it is inferred that introducing the ferric recalculation introduces additional error in the calculations. It is thus assumed that the *all ferrous* calibration yields a more consistent and better approximation of apparent peak *P-T* conditions even though this assumption may result in overestimation of peak temperature conditions in some samples.

Appendix F: P-T determinations for the Goose Bay region.

Samples with an * indicate that the *P-T* estimates for those analyses have been altered to reflect the true activity of silica ($aSiO_2 \neq 1$) in the analysis area or sample. The activity of silica and respective *P-T* values are located in Table 7-3. Temperature is in °C and pressure is in kbars.

Sample	Assem.	T	P Opx core	P Opx rim	P Cpx core	P Cpx rim	P Hbl core	P Hbl rim
008-1*	GCPQ	915			16.1			
008-11*	GCPQ	798				12.8		
008-2	GCPQ	838			13.9			
008-2	GHPQ	751					11.6	
008-21	GCPQ	658				10.7		
008-21	GHPQ	656						12.1
012-11*	GCPQ	902			15.8			
012-12*	GCPQ	843				14.2		
012-13*	GHPQ	815					14.1	
012-14*	GCPQ	809				13.3		
012-21	GCPQ	846			13.6			
012-22	GCPQ	751				11.4		
012-31	GCPQ	852			14.7			
012-32	GCPQ	709				11.3		
012-41	GHPQ	927					17.4	
012-42	GHPQ	843						15.8
017-1*	GCPQ	863			14.3			
017-1*	GHPQ	842					14.2	
017-11	GHPQ	N\A						
017-2*	GCPQ	887			15.1			
017-3*	GCPQ	818			13.4			
028-1	GOPQ	909	12.8					
028-1-2	GOPQ	781	10.8					
028-1-3	GCPQ	906			11.1			
028-1-32	GOPQ	780		8.9				
028-1-32	GCPQ	872				10.6		
028-1-32	GHPQ	786						8.1
028-1-rim	GOPQ	691		9.0				
029-1-1	GCPQ	900			14.5			
029-1-12	GCPQ	833				13.5		
029-1-2	GCPQ	845			14.2			
029-1-2	GHPQ	888					15.9	
029-1-22	GCPQ	828				13.9		
029-1-23	GHPQ	765						12.2
029-1-4	GCPQ	854			14.7			
029-1-41	GCPQ	866			14.2			
029-1-42	GCPQ	818				14.1		
029-1-43	GCPQ	793				13.1		

Sample	Assem.	T	P Opx core	P Opx rim	P Cpx core	P Cpx rim	P Hbl core	P Hbl rim
049-1	GCPQ	855			12.1			
049-12	GCPQ	806				11.5		
049-2	GCPQ	802			11.7			
049-21	GCPQ	809				11.8		
056-1	GHPQ	767					9.2	
056-11	GHPQ	645						6.1
056-2	GHPQ	740					8.7	
056-21	GHPQ	661						7.2
056-3	GHPQ	718					8.9	
056-31	GHPQ	677						7.6
059a-1	GHPQ	874					12.6	
059a-12	GHPQ	776						11.5
059a-13	GCPQ	889			13.5			
059a-14	GCPQ	790				11.8		
059a-2	GCPQ	831			12.4			
059a-21	GCPQ	844				12.5		
059a-22	GCPQ	881			12.8			
059a-23	GCPQ	790				12.0		
059a-3	GCPQ	941			14.6			
059a-31	GCPQ	826				12.0		
059a-4	GCPQ	878			13.4			
059a-41	GCPQ	780				11.3		
065a-1	GCPQ	824			13.1			
065a-12	GCPQ	614				9.3		
065a-2	GCPQ	874			14.2			
065a-21	GCPQ	755				12.1		
071-1	GCPQ	920			14.6			
071-12	GCPQ	880				13.9		
071-2	GCPQ	877			14.6			
071-21	GCPQ	862				14.5		
071-3	GCPQ	872			14.0			
071-31	GCPQ	858			13.9			
071-32	GCPQ	833				13.7		
072-1	GCPQ	868			13.8			
072-12	GCPQ	849				13.5		
072-2	GCPQ	858			13.8			
072-21	GCPQ	835				13.6		
072-3	GCPQ	877			14.0			
072-31	GCPQ	836				13.0		
072-4	GCPQ	893			14.3			
072-41	GCPQ	827				13.3		
074-11	GCPQ	728			12.7			
074-12	GCPQ	738			13.1			
074-13	GCPQ	689				11.3		
074-14	GCPQ	664				10.3		
074-2	GCPQ	722			12.7			
074-21	GCPQ	705				12.0		
074-31	GCPQ	735			13.6			
074-32	GCPQ	710			12.5			
074-33	GCPQ	695				11.5		

Sample	Assem.	T	P Opx core	P Opx rim	P Cpx core	P Cpx rim	P Hbl core	P Hbl rim
084-1*	GCPQ	907			15.8			
084-12*	GCPQ	851				14.5		
084-2	GCPQ	835			13.6			
084-21	GCPQ	815				13.9		
084-3*	GCPQ	948			15.1			
084-31*	GCPQ	865				14.6		
086-1-1	GCPQ	923			13.6			
086-1-1	GHPQ	967					12.7	
086-1-12	GCPQ	769				11.6		
086-1-12	GHPQ	781						10.7
090-1	GCPQ	850			13.9			
090-2	GCPQ	802				12.7		
090-2	GHPQ	785						9.7
122-31	GOPQ	781	9.7					
122-31	GCPQ	797			10.7			
122-312	GHPQ	774					9.1	
122-313	GOPQ	739		9.6				
122-314	GHPQ	782						9.2
122-321	GCPQ	802			11.9			
122-322	GCPQ	739				10.7		
122-323	GCPQ	846			14.1			
122-324	GCPQ	763			11.4			
122-325	GCPQ	780				11.2		
122-331	GCPQ	828			11.7			
122-332	GCPQ	810				11.7		
142-1	GCPQ	832			12.6			
142-12	GCPQ	824				12.4		
142-13	GHPQ	825					11.2	
142-14	GCPQ	926				14.5		
142-2	GCPQ	791			11.4			
142-21	GCPQ	733				10.6		
142-22	GHPQ	853					12.4	
142-3	GCPQ	896			13.8			
142-31	GCPQ	772				11.0		
196a-11	GCPQ	790			10.7			
196a-11	GHPQ	722					8.9	
196a-12	GCPQ	776				10.6		
196a-13	GHPQ	688						7.7
196a-14	GHPQ	705					7.9	
196a-15	GHPQ	686						7.5
196a-21	GCPQ	777			10.9			
196a-22	GHPQ	641						6.7
196a-23	GCPQ	830			11.5			
196a-24	GCPQ	805				11.2		
196a-25	GHPQ	766					8.9	
196a-26	GHPQ	737						8.5
196a-31	GCPQ	814			11.5			
196a-32	GCPQ	780				11.2		
196a-33	GHPQ	812					10.0	
196a-34	GHPQ	708						7.9

Jason B. Krauss Thesis map

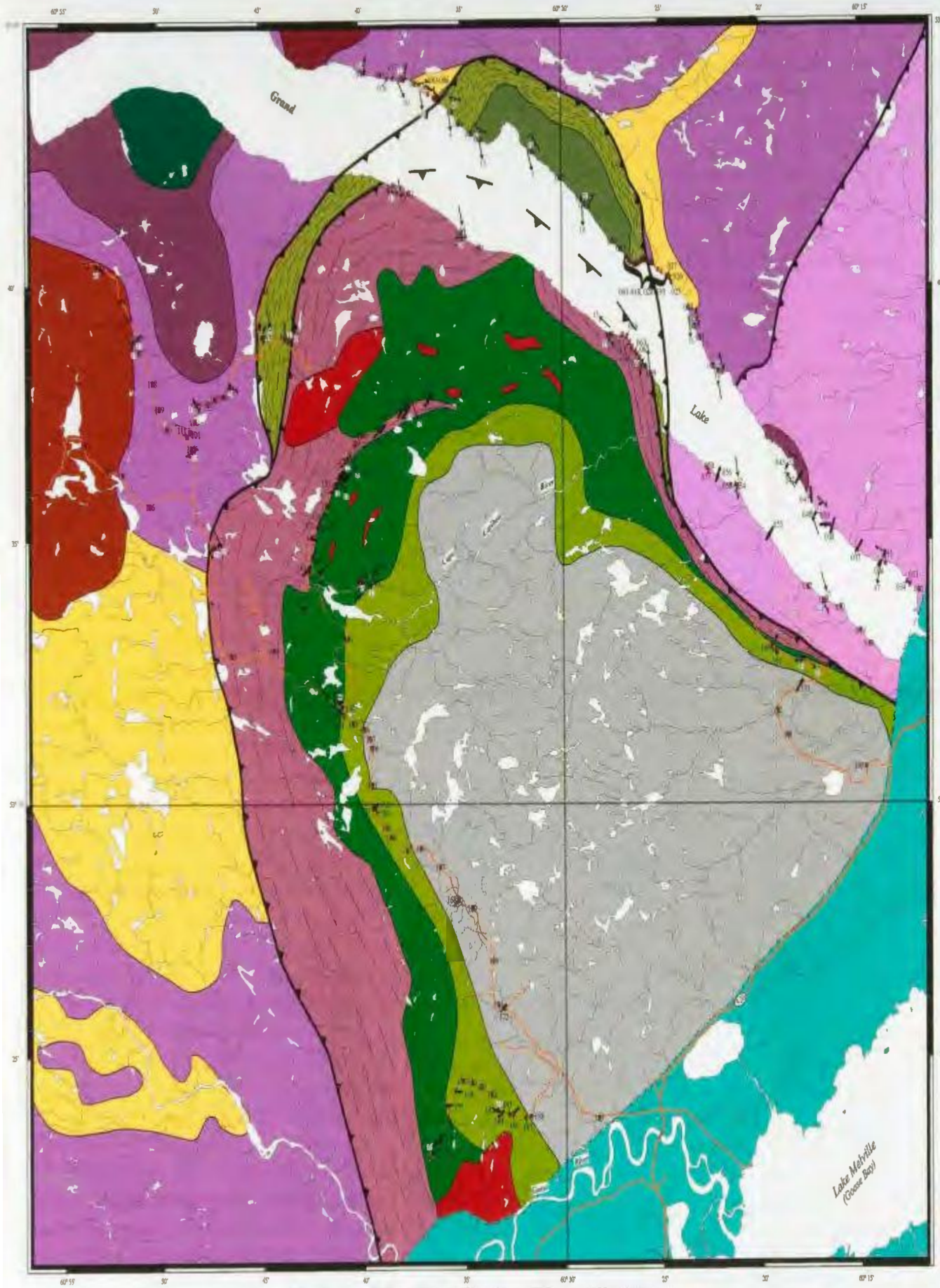

Legend

Cape Caribou River Allochthon

- Mylonite Zone
- Mafic Gneiss unit
- Dome Mountain Suite
- Granitoid Gneiss
- Recrystallized Gabbro-Diorite
- Layered Gabbro Monzonite
- NorthWest River Anorthosite

Groswater Bay terrane

- Paragneiss
- Orthogneiss
- Trans Labrador Batholith
- Unnamed Metadiorite
- Susan River Quartz Diorite
- Arrowhead Lake pluton

Lake Meville terrane

- Lake Melville Orthogneiss
- Susan River Quartz Diorite

- Northwest River Dykes
- Lake Melville Rift System

Symbols

- Mapping Station
- Mineral Lineation
- Foliation
- Gneissic Foliation
- Foliation Parallel to Igneous Layering
- Igneous layering and/or lamination
- Thrust/ductile shear zone
- Normal Fault
- Geological Contact: known, inferred
- Roads: Two lanes (paved)
- logging road (dirt)
- not maintained

N

Geology of the Cape Caribou River Allochthon

Scale
1:125,000

0 2 4 6 8 10 Kilometers